**NASA Technical Paper 2772**

1987

# Wind-Tunnel Investigation of a Full-Scale General Aviation Airplane Equipped With an Advanced Natural Laminar Flow Wing

Daniel G. Murri and
Frank L. Jordan, Jr.

*Langley Research Center*
*Hampton, Virginia*

National Aeronautics
and Space Administration

**Scientific and Technical
Information Division**

## Summary

An investigation has been conducted in the Langley 30- by 60-Foot Tunnel to evaluate the performance, stability, and control characteristics of a full-scale general aviation airplane equipped with an advanced natural laminar flow wing. The study focused on the effects of natural laminar flow and premature boundary-layer transition on performance, stability, and control, and also on the effects of several wing leading-edge modifications on the stall/departure resistance of the configuration. Data were measured over an angle-of-attack range from $-6°$ to $40°$ and an angle-of-sideslip range from $-6°$ to $20°$. The Reynolds number was varied from $1.4 \times 10^6$ to $2.4 \times 10^6$ based on the mean aerodynamic chord. Additional measurements were made using hot-film and sublimating chemical techniques to determine the condition of the wing boundary layer, and wool tufts were used to study the wing stall characteristics.

The investigation showed that large regions of natural laminar flow existed on the wing which would significantly enhance the cruise performance of the configuration. Also, because of the characteristics of the airfoil section, artificially tripping the wing boundary layer to a turbulent condition did not significantly affect the lift, stability, and control characteristics. The addition of a leading-edge droop arrangement was found to increase the stall angle of attack at the wingtips and, therefore, was considered to be effective in improving the stall/departure resistance of the configuration. Also, the addition of the droop arrangement resulted in only minor increases in drag. The configuration exhibited good longitudinal stability and control characteristics for all test conditions and stable effective dihedral up to the angle of attack for wing stall. The directional stability characteristics were generally poor at the higher angles of attack because of the loss of vertical tail effectiveness as angle of attack increased. The lateral-directional control characteristics were satisfactory, except near wing stall where large yawing and rolling moments were encountered as a result of asymmetric wing stall.

## Introduction

In recent years, studies have shown that significant improvements in the performance of general aviation and commuter aircraft are possible from the realization of increased amounts of natural laminar flow (NLF) (refs. 1 to 5). These results have been achieved in part through advanced NLF airfoil design and modern construction materials and fabrication techniques such as composites and milled or bonded aluminum skins. The emphasis in airfoil design has been directed toward developing airfoils with extensive natural laminar flow in an attempt to obtain lower cruise drag coefficients while maintaining acceptable maximum lift and stall characteristics. One airfoil designed with these considerations is designated the NASA NLF(1)-0414F. (See refs. 4 and 5.)

The current tests were conducted in a cooperative program between the NASA Langley Research Center and the Cessna Aircraft Company by testing a full-scale modified Cessna T-210 airplane in the Langley 30- by 60-Foot Tunnel (figs. 1 and 2). This airplane features a modified wing of increased aspect ratio and incorporates the NASA NLF(1)-0414F airfoil. A primary objective of these tests was to document the characteristics of the airfoil in this application and to determine the effects of premature boundary-layer transition on the overall airplane performance, stability, and control. In addition, results are presented concerning the effects of power and flap deflections on the longitudinal characteristics and the lateral-directional stability and control, and also the effects of fairing the airfoil trailing-edge reflex. The tests with the faired trailing-edge reflex were conducted to evaluate the effects of changing the airfoil contour to a shape that would be much easier and less expensive to fabricate.

Additional results are presented concerning the effects of several wing leading-edge modifications applied to the modified Cessna T-210. These tests were conducted to determine whether leading-edge modifications previously shown to provide excellent stall/spin resistance on more conventional wing/airfoil configurations (refs. 6 to 8) could be developed for application to an NLF wing design of high aspect ratio.

One approach recently studied in exploratory research (ref. 9) was to use the NASA NLF(1)-0414F airfoil for enhanced performance and to use another NLF airfoil of current interest, the NASA NLF(1)-0215F (ref. 3), for the leading-edge droop design. A leading-edge droop was developed for the current configuration in subscale tests in the Langley 12-Foot Low-Speed Tunnel using a wingtip balance to measure the aerodynamics of the outer wing panel. The droop was developed from the NLF(1)-0215F airfoil by gloving over the leading-edge outboard panel of the basic wing. An important feature of the droop is the abrupt discontinuity of the droop inboard leading edge. This discontinuity is effective in generating a vortex that acts as an aerodynamic fence to stop the spanwise flow from the inboard portion of the wing as stall progresses outward. The leading-edge droop extends to near the wingtip such that the outer

portion of the wing performs as a low-aspect-ratio wing with a very high stall angle of attack. This earlier research also revealed that on this particular configuration the effectiveness of the outboard droop could be enhanced by the addition of a small-span droop located inboard on the wing. Results are presented from the current tests which show the effects of the leading-edge modifications on the wing stall characteristics and the associated effects on stability and control, roll damping, and calculated cruise performance.

## Symbols

All longitudinal forces and moments are referred to the wind axis system, and all lateral-directional forces and moments are referred to the body axis system. Moment data are presented with respect to a center-of-gravity position of 25 percent of the wing mean aerodynamic chord.

| | |
|---|---|
| $b$ | wing span, ft |
| $C_D$ | drag coefficient, $\frac{\text{Drag}}{q_\infty S}$ |
| $\Delta C_D$ | incremental drag coefficient |
| $C_L$ | lift coefficient, $\frac{\text{Lift}}{q_\infty S}$ |
| $C_l$ | rolling-moment coefficient, positive with right wing down, $\frac{\text{Rolling moment}}{q_\infty S b}$ |
| $\Delta C_l$ | incremental rolling-moment coefficient |
| $C_m$ | pitching-moment coefficient, positive with nose up, $\frac{\text{Pitching moment}}{q_\infty S \bar{c}}$ |
| $\Delta C_m$ | incremental pitching-moment coefficient |
| $C_n$ | yawing-moment coefficient, positive with nose to right, $\frac{\text{Yawing moment}}{q_\infty S b}$ |
| $\Delta C_n$ | incremental yawing-moment coefficient |
| $C_T$ | thrust coefficient, $\frac{\text{Thrust}}{q_\infty S}$ |
| $C_Y$ | side-force coefficient, positive to right, $\frac{\text{Side force}}{q_\infty S}$ |
| $\Delta C_Y$ | incremental side-force coefficient |
| $c$ | local wing chord, ft |
| $\bar{c}$ | mean aerodynamic chord (reference), ft |
| $f$ | frequency of oscillation, Hz |
| $h$ | altitude, ft |
| $k$ | reduced-frequency parameter, $\omega b/2V$ |
| $p$ | roll rate, rad/sec |
| $q_\infty$ | free-stream dynamic pressure, $lb/ft^2$ |
| $R$ | Reynolds number based on $\bar{c}$ |
| $S$ | wing reference area, $ft^2$ |
| $V$ | velocity, ft/sec (or knots as indicated) |
| $W$ | weight, lb |
| $x$ | chordwise distance from wing leading edge, positive aft, ft |
| $z$ | vertical distance from wing leading edge, positive up, ft |
| $\alpha$ | angle of attack, deg |
| $\beta$ | angle of sideslip, deg |
| $\dot{\beta}$ | time rate of change of angle of sideslip, rad/sec |
| $\delta_a$ | aileron deflection, positive with trailing edge down, deg |
| $\delta_{a,\text{eff}}$ | effective aileron deflection, $\frac{\delta_{a,\text{right}} - \delta_{a,\text{left}}}{2}$, deg |
| $\delta_{\text{cf}}$ | cruise flap deflection, positive with trailing edge down, deg |
| $\delta_e$ | elevator deflection, positive with trailing edge down, deg |
| $\delta_r$ | rudder deflection, positive with trailing edge to left, deg |
| $\delta_s$ | spoiler deflection, positive with trailing edge up, deg |

| | |
|---|---|
| $\delta_{sf}$ | split flap deflection, positive with trailing edge down, deg |
| $\eta$ | propeller efficiency |
| $\rho$ | density of air, slugs/ft$^3$ |
| $\Delta\phi$ | amplitude of roll oscillation, deg |
| $\omega$ | angular frequency, $2\pi f$, rad/sec |

Stability derivatives:

$$C_{l_\beta} = \frac{\partial C_l}{\partial \beta} \quad C_{n_\beta} = \frac{\partial C_n}{\partial \beta} \quad C_{Y_\beta} = \frac{\partial C_Y}{\partial \beta}$$

$$C_{l_p} = \frac{\partial C_l}{\partial \frac{pb}{2V}} \quad C_{l_{\dot\beta}} = \frac{\partial C_l}{\partial \frac{\dot\beta b}{2V}}$$

Abbreviations:

| | |
|---|---|
| F.S. | fuselage station, in. |
| NLF | natural laminar flow |
| T.E. | trailing edge |
| T.E.D. | trailing edge down |
| T.E.U. | trailing edge up |
| V.G. | vortex generator |
| W.L. | waterline, in. |
| W.S. | wing station, in. |

## Model Description and Test Apparatus

The configuration tested in the study was a 1985 full-scale Cessna T-210 airplane modified with a high-aspect-ratio wing using a natural laminar flow airfoil section. The model was constructed primarily of formed aluminum; however, a polyester resin filler material was applied to the wing to obtain the desired airfoil section contours. The waviness of the wing surface when measured in a chordwise direction was maintained within ±0.003 in. per 2 inches of wavelength. Drawings of the model geometry and photographs of the model mounted in the Langley 30- by 60-Foot Tunnel are shown in figures 1 and 2, respectively. Also, a summary of the model geometric characteristics is presented in table I. The wing incorporates a small 12.5-percent-chord trailing-edge "cruise" flap that is designed to vary the low-drag lift coefficient range with small flap deflections. This cruise flap could also be set to large trailing-edge-down deflections (to 40°) to enhance the maximum lift characteristics. Roll control is provided by a combination of ailerons and spoilers.

The NASA NLF(1)-0414F airfoil section, shown in figure 3, is designed to achieve low-profile drag coefficients at a cruise condition of $R = 10 \times 10^6$ by maintaining natural laminar flow to about 70 percent chord on both upper and lower surfaces. Airfoil coordinates are provided in table II, and a more-detailed description of the airfoil and its characteristics can be found in reference 5.

The control settings were tested in the following ranges: $\delta_e = -25°$ to 15°, $\delta_{cf} = -3°$ to 40°, $\delta_r = -22°$ to 22°, $\delta_a = -22°$ to 16°, and $\delta_s = 0°$ to 48°. The ailerons and spoilers were tested both individually and combined for lateral control effectiveness. The ratio of spoiler deflection to aileron deflection is presented in figure 4 for the case where simultaneous deflections were used. The data of figure 4 are presented in terms of an effective aileron deflection, as defined in the "Symbols" section. In addition to deflecting the cruise flaps in the range indicated previously, a bolted-on sheet-metal split flap was tested at a deflection angle of 45°. The geometry of the split flap is presented in figure 1(c) and in table I.

The basic model configuration is defined in the following list:

| Basic model configuration |
|---|
| Boundary-layer transition free |
| Wing leading-edge modifications removed |
| All control surfaces undeflected |
| Landing gear retracted |
| Propeller fully feathered |

Variations to the basic model configuration are given in the following list:

| Variations to basic model configuration |
|---|
| Boundary-layer transition fixed |
| Wing leading-edge modifications added |
| All control surfaces deflected |
| Split flap simulated |
| Airfoil contour varied |
| Power effects added |
| Propeller removed |
| Engine cowling faired |
| Horizontal and vertical tails removed |

The wing leading-edge modifications tested included an outboard leading-edge droop, a segmented leading-edge droop, and a combination of an outboard droop and an inboard vortex generator. The droop airfoil section was derived by gloving the leading edge of the NLF(1)-0215F airfoil (ref. 3) to the NLF(1)-0414F airfoil. The resulting droop airfoil

coordinates are listed in table III, and drawings of all the leading-edge modifications are presented in figure 5.

The airfoil section contour was varied by fairing the upper and lower surface trailing-edge reflexes with sheet aluminum. These tests were conducted to evaluate the effects of changing the airfoil contour to a shape that would be much easier and less expensive to fabricate. The resulting airfoil section is shown in figure 6.

Powered tests were conducted using the standard 325-hp reciprocating engine to determine the effect of power on the longitudinal and lateral-directional stability characteristics. Also, the effects of the power plant installation were determined by testing with the propeller removed and with an auxiliary engine cowling installed with sealed and faired inlet and exit areas.

Overall aerodynamic forces and moments acting on the model were measured on the external scale balance system of the Langley 30- by 60-Foot Tunnel. (See ref. 10.) Tufts made of wool yarn were used on the wing upper surface to provide flow-visualization information when boundary-layer transition was artificially fixed near the leading edge of the wing. The tufts were removed from the model when free boundary-layer transition was desired. Boundary-layer transition was measured using both sublimating chemical (ref. 1) and hot-film techniques (ref. 11).

## Test Conditions and Corrections

Test conditions included an angle-of-attack range from $-6°$ to $40°$ and an angle-of-sideslip range from $-6°$ to $20°$. Aerodynamic data were obtained at free-stream tunnel velocities of 40, 60, and 72 mph which correspond to Reynolds numbers based on $\bar{c}$ of about $1.4 \times 10^6$, $2.0 \times 10^6$, and $2.4 \times 10^6$, respectively. Most of the force and moment tests, however, were conducted at a free-stream velocity of 60 mph. The Langley 30- by 60-Foot Tunnel has a turbulence factor of 1.1 which corresponds to an average turbulence level of approximately 0.1 percent (ref. 12).

A wind-tunnel calibration was made prior to model installation to determine horizontal buoyancy and flow-angularity corrections, and flow-field surveys ahead of the model were made in the manner of reference 13 to determine the flow-blockage corrections. Jet boundary corrections were made in accordance with the method of reference 14. Also, tares have been applied to the data to account for the aerodynamic loads applied to the exposed portions of the model support struts.

## Presentation of Results

The test results, which are presented in figures 7 to 51, are grouped in the following order of discussion:

## Discussion of Results

### Basic Airplane Characteristics

***Reynolds number effects.*** Before discussing the characteristics measured with the full-scale modified Cessna T-210 airplane, some of the Reynolds number effects on the NASA NLF(1)-0414F airfoil are presented. Data are presented in figure 7 from reference 15 that show the effect of Reynolds number on the two-dimensional-airfoil characteristics. The data at $R = 2.0 \times 10^6$ correspond approximately to the high-lift (landing) condition of the modified Cessna T-210, and this was the Reynolds number used for the majority of tests in the Langley 30- by 60-Foot Tunnel. The data at a Reynolds number of $6.0 \times 10^6$ correspond approximately to the cruise condition of the modified Cessna T-210.

The differences in lift and drag shown in figure 7 illustrate the importance of accounting for the Reynolds number effects on airfoils such as the NLF(1)-0414F. The data measured at $R = 6.0 \times 10^6$ could be used to predict the cruise performance of the airplane, but they would indicate unrealistically high levels of lift available for landing. The data measured at $R = 2.0 \times 10^6$ would accurately represent the landing condition, but they would indicate higher values of drag at cruise conditions. The two-dimensional-airfoil data suggest that drag measurements made in the Langley 30- by 60-Foot Tunnel ($R = 2.0 \times 10^6$) would be somewhat higher than those made at the actual cruise condition of the airplane. However, it was found that the incremental changes in total airplane drag due to fixing transition using roughness at $R = 2.0 \times 10^6$ (shown in later figures) agreed reasonably well with the increments obtained in flight at a Reynolds number of approximately $6.0 \times 10^6$.

The effects of Reynolds number on the longitudinal aerodynamic characteristics of the airplane are presented in figure 8. The data presented in figure 8 were measured with an external pressure belt installed on the right wing and with the propeller in flat pitch. These test runs were conducted as a preliminary part of the program to determine the best tunnel speed for the study. Because of the differences between the airplane configuration and the basic configuration for these runs, care should be taken in comparing the data of figure 8 with the data of other figures.

A primary effect of increasing Reynolds number, as shown in figure 8, is an increase in maximum lift coefficient and stall angle of attack. This is a well-known phenomenon and is due to an increased resistance of the boundary layer to separate near the wing trailing edge at higher Reynolds numbers. Another significant effect shown in figure 8 is a nonlinear variation of pitching-moment coefficient with angle of attack below 2°. This characteristic was most pronounced at the lowest Reynolds number.

The two-dimensional-airfoil data in figure 7, however, show no such characteristic down to $R = 2.0 \times 10^6$.

Examination of the lift-drag polars for various Reynolds numbers (fig. 8(b)) indicates that the drag data obtained at $R = 2.0 \times 10^6$ were nearly equal to those obtained at $R = 2.4 \times 10^6$. For this reason and because of support system and airplane structural limitations at high angles of attack and high tunnel speeds, the majority of the tests were conducted at a Reynolds number of $2.0 \times 10^6$, which corresponds to a tunnel speed of about 60 mph.

***Longitudinal characteristics.*** Results are presented in figure 9 for the basic airplane configuration. The data of figure 9 indicate that a maximum lift coefficient of about 1.65 was measured at an angle of attack $\alpha$ of 17° and was followed by a sharp stall between $\alpha = 17°$ and 18°. An interesting characteristic exhibited in the data is the change in lift-curve slope that occurred at about $\alpha = 2°$. This characteristic was caused by an upper surface trailing-edge separation behind about $0.8c$ and is evident in the two-dimensional pressure distributions measured for this airfoil in reference 5. However, the data presented in reference 5 indicate that the trailing separation is delayed to higher angles of attack at higher Reynolds numbers ($\alpha \approx 5°$ at $R = 10 \times 10^6$). The change in lift-curve slope was also accompanied by a slight increase in longitudinal stability at about $C_L = 0.47$, which is most evident in the plot of $C_L$ versus $C_m$. Although this characteristic did not significantly affect the longitudinal stability of this configuration, more-pronounced effects could be encountered on canard configurations where the distances between the lifting surfaces and the center of gravity are much greater. More-detailed discussions of the relationship between canard/wing-section characteristics and overall stability characteristics for canard configurations can be found in references 2, 16, and 17. In addition to the effects on the longitudinal characteristics, it will be shown in later sections that this trailing-edge separation also reduced the effectiveness of the ailerons and spoilers to provide roll-control moments.

The drag characteristics of the basic airplane configuration are presented in figure 9(b). The data show that the minimum drag coefficient of the basic configuration was about 0.0275 at a lift coefficient of about 0.1 and occurred at an angle of attack between −2° and −1°.

***Flow visualization using tufts.*** Presented in figure 10 are tuft flow-visualization photographs used to examine the stall progression characteristics of the basic wing for angles of attack ranging from −6° to 40°. Since the tufts would be expected to trigger boundary-layer transition, a transition strip was applied at $x/c = 0.05$ to identify the point of transition. An interesting characteristic discussed previously is an initial trailing-edge separation that occurs above an angle of attack of about 2° and is evident beginning in figure 10(f). This trailing-edge separation was shown to cause a decrease in lift-curve slope and an increase in longitudinal stability. Beginning at $\alpha = 16°$, stalled flow is shown to begin at the spoiler area and to propagate outboard and inboard from this point. (See fig. 10(n).) At an angle of attack of 18°, the wing has completely stalled (fig. 10(p)) which results in a sharp loss in lift and a highly negative lift-curve slope. An interesting characteristic observed during the flow-visualization tests was an unsteady stalling and reattaching behavior exhibited on a small inboard area on the wing upper surface as wing stall progressed. Because of its unsteady nature, this characteristic is not evident in the photographs presented in figure 10. However, this unsteady characteristic was observed for all wing configurations during the flow-visualization tests.

***Effect of airplane components.*** The results of tests conducted to determine the effects of various airplane components are presented in figures 11 and 12. As expected, the primary effect on the longitudinal characteristics of removing the horizontal and vertical tails was a reduction in longitudinal static stability (fig. 11). However, at angles of attack above 20°, the slope of the $C_m$ versus $\alpha$ curve is nearly the same for the tail-off and tail-on configurations. This result would indicate that the horizontal tail loses its effectiveness in providing longitudinal stability above $\alpha = 20°$. Such an effect could result from horizontal tail stall, but it could also be aggravated by the wake from the model support fairings impinging on the horizontal tail at extreme angles of attack. (See fig. 2.)

As mentioned previously, tests were conducted to determine the effect of the power plant installation. The primary effect of fairing the engine cowling and removing the propeller was a reduction in drag coefficient as shown in figure 11(b). The data show that an almost constant drag increment $\Delta C_D$ of about 0.0030 was measured between the basic configuration and the configuration with the propeller removed and the engine cowling faired.

***Lateral-directional stability.*** The results of tests to determine the static lateral-directional stability of the airplane are presented in figure 12 in terms of the derivatives $C_{Y_\beta}$, $C_{n_\beta}$, and $C_{l_\beta}$ as functions of angle of attack. These derivatives were obtained by taking slopes between $\beta = 6°$ and −6° and are referred to the airplane body axes. The results for the

complete airplane indicate stable effective dihedral ($-C_{l_\beta}$) up to the angle of attack for wing stall ($\alpha \approx 17°$). However, the directional stability ($C_{n_\beta}$) characteristics are shown to become low or negative from about $\alpha = 3°$ up to the stall. A comparison of the tail-on and tail-off directional stability data indicates that the vertical tail lost effectiveness in providing directional stability near $\alpha = 13°$.

***Control-effectiveness characteristics.*** The results of tests to determine the effectiveness of the airplane flight control surfaces are presented in figures 13 to 16 for the basic airplane configuration.

In figure 13(a) good longitudinal control effectiveness is indicated, with elevator control providing a trim angle-of-attack range from about $-4°$ to $20°$. The variation in pitching moment with elevator deflection is shown in figure 13(c) for $\alpha = 0°$ and $15°$. The data show a linear variation of $C_m$ with $\delta_e$ over a fairly large range of elevator deflections. Elevator effectiveness is shown to be about equal at $\alpha = 0°$ and $15°$; however, the data of figure 13(a) indicate reduced elevator effectiveness at angles of attack above wing stall.

The directional control effectiveness of the rudder is summarized in figure 14. The data indicate that the rudder generally maintains yaw-control effectiveness up to the angle of attack for wing stall ($\alpha \approx 17°$) and exhibits reduced effectiveness at higher angles of attack. At an angle of attack of 17°, however, large yawing and rolling moments are encountered that are a result of asymmetric wing stall. The data of figure 14(a) indicate that these large moments at the stall are greater than the yawing moment provided by full rudder deflection.

In order to determine the isolated effects of the lateral control surfaces, tests were conducted using individual aileron and spoiler deflections. Presented in figure 15 is the effect of deflecting the left aileron alone. The data show an initial reduction in aileron effectiveness at an angle of attack of about 5°, probably because of wing trailing-edge separation. This reduction in aileron effectiveness may be delayed to higher angles of attack at higher Reynolds numbers because of the effect of increasing Reynolds number to delay trailing-edge separation (discussed earlier). Nonetheless, good control effectiveness is indicated up to wing stall, and then reduced effectiveness is shown at higher angles of attack. The data of figure 16 show that the spoilers were much less effective in providing roll control than the ailerons. A comparison of the data in figures 16(a) and 16(b) indicates that spoiler deflections of 18° or less were ineffective in providing roll control, except at negative angles of attack. At $\alpha = 0°$, spoiler deflections greater than 18° are shown to provide a fairly linear variation in rolling moment; however, all usable spoiler roll-control effectiveness is lost by an angle of attack of about 12°. Therefore, the only roll control available at the stall is provided by the ailerons. The aileron-effectiveness results of figure 15 (for the left aileron alone), however, suggest that the total roll control provided by the ailerons may become marginal at wing stall.

## Boundary-Layer Study

***Free-transition characteristics.*** The boundary-layer transition characteristics of the basic wing were measured using both the sublimating chemical technique (ref. 1) and the hot-film technique (ref. 11). An example of one of the sublimating chemical tests is shown in figure 17(a) for $\alpha = 1°$ and $R = 2.4 \times 10^6$. The test results showed that laminar flow was maintained to about 70 percent chord on both upper and lower surfaces at the cruise angle of attack. These results agree well with the theoretical predictions and the two-dimensional-airfoil transition measurements from references 4 and 5. These data also agree well with the transition measurements made in flight by Cessna with the same modified Cessna T-210. (See ref. 18.)

Presented in figures 17(b) and 17(c) are the upper and lower surface boundary-layer transition characteristics measured using the hot-film technique. The data show the movement of the transition location with changes in angle of attack and cruise flap deflection. Some exceptions were noted when comparing the forward movement of transition with changes in angle of attack from present test results with those of the flight tests (ref. 18). For example, the wind-tunnel data indicate earlier forward movement of transition on the upper surface as angle of attack is decreased and on the lower surface as angle of attack is increased. These differences are probably due to differences in Reynolds number and turbulence level between the conditions in the wind tunnel and in cruise flight and are discussed further in reference 18.

***Boundary-layer transition.*** With such a large extent of natural laminar flow occurring on the wing of this configuration, the obvious question that arises is the effect of artificially tripping the laminar boundary layer to a turbulent condition. In an operational environment, periodic wing cleaning (possibly before each flight) would probably be required to ensure the performance benefit from natural laminar flow. Once airborne, however, premature boundary-layer transition could occur after insect contamination or during flight in moisture, and it could potentially result in changing the trim or stability and control

characteristics (ref. 9). Therefore, designing a wing with a natural laminar flow airfoil to minimize these characteristics is very desirable.

The effects on the total airplane characteristics of artificially tripping the boundary layer at $x/c = 0.05$ are presented in figure 18. The data of figure 18(a) indicate the very desirable characteristic that boundary-layer transition results in essentially no change in the lift and pitching-moment characteristics. Of particular interest is the characteristic that maximum lift and the angle of attack for maximum lift remain unchanged for either boundary-layer condition. The total airplane drag characteristics with artificial boundary-layer transition are shown in figure 18(b). As would be expected, the turbulent boundary-layer condition results in large increases in drag at cruise lift coefficients. The total increase in drag $\Delta C_D$ at a cruise lift coefficient $C_L$ of 0.3 is shown to be about 0.0070.

The calculated performance increases of the modified Cessna T-210 due to the large extent of laminar flow are illustrated in figure 19. These performance calculations are based on trimmed values of $C_L$ and $C_D$ and are made for an altitude of 10 000 ft, a weight of 3500 lb, and at 75 percent power. Also, a propeller efficiency $\eta$ of 0.80 has been assumed for the cruise condition, and a drag increment of −0.0015 has been subtracted from the data to account for the feathered propeller. The equations used for the performance calculations are as follows:

For velocity ($V$),

$$V = \sqrt{\frac{2W}{\rho C_L S}} \qquad \text{(ft/sec)}$$

or

$$V = \frac{3600}{6076}\sqrt{\frac{2W}{\rho C_L S}} \qquad \text{(knots)}$$

For power available ($P_a$), with engine power setting in percent,

$$P_a = 325\eta\ (\text{Engine power setting}/100) \qquad \text{(hp)}$$

For power required ($P_r$), with $V$ in feet per second,

$$P_r = \frac{\frac{1}{2}\rho V^3 S(C_D - 0.0015)}{550} \qquad \text{(hp)}$$

It is noted that these calculations are derived from the wind-tunnel data measured at $R = 2.0 \times 10^6$, where the airfoil is not performing as well (in terms of drag) as at the true cruise Reynolds number ($R \approx 6.0 \times 10^6$). As a result, the calculated performance would be expected to be less than that obtained in flight; however, the calculations were found to give a reasonable estimate of the incremental effects of fixing transition.

The calculations presented in figure 19 indicate that the large extent of laminar flow would be responsible for about a 10-percent increase in speed and range for the same power setting. These incremental effects agree reasonably well with the performance measurements made by Cessna during flight tests of the same modified Cessna T-210 (ref. 18). The calculations also show that if power were reduced to fly at the same cruise speed, then the large extent of laminar flow would be responsible for about a 29-percent increase in range. This example indicates the desirability of maintaining the quality of the wing surface in an operational environment in order to take advantage of the performance gains resulting from natural laminar flow.

As would be expected, given the insignificant effects of boundary-layer transition on the lift and pitching-moment characteristics (shown previously), only minor effects on lateral-directional stability and control are experienced. The only data available indicating the effect of transition on lateral-directional stability were measured on the basic configuration modified with the outboard-droop and vortex-generator (droop/V.G.) configuration. These data, presented in figure 20, show very minor effects of transition. Data describing the effect of transition on the lateral-directional stability are not available for the basic configuration. However, all the results discussed above would suggest that only very minor effects on lateral-directional stability would be encountered with the basic configuration. The aileron and spoiler effectiveness of the configuration, shown in figure 21, is also very similar for the free- and fixed-transition cases.

### Leading-Edge Modifications

As discussed in the "Introduction," several of the leading-edge modifications tested were developed during preliminary subscale model tests. The only data from these preliminary tests (reported in ref. 9) that are presented herein are results of subscale forced-oscillation tests to determine roll damping characteristics. These forced-oscillation tests were conducted in the Langley 30- by 60-Foot Tunnel using a 28-percent-scale wing/body model of the present configuration. The tests were conducted at a free-stream dynamic pressure of 10 lb/ft$^2$ ($R = 0.65 \times 10^6$ based on $\bar{c}$), a reduced frequency $k$ of 0.2, and a roll oscillation amplitude $\Delta\phi$ of ±5°.

***Subscale roll damping results.*** The roll damping characteristics of the outboard-droop and segmented-droop leading-edge configurations are compared with the roll damping characteristics of the basic configuration in figure 22. The data of figure 22(a) show that the basic wing configuration exhibited highly unstable values of damping in roll at angles of attack both at and slightly beyond wing stall. (For the lower Reynolds number subscale tests, stall occurred at a slightly lower angle of attack.) These unstable values of damping in roll are due primarily to the highly negative lift-curve slope exhibited by this configuration immediately after wing stall. The data for the outboard-droop configuration show significantly enhanced roll damping characteristics at the stall; however, unstable roll damping characteristics are not completely eliminated with the outboard droop alone. On the other hand, the data of figure 22(b) show that the segmented-droop configuration maintained stable characteristics over the test angle-of-attack range. The reasons for these characteristics will be illustrated in the following section on flow visualization using tufts.

***Flow visualization using tufts.*** The effects of the leading-edge modifications on the stall progression characteristics are presented in figures 23 to 25 for the cases with no cruise flap deflection. As with the basic wing when tufts were installed, a transition strip was applied at $x/c = 0.05$ to identify the point of transition. The results of figure 23 show that as stalled flow develops on the outboard-droop configuration, attached flow is maintained at the wingtips to an angle of attack as high as 30°. This result would tend to improve the post-stall roll damping characteristics as indicated in figure 22. At the initial stall, however, the large inboard portion of the wing stalls very rapidly, a result probably accounting for the small unstable values of roll damping for the outboard-droop configuration. With the segmented-droop configuration, however, the inboard-droop segment is shown in figure 24 to be effective in delaying the complete stall of the inboard portion of the wing. Therefore, the stable roll damping characteristics exhibited by the segmented-droop configuration appear to be due in part to an effectiveness of the inboard-droop segment in delaying inboard wing stall.

For drag considerations (discussed in a later section), tests were also conducted with the inboard-droop segment replaced by a vortex generator. The results of figure 25 show that the stall progression characteristics for the droop/V.G. configuration are very similar to those of the segmented-droop configuration. Roll damping data are not available for the droop/V.G. configuration; however, the stall progression results of figures 24 and 25 suggest that the roll damping characteristics for the droop/V.G. configuration would be similar to those of the segmented-droop configuration. Also, an interesting characteristic exhibited in figures 25(e) and 25(f) was an unsteady stalling and reattaching behavior occurring inboard on the wing upper surface as wing stall progressed. As discussed previously, this characteristic was observed for all wing configurations but was not always evident in the photographs because of its unsteady nature.

***Longitudinal characteristics.*** The effects of the leading-edge modifications on the longitudinal characteristics are presented in figures 26 and 27. The primary effects shown in these figures are changes in the lift characteristics at wing stall and in the drag at lower angles of attack. As would be expected based on the tuft flow photographs, the outboard-droop and segmented-droop configurations show successive reductions in the abruptness of the lift loss at wing stall (fig. 26(a)). Also, the data of figure 27(a) show that the droop/V.G. and segmented-droop configurations have similar stall characteristics. In all cases, the increased values of lift for the leading-edge modifications result from maintaining areas of attached flow at angles of attack above normal wing stall.

The drag characteristics of the leading-edge modifications are presented in figures 26(b) and 27(b). In general, the leading-edge modifications were responsible for small drag increases at low angles of attack. For example, at a cruise lift coefficient of 0.3, the addition of the outboard droop resulted in an untrimmed drag penalty $\Delta C_D$ of about 0.0009. The segmented droop, however, shows an untrimmed drag penalty of about 0.0021 at $C_L = 0.3$. The reason for the disproportionate increase in drag with the addition of the inboard-droop segment is probably due to an increase in the number of discontinuities at the wing leading edge which introduced several regions of vortex flow over the wing. The data measured for the configuration with the vortex generator installed inboard of the leading-edge droop generally show a slight drag reduction at low lift coefficients compared with data for the configuration with the segmented-droop leading edge (fig. 27(b)). This result is probably due to eliminating disturbances inboard on the lower wing surface introduced by the segmented-droop arrangement. In this case, at a lift coefficient $C_L$ of 0.3, the addition of the droop/V.G. modification resulted in an untrimmed drag penalty $\Delta C_D$ of about 0.0018.

***Boundary-layer transition with wing leading-edge modifications.*** Boundary-layer transition was measured using the sublimating chemical technique on the upper and lower wing surfaces with the segmented-droop modification installed. The photograph presented in figure 28 shows the extent of NLF on the wing upper surface at $R = 2.4 \times 10^6$ and $\alpha = 1°$. The photograph shows that NLF was maintained on the upper surface of the droop sections to $x/c \approx 0.70$, and turbulent wedges can be seen emanating from the droop discontinuities. On the lower surface, however, transition was found to occur very near the leading edge of the droop section.

***Cruise performance.*** The calculated cruise performance characteristics for the configuration with the leading-edge modifications are summarized in figure 29 using the same cruise example explained previously. The data show that the outboard-droop and segmented-droop modifications would be responsible for decreases in cruise speed of about 2 knots and 5 knots, respectively. These penalties are considered relatively small (about 1.1 percent and 2.8 percent, respectively), especially in view of the potential improvements in stall/departure resistance provided by the modifications. The data for the droop/V.G. modification show a cruise speed reduction of about 3 knots. In this case, it may be possible to realize the potential improvements in stall/departure resistance of the segmented droop and minimize the performance penalty of the modification.

***Lateral-directional stability.*** The lateral-directional stability characteristics with the droop/V.G. and segmented-droop modifications are presented in figure 30. As would be expected, the data show that the primary effects on lateral-directional stability of adding the leading-edge modifications are on the stall and post-stall characteristics. At an angle of attack of 18°, the basic airplane is shown to exhibit a high level of directional stability ($+C_{n_\beta}$) and highly unstable effective dihedral ($+C_{l_\beta}$). These characteristics are a result of large yawing and rolling moments caused by asymmetric wing stall in a sideslip condition. Addition of the leading-edge modifications tends to reduce the level of asymmetric wing stall at sideslip. Therefore, at $\alpha = 18°$, the leading-edge modifications tend to reduce directional stability and enhance effective dihedral. At post-stall angles of attack, however, the data show that the leading-edge modifications generally improve directional stability and reduce effective dihedral.

***Aileron and spoiler effectiveness.*** The aileron and spoiler effectiveness of the configuration with and without the segmented-droop modification is presented in figure 31 for $\alpha = 15°$. The data show only a minor effect of the segmented-droop modification on the roll-control effectiveness of the aileron and spoiler combination. The roll-control effectiveness is shown to be slightly improved at sideslip with the leading-edge modification installed.

### Wing Contour Study

The effects of fairing the airfoil upper and lower surface trailing-edge reflexes are summarized in figure 32. The data of figure 32 show that fairing the trailing-edge reflex resulted in minor changes in the aerodynamic characteristics of the airplane. Maximum lift is shown to be reduced by about 0.08, and a minor increase in drag is shown to occur between about $C_L = 0$ and 0.2. At a cruise lift coefficient of 0.3, the data indicate that fairing the trailing-edge reflex would have very minor effects on drag. It should be noted, however, that these characteristics were measured at $R = 2.0 \times 10^6$ and that the effects of fairing the trailing-edge reflex on the drag characteristics at higher Reynolds number are unknown.

### Flap Configurations

***Longitudinal characteristics.*** The longitudinal characteristics as affected by deflection of the cruise flap are presented in figure 33 for the basic airplane configuration. As implied, the cruise flaps for this configuration were designed to be deflected at small angles during cruise flight. Reference 5 explains that this concept can be used to minimize drag at a given cruise lift coefficient by deflecting the flap to keep the stagnation point at the leading edge. The data of figure 33(b) indicate, however, that small cruise flap deflections resulted in values of total airplane drag that were no better than those for the $\delta_{cf} = 0°$ case.

The effectiveness of large cruise flap deflections in providing increased values of maximum lift is shown in figure 33(c). Values of lift coefficient are shown to increase progressively with increasing cruise flap deflection. The maximum untrimmed lift coefficient obtained with power off was approximately 2.05 with a cruise flap deflection of 40°. Another characteristic evident in figure 33(c) is that only minor pitching-moment changes occur with cruise flap deflections. Apparently, the diving moments produced by trailing-edge-down cruise flap deflections (evident in the tail-off data of fig. 34) are about equally offset by the effects of increased downwash at the horizontal tail. The longitudinal characteristics with the split flap deflected and with combined split flap and cruise flap deflections are presented in figure 35. The data show that the maximum lift coefficient (untrimmed) obtained with the split flap alone was about 1.9,

which is slightly less than that provided with a cruise flap deflection of 40° (fig. 33(c)). Also, combined split flap and cruise flap deflections did not yield higher values of maximum lift than those with the split flap alone. As in the case of the cruise flap, deflection of the split flap showed only minor effects on pitching moment.

***Flow visualization using tufts.*** Presented in figures 36 to 39 are tuft flow-visualization photographs used to observe the stall progression of the wing with the cruise flaps deflected to 40°. As explained previously, since the tufts would be expected to trigger boundary-layer transition, a transition strip was applied at $x/c = 0.05$ to identify the point of transition. The primary effects of deflecting the cruise flap on the stall characteristics of the basic wing are illustrated in figure 36. With the cruise flaps deflected to $\delta_{cf} = 40°$, stalled flow is shown to begin at a point more inboard than that with the flaps undeflected (fig. 10), and total wing stall occurs at a slightly lower angle of attack ($\alpha = 17°$). Also evident in figures 36(c) and 36(d) is the unsteady stalling and reattaching behavior that was noted previously.

The effects of cruise flap deflection on the stall progression characteristics of the configuration with leading-edge modifications installed are presented in figures 37, 38, and 39. The effect of cruise flap deflection on the stall pattern of the modified wing is very similar to that for the basic wing (no leading-edge modifications). That is, wing stall begins at slightly lower angles of attack with the cruise flap $\delta_{cf}$ deflected to 40°. Also, for each leading-edge modification, the stall progression characteristics are very similar to those for the corresponding configuration with the flaps undeflected.

***Lateral-directional stability.*** The effect of cruise flap deflection on lateral-directional stability for the basic configuration is presented in figure 40. The directional stability characteristics of the configuration remain relatively unchanged with cruise flap deflection above about $\alpha = 2°$. Below $\alpha = 2°$, trailing-edge-down cruise flap deflections are shown to generally degrade the directional stability characteristics. The decrease in directional stability could be a result of reduced dynamic pressure over the vertical tail when the flaps are deflected. Deflection of the cruise flap is shown to have little effect on effective dihedral characteristics.

***Control effectiveness.*** The results of tests to evaluate the effects of flap deflection on the control-effectiveness characteristics are summarized in figures 41 to 44. The data of figure 41 indicate that the pitch-control effectiveness of the elevator was essentially unchanged with any combination of split flap and cruise flap deflections. Other than slight offsets in $C_m$ due to the flap deflection, the variation of pitching moment with elevator deflection was unaffected. The yaw-control effectiveness of the rudder was found to be independent of cruise flap deflection at $\alpha = 0°$ (fig. 42(a)). However, at $\alpha = 15°$, somewhat erratic variations in yawing moment with rudder deflection are observed; but the data indicate no clear trend due to cruise flap deflection.

The effects of cruise flap deflection on the roll-control characteristics of the left aileron and the left spoiler are shown in figures 43 and 44, respectively. The data of figure 43 indicate that the roll-control effectiveness of the ailerons is generally unaffected by cruise flap deflection. The data of figure 44, however, show that trailing-edge-down cruise flap deflections can improve the roll-control effectiveness of the spoilers at low angles of attack. As discussed previously for the basic configuration ($\delta_{cf} = 0°$), spoiler deflections of 18° or less are ineffective in providing roll control at $\alpha = 0°$. With trailing-edge-down cruise flap deflections, however, the data of figure 44 show an increase in spoiler effectiveness and a relatively linear variation of rolling moment with spoiler deflection over the entire spoiler deflection range. The increase in spoiler effectiveness with the cruise flaps deflected is probably due to an acceleration of the airflow at the spoiler location caused by trailing-edge-down cruise flap deflections. At higher angles of attack ($\alpha = 15°$) where spoiler roll-control effectiveness is completely lost, the data show no beneficial effect of trailing-edge-down cruise flap deflections.

***Flap effectiveness with transition.*** The effects of transition with cruise flaps deflected were found to be very similar to those for the basic configuration discussed previously. The data of figure 45 show that the lift and pitching-moment characteristics are not significantly affected by transition for any cruise flap deflection. The drag data for all cruise flap deflections (fig. 45(b)) show significant increases in total airplane drag with transition fixed at $x/c = 0.05$.

## Power Effects

***Longitudinal characteristics.*** The results of tests to determine the effect of power on the longitudinal characteristics are presented in figures 46, 47, and 48 for cruise flap deflections of 0°, 20°, and 40°, respectively. Values of thrust coefficient were determined by measuring the difference in total airplane drag between the power-off and power-on conditions at $\alpha = 0°$ and $\delta_{cf} = 0°$. The engine/propeller settings corresponding to these conditions were then used to set the thrust coefficient for all angles of attack and cruise flap deflections.

In general, the results of figures 46 to 48 show increases in both lift-curve slope and maximum lift for increasing $C_T$ for all cruise flap deflections. These effects are partially due to direct thrust components and partially due to propeller-slipstream-induced effects over the wings and flaps. No significant effects of power on the longitudinal stability or trim characteristics are indicated except for the $\delta_{cf} = 40°$ case (fig. 48(a)). With the cruise flaps deflected to $\delta_{cf} = 40°$, the data show a moderate change in trim characteristics and reduced levels of longitudinal stability with increasing $C_T$. The increased pitching-moment changes with power when $\delta_{cf} = 40°$ are probably caused by increased downwash at the tail for the flap-down, high-power condition and are not serious when considering the already high levels of longitudinal stability and good longitudinal control power.

***Lateral-directional stability.*** The effects of power on lateral-directional stability are shown in figure 49. Increasing $C_T$ is shown to have a stabilizing effect on directional stability between angles of attack of about 2° and 18°, probably as a result of increased dynamic pressure at the tail. Although the data show unstable directional stability occurring by $\alpha = 3°$ for the power-off case, the data for $C_T = 0.28$ show stable directional stability characteristics up to an angle of attack of about 12°.

The effective dihedral characteristics generally show increased stability due to power below an angle of attack of about 2°. At low angles of attack where the data of figure 46 show that the addition of power tends to decrease lift, propeller slipstream effects at sideslip would tend to enhance effective dihedral.

***Control effectiveness.*** The effects of power on the elevator- and rudder-effectiveness characteristics are presented in figures 50 and 51, respectively. The data presented in these figures are in the form of incremental moment coefficients generated by a control deflection away from zero. As expected, the data show increased elevator and rudder effectiveness with increased thrust coefficient because of increased dynamic pressure at the horizontal and vertical tails.

## Summary of Results

A wind-tunnel investigation has been conducted to evaluate the aerodynamic performance, stability, and control of a full-scale general aviation airplane equipped with an advanced natural laminar flow wing. The following remarks summarize the most significant results of the investigation:

1. Natural laminar flow was maintained to about 70 percent chord on both upper and lower wing surfaces at the cruise angle of attack (at a lift coefficient of approximately 0.3 and a Reynolds number of $2.4 \times 10^6$). The large extent of laminar flow was in agreement with airfoil data and flight test results obtained at cruise Reynolds numbers ($6.0 \times 10^6$). Calculated cruise performance based on the data indicates significant increases in performance due to natural laminar flow.

2. Artificially tripping the wing boundary layer to a turbulent condition did not significantly affect the lift, stability, and control characteristics. These characteristics are very desirable since the effects of premature boundary-layer transition (due to insect contamination, etc.) must be considered.

3. The leading-edge modifications were found to enhance the roll damping characteristics at the stall significantly, and they were therefore considered effective in improving the stall/departure resistance. Also, the modifications were found to be responsible for only minor increases in drag ($\Delta C_D = 0.0009$ to 0.0021) at a cruise lift coefficient of 0.3.

4. The configuration exhibited good longitudinal stability and control characteristics for all flap, power, and wing leading-edge conditions.

5. The airplane exhibited stable effective dihedral up to the angle of attack for wing stall (approximately 17°) for all configurations tested. The power-off directional stability was generally poor at the higher angles of attack because of the loss of vertical tail effectiveness. However, power-on directional stability is somewhat improved because of slipstream effects at the tail.

6. The lateral-directional control characteristics were generally satisfactory except near wing stall where large yawing and rolling moments were encountered as a result of asymmetric wing stall. The roll-control effectiveness of the ailerons and spoilers was reduced at angles of attack above 5° because of trailing-edge flow separation on the wing upper surface. Furthermore, the spoilers were found to be ineffective in providing roll control at angles of attack above 12°.

7. Deflection of the cruise flaps was more effective in providing increased levels of maximum lift than deflection of the simulated split flap. The maximum untrimmed lift coefficient obtained with power off was approximately 2.05 with a cruise flap deflection of 40°.

NASA Langley Research Center
Hampton, Virginia 23665-5225
September 1, 1987

## References


1. Holmes, Bruce J.; Obara, Clifford J.; and Yip, Long P.: *Natural Laminar Flow Experiments on Modern Airplane Surfaces.* NASA TP-2256, 1984.
2. Yip, Long P.: *Wind-Tunnel Investigation of a Full-Scale Canard-Configured General Aviation Airplane.* NASA TP-2382, 1985.
3. Somers, Dan M.: *Design and Experimental Results for a Natural-Laminar-Flow Airfoil for General Aviation Applications.* NASA TP-1861, 1981.
4. Viken, Jeffrey K.: Aerodynamic Design Considerations and Theoretical Results for a High Reynolds Number Natural Laminar Flow Airfoil. M.S. Thesis, George Washington Univ., Jan. 1983.
5. McGhee, Robert J.; Viken, Jeffrey K.; Pfenninger, Werner; Beasley, William D.; and Harvey, William D.: *Experimental Results for a Flapped Natural-Laminar-Flow Airfoil With High Lift/Drag Ratio.* NASA TM-85788, 1984.
6. Staff, Langley Research Center: *Exploratory Study of the Effects of Wing-Leading-Edge Modifications on the Stall/Spin Behavior of a Light General Aviation Airplane.* NASA TP-1589, 1979.
7. Newsom, William A., Jr.; Satran, Dale R.; and Johnson, Joseph L., Jr.: *Effects of Wing-Leading-Edge Modifications on a Full-Scale, Low-Wing General Aviation Airplane—Wind-Tunnel Investigation of High-Angle-of-Attack Aerodynamic Characteristics.* NASA TP-2011, 1982.
8. DiCarlo, Daniel J.; Glover, Kenneth E.; Stewart, Eric C.; and Stough, H. Paul: Discontinuous Wing Leading Edge To Enhance Spin Resistance. *J. Aircr.*, vol. 22, no. 4, Apr. 1985, pp. 283–288.
9. Johnson, Joseph L., Jr.; Yip, Long P.; and Jordan, Frank L., Jr.: Preliminary Aerodynamic Design Considerations for Advanced Laminar Flow Aircraft Configurations. *Laminar Flow Aircraft Certification,* Louis J. Williams, compiler, NASA CP-2413, 1986, pp. 185–225.
10. DeFrance, Smith J.: *The N.A.C.A. Full-Scale Wind Tunnel.* NACA Rep. 459, 1933.
11. Obara, Clifford J.; and Holmes, Bruce J.: *Flight-Measured Laminar Boundary-Layer Transition Phenomena Including Stability Theory Analysis.* NASA TP-2417, 1985.
12. Rae, William H., Jr.; and Pope, Alan: *Low-Speed Wind Tunnel Testing, Second ed.* John Wiley & Sons, Inc., c.1984.
13. Theodorsen, Theodore; and Silverstein, Abe: *Experimental Verification of the Theory of Wind-Tunnel Boundary Interference.* NACA Rep. 478, 1934.
14. Heyson, Harry H.: *Use of Superposition in Digital Computers To Obtain Wind-Tunnel Interference Factors for Arbitrary Configurations, With Particular Reference to V/STOL Models.* NASA TR R-302, 1969.
15. Murri, Daniel G.; Jordan, Frank L., Jr.; Nelson, Randy; and Davis, Patrick J.: Wind-Tunnel Investigation of a General Aviation Airplane Equipped With a High Aspect-Ratio, Natural-Laminar-Flow Wing. SAE Tech. Paper Ser. 871019, Apr. 1987.
16. Chambers, Joseph R.; Yip, Long P.; and Moul, Thomas M.: *Wind-Tunnel Investigation of an Advanced General Aviation Canard Configuration.* NASA TM-85760, 1984.
17. Williams, L. J.; Johnson, J. L., Jr.; and Yip, L. P.: Some Aerodynamic Considerations for Advanced Aircraft Configurations. AIAA-84-0562, Jan. 1984.
18. Befus, Jack; Nelson, E. Randel; Ellis, David R.; and Latas, Joe: Flight Test Investigations of a Wing Designed for Natural Laminar Flow. SAE Tech. Paper Ser. 871044, Apr. 1987.

Table I. Model Geometric Characteristics

| | |
|---|---|
| Wing: | |
| Area, $ft^2$ | 161.051 |
| Area (reference), $ft^2$ | 160.735 |
| Span, ft | 42.0 |
| Mean aerodynamic chord, ft | 3.913 |
| Mean aerodynamic chord (reference), ft | 3.908 |
| Root chord (centerline), ft | 4.787 |
| Tip chord, ft | 2.882 |
| Aspect ratio | 10.95 |
| Taper ratio | 0.60 |
| Wing incidence (root), deg | 0 |
| Dihedral angle, deg | 2.0 |
| Washout angle, deg | 0 |
| Leading-edge sweep angle, deg | 0 |
| Trailing-edge sweep angle, deg | −5.18 |
| Airfoil | NASA NLF(1)-0414F |
| Cruise flap: | |
| Area (one), $ft^2$ | 7.306 |
| Inboard wing station, in. | 23.0 |
| Outboard wing station, in. | 201.0 |
| Span (per side), ft | 14.833 |
| Chord, percent $c$ | 12.5 |
| Split flap: | |
| Area (one), $ft^2$ | 8.653 |
| Inboard wing station, in. | 23.0 |
| Outboard wing station, in. | 201.0 |
| Span (per side), ft | 14.833 |
| Chord, ft | 0.583 |
| Aileron: | |
| Area (one), $ft^2$ | 2.517 |
| Inboard wing station, in. | 201.0 |
| Outboard wing station, in. | 250.0 |
| Span (per side), ft | 4.083 |
| Chord, percent $c$ | 20.0 |
| Spoiler: | |
| Area (one), $ft^2$ | 2.251 |
| Inboard wing station, in. | 125.0 |
| Outboard wing station, in. | 201.0 |
| Span (per side), ft | 6.333 |
| Leading edge, percent $c$ | 77.5 |
| Trailing edge, percent $c$ | 87.5 |
| Chord, percent $c$ | 10.0 |
| Horizontal tail (including elevator): | |
| Area, $ft^2$ | 48.0 |
| Span, ft | 16.0 |
| Root chord, ft | 4.0 |
| Tip chord, ft | 2.0 |
| Incidence, deg | −1.0 |
| Elevator area, $ft^2$ | 17.10 |

Table I. Concluded

| | |
|---|---|
| Vertical tail (including rudder): | |
| Area (less dorsal), $ft^2$ | 16.0 |
| Span, ft | 4.80 |
| Root chord (less dorsal), ft | 4.33 |
| Tip chord, ft | 2.33 |
| Rudder area, $ft^2$ | 6.40 |

Table II. NASA NLF(1)-0414F Airfoil Coordinates

[Data taken from reference 5]

(a) Upper surface

| $x/c$ | $z/c$ |
|---|---|
| 0.000000 | 0.000000 |
| .000085 | .001585 |
| .000299 | .003274 |
| .001231 | .007144 |
| .002695 | .010618 |
| .004989 | .014163 |
| .008005 | .017552 |
| .011774 | .020769 |
| .016268 | .023816 |
| .021468 | .026795 |
| .027356 | .029735 |
| .033891 | .032633 |
| .041042 | .035480 |
| .048811 | .038317 |
| .057201 | .041092 |
| .066189 | .043825 |
| .075767 | .046482 |
| .085915 | .049070 |
| .096610 | .051588 |
| .107826 | .054033 |
| .119545 | .056398 |
| .131756 | .058692 |
| .144443 | .060917 |
| .157592 | .063092 |
| .171193 | .065206 |
| .185212 | .067240 |
| .199628 | .069172 |
| .214447 | .071009 |
| .229647 | .072735 |
| .245187 | .074349 |
| .261054 | .075830 |
| .277233 | .077161 |
| .293699 | .078380 |
| .310424 | .079454 |
| .327391 | .080369 |
| .344571 | .081151 |
| .361925 | .081781 |
| .379421 | .082240 |
| .397052 | .082536 |
| .414812 | .082677 |
| .432667 | .082633 |
| .450558 | .082429 |
| .468450 | .082047 |

| $x/c$ | $z/c$ |
|---|---|
| 0.486327 | 0.081507 |
| .504159 | .080794 |
| .521931 | .079893 |
| .539641 | .078779 |
| .557254 | .077489 |
| .574742 | .075988 |
| .592064 | .074285 |
| .609177 | .072377 |
| .626040 | .070245 |
| .642629 | .067900 |
| .658928 | .065348 |
| .674926 | .062510 |
| .690586 | .059376 |
| .705860 | .055889 |
| .720751 | .051944 |
| .735392 | .047492 |
| .750058 | .042542 |
| .764925 | .037208 |
| .779951 | .031694 |
| .795034 | .026178 |
| .810124 | .020750 |
| .825179 | .015483 |
| .840076 | .010464 |
| .854693 | .005783 |
| .868960 | .001467 |
| .882768 | −.002475 |
| .896006 | −.006044 |
| .908644 | −.009267 |
| .920659 | −.012161 |
| .931980 | −.014739 |
| .942511 | −.017008 |
| .952200 | −.018994 |
| .961042 | −.020722 |
| .969034 | −.022206 |
| .976155 | −.023456 |
| .982370 | −.024492 |
| .987660 | −.025333 |
| .992021 | −.026006 |
| .995456 | −.026519 |
| .997952 | −.026872 |
| .999480 | −.027067 |
| 1.000000 | −.027122 |

Table II. Concluded

(b) Lower surface

| $x/c$ | $z/c$ |
|---|---|
| 0.000000 | 0.000000 |
| .000085 | −.001535 |
| .000164 | −.002120 |
| .000740 | −.004536 |
| .002095 | −.006984 |
| .004174 | −.009008 |
| .007129 | −.010993 |
| .010874 | −.012933 |
| .015540 | −.014882 |
| .021096 | −.016854 |
| .027380 | −.018787 |
| .034569 | −.020742 |
| .042393 | −.022654 |
| .050985 | −.024572 |
| .060274 | −.026487 |
| .070243 | −.028383 |
| .080881 | −.030259 |
| .092159 | −.032116 |
| .104058 | −.033945 |
| .116557 | −.035741 |
| .129635 | −.037497 |
| .143277 | −.039212 |
| .157457 | −.040888 |
| .172148 | −.042521 |
| .187328 | −.044107 |
| .202969 | −.045646 |
| .219043 | −.047125 |
| .235525 | −.048542 |
| .252387 | −.049901 |
| .269586 | −.051189 |
| .287087 | −.052411 |
| .304866 | −.053561 |
| .322901 | −.054635 |
| .341156 | −.055635 |
| .359611 | −.056539 |
| .378260 | −.057344 |
| .397074 | −.058052 |
| .416017 | −.058658 |
| .435049 | −.059142 |
| .454127 | −.059517 |
| .473222 | −0.059785 |
| .492319 | −.059950 |
| .511402 | −.060012 |
| .530430 | −.059979 |
| .549361 | −.059792 |
| .568160 | −.059456 |
| .586782 | −.058982 |
| .605204 | −.058340 |
| .623397 | −.057533 |
| .641303 | −.056524 |
| .658920 | −.055246 |
| .676262 | −.053698 |
| .693229 | −.051845 |
| .709795 | −.049388 |
| .726433 | −.046065 |
| .743743 | −.042296 |
| .761642 | −.038850 |
| .779550 | −.035991 |
| .797188 | −.033529 |
| .814513 | −.031444 |
| .831368 | −.029735 |
| .847719 | −.028310 |
| .863493 | −.027230 |
| .878523 | −.026450 |
| .892802 | −.025925 |
| .906336 | −.025641 |
| .919043 | −.025539 |
| .930841 | −.025569 |
| .941715 | −.025689 |
| .951668 | −.025861 |
| .960696 | −.026061 |
| .968804 | −.026275 |
| .975996 | −.026483 |
| .982266 | −.026675 |
| .987613 | −.026858 |
| .992033 | −.027036 |
| .995503 | −.027211 |
| .997994 | −.027367 |
| .999497 | −.027475 |
| 1.000000 | −.027514 |

Table III. Airfoil Coordinates With Leading-Edge Droop Modification

(a) Upper surface

| $x/c$ | $z/c$ |
|---|---|
| −0.30000 | −0.023843 |
| −.029482 | −.019923 |
| −.027929 | −.015199 |
| −.025346 | −.010322 |
| −.021747 | −.005285 |
| −.017143 | −.000114 |
| −.011553 | .005229 |
| −.004999 | .010634 |
| .002493 | .015994 |
| .010894 | .021239 |
| .020170 | .026283 |
| .030000 | .030948 |
| .040000 | .035082 |
| .050000 | .038727 |
| .060000 | .041969 |
| .070000 | .044911 |
| .080000 | .047588 |
| .090000 | .050055 |
| .100000 | .052347 |
| .110000 | .054485 |
| .120000 | .056486 |
| .130000 | .058372 |
| .140000 | .060154 |
| .150000 | .061852 |
| .160000 | .063476 |
| .170000 | .065026 |
| .180000 | .066501 |
| .190000 | .067899 |
| .200000 | .069220 |
| .210000 | .070474 |
| .220000 | .071657 |
| .230000 | .072773 |
| .240000 | .073828 |
| .250000 | .074816 |
| .260000 | .075737 |
| .270000 | .076685 |
| .280000 | .077376 |
| .290000 | .078119 |
| .300000 | .078804 |
| .310000 | .079429 |
| .320000 | .079990 |
| .330000 | .080497 |
| .340000 | .080958 |
| .350000 | .081366 |
| .360000 | .081719 |
| .370000 | .082014 |
| .380000 | .082252 |
| .390000 | .082437 |
| .410000 | .082656 |
| .420000 | .082682 |
| .430000 | .082650 |
| .440000 | .082570 |

| $x/c$ | $z/c$ |
|---|---|
| 0.450000 | 0.082438 |
| .460000 | .082248 |
| .470000 | .082007 |
| .480000 | .081717 |
| .490000 | .081375 |
| .510000 | .080520 |
| .520000 | .080001 |
| .530000 | .079410 |
| .540000 | .078755 |
| .550000 | .078045 |
| .560000 | .077268 |
| .570000 | .076417 |
| .580000 | .075494 |
| .590000 | .074500 |
| .610000 | .072279 |
| .620000 | .071038 |
| .630000 | .069708 |
| .640000 | .068288 |
| .650000 | .066782 |
| .660000 | .065169 |
| .670000 | .063421 |
| .680000 | .061538 |
| .690000 | .059501 |
| .710000 | .054848 |
| .720000 | .052157 |
| .730000 | .049193 |
| .740000 | .045981 |
| .750000 | .042562 |
| .760000 | .038998 |
| .770000 | .035352 |
| .780000 | .031676 |
| .790000 | .028012 |
| .810000 | .020794 |
| .820000 | .017275 |
| .830000 | .013835 |
| .840000 | .010489 |
| .850000 | .007258 |
| .860000 | .004149 |
| .870000 | .001162 |
| .880000 | −.001703 |
| .890000 | −.004450 |
| .910000 | −.009602 |
| .920000 | −.012006 |
| .930000 | −.014298 |
| .940000 | −.016478 |
| .950000 | −.018552 |
| .960000 | −.020523 |
| .970000 | −.022380 |
| .980000 | −.024104 |
| .990000 | −.025696 |
| 1.000000 | −.027122 |

Table III. Concluded

(b) Lower surface

| $x/c$ | $z/c$ |
|---|---|
| −0.030000 | −0.023843 |
| −.029482 | −.026943 |
| −.027929 | −.029825 |
| −.025346 | −.032399 |
| −.021747 | −.034730 |
| −.017143 | −.036789 |
| −.011553 | −.038547 |
| −.004999 | −.040220 |
| .002493 | −.041844 |
| .010894 | −.043394 |
| .020170 | −.044874 |
| .030285 | −.046285 |
| .041198 | −.047630 |
| .052868 | −.048880 |
| .065246 | −.050061 |
| .078286 | −.051167 |
| .091936 | −.052195 |
| .106140 | −.053152 |
| .120844 | −.054038 |
| .135990 | −.054850 |
| .151517 | −.055590 |
| .167364 | −.056258 |
| .183470 | −.056855 |
| .199769 | −.057383 |
| .216199 | −.057841 |
| .232694 | −.058233 |
| .249189 | −.058562 |
| .265618 | −.058833 |
| .281918 | −.059035 |
| .298023 | −.059164 |
| .313871 | −.059248 |
| .337149 | −.059356 |
| .360427 | −.059459 |
| .383704 | −.059557 |
| .406982 | −.059652 |
| .430260 | −.059743 |
| .453538 | −.059830 |
| .460000 | −.059611 |
| .470000 | −.059747 |
| .480000 | −.059855 |
| .490000 | −.059935 |
| .500000 | −.059987 |
| .510000 | −.060011 |
| .520000 | −.060012 |
| .530000 | −.059981 |
| .540000 | −.059904 |

| $x/c$ | $z/c$ |
|---|---|
| 0.550000 | −0.059783 |
| .560000 | −.059620 |
| .570000 | −.059416 |
| .580000 | −.059173 |
| .590000 | −.058882 |
| .600000 | −.058538 |
| .610000 | −.058146 |
| .620000 | −.057699 |
| .630000 | −.057190 |
| .640000 | −.056606 |
| .650000 | −.055929 |
| .660000 | −.055159 |
| .670000 | −.054294 |
| .680000 | −.053330 |
| .690000 | −.052239 |
| .700000 | −.050930 |
| .710000 | −.049351 |
| .720000 | −.047416 |
| .730000 | −.045291 |
| .740000 | −.043101 |
| .750000 | −.041033 |
| .760000 | −.039144 |
| .770000 | −.037456 |
| .780000 | −.035924 |
| .790000 | −.034491 |
| .800000 | −.033168 |
| .810000 | −.031955 |
| .820000 | −.030857 |
| .830000 | −.029864 |
| .840000 | −.028949 |
| .850000 | −.028136 |
| .860000 | −.027445 |
| .870000 | −.026863 |
| .880000 | −.026386 |
| .890000 | −.026010 |
| .900000 | −.025750 |
| .910000 | −.025596 |
| .920000 | −.025537 |
| .930000 | −.025563 |
| .940000 | −.025665 |
| .950000 | −.025828 |
| .960000 | −.026044 |
| .970000 | −.026308 |
| .980000 | −.026604 |
| .990000 | −.026947 |
| 1.000000 | −.027514 |

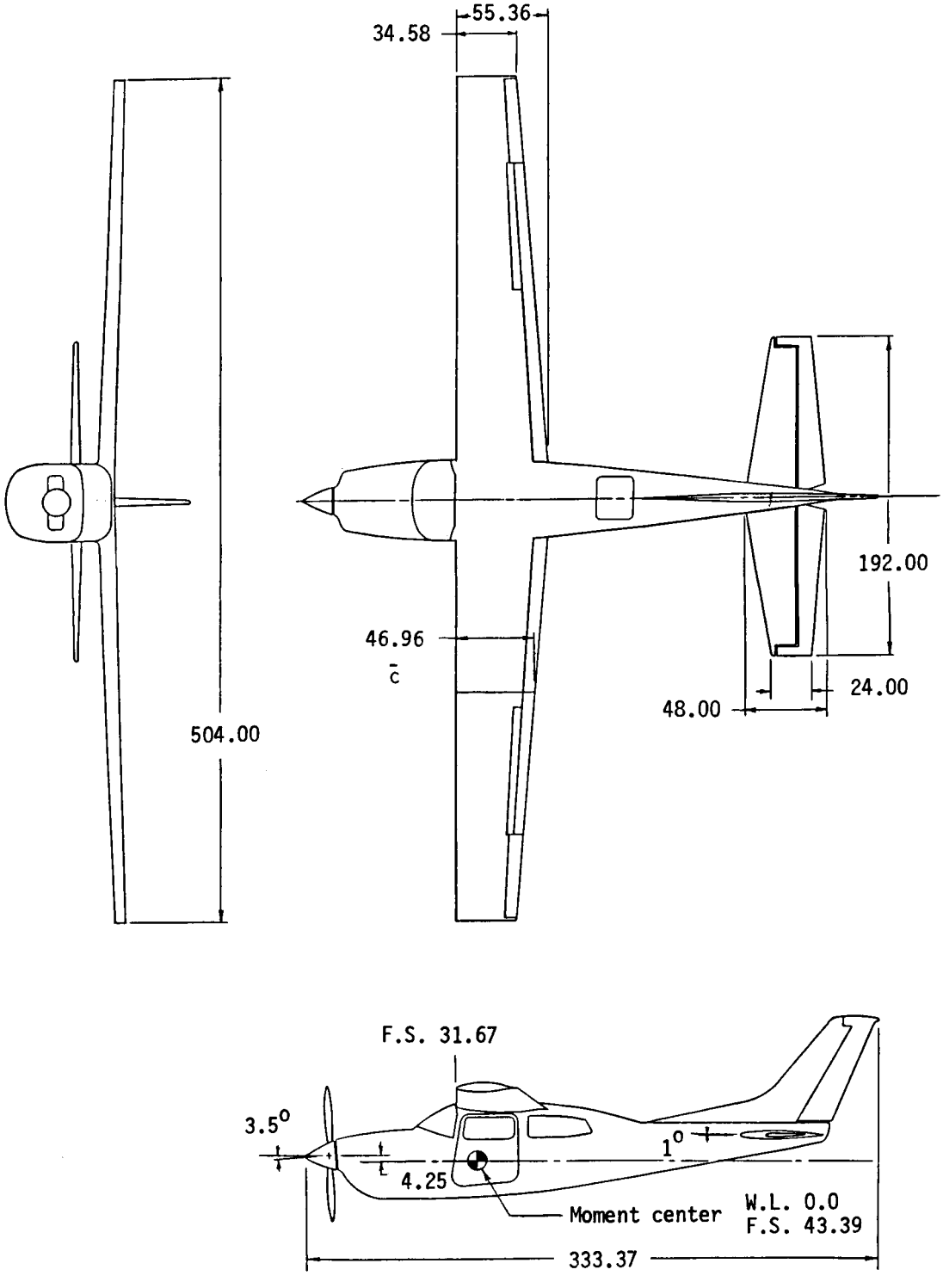


(a) Three-view drawing.

Figure 1. Geometric characteristics of model. Linear dimensions are in inches.

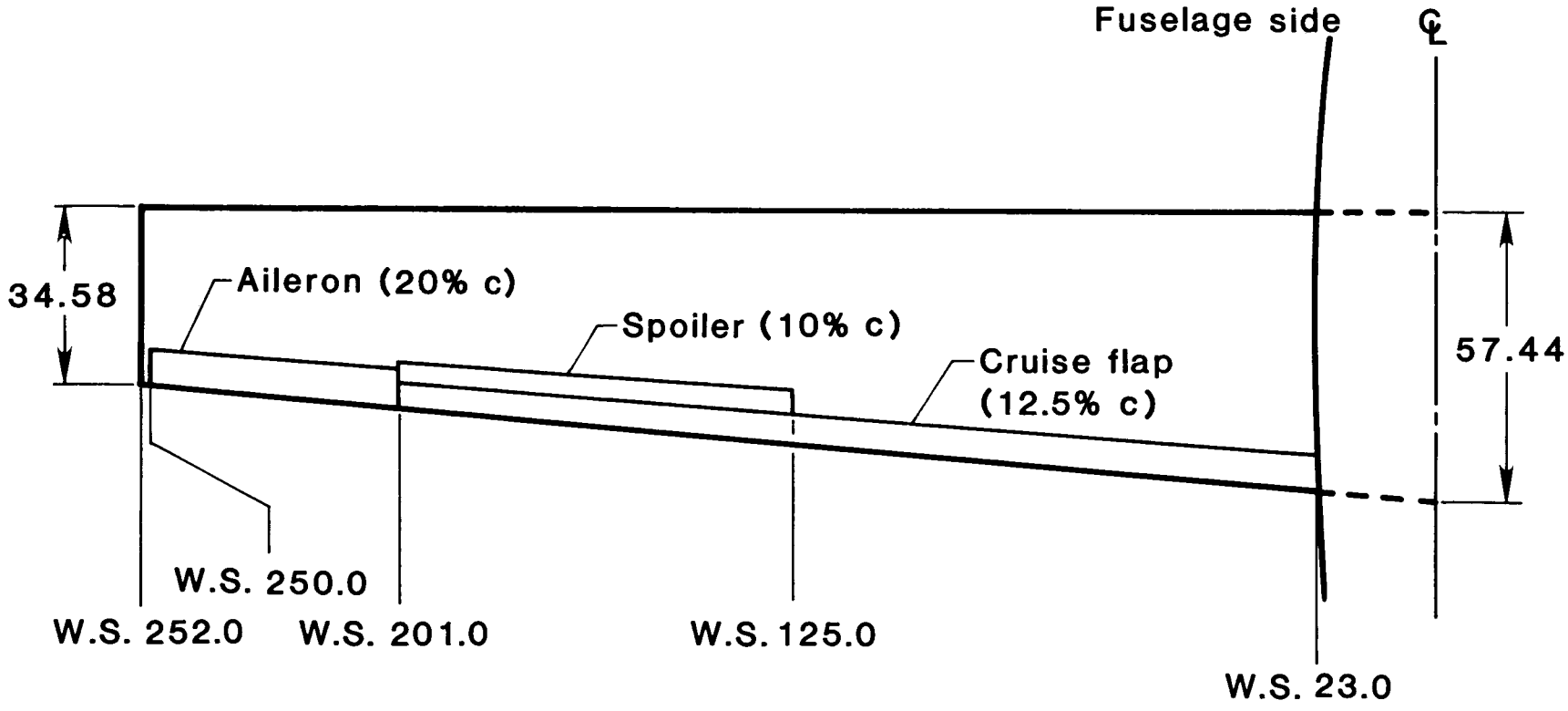


(b) Wing details.

Figure 1. Continued.

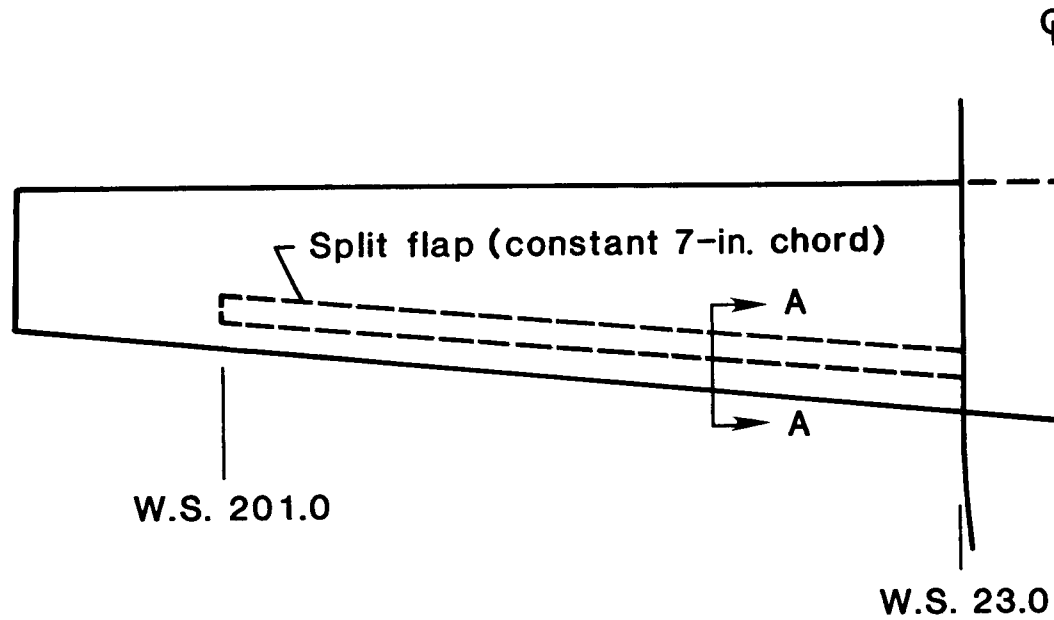


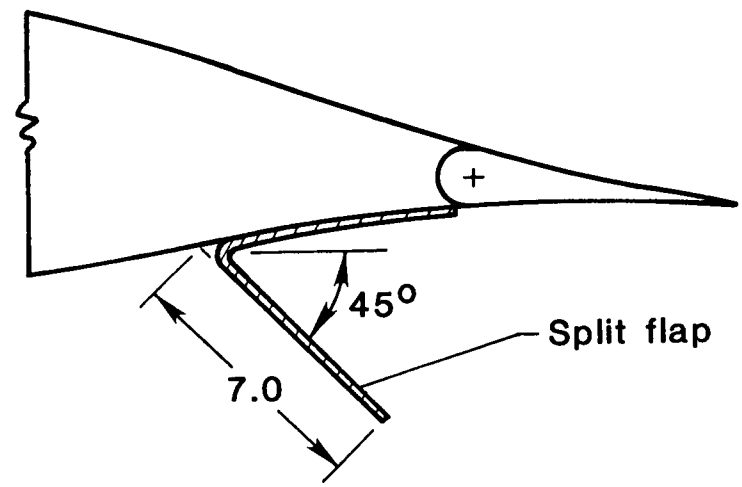


Section A–A

(c) Split flap details.

Figure 1. Concluded.

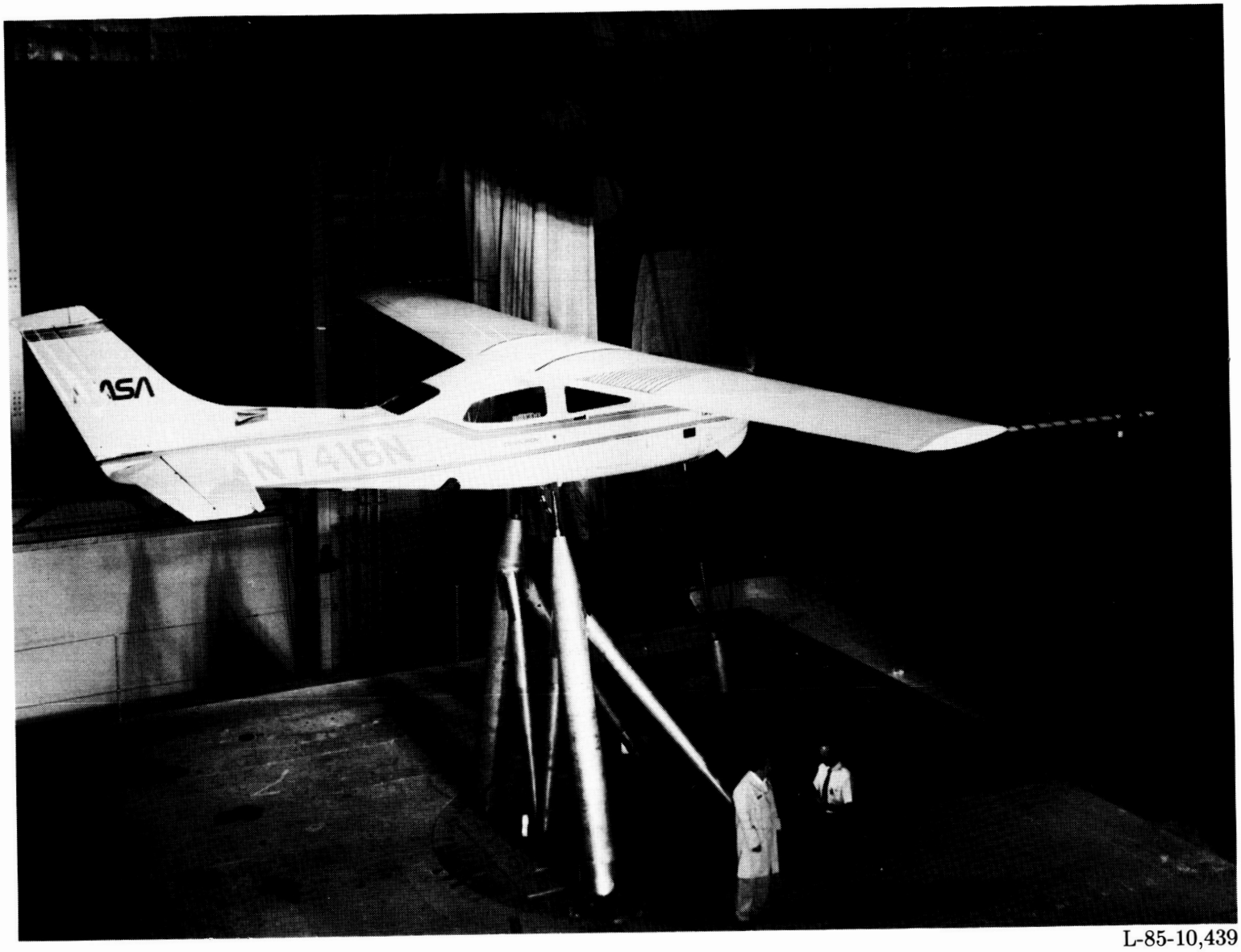


L-85-10,439

(a) Three-quarter rear view.

Figure 2. Model installed in the Langley 30- by 60-Foot Tunnel.


L-85-10,605

(b) Side view.

Figure 2. Continued.

L-85-10,074

(c) Front view.

Figure 2. Concluded.

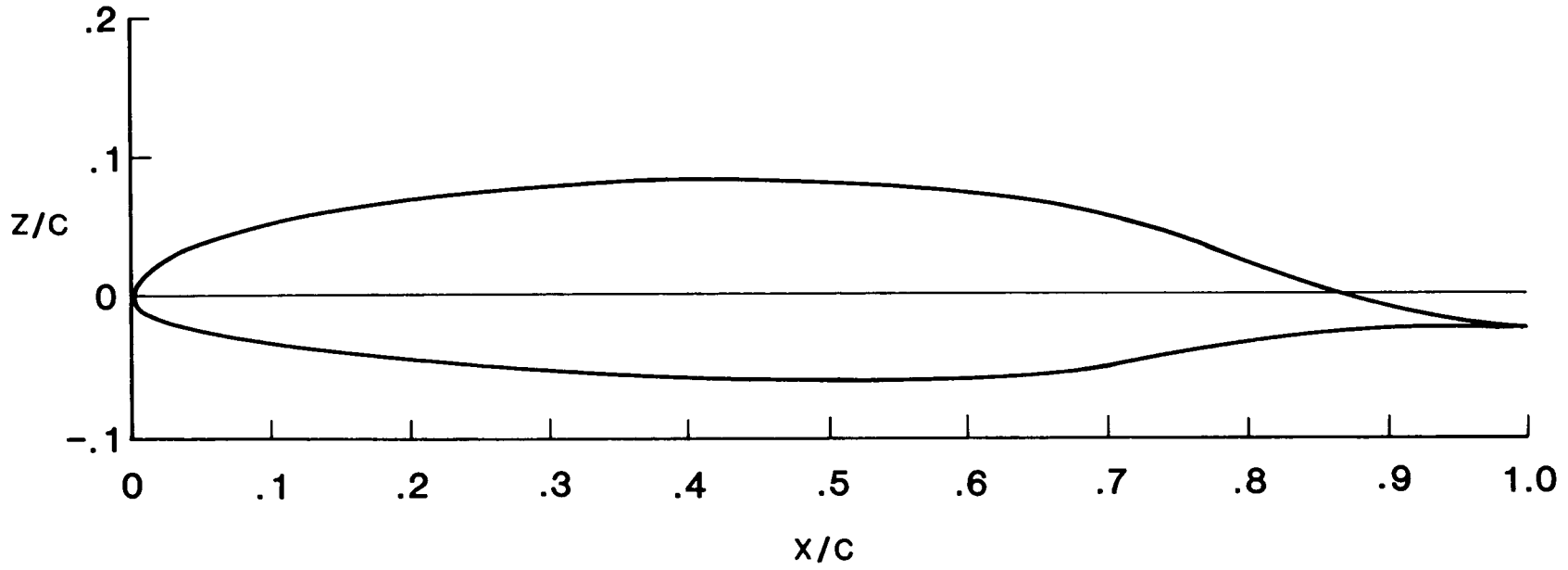


Figure 3. Section shape for NASA NLF(1)-0414F airfoil.

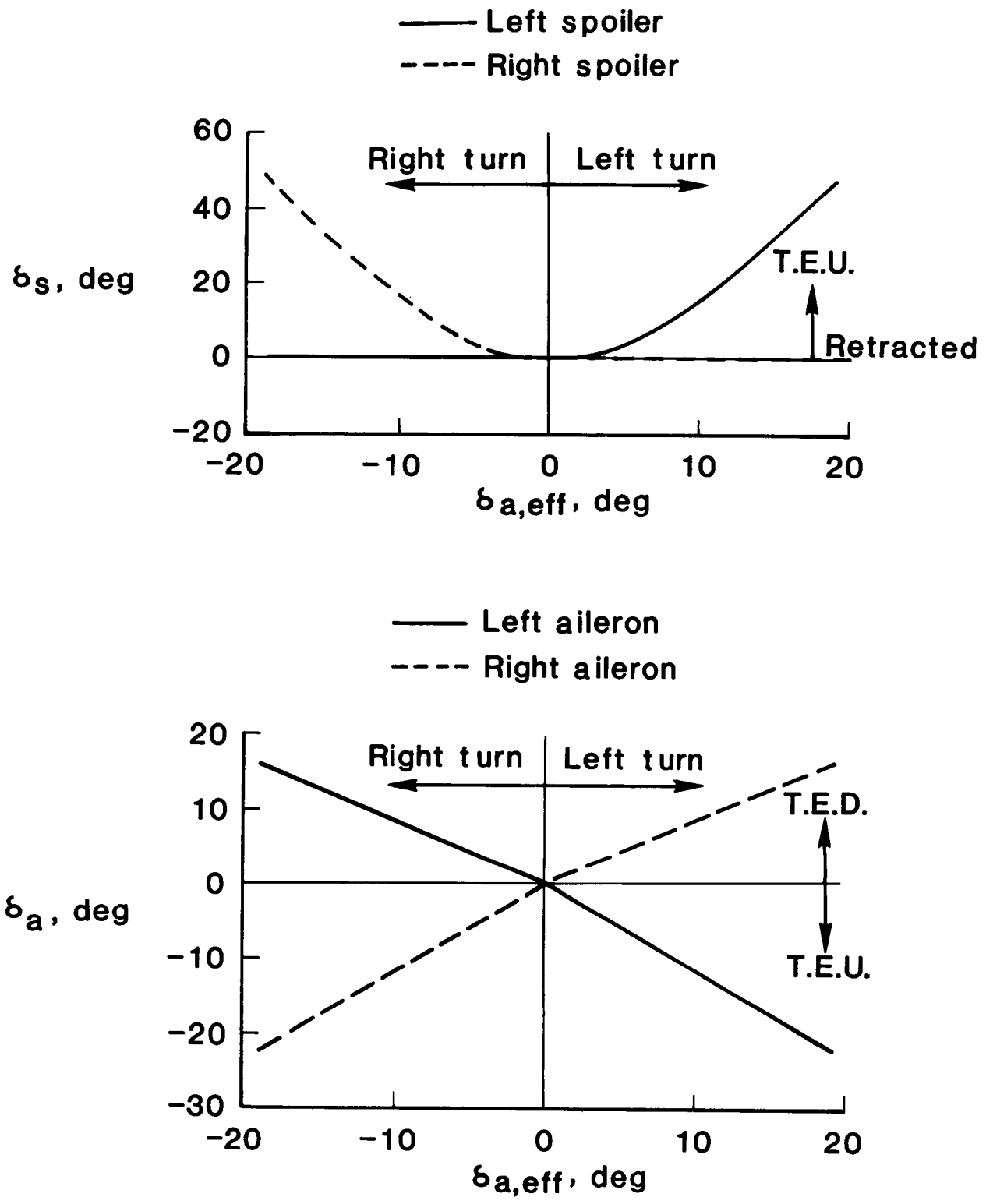


Figure 4. Ratio of spoiler deflection to aileron deflection.

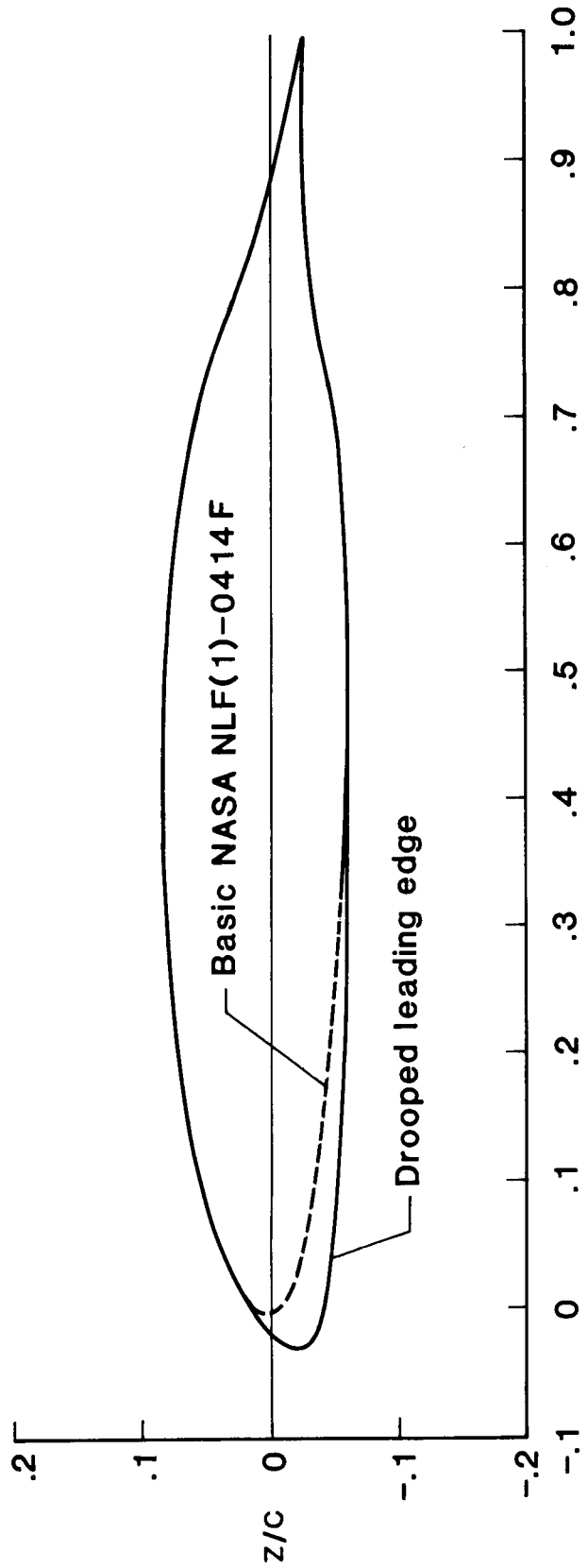


(a) Airfoil section shape with leading-edge droop.

Figure 5. Geometry of wing leading-edge modifications.

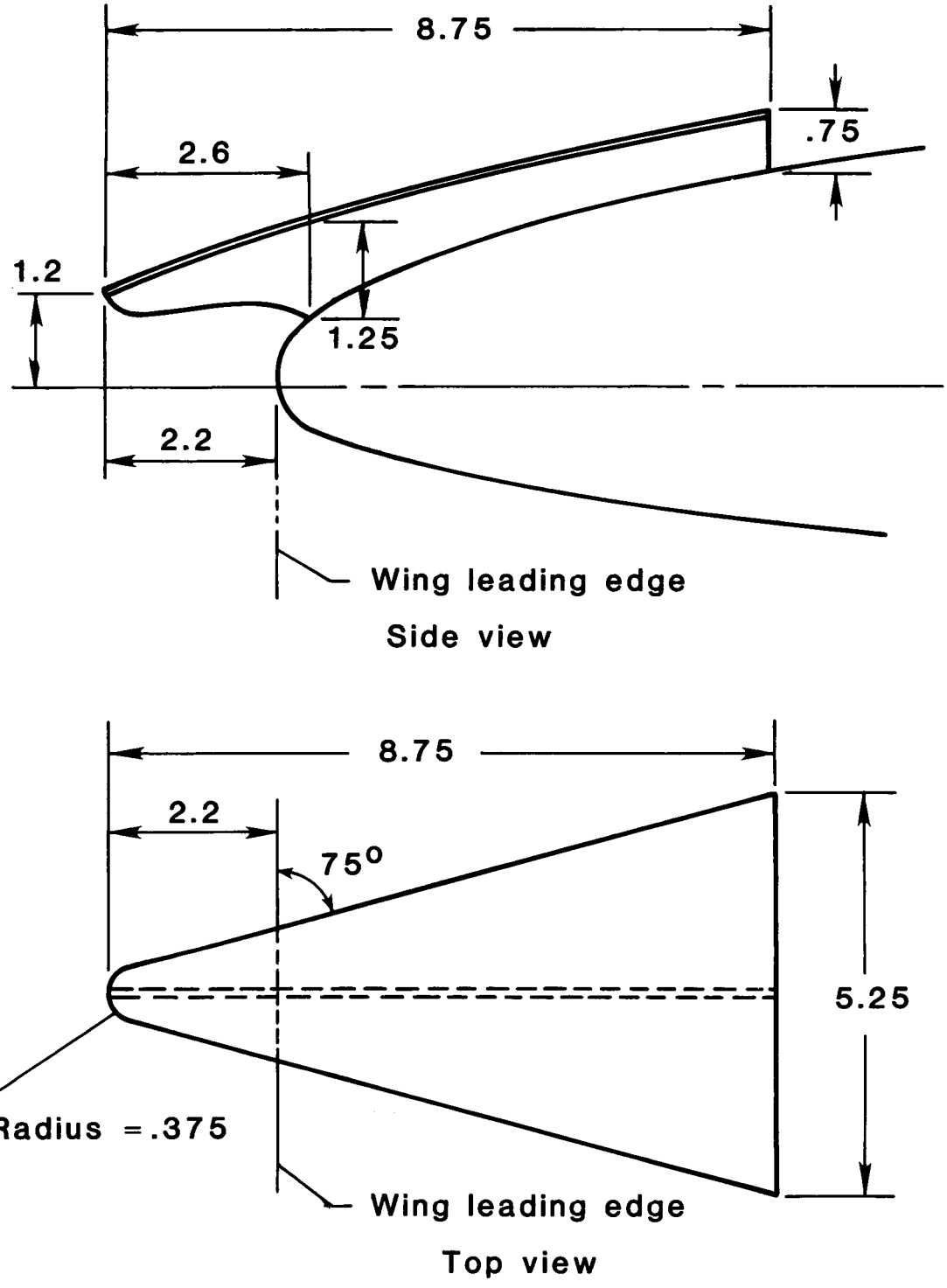


(b) Vortex generator. Linear dimensions are in inches.

Figure 5. Continued.

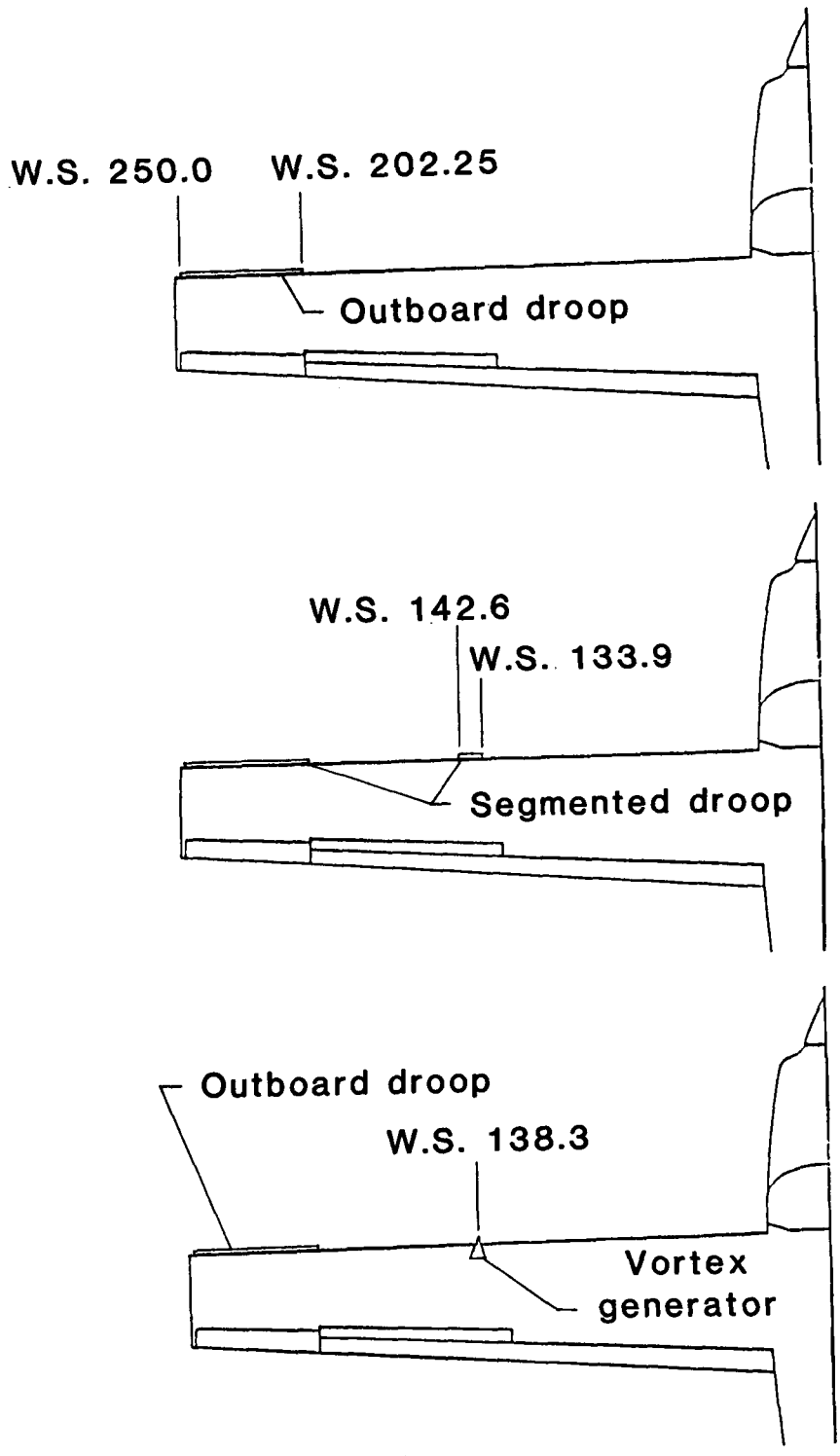


(c) Placement of leading-edge modifications.

Figure 5. Concluded.

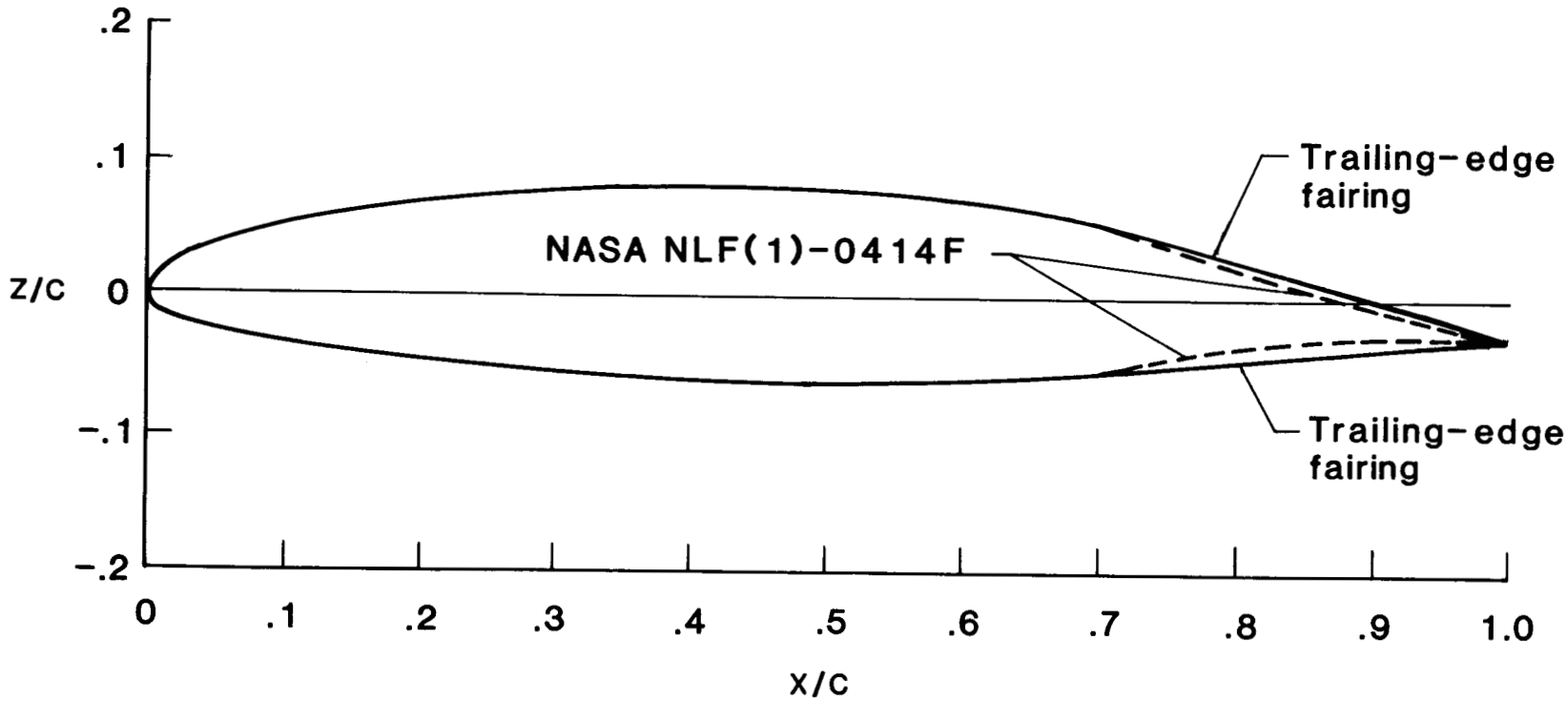


Figure 6. Airfoil section shape with trailing-edge reflex faired.

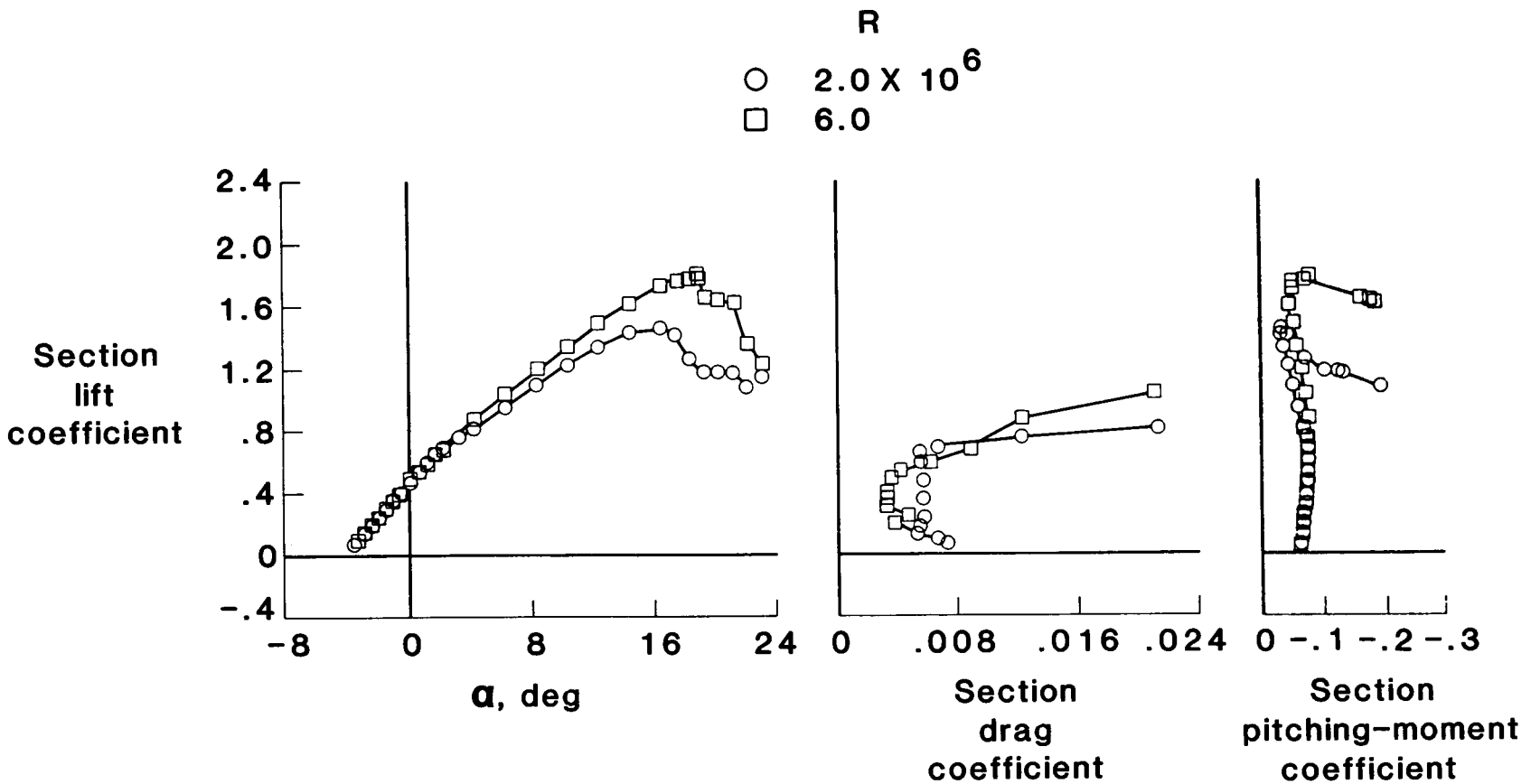


Figure 7. Effect of Reynolds number on two-dimensional-airfoil characteristics. Data taken from reference 15.

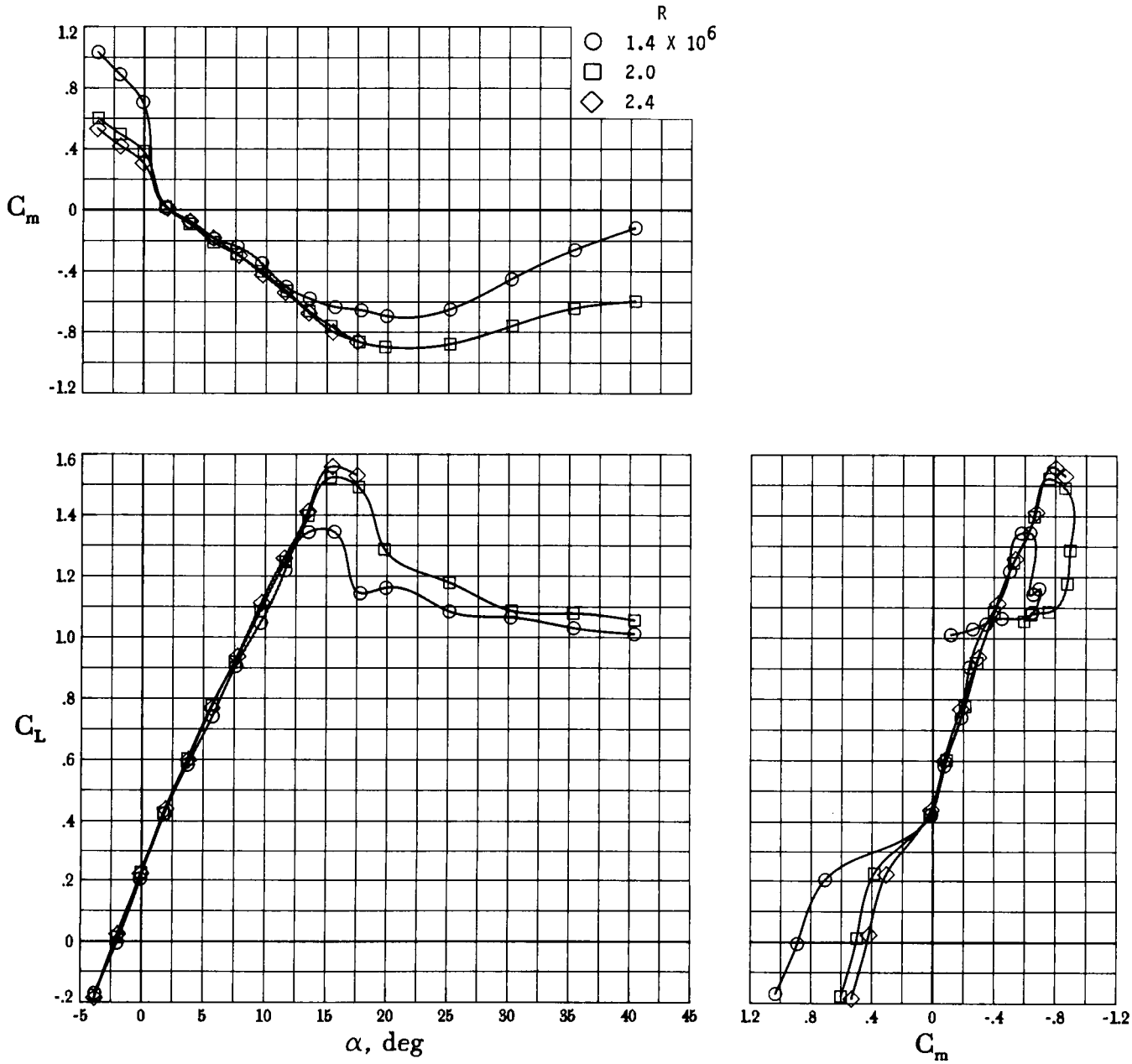


(a) Lift and pitching moment.

Figure 8. Effect of Reynolds number on longitudinal characteristics of basic configuration with pressure belt installed and propeller in flat pitch. All controls at zero; $C_T = 0$.

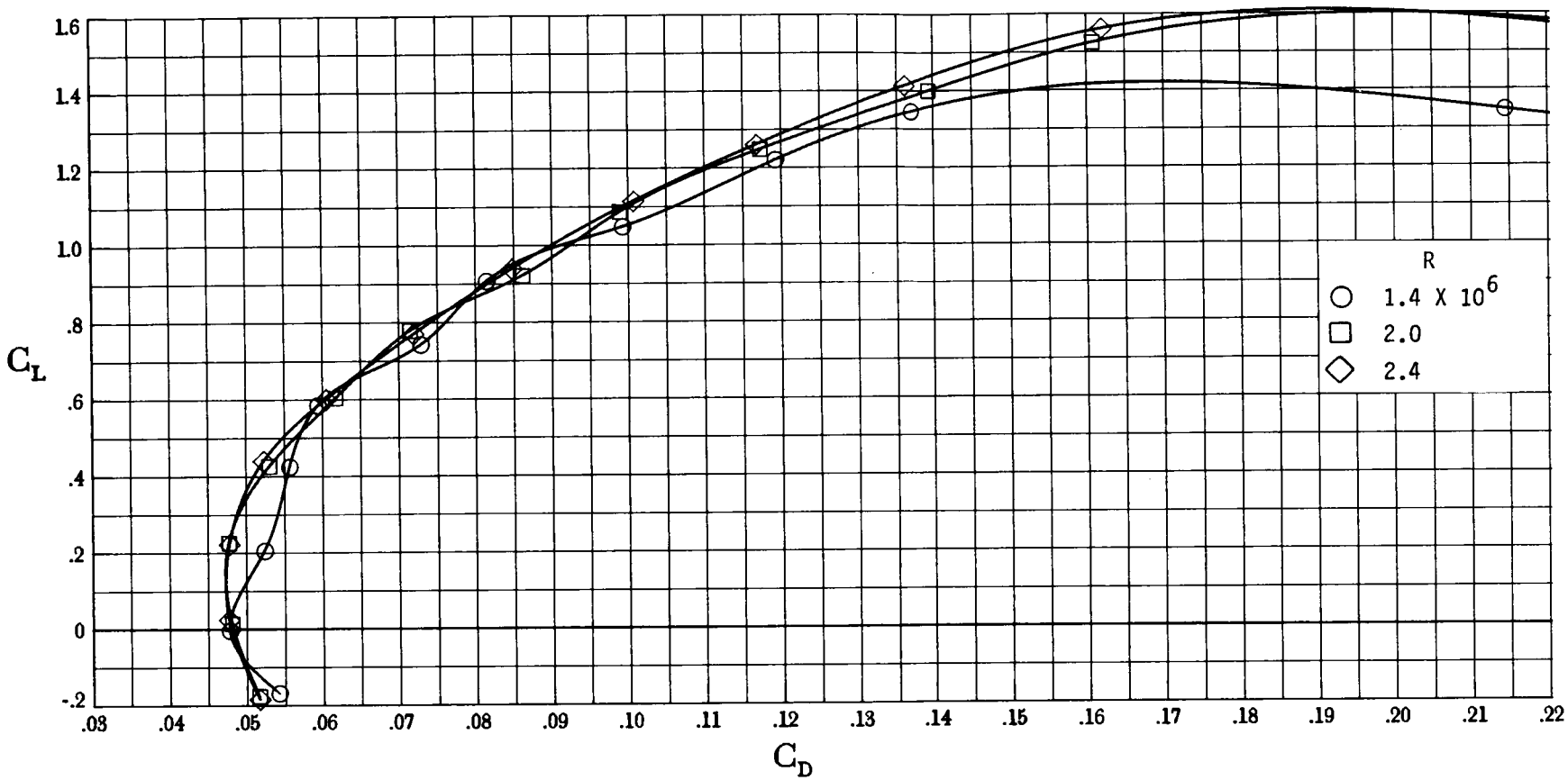


(b) Lift-drag polars.

Figure 8. Concluded.

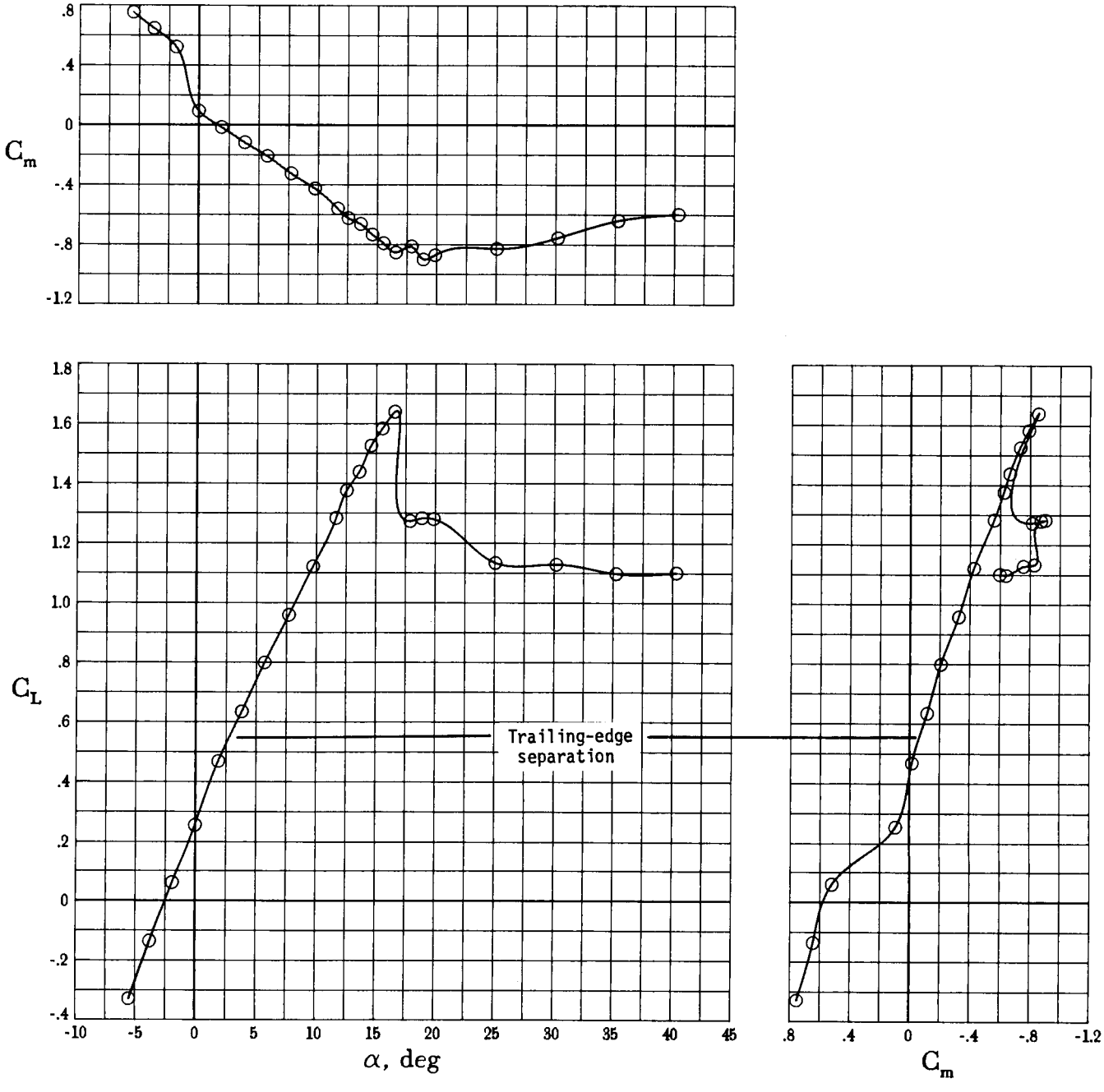


(a) Lift and pitching moment.

Figure 9. Longitudinal characteristics of basic configuration. All controls at zero; $C_T = 0$; $R = 2.0 \times 10^6$.

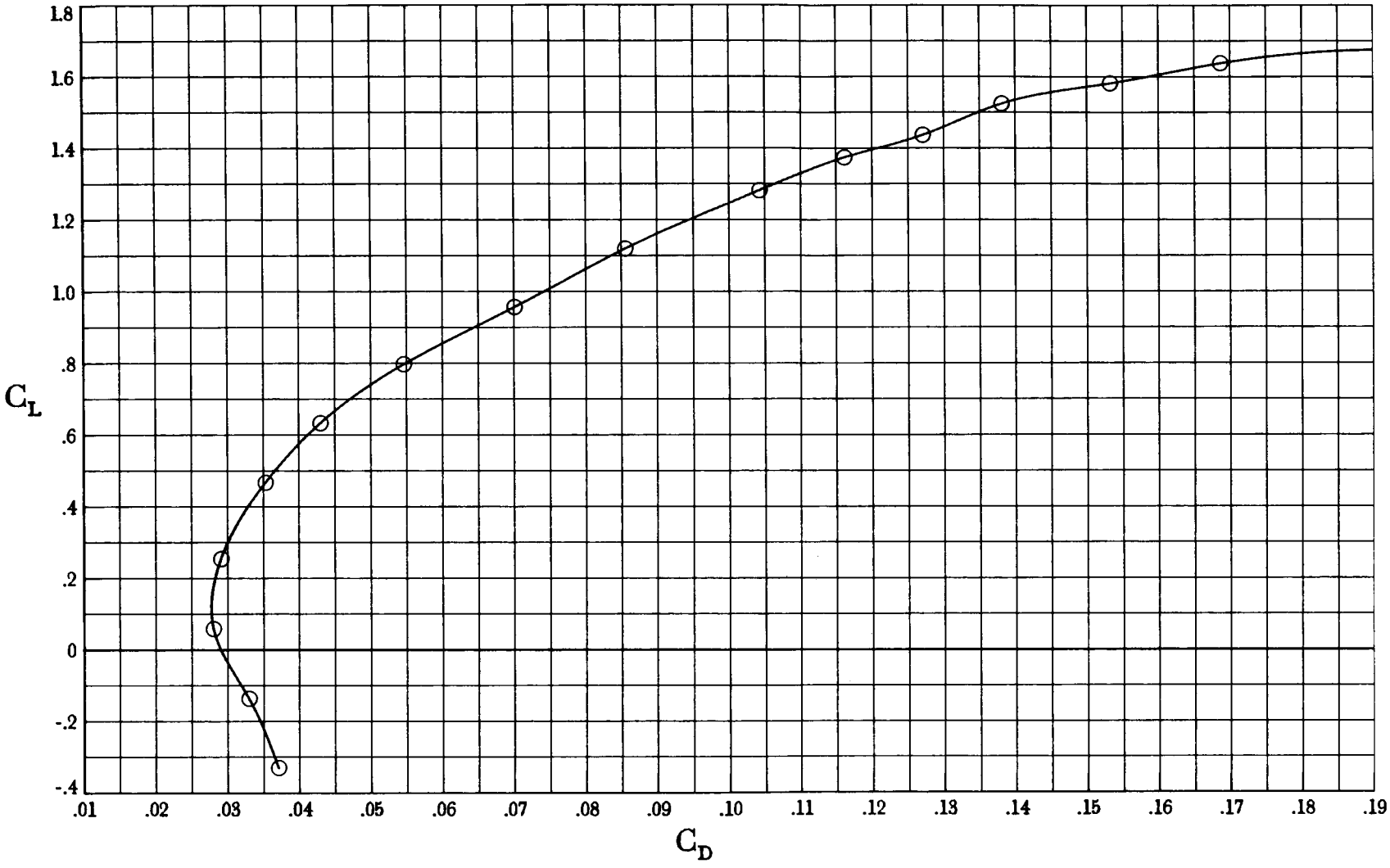


(b) Lift-drag polars.

Figure 9. Concluded.

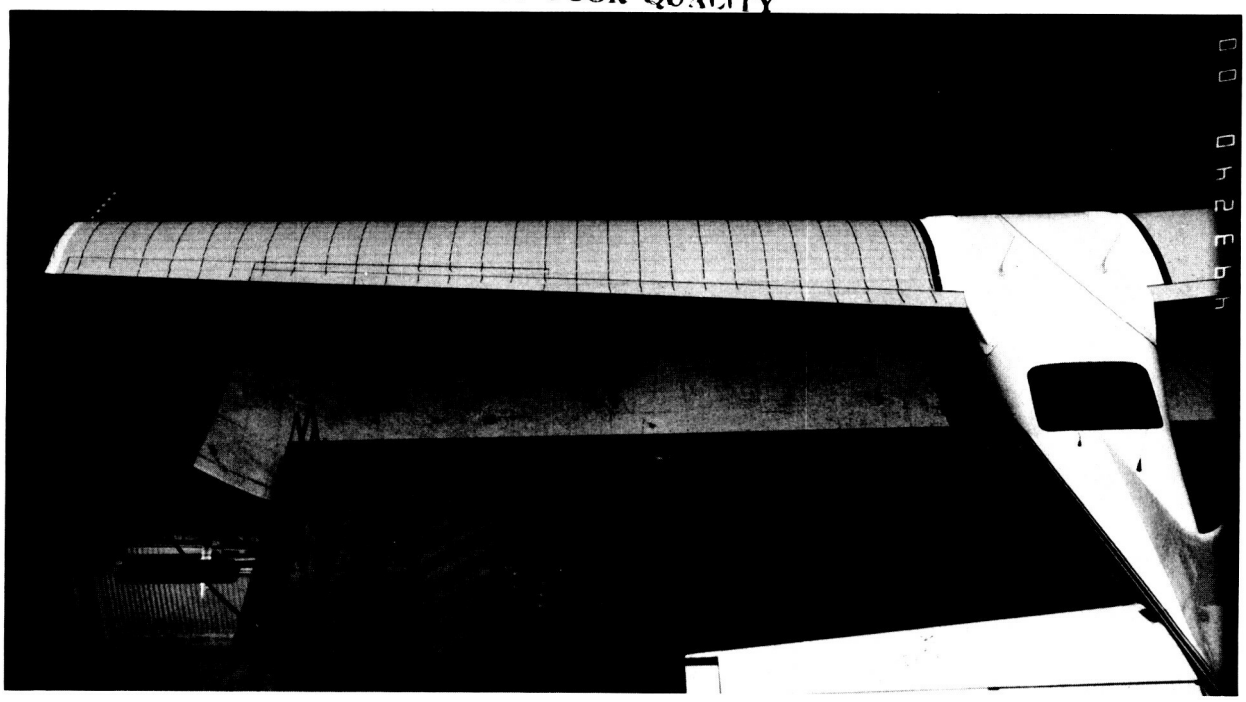

(a) $\alpha = -6°$.

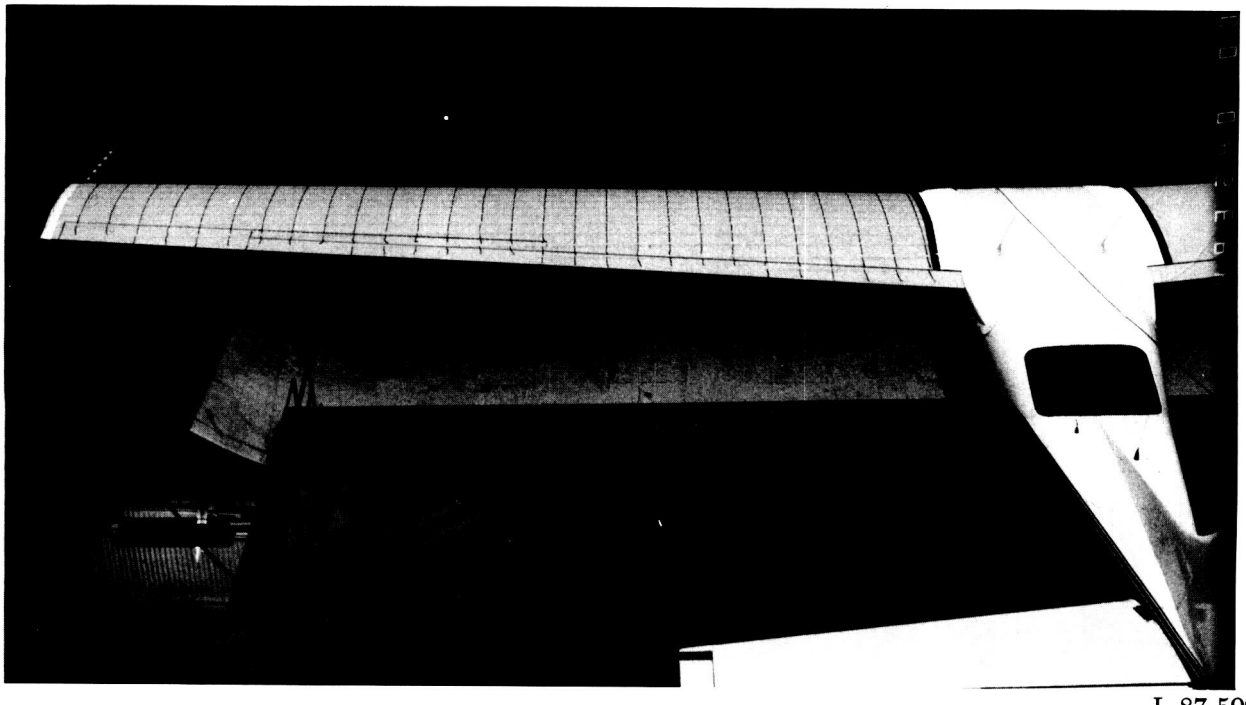

L-87-599

(b) $\alpha = -4°$.

Figure 10. Tuft flow-visualization photographs of basic configuration with transition fixed at $x/c = 0.05$. All controls at zero; $C_T = 0$; $R = 2.0 \times 10^6$.

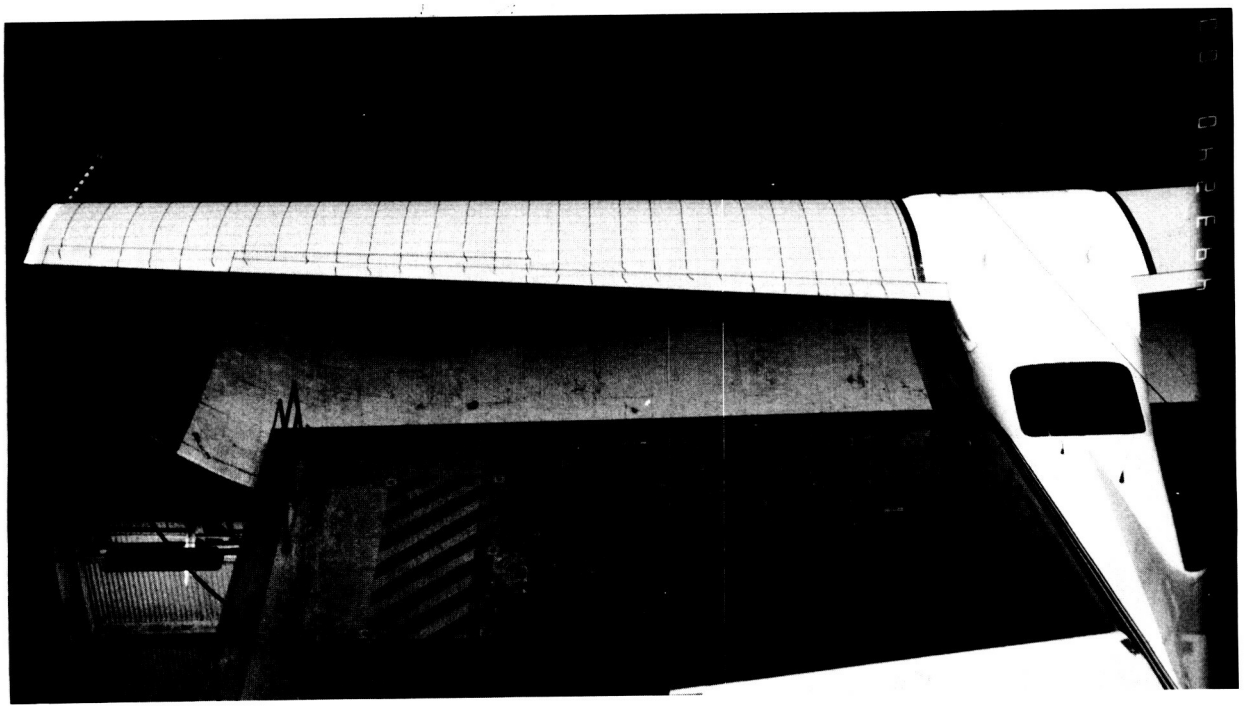

(c) $\alpha = -2°$.

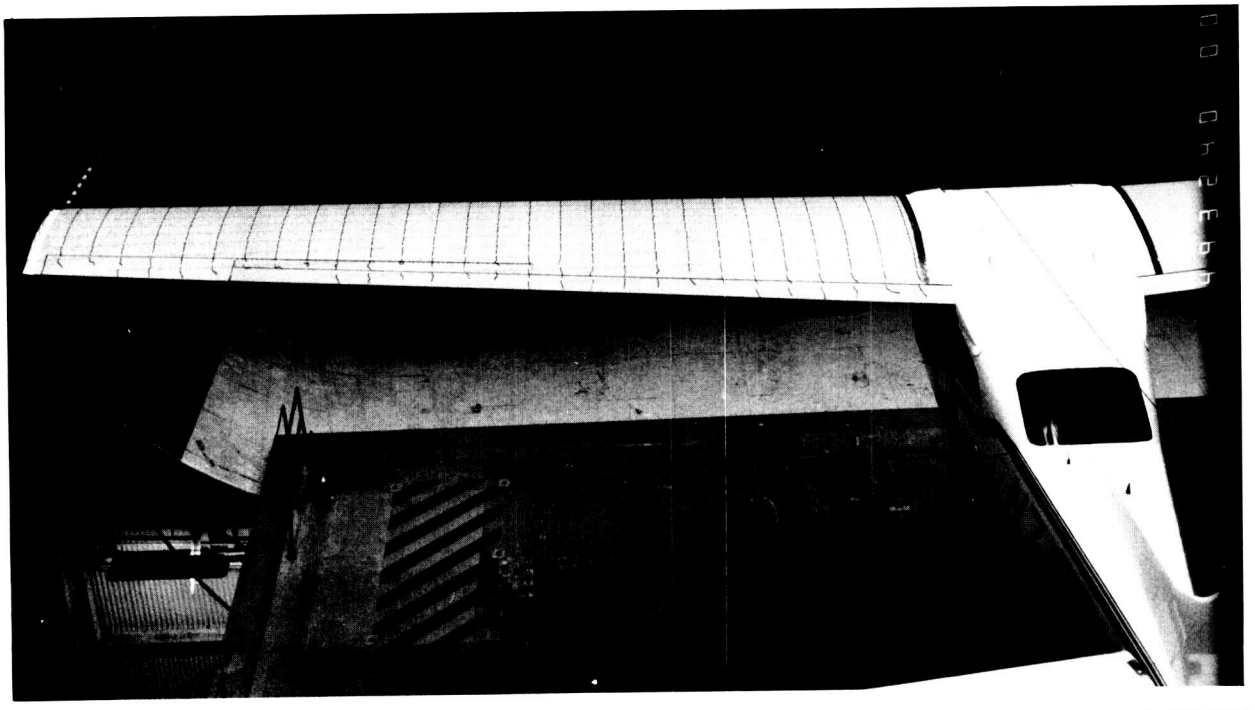

L-87-600

(d) $\alpha = 0°$.

Figure 10. Continued.

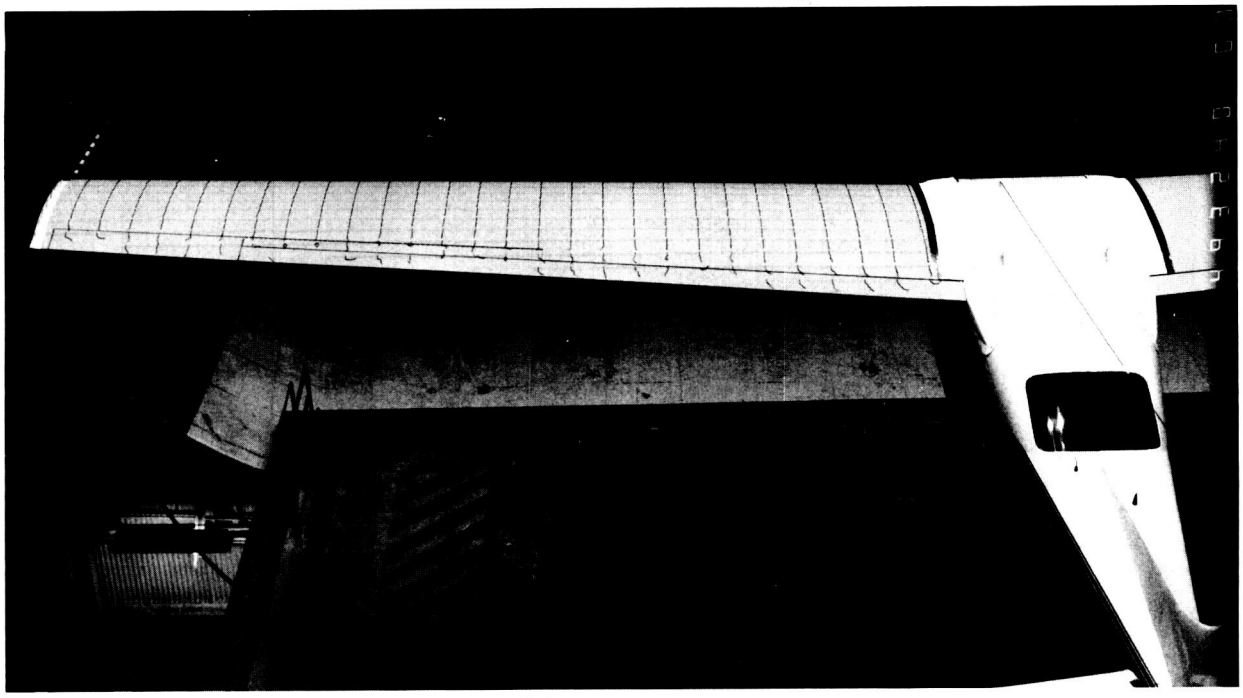

(e) $\alpha = 2°$.

L-87-601

(f) $\alpha = 4°$.

Figure 10. Continued.

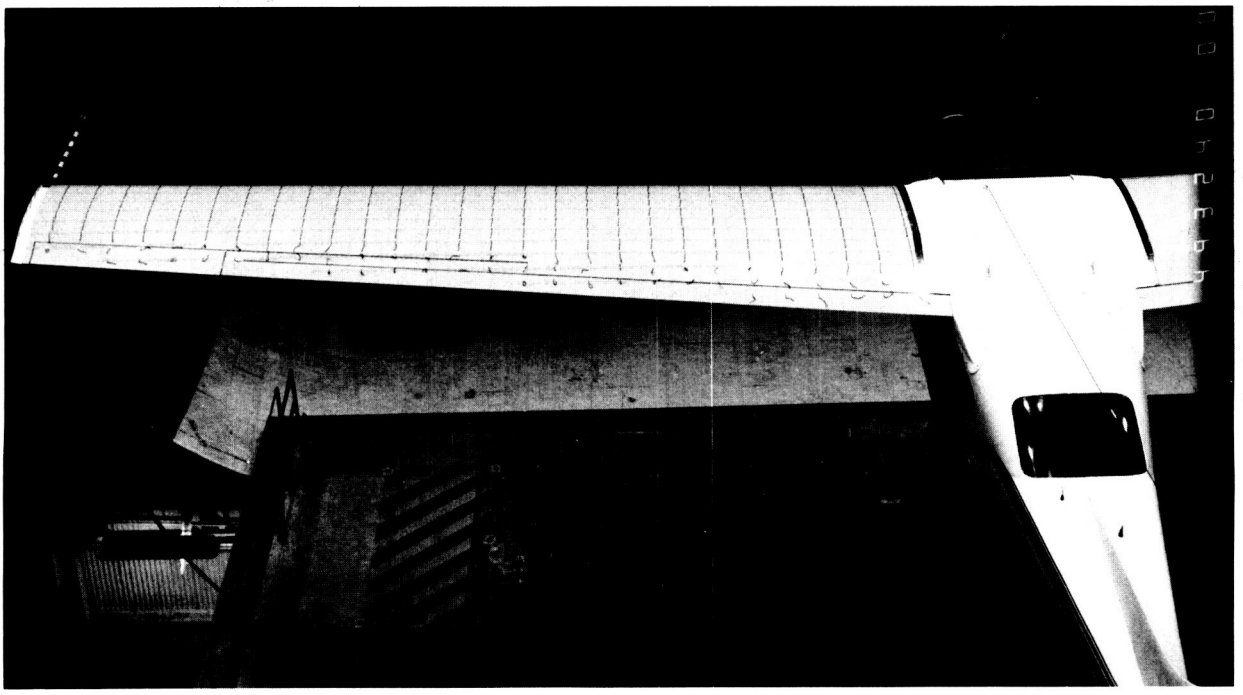

(g) $\alpha = 6°$.

(h) $\alpha = 8°$.

L-87-602

Figure 10. Continued.

(i) $\alpha = 10°$.

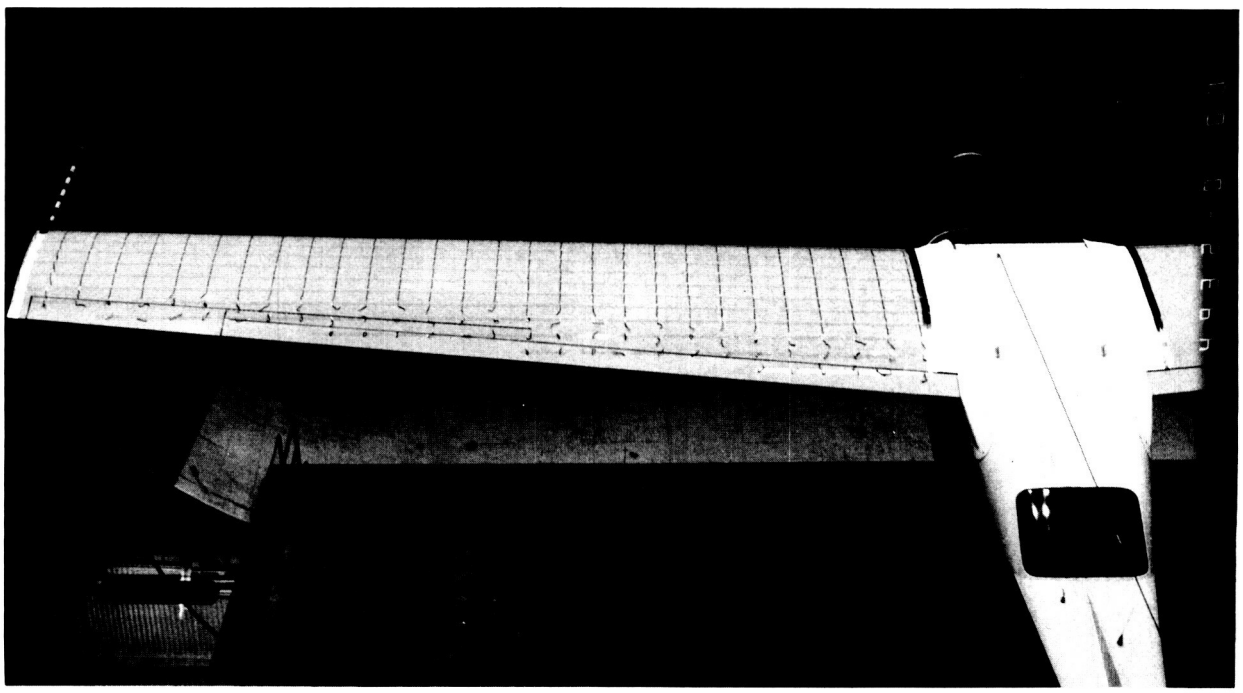

(j) $\alpha = 12°$. L-87-603

Figure 10. Continued.

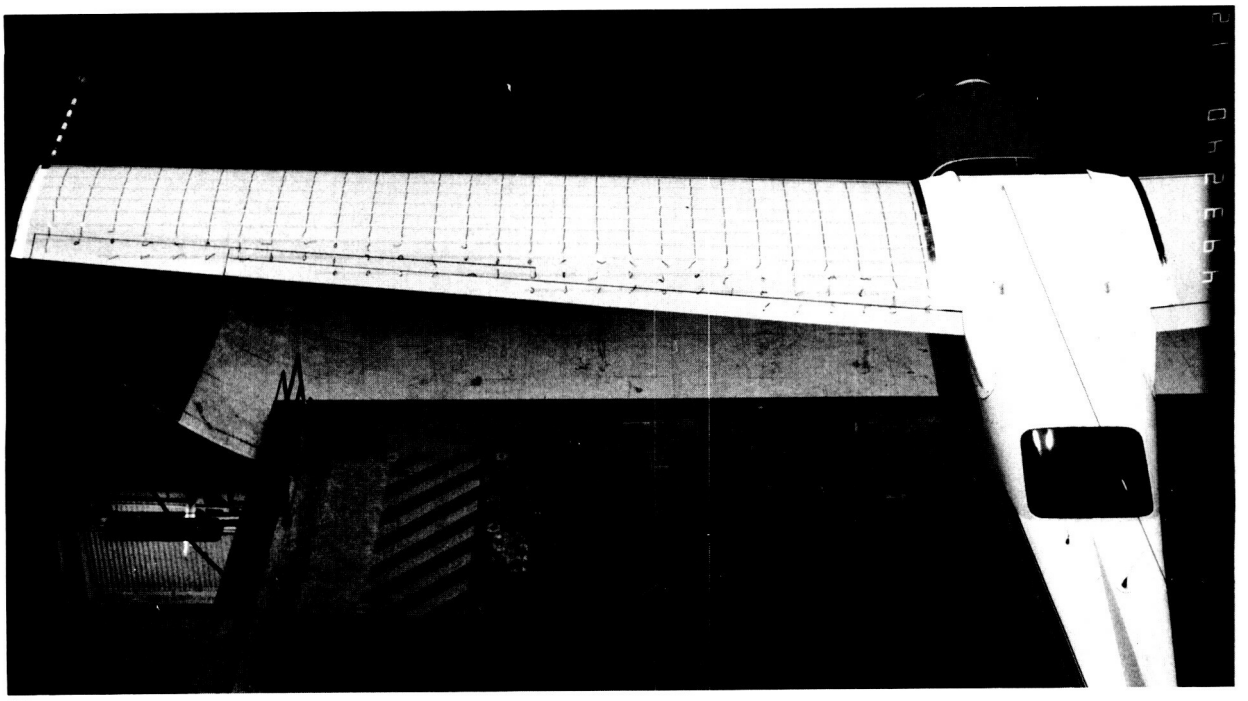

(k) $\alpha = 13°$.

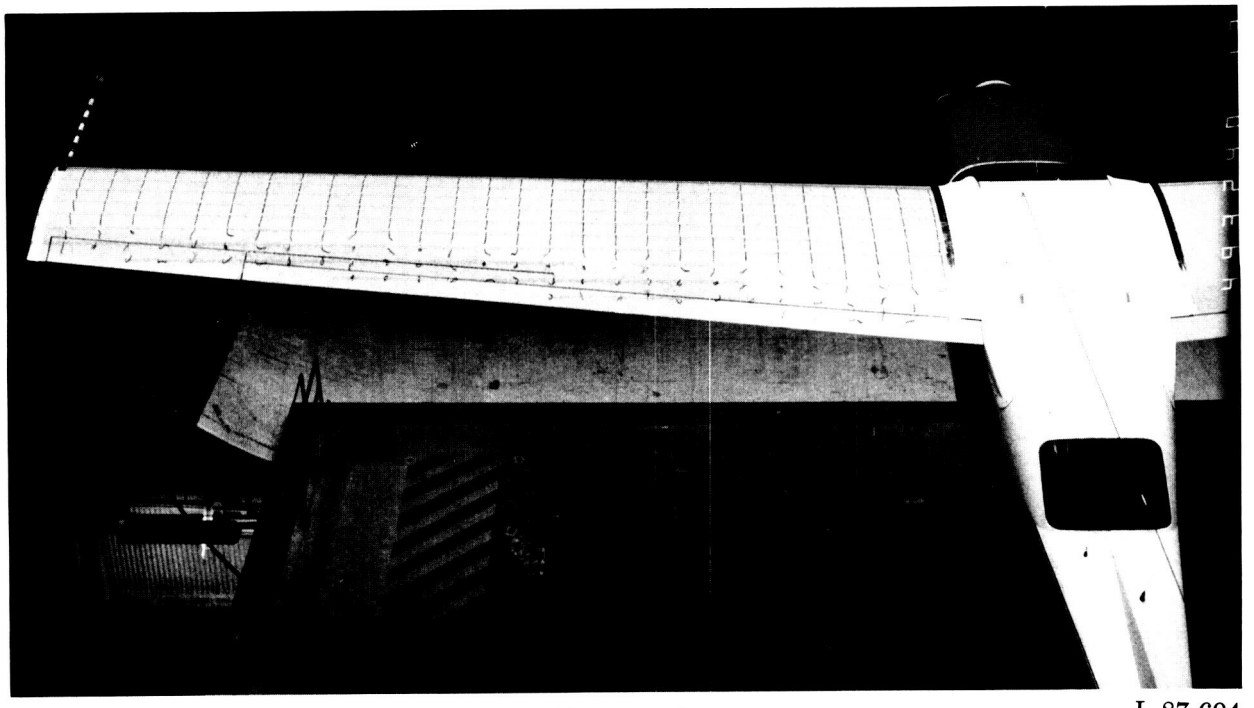

(l) $\alpha = 14°$.

L-87-604

Figure 10. Continued.

(m) $\alpha = 15°$.

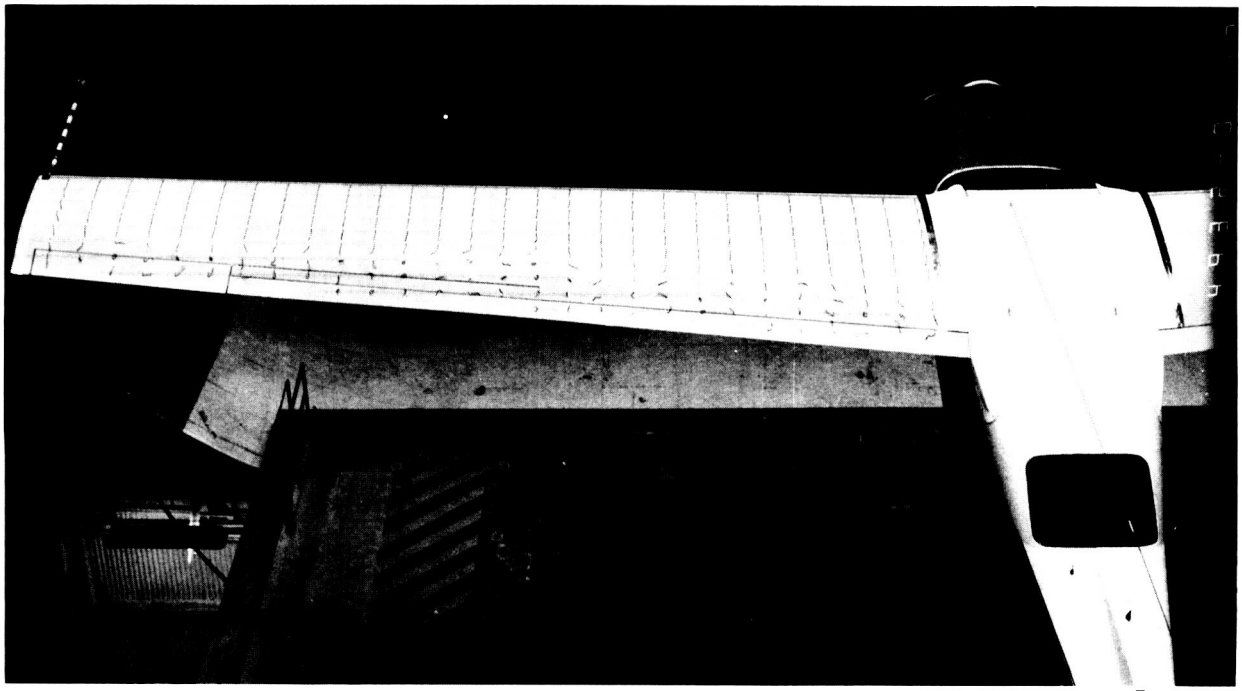

L-87-605

(n) $\alpha = 16°$.

Figure 10. Continued.

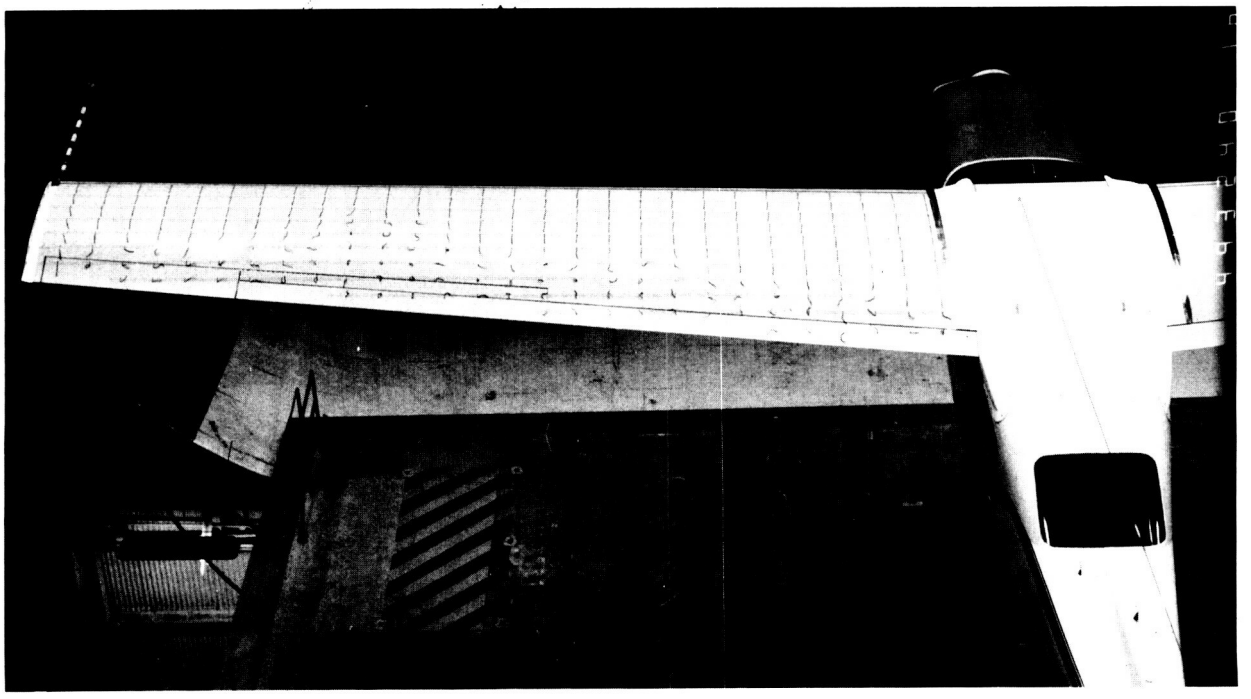

(o) $\alpha = 17°$.

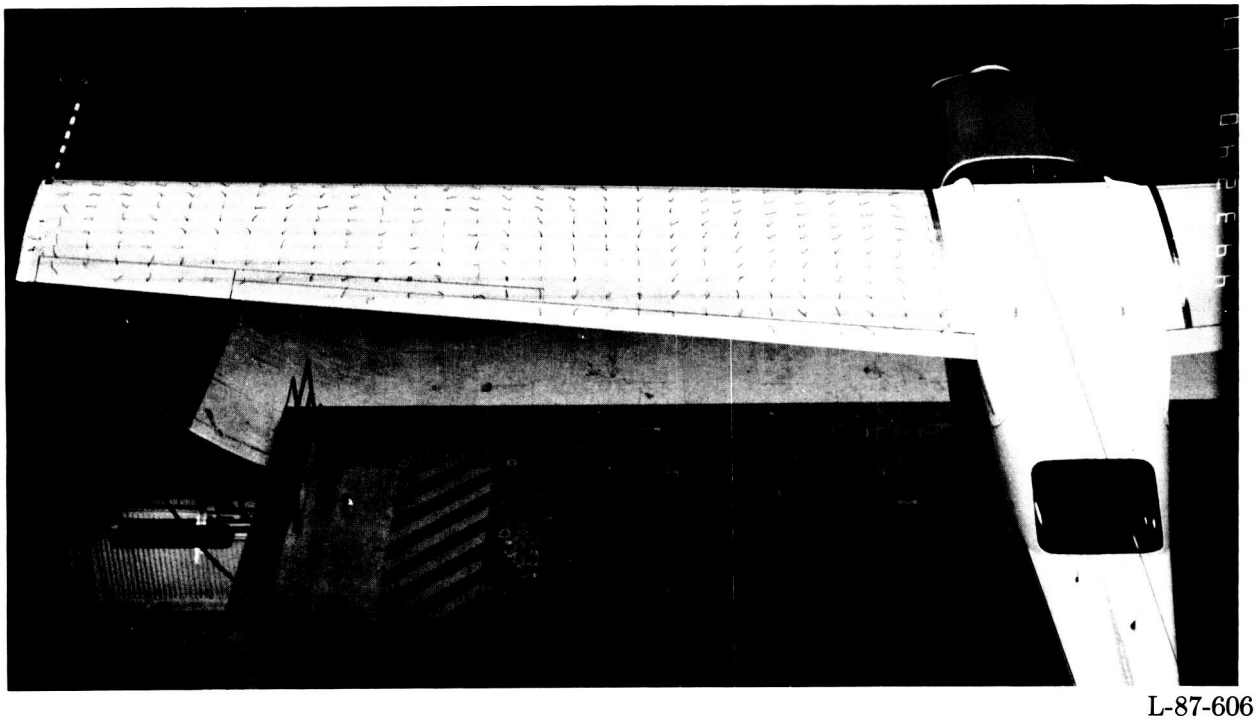

L-87-606

(p) $\alpha = 18°$.

Figure 10. Continued.

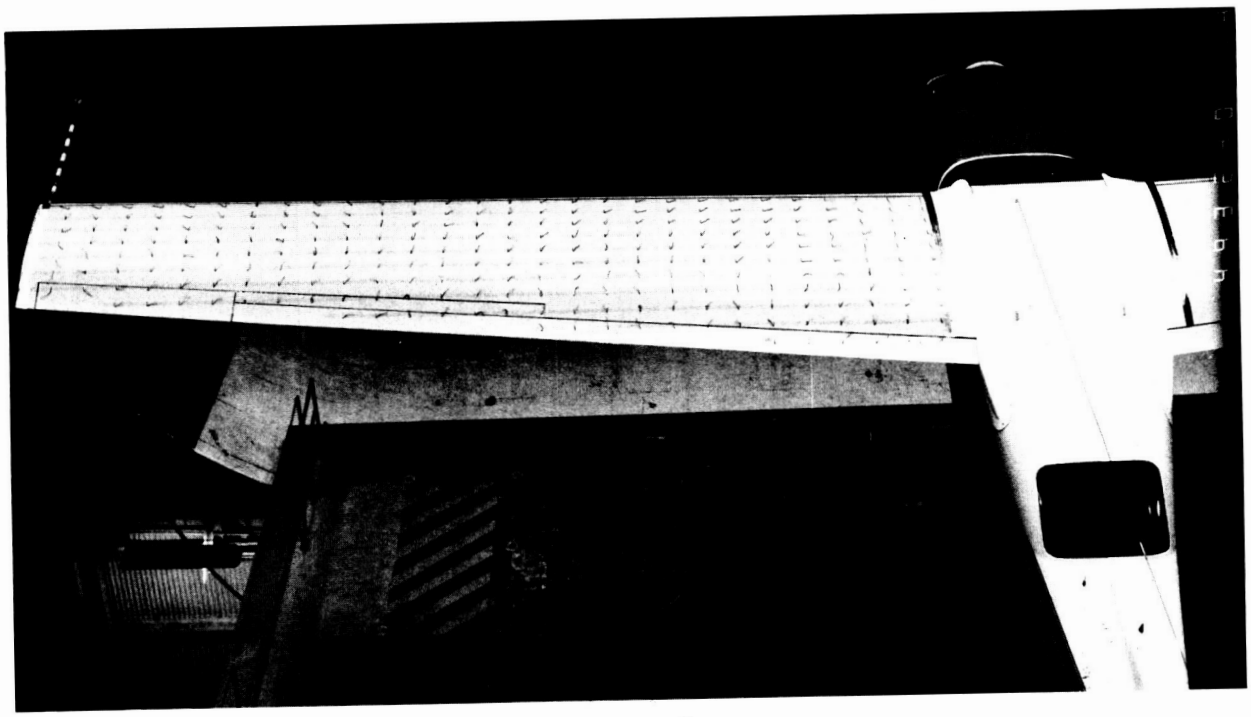

(q) $\alpha = 19°$.

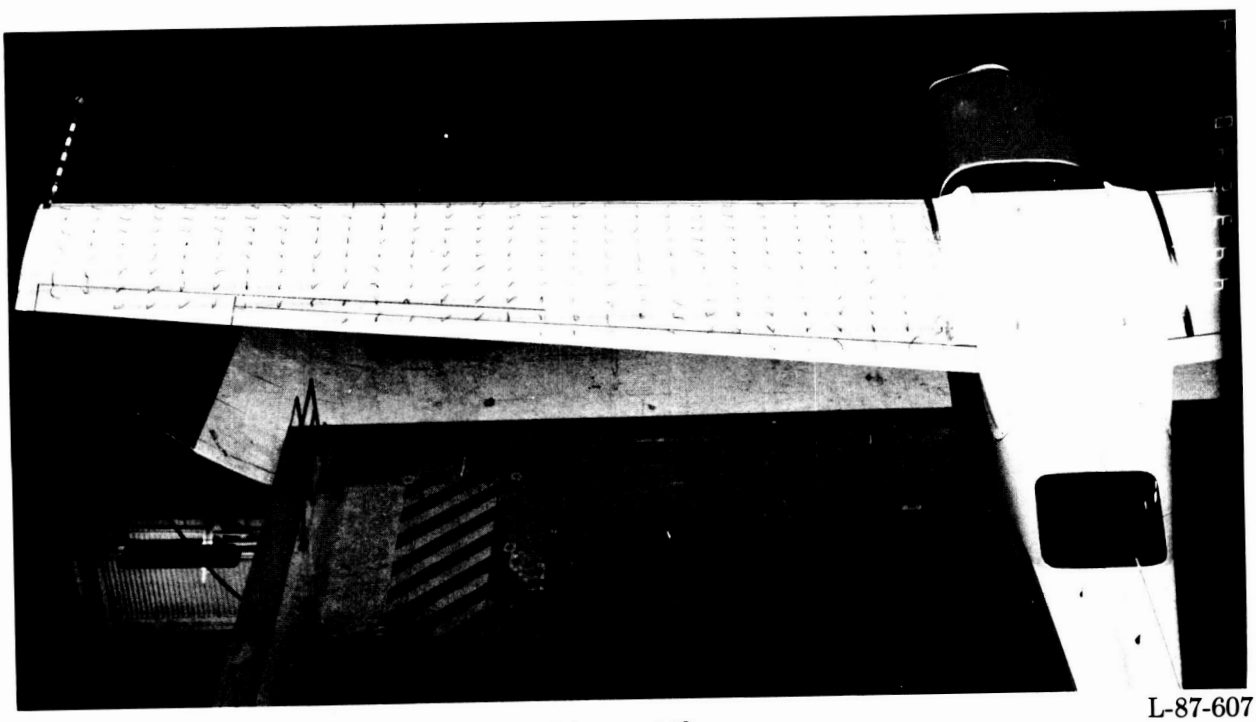

L-87-607

(r) $\alpha = 20°$.

Figure 10. Continued.

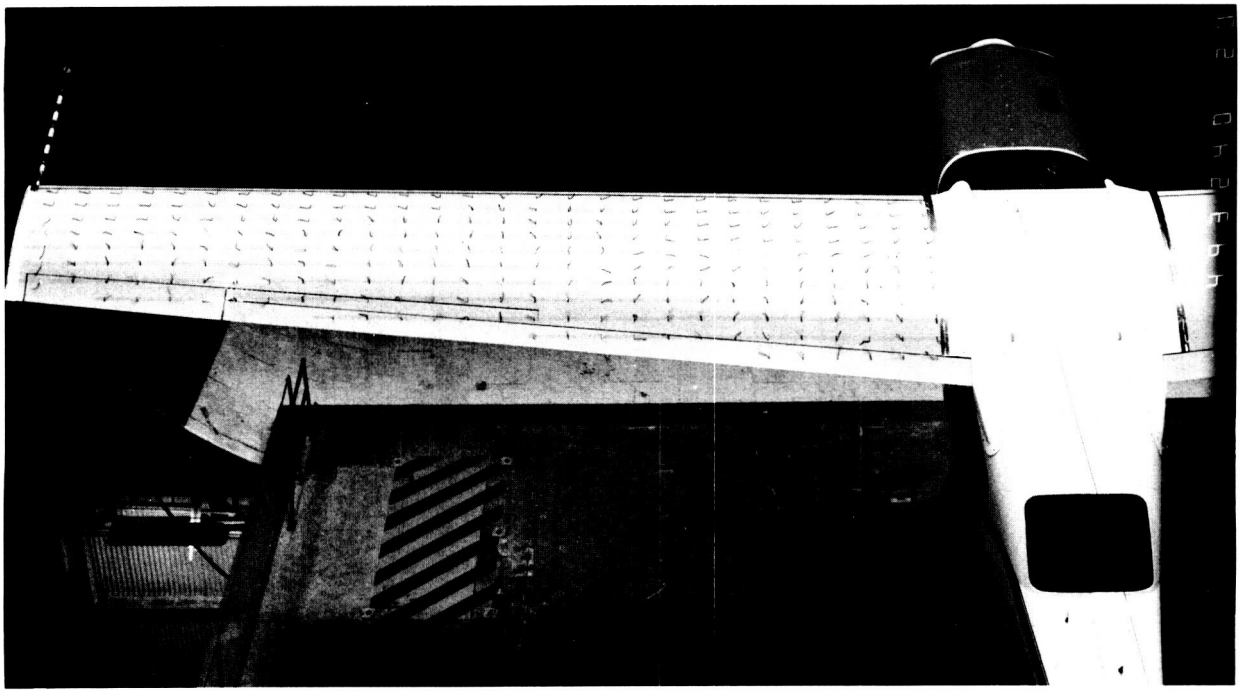

(s) $\alpha = 25°$.

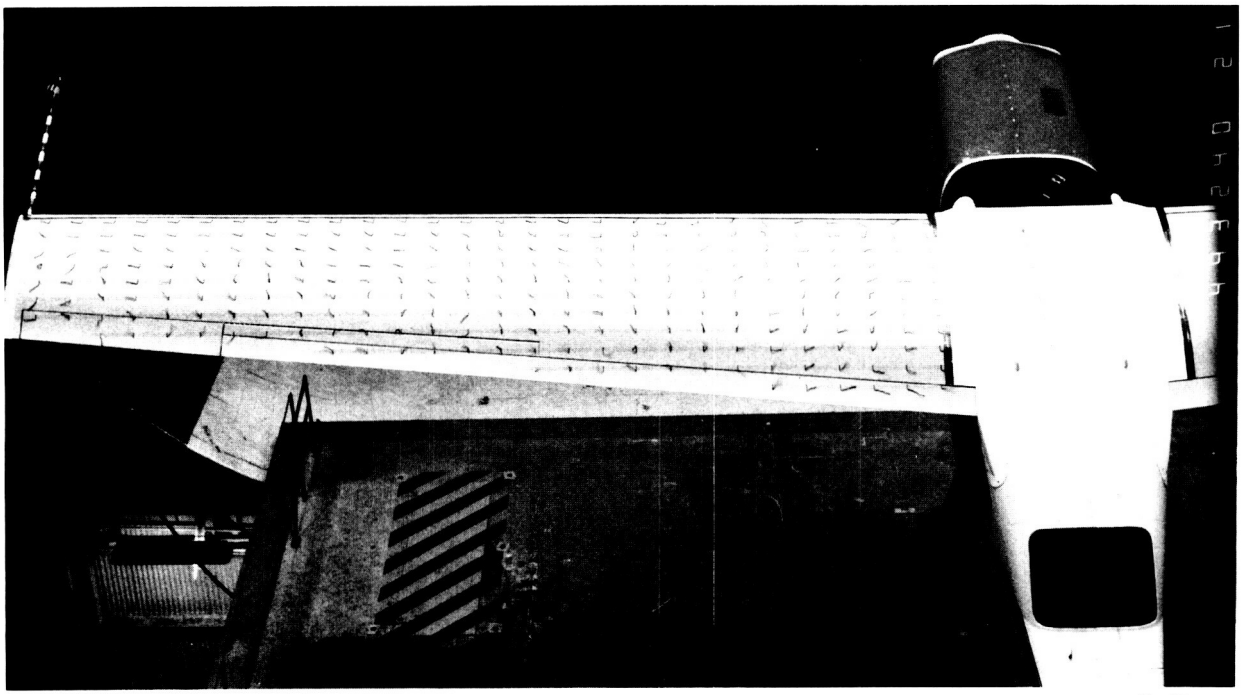

L-87-608

(t) $\alpha = 30°$.

Figure 10. Continued.

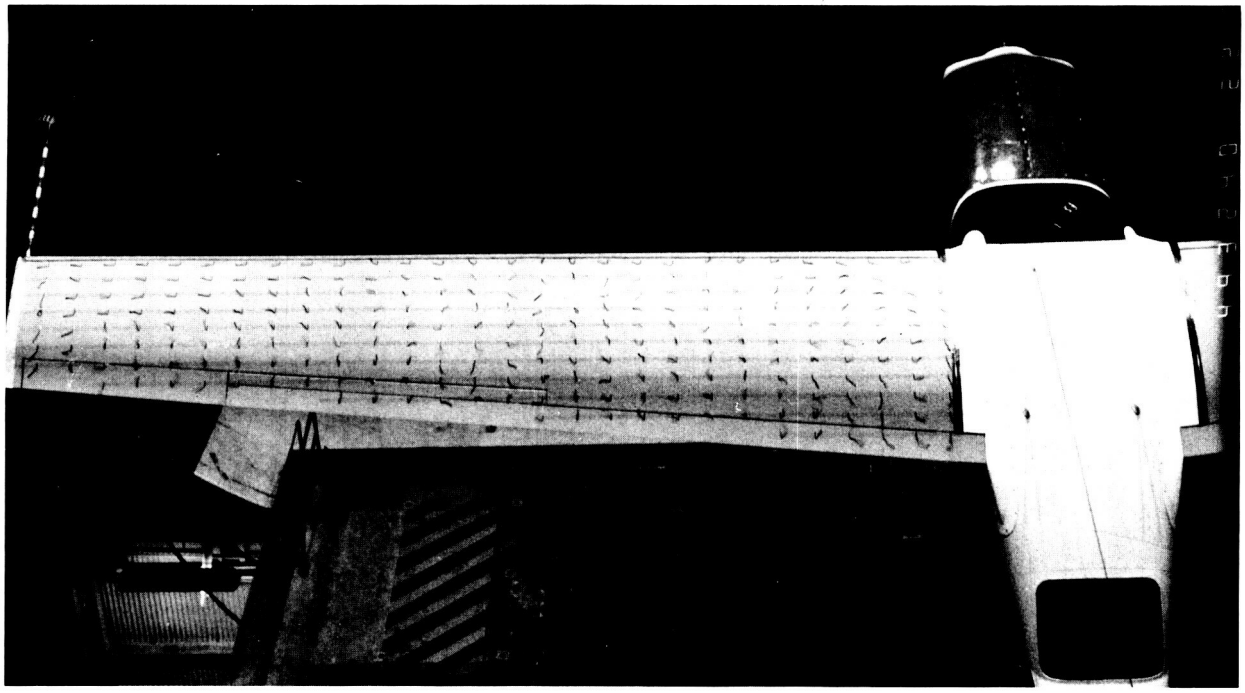

(u) $\alpha = 35°$.

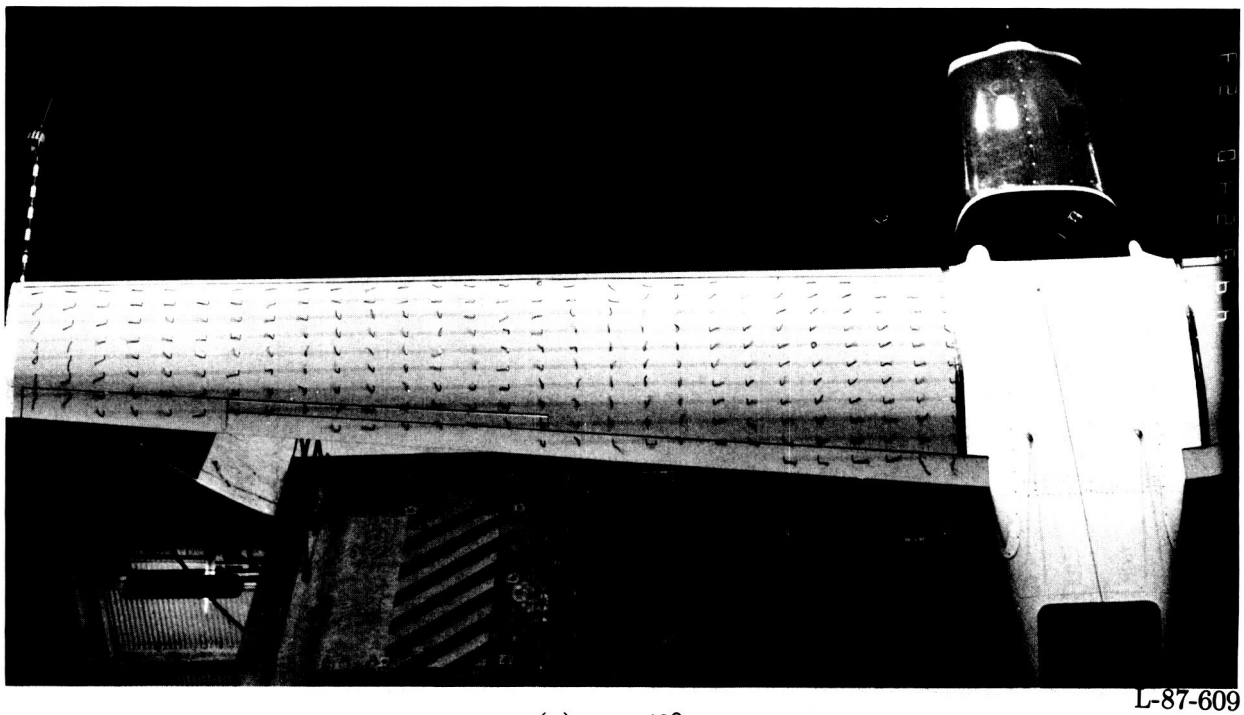

L-87-609

(v) $\alpha = 40°$.

Figure 10. Concluded.

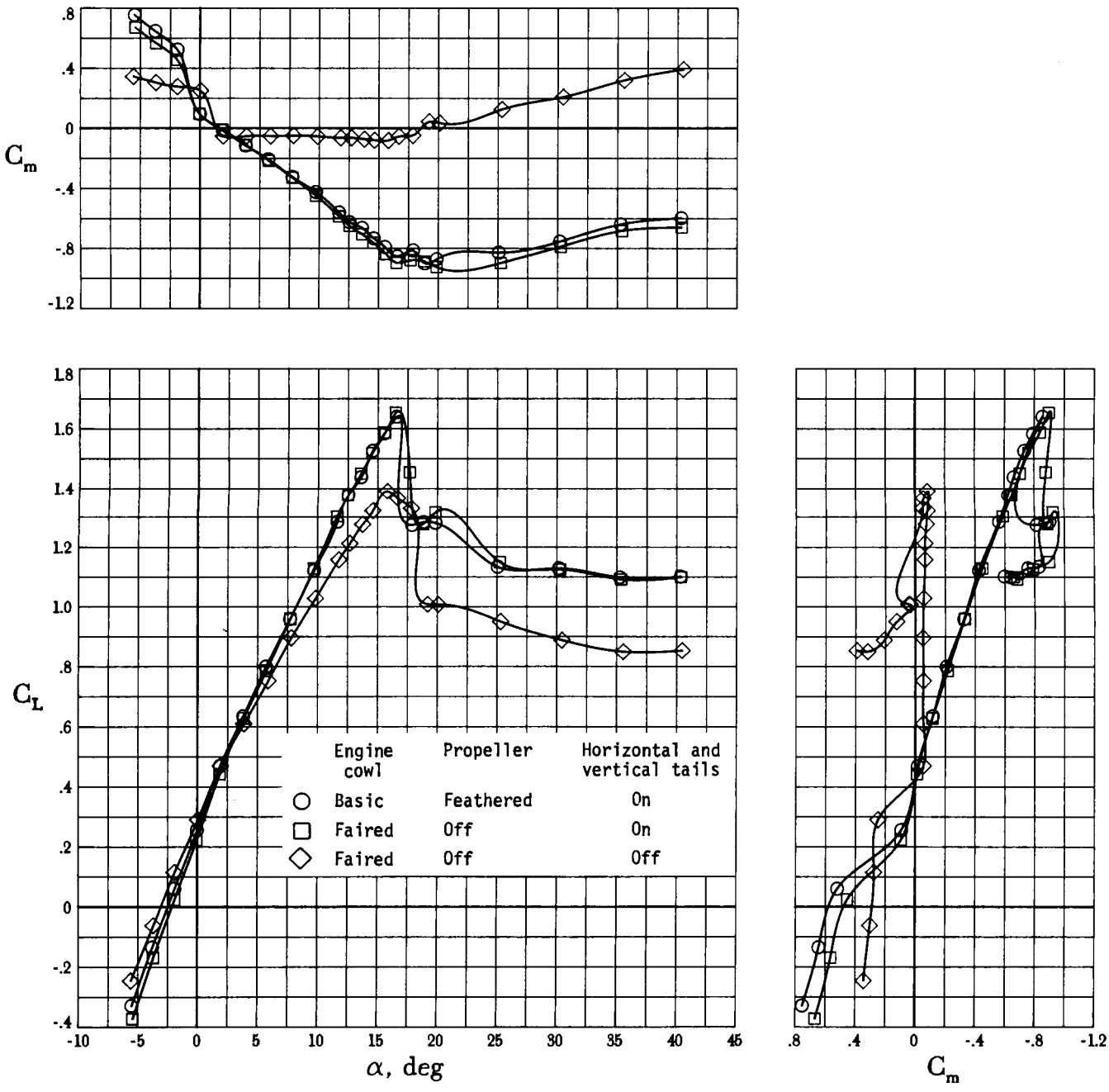


(a) Lift and pitching moment.

Figure 11. Effect of airplane components on longitudinal characteristics of basic configuration. All controls at zero; $C_T = 0$; $R = 2.0 \times 10^6$.

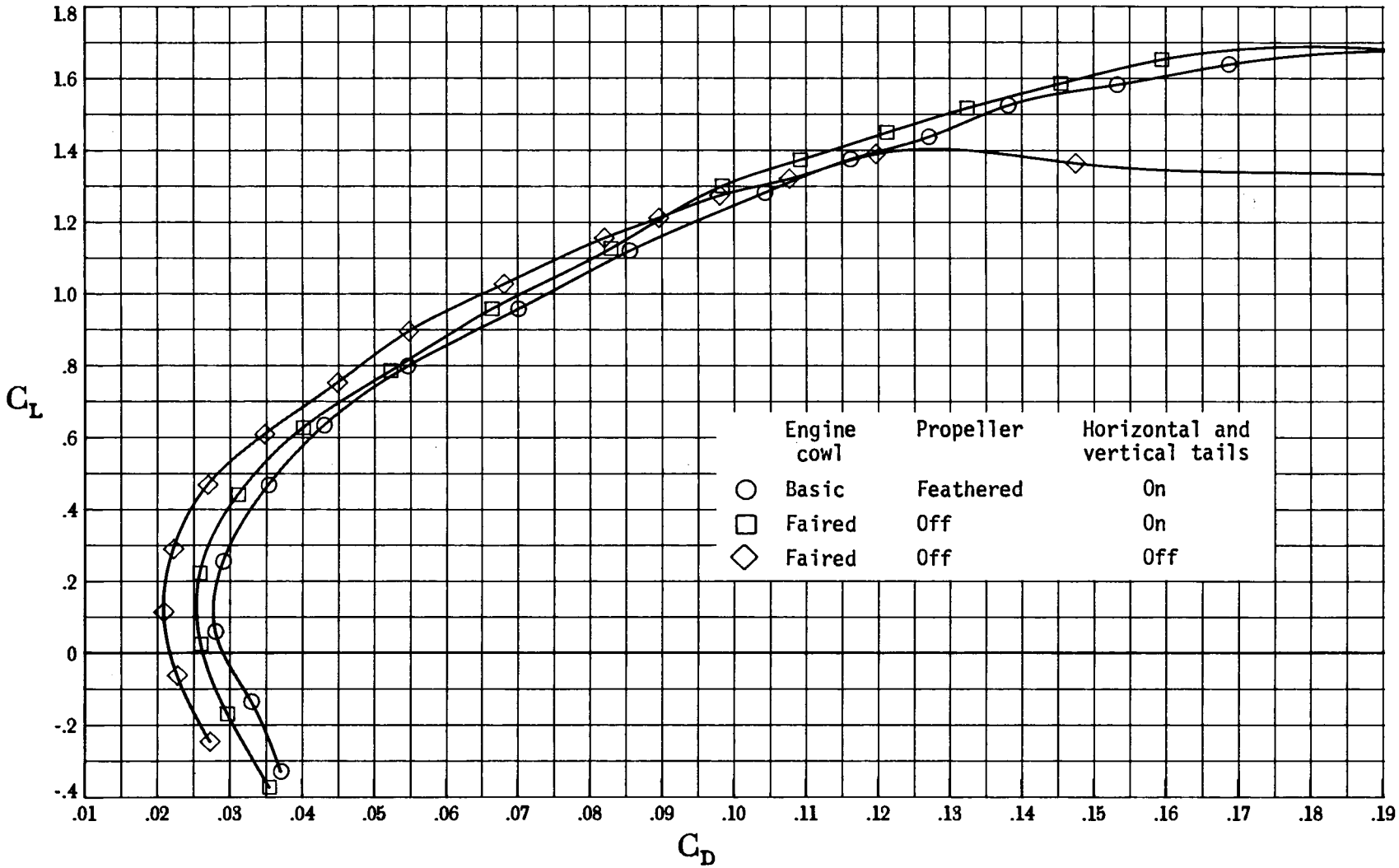


(b) Lift-drag polars.

Figure 11. Concluded.

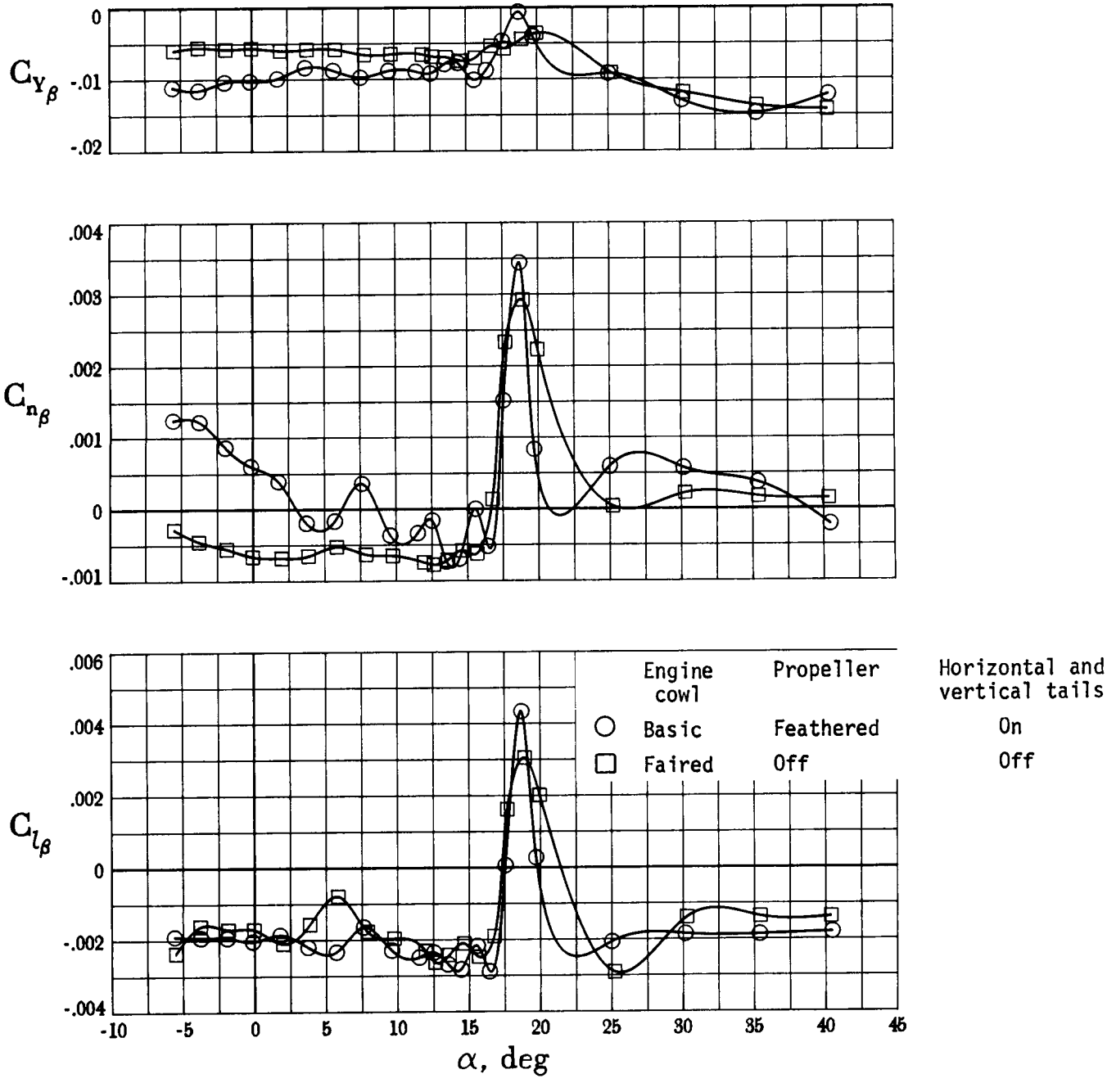


Figure 12. Effect of airplane components on lateral-directional stability characteristics of basic configuration. All controls at zero; $C_T = 0$; $R = 2.0 \times 10^6$.

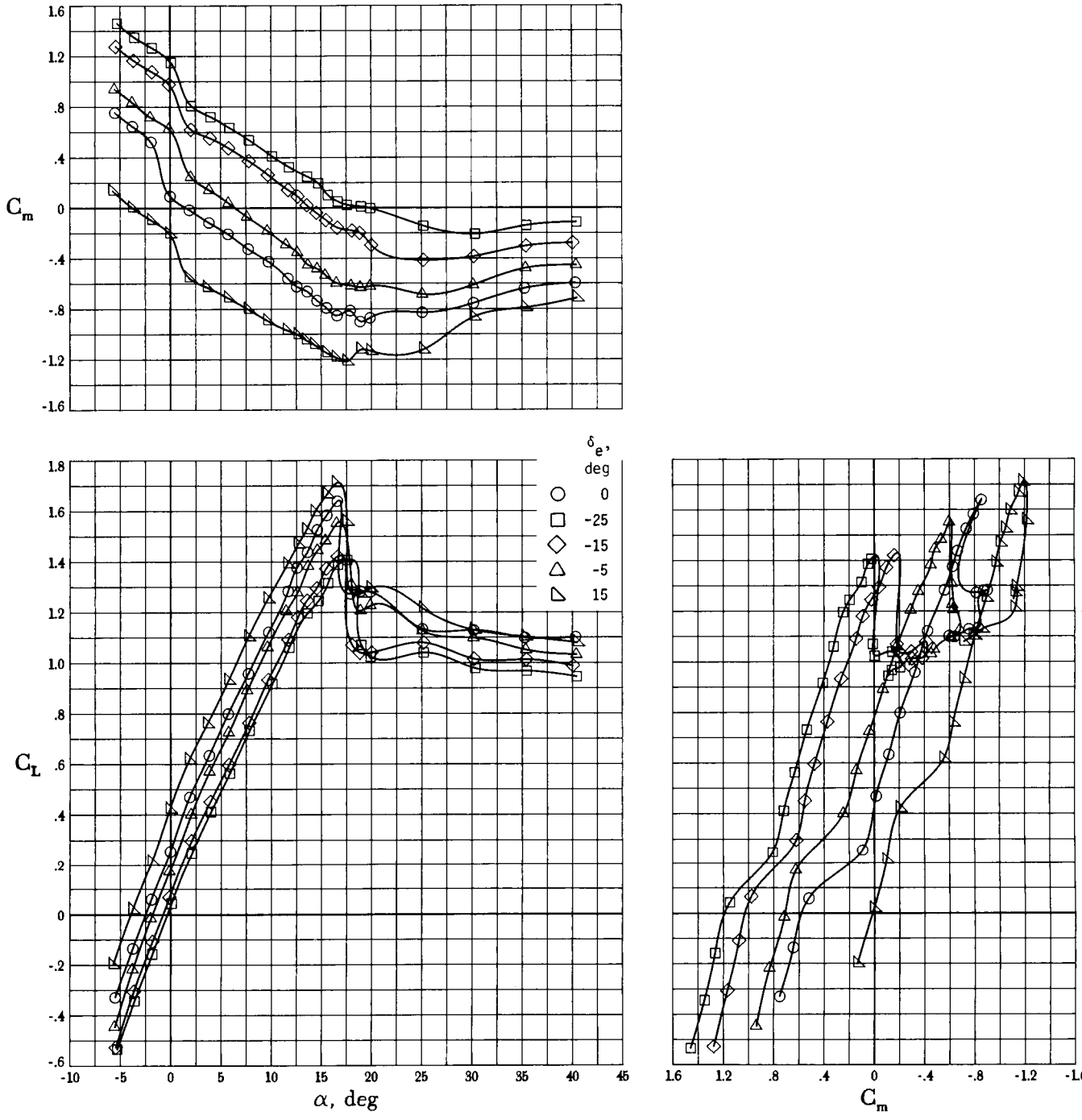


(a) Lift and pitching moment.

Figure 13. Effect of elevator deflection on longitudinal characteristics of basic configuration. All other controls at zero; $C_T = 0$; $R = 2.0 \times 10^6$.

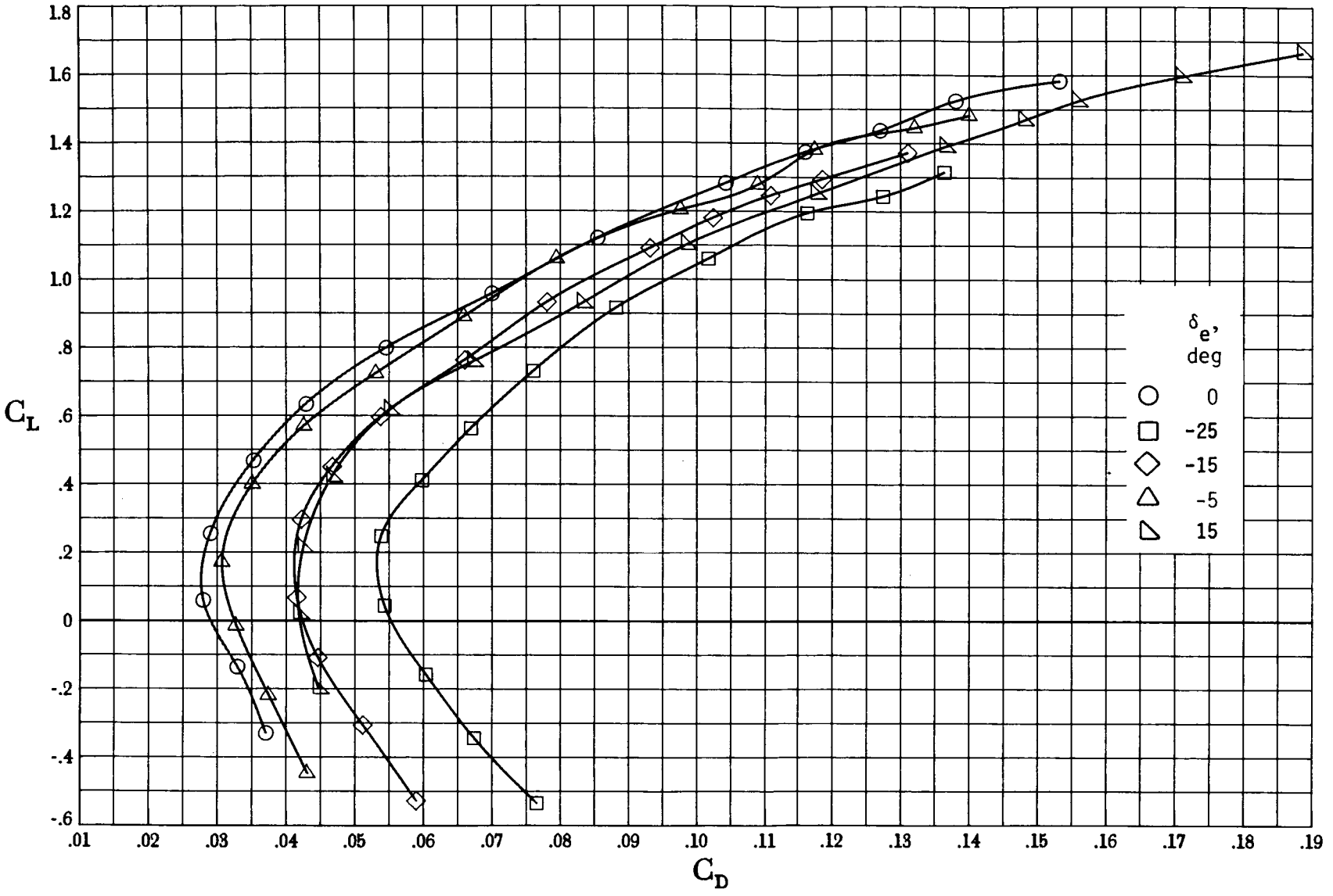


(b) Lift-drag polars.

Figure 13. Continued.

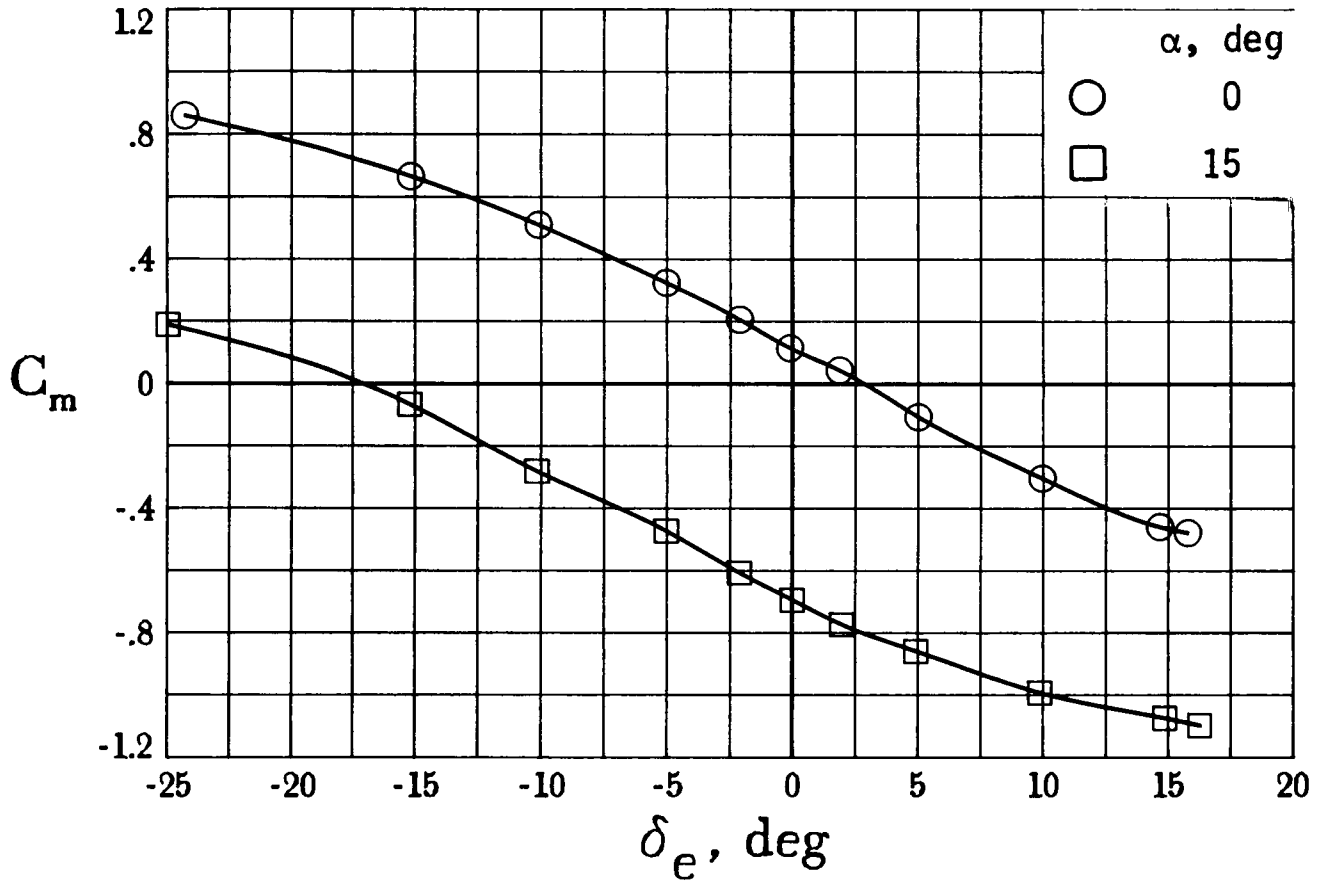


(c) Pitching moment versus $\delta_e$.

Figure 13. Concluded.

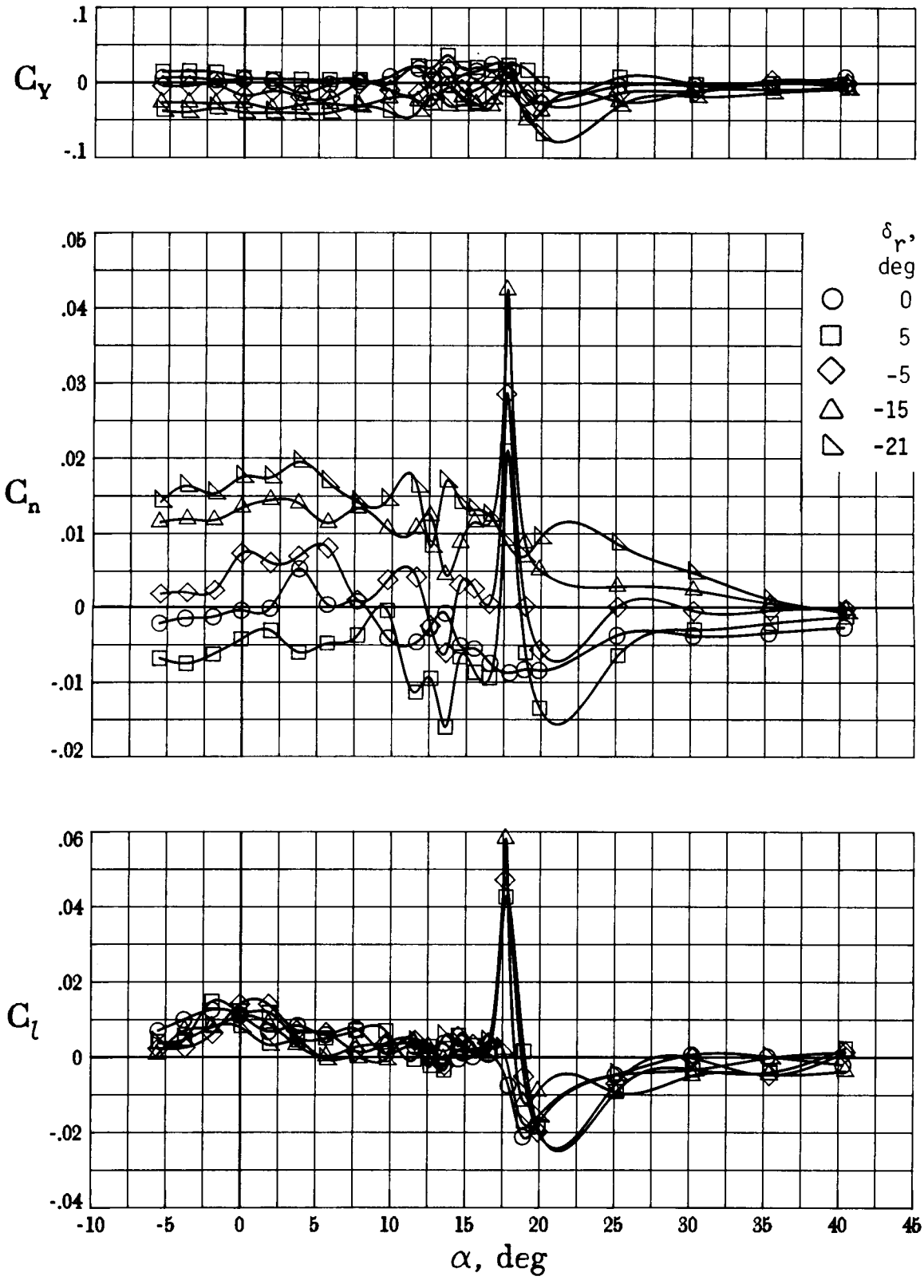


(a) Characteristics versus $\alpha$.

Figure 14. Effect of rudder deflection on lateral-directional characteristics of basic configuration. All other controls at zero; $C_T = 0$; $R = 2.0 \times 10^6$.

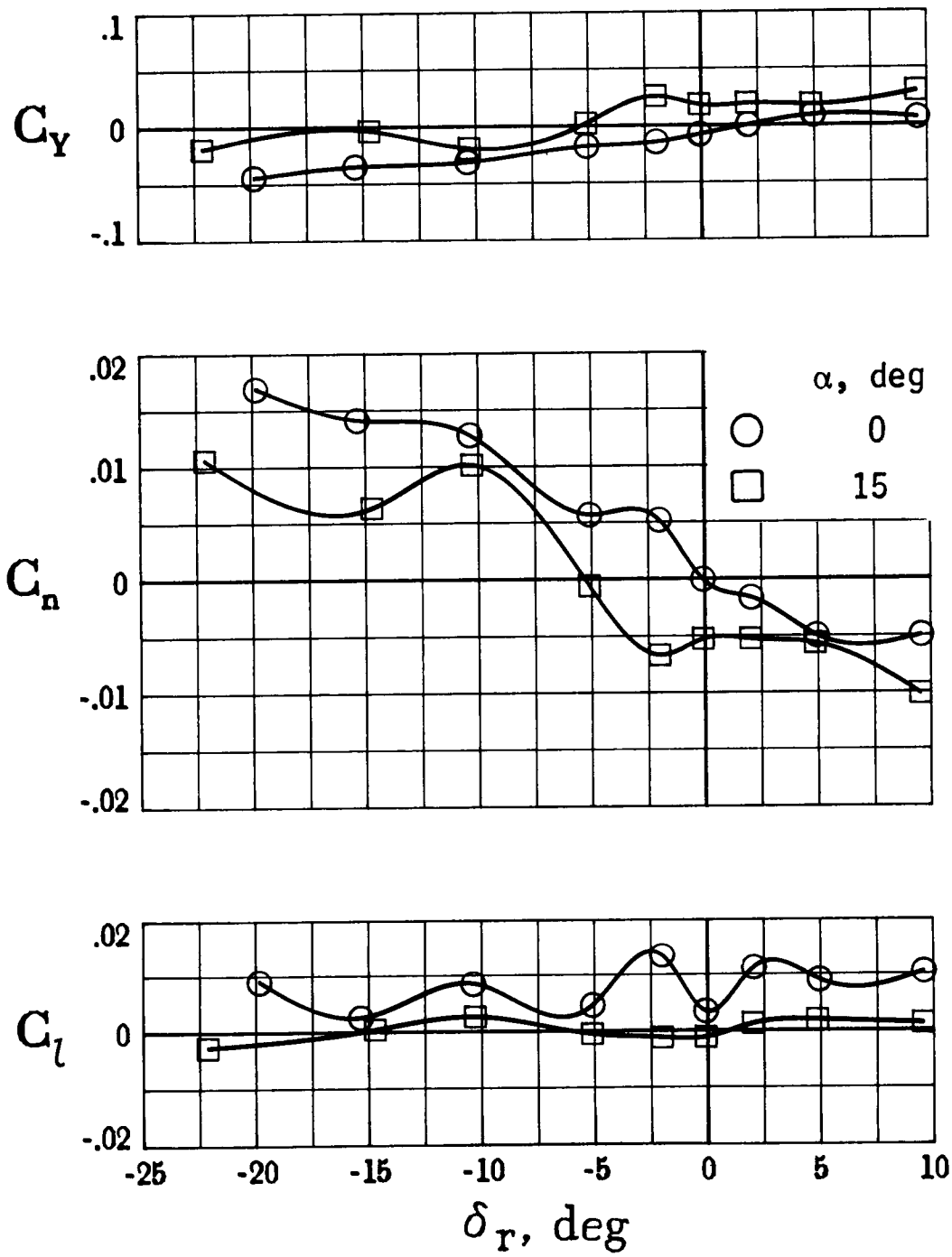


(b) Characteristics versus $\delta_r$.

Figure 14. Concluded.

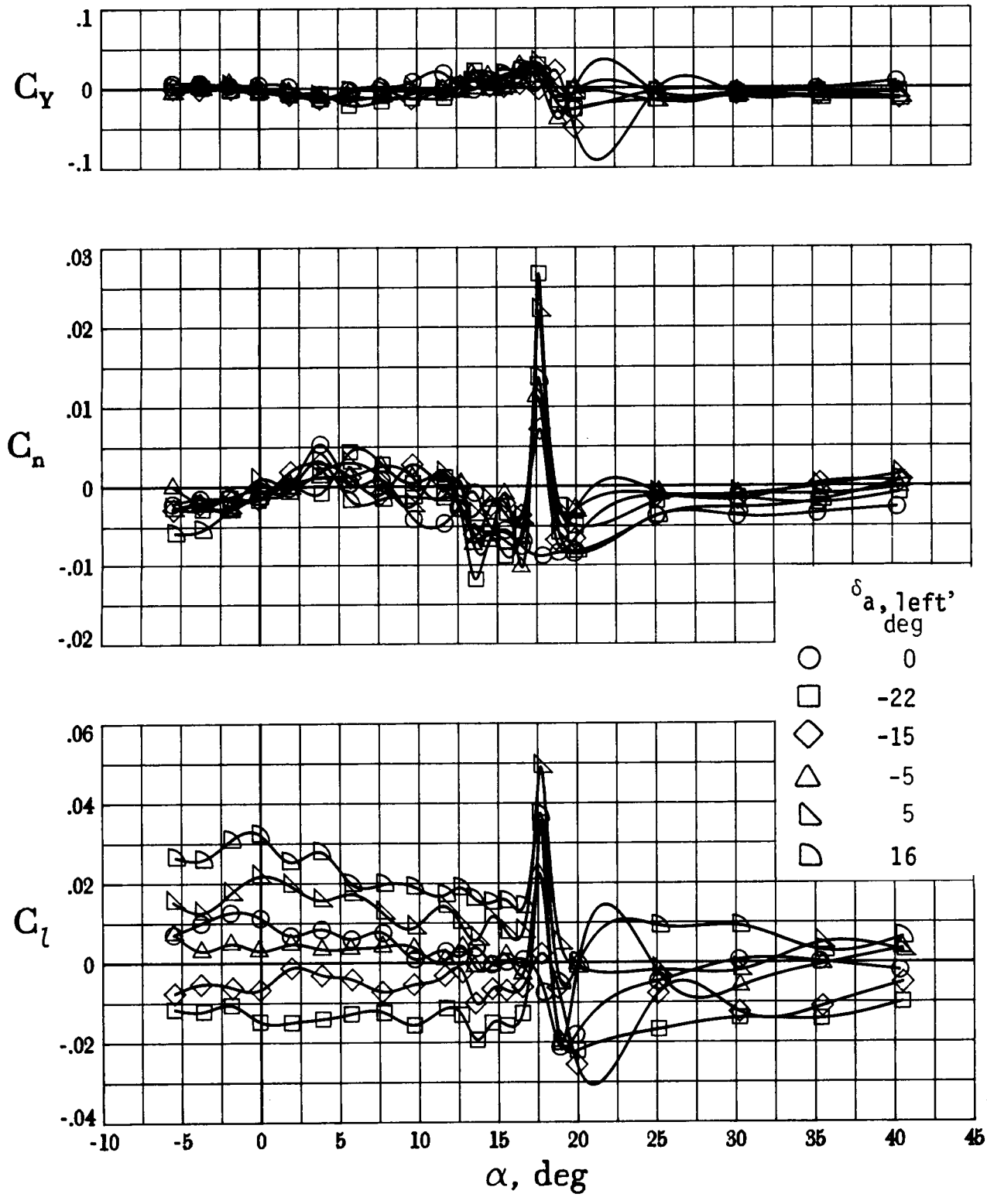


(a) Characteristics versus $\alpha$.

Figure 15. Effect of left aileron deflection on lateral-directional characteristics of basic configuration. All other controls at zero; $C_T = 0$; $R = 2.0 \times 10^6$.

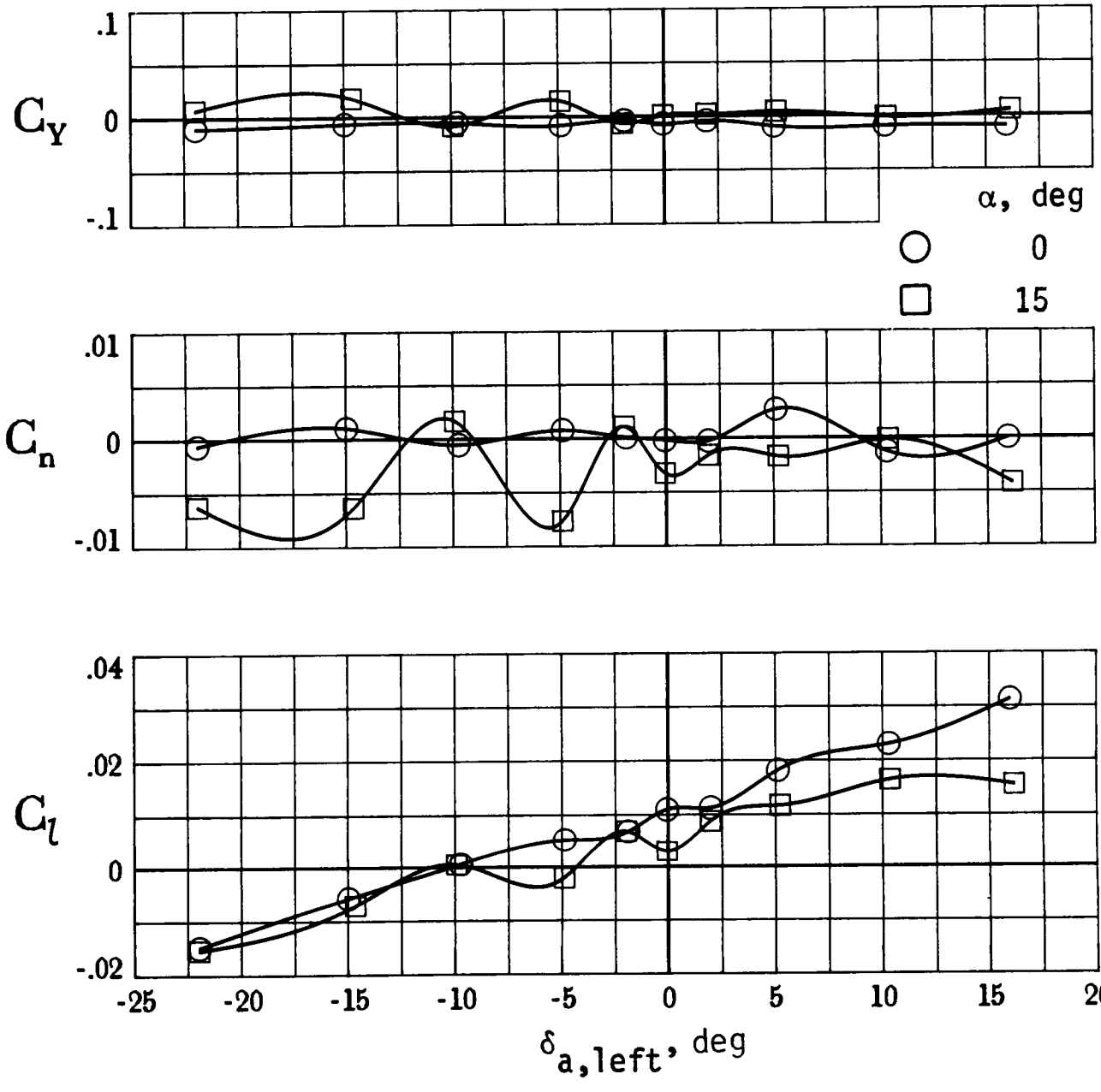


(b) Characteristics versus $\delta_{a,\text{left}}$.

Figure 15. Concluded.

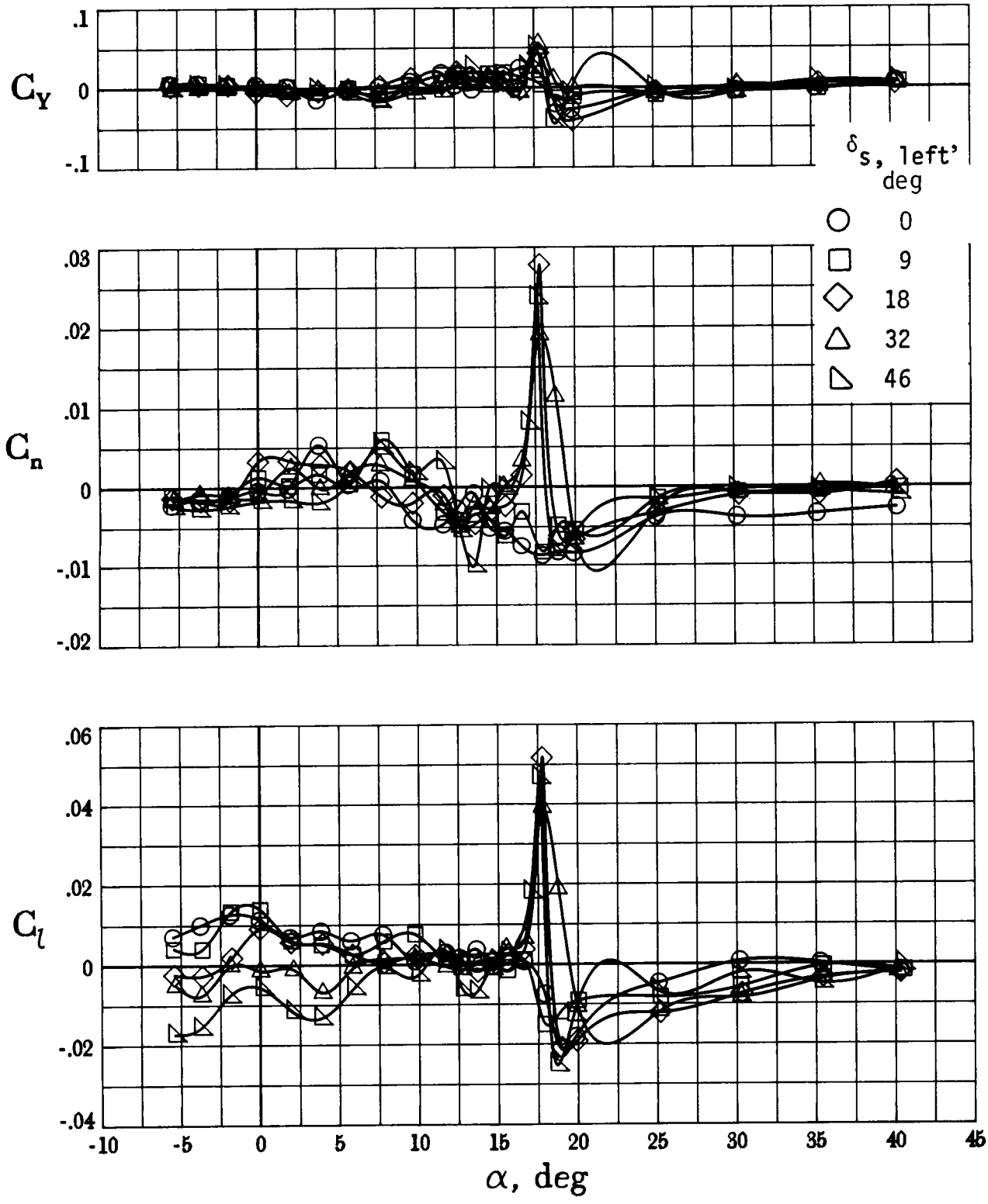


(a) Characteristics versus $\alpha$.

Figure 16. Effect of left spoiler deflection on lateral-directional characteristics of basic configuration. All other controls at zero; $C_T = 0$; $R = 2.0 \times 10^6$.

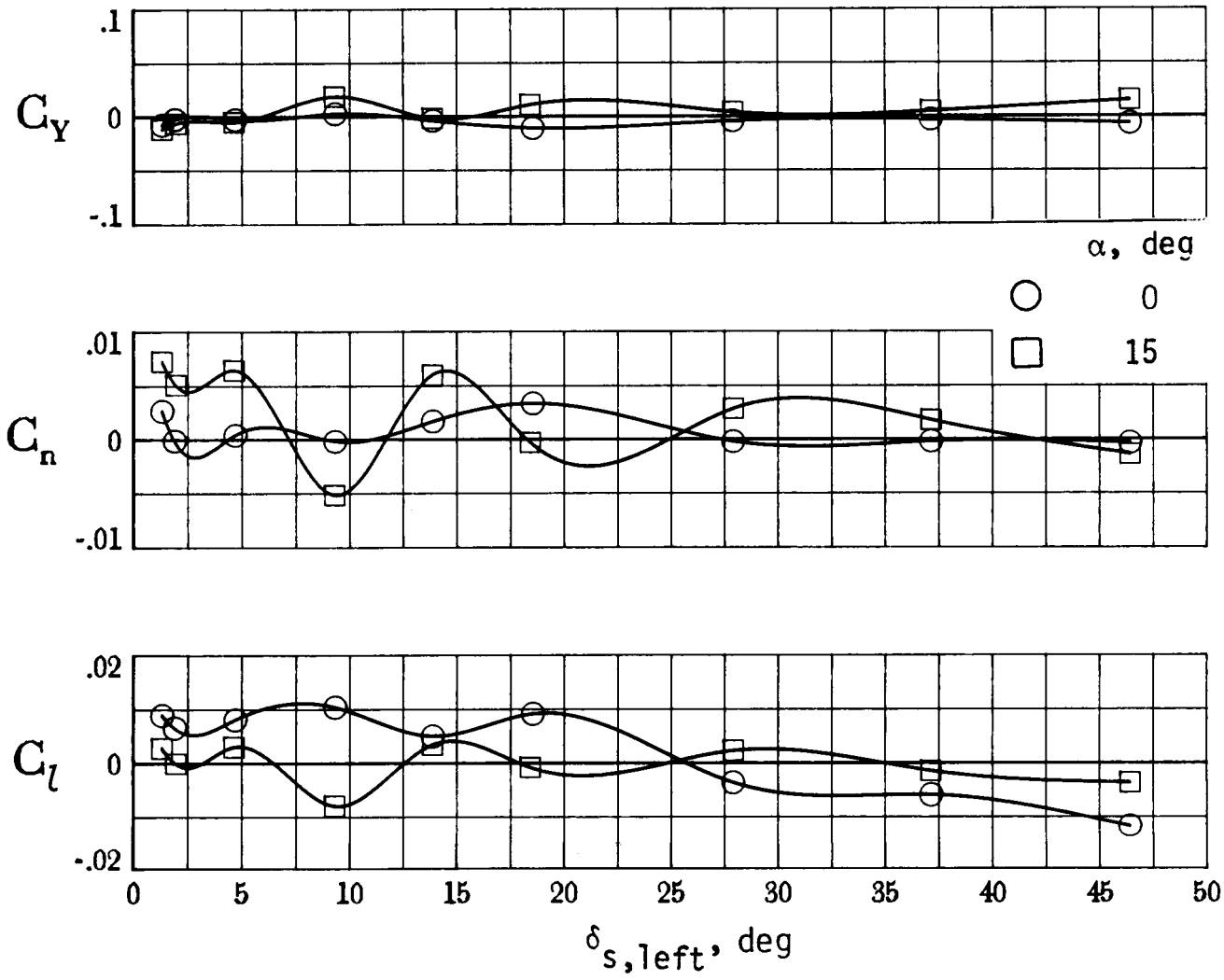


(b) Characteristics versus $\delta_{s,\text{left}}$.

Figure 16. Concluded.

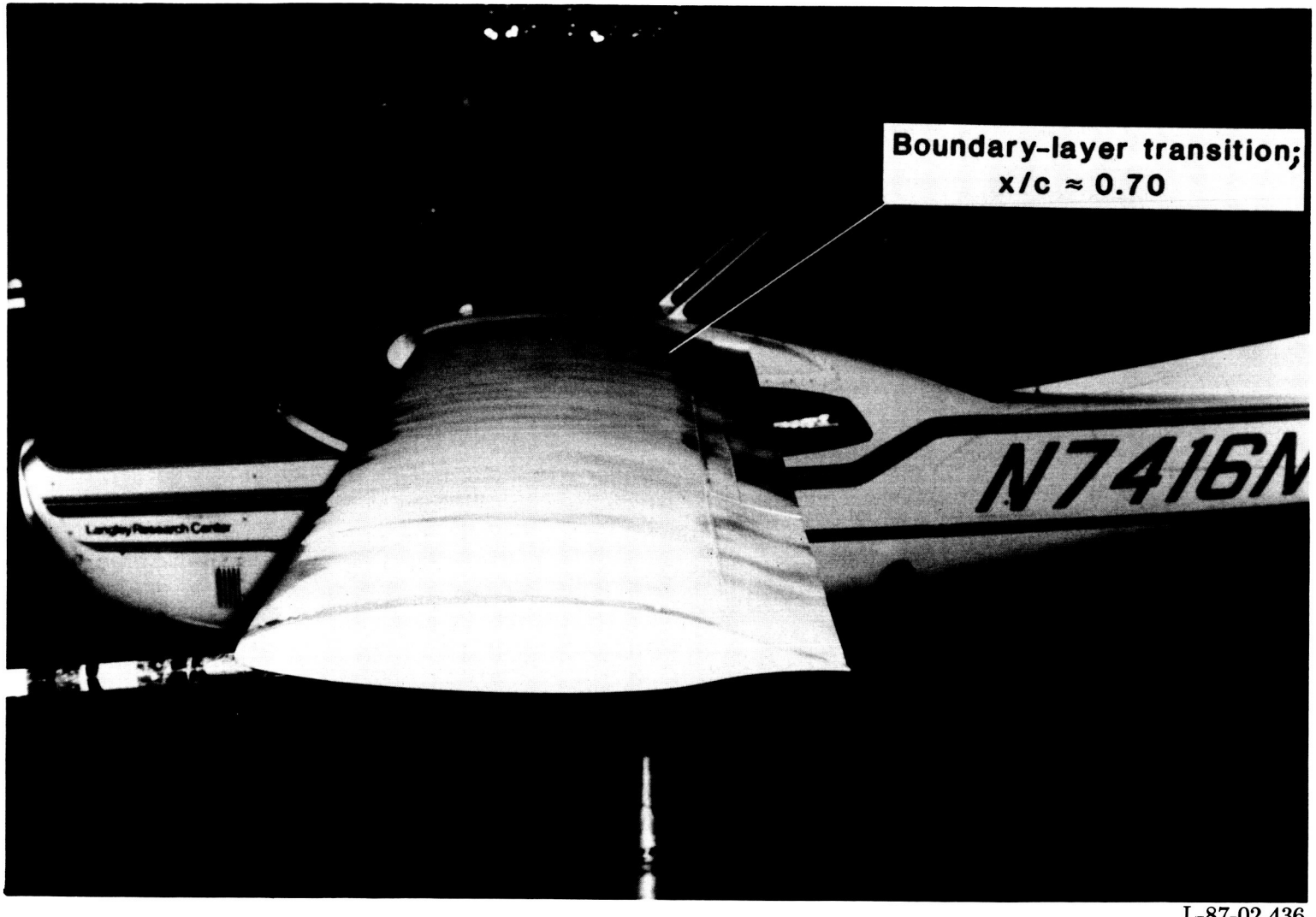


L-87-02,436

(a) Photograph of sublimating chemical technique. $\alpha = 1°$.

Figure 17. Boundary-layer transition characteristics of basic configuration. All controls at zero; $C_T = 0$; $R = 2.4 \times 10^6$.

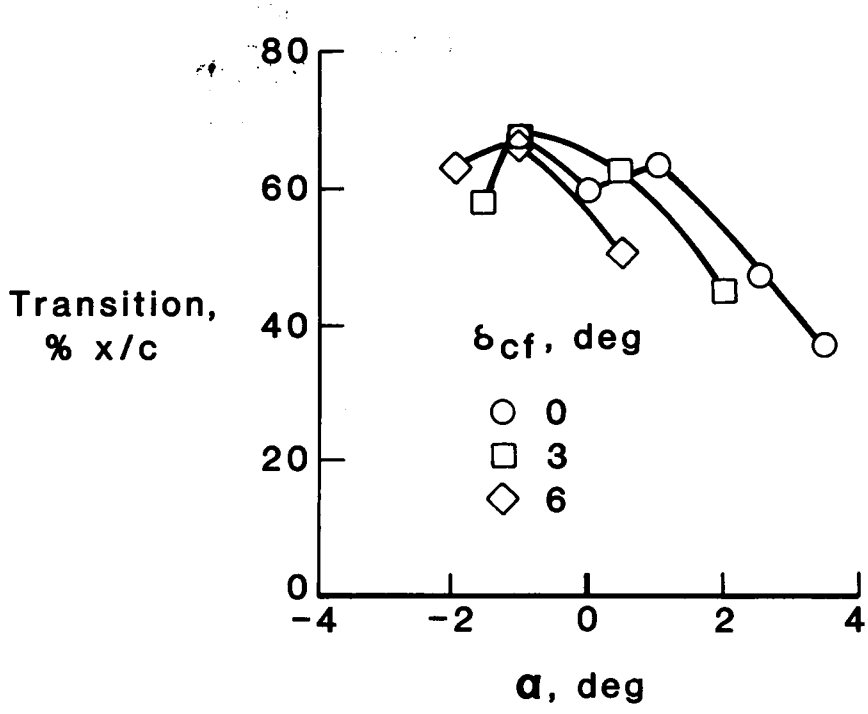


(b) Hot-film technique for upper surface.

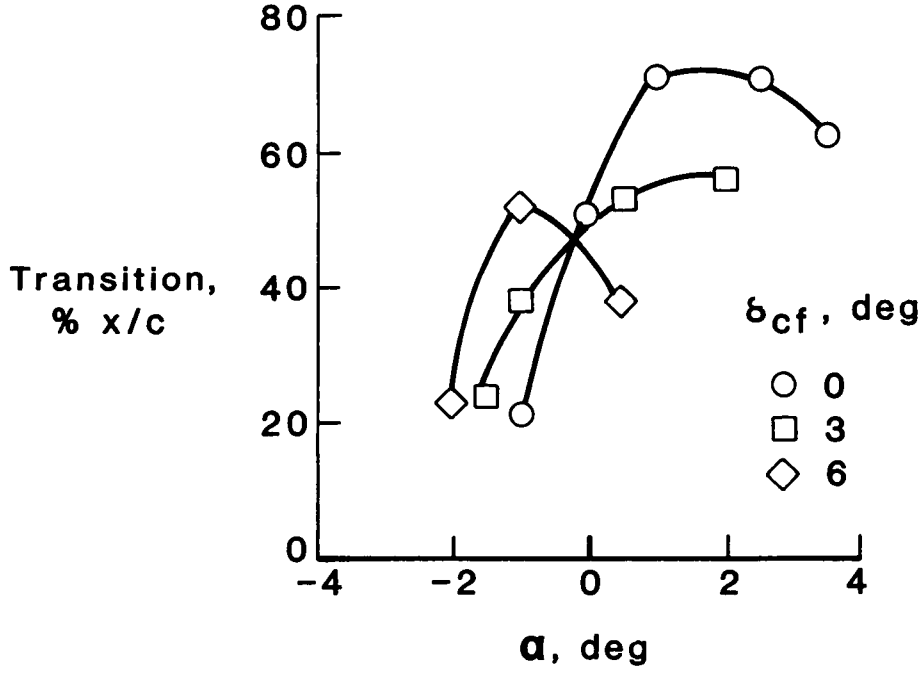


(c) Hot-film technique for lower surface.

Figure 17. Concluded.

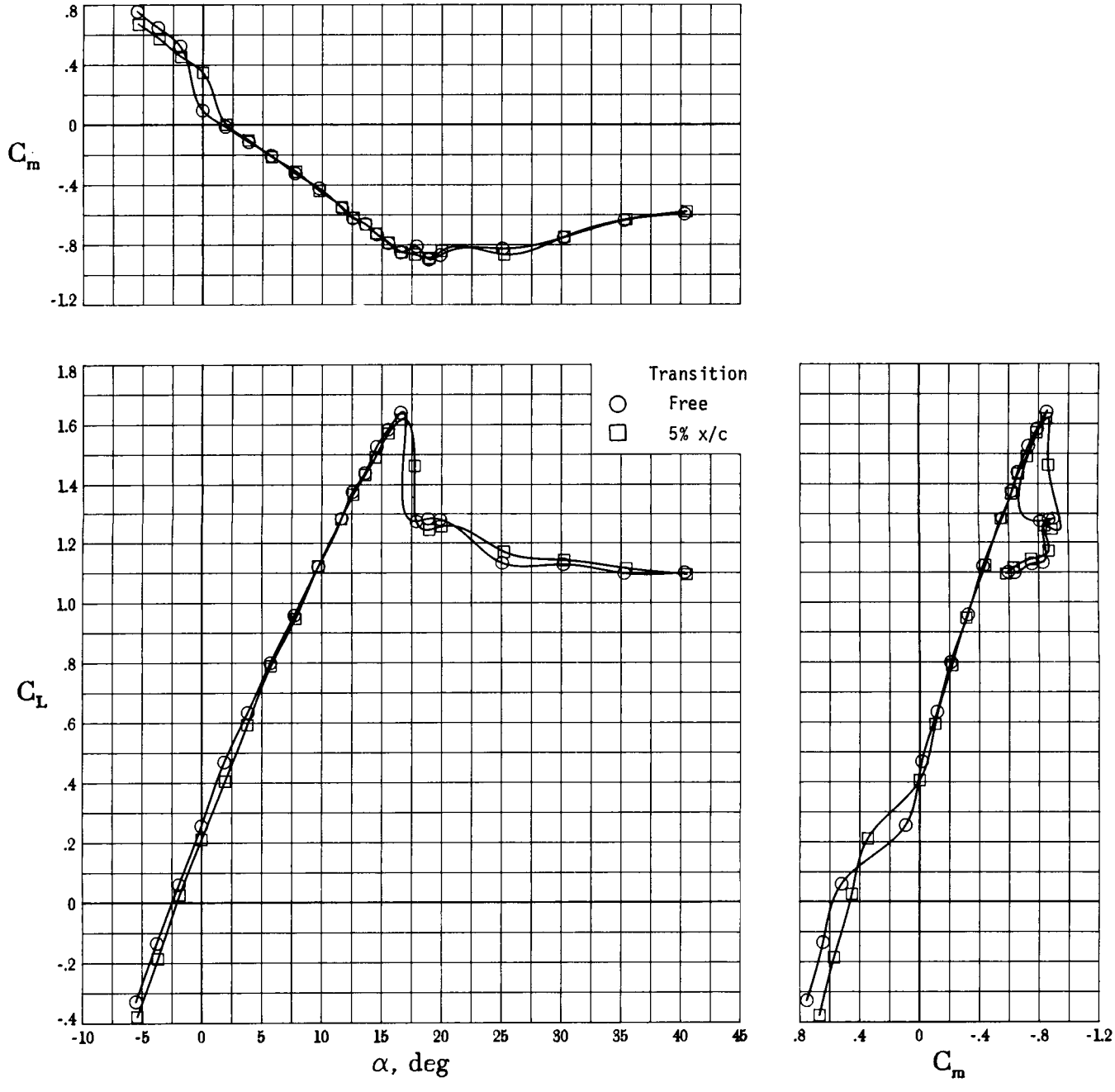


(a) Lift and pitching moment.

Figure 18. Effect of transition on longitudinal characteristics of basic configuration. All controls at zero; $C_T = 0$; $R = 2.0 \times 10^6$.

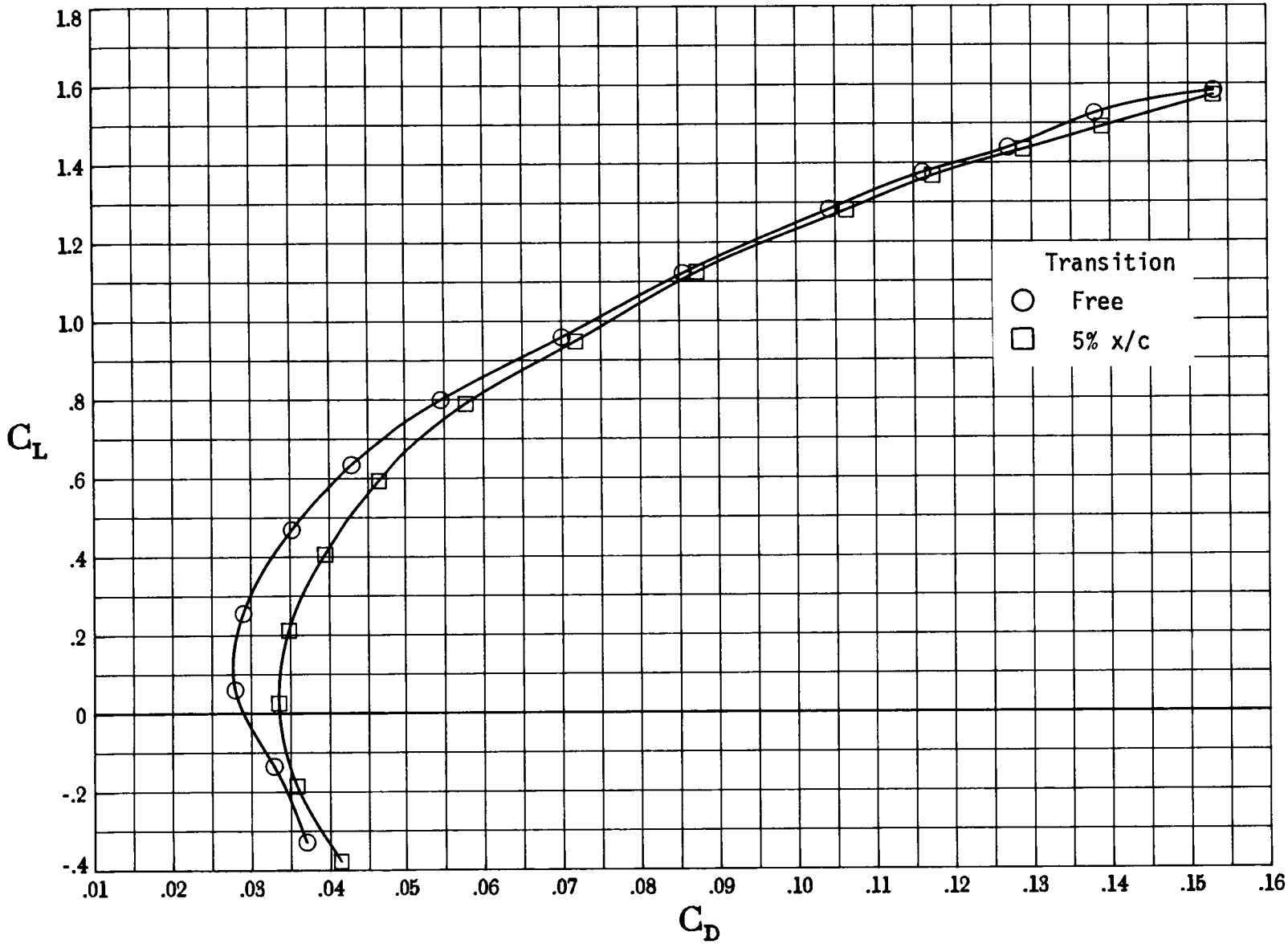


(b) Lift-drag polars.

Figure 18. Concluded.

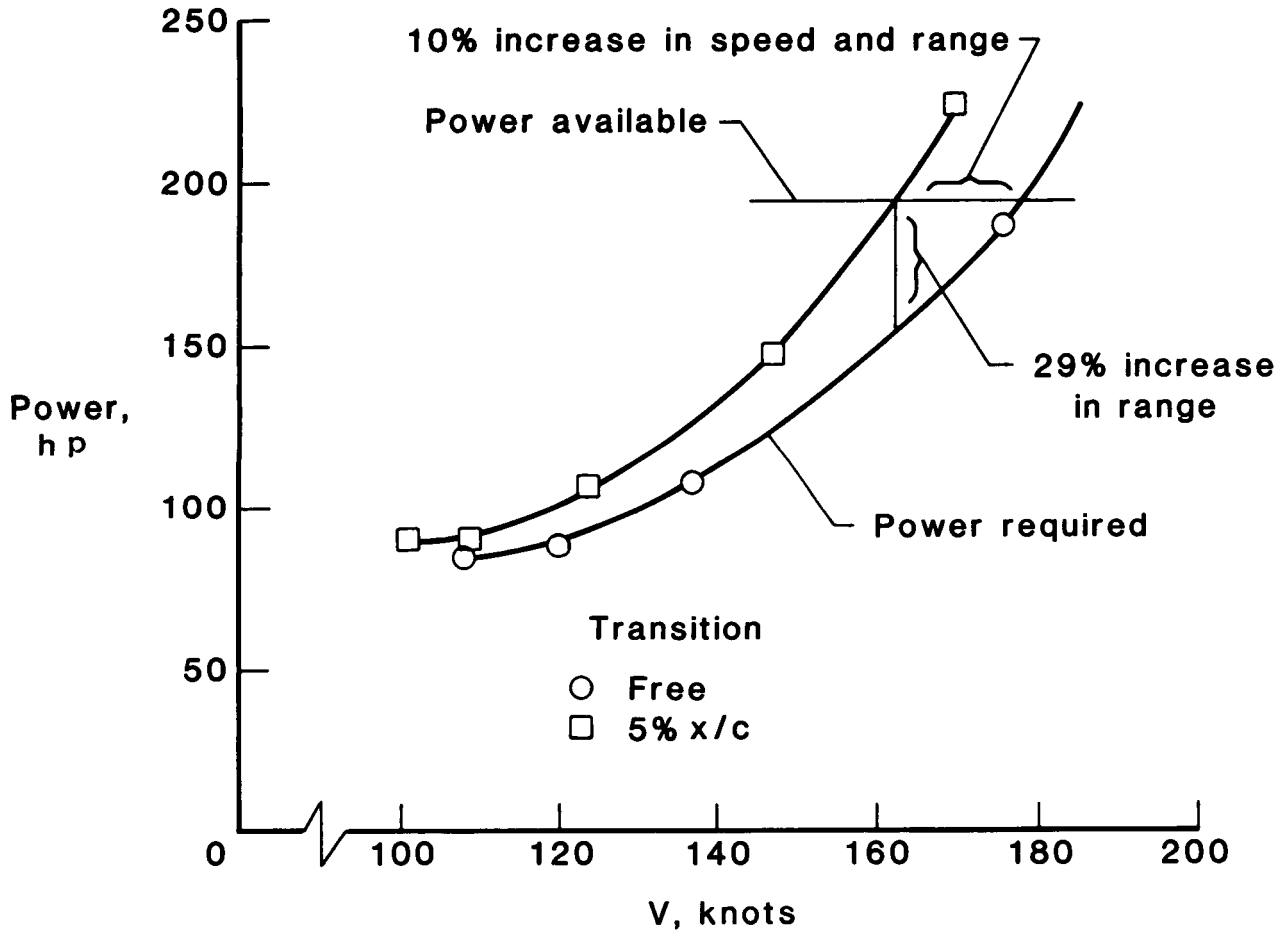


Figure 19. Effect of transition on calculated cruise performance of basic configuration. $h$ = 10000 ft; $W$ = 3500 lb; Power = 75 percent; $\eta$ = 0.80; Propeller $\Delta C_D$ = −0.0015. Results based on trimmed lift and drag calculated from tests with $C_T = 0$ and $R = 2.0 \times 10^6$.

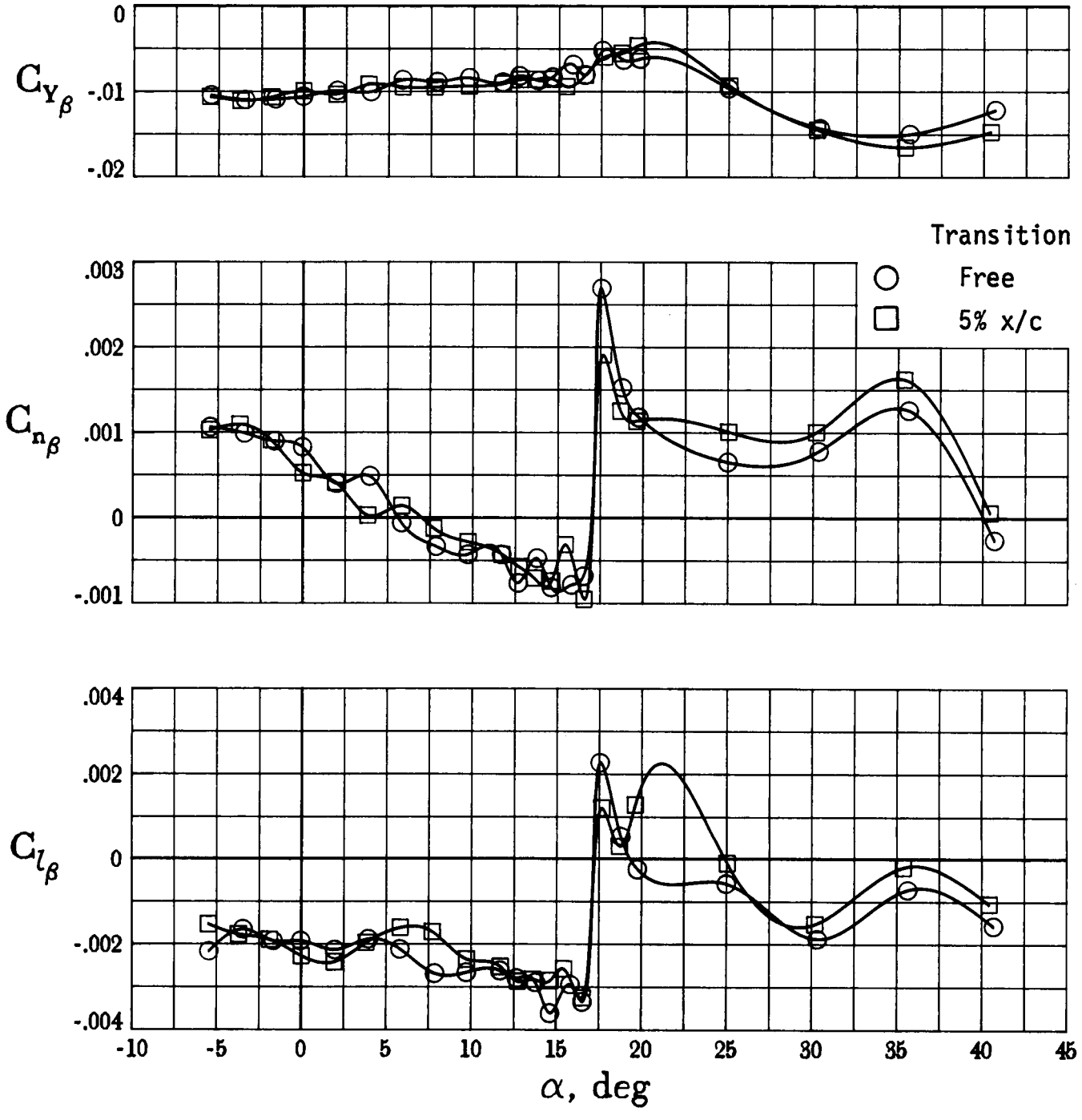


Figure 20. Effect of transition on lateral-directional stability characteristics of basic configuration with droop/V.G. leading-edge modifications. All controls at zero; $C_T = 0$; $R = 2.0 \times 10^6$.

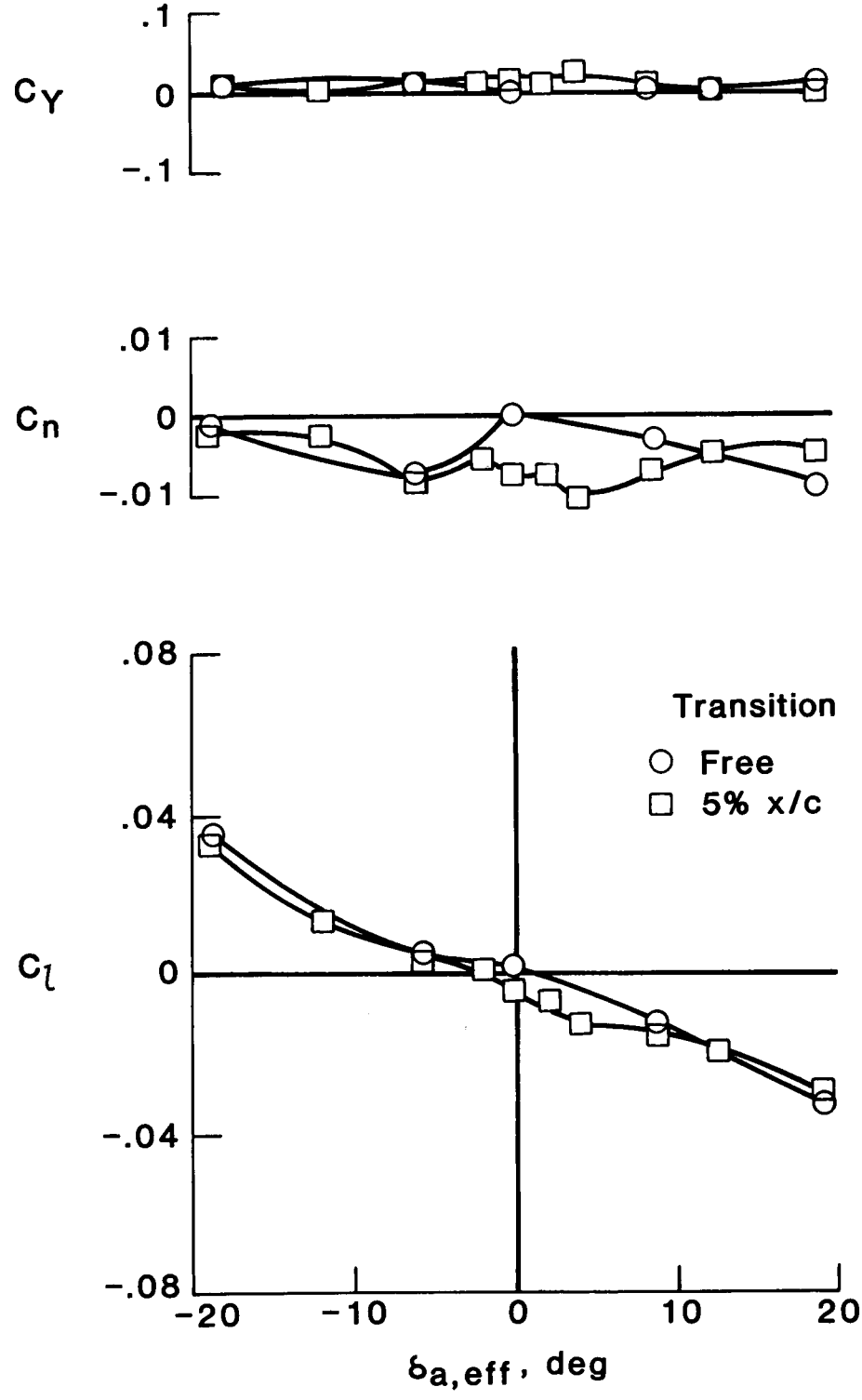


Figure 21. Effect of transition on combined aileron and spoiler effectiveness of basic configuration at $\alpha = 15°$. All other controls at zero; $C_T = 0$; $R = 2.0 \times 10^6$.

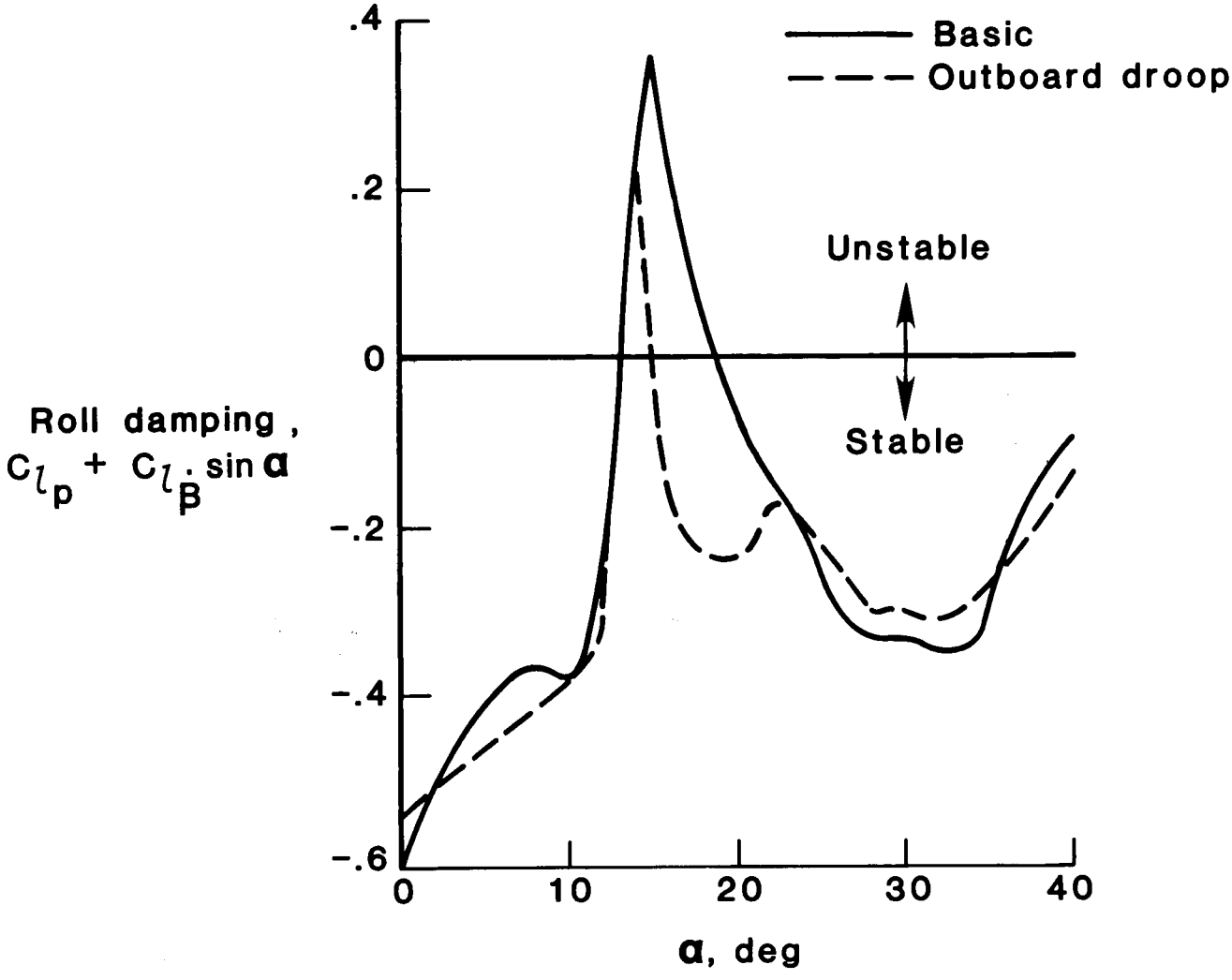


(a) Basic and outboard-droop configurations.

Figure 22. Effect of leading-edge modifications on roll damping characteristics measured during preliminary subscale model tests. Horizontal and vertical tails off; all controls at zero; $C_T = 0$; $R = 0.65 \times 10^6$.

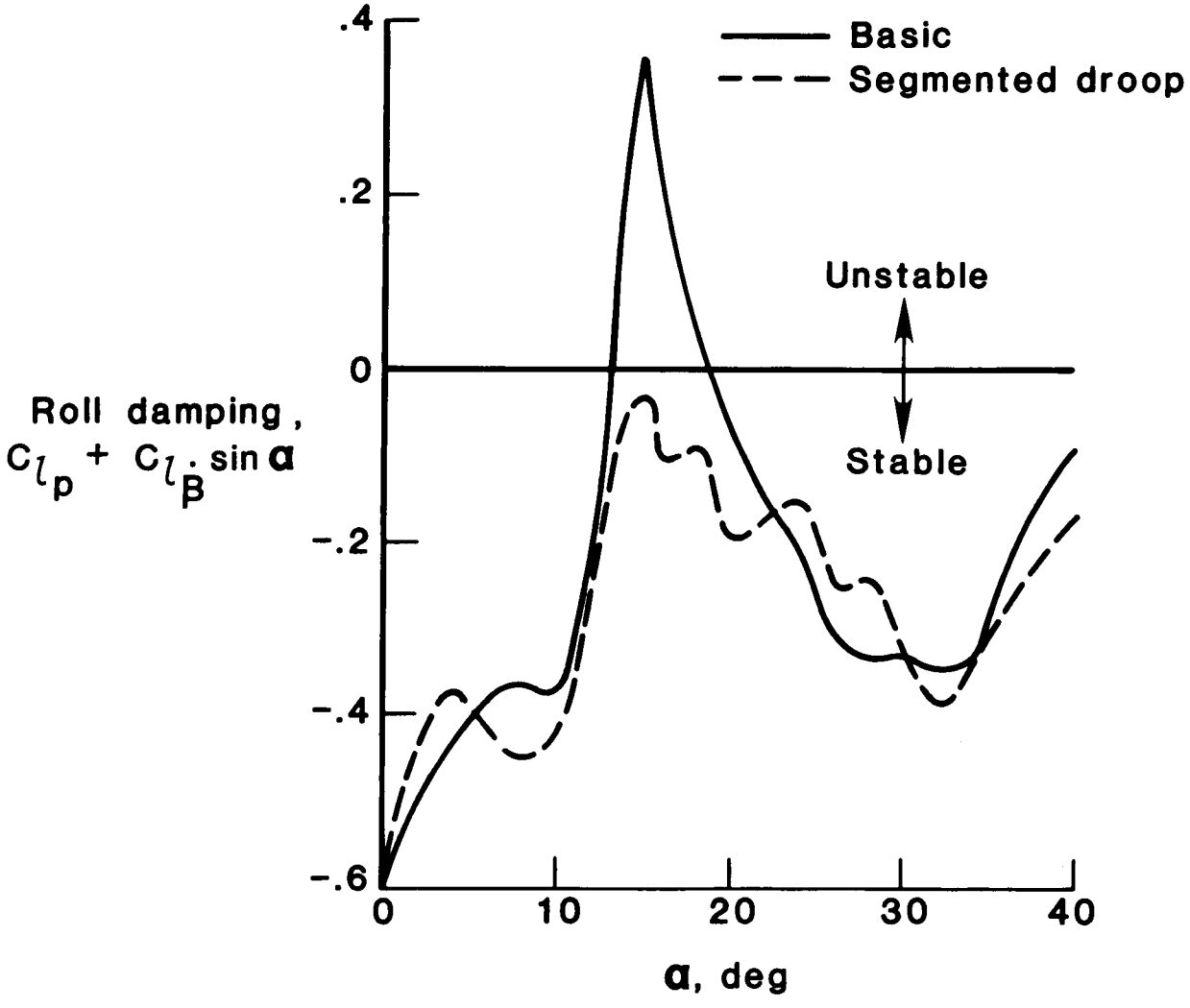


(b) Basic and segmented-droop configurations.

Figure 22. Concluded.

ORIGINAL PAGE IS
OF POOR QUALITY

(a) $\alpha = 15°$.

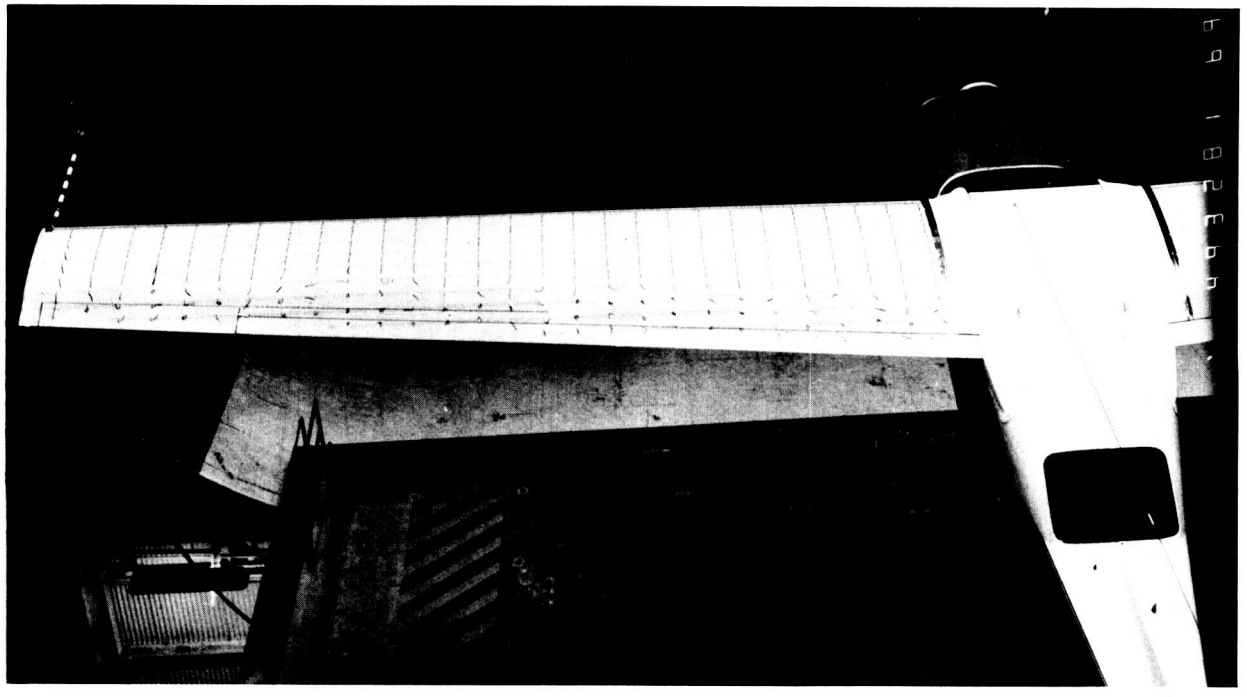

(b) $\alpha = 16°$.

L-87-610

Figure 23. Tuft flow-visualization photographs of basic configuration with outboard-droop leading-edge modification. Transition fixed at $x/c = 0.05$; all controls at zero; $C_T = 0$; $R = 2.0 \times 10^6$.

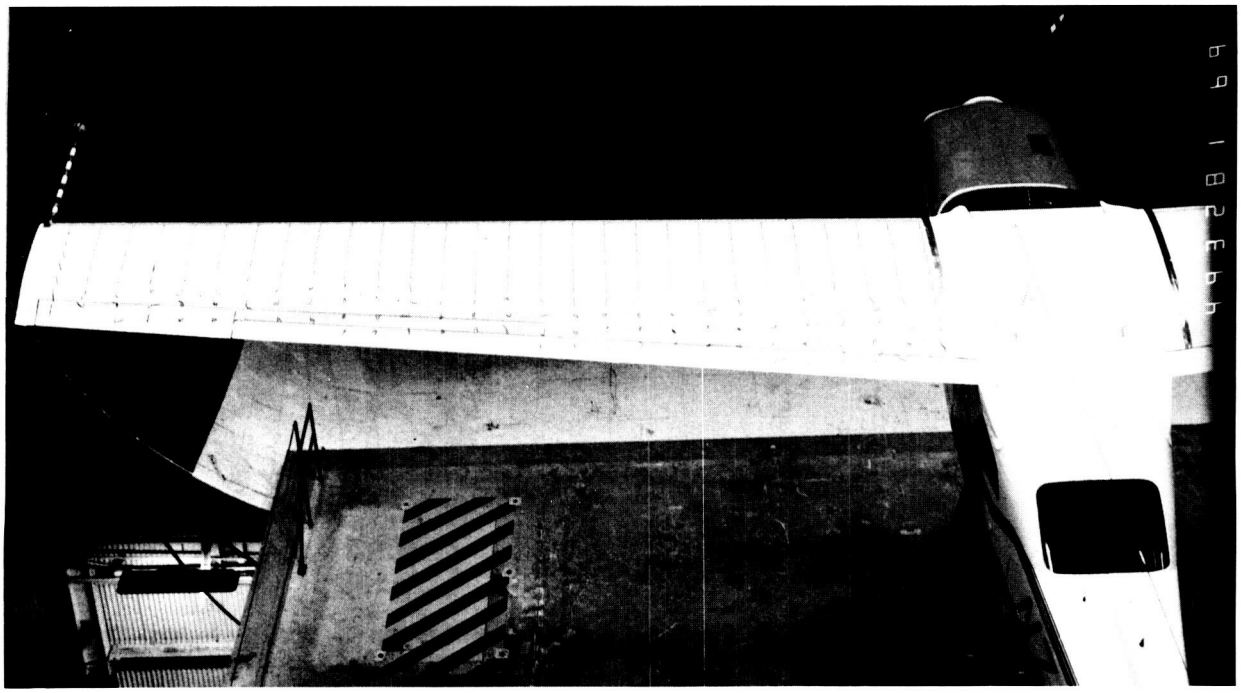

(c) $\alpha = 17°$.

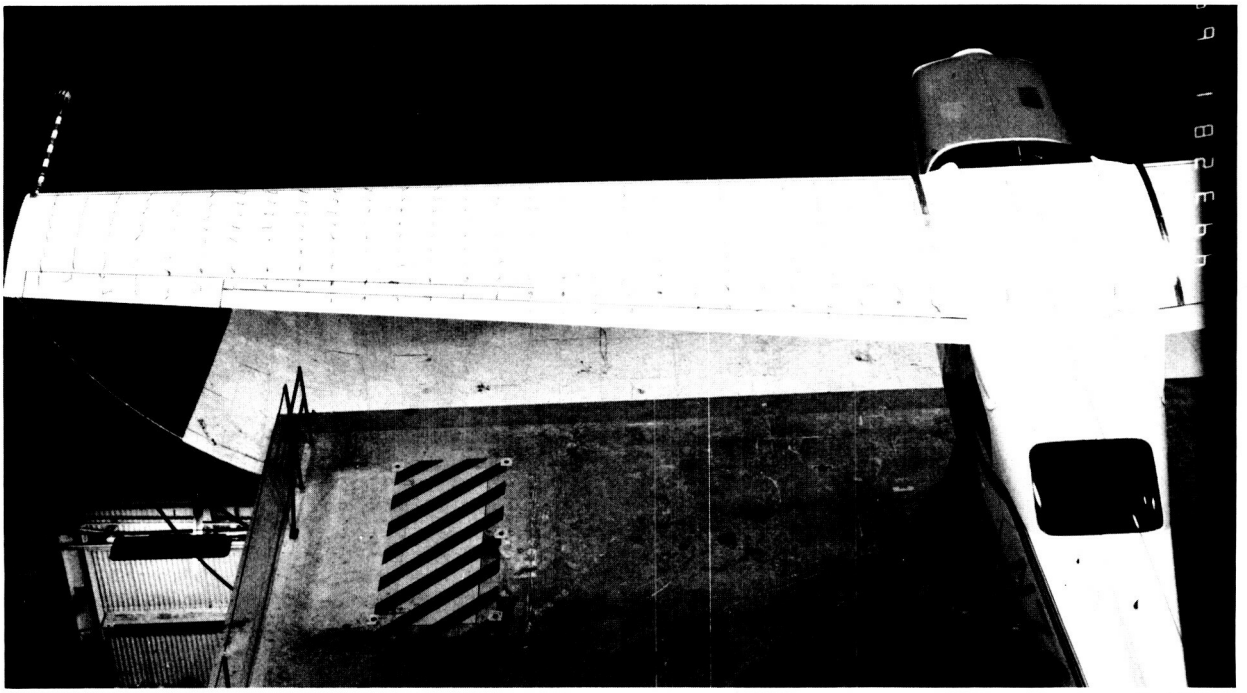

L-87-611

(d) $\alpha = 18°$.

Figure 23. Continued.

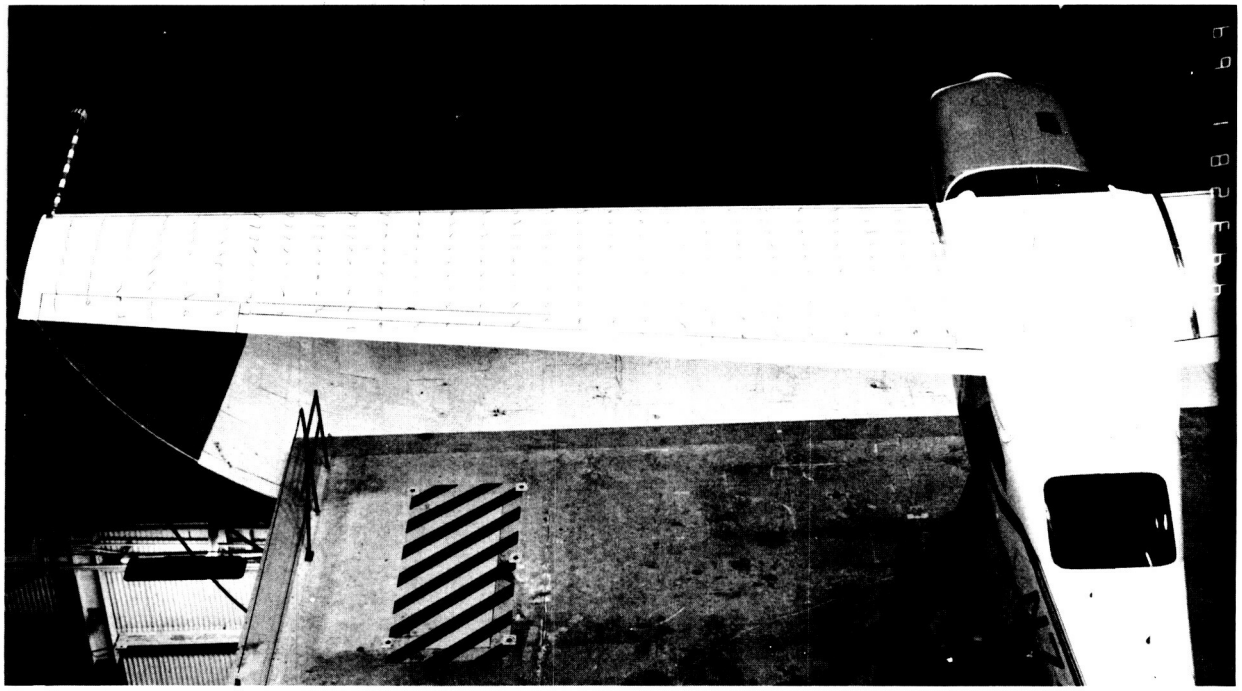

(e) $\alpha = 19°$.

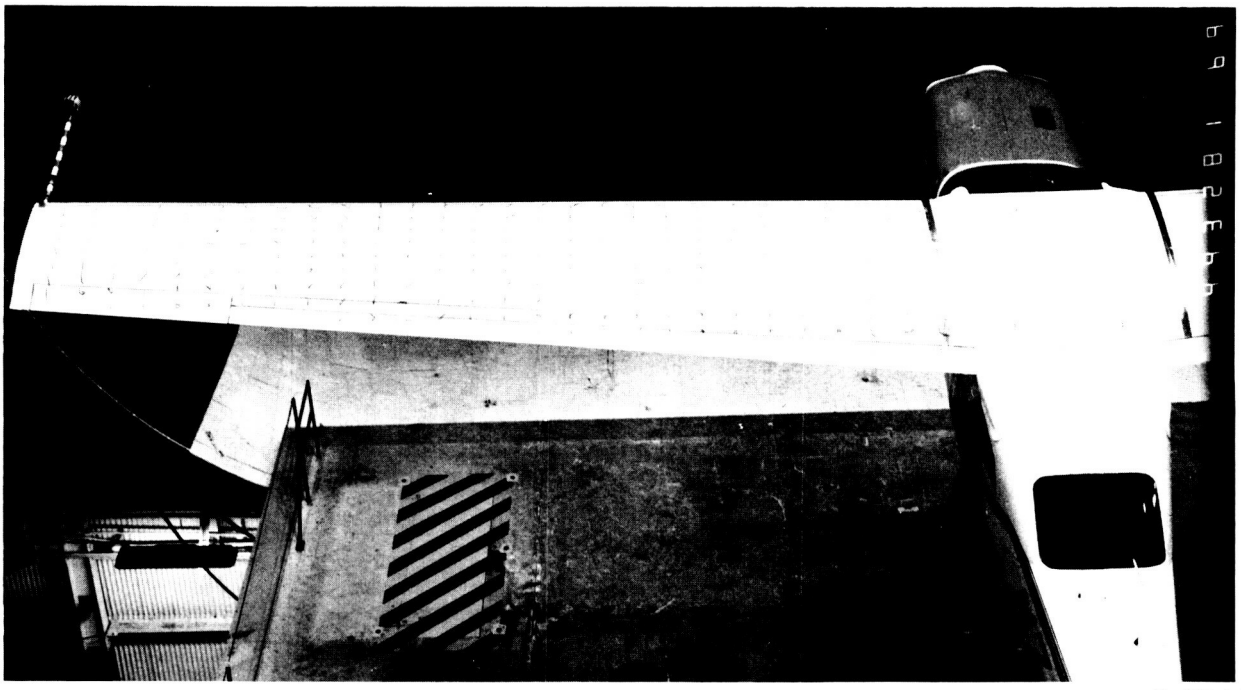

(f) $\alpha = 20°$.

L-87-612

Figure 23. Continued.

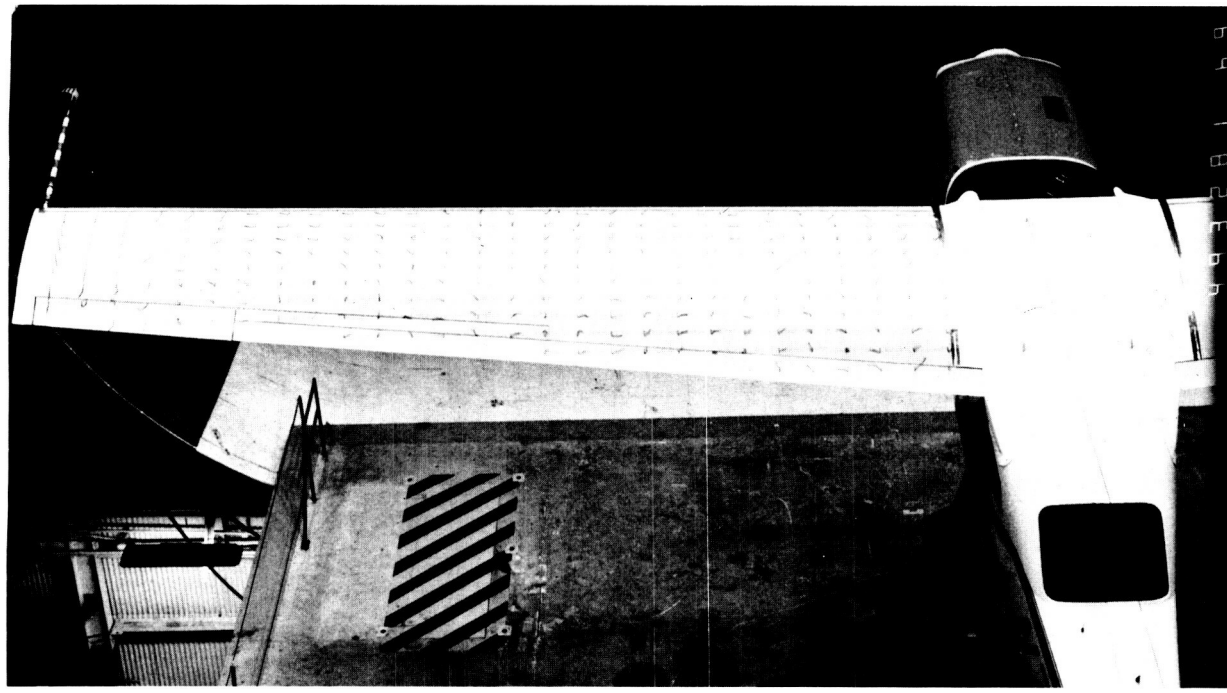

(g) $\alpha = 25°$.

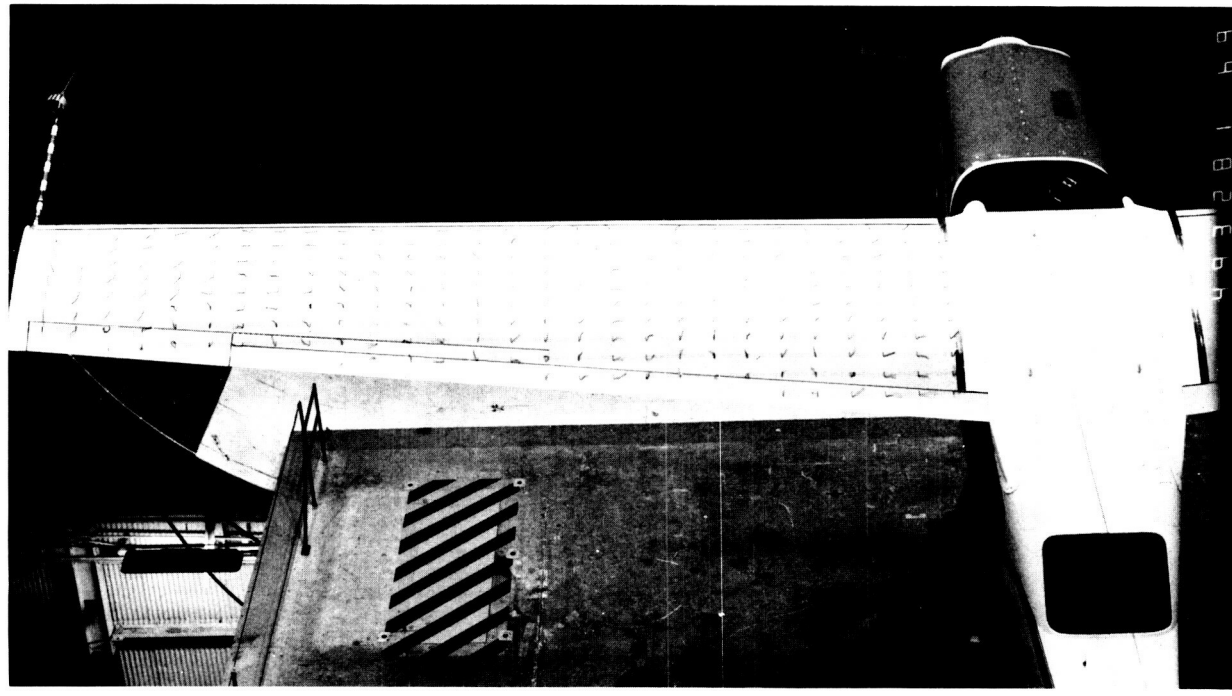

L-87-613

(h) $\alpha = 30°$.

Figure 23. Concluded.

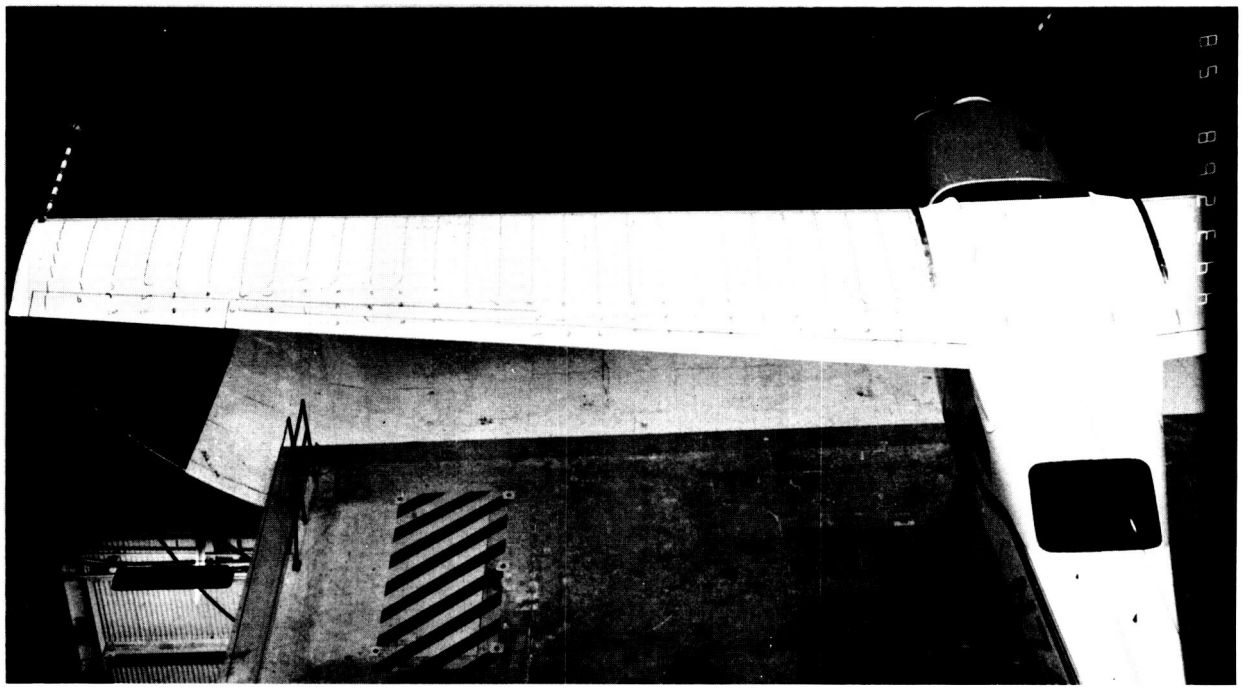

(a) $\alpha = 15°$.

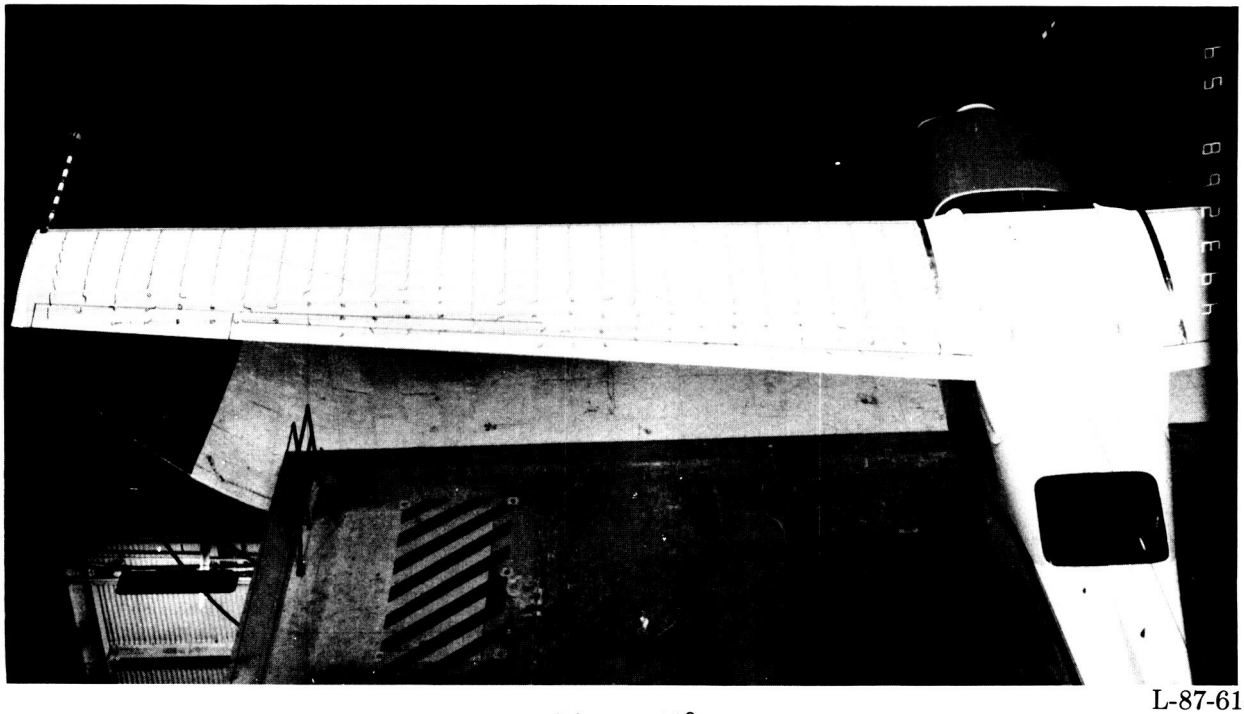

L-87-614

(b) $\alpha = 16°$.

Figure 24. Tuft flow-visualization photographs of basic configuration with segmented-droop leading-edge modification. Transition fixed at $x/c = 0.05$; all controls at zero; $C_T = 0$; $R = 2.0 \times 10^6$.

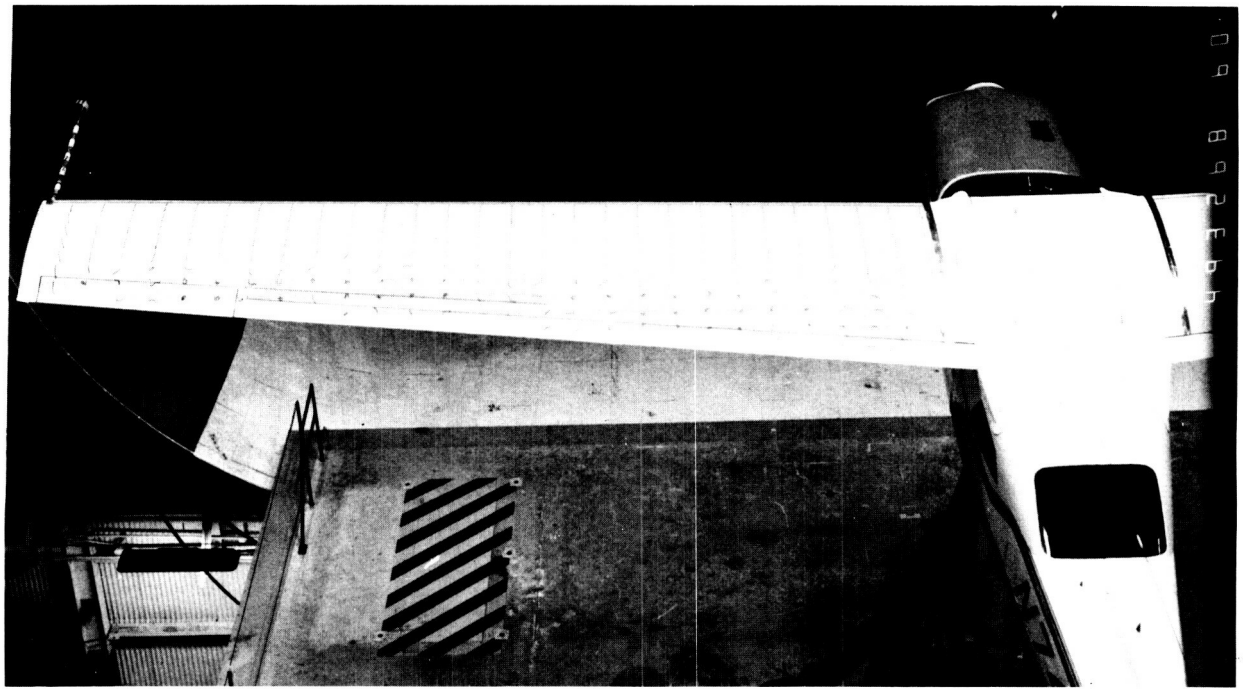

(c) $\alpha = 17°$.

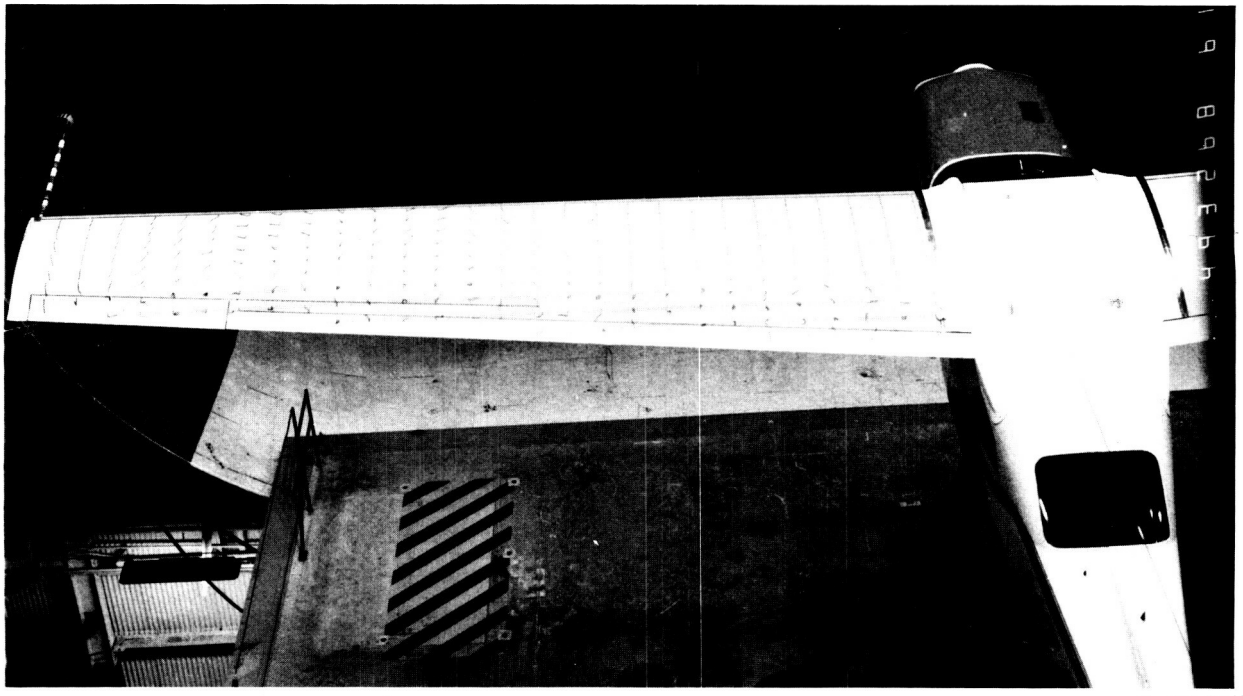

L-87-615

(d) $\alpha = 18°$.

Figure 24. Continued.

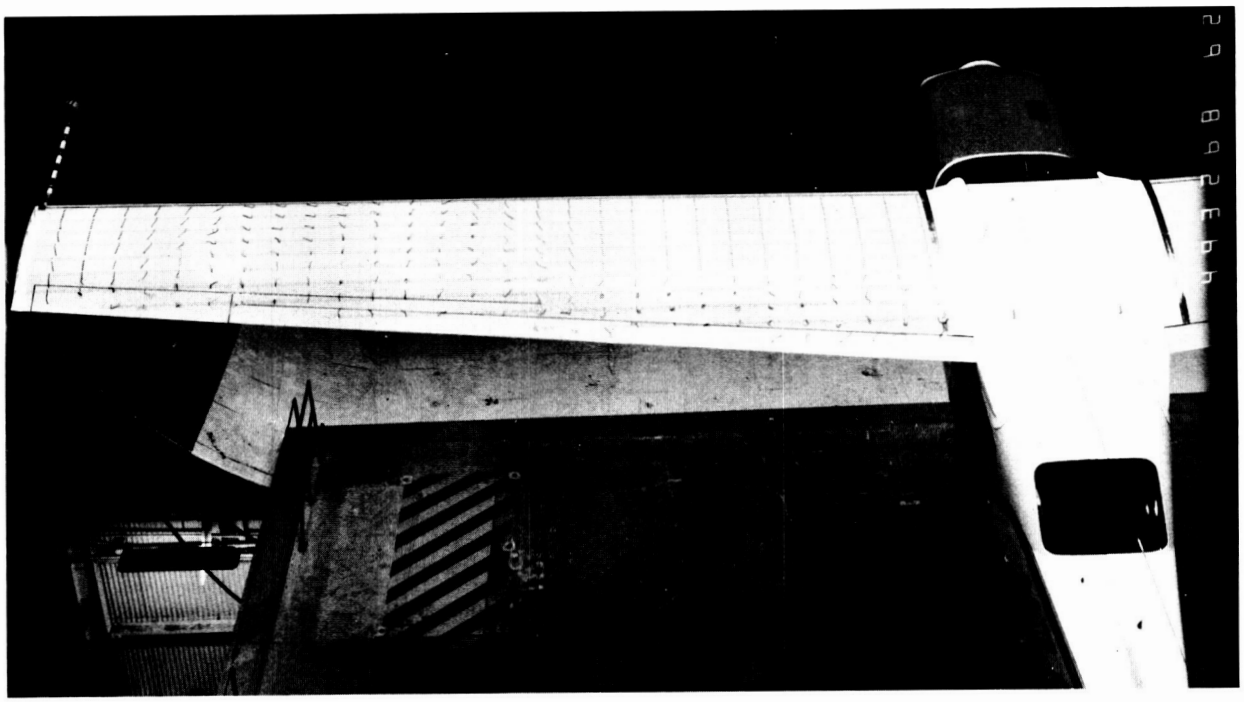

(e) $\alpha = 19°$.

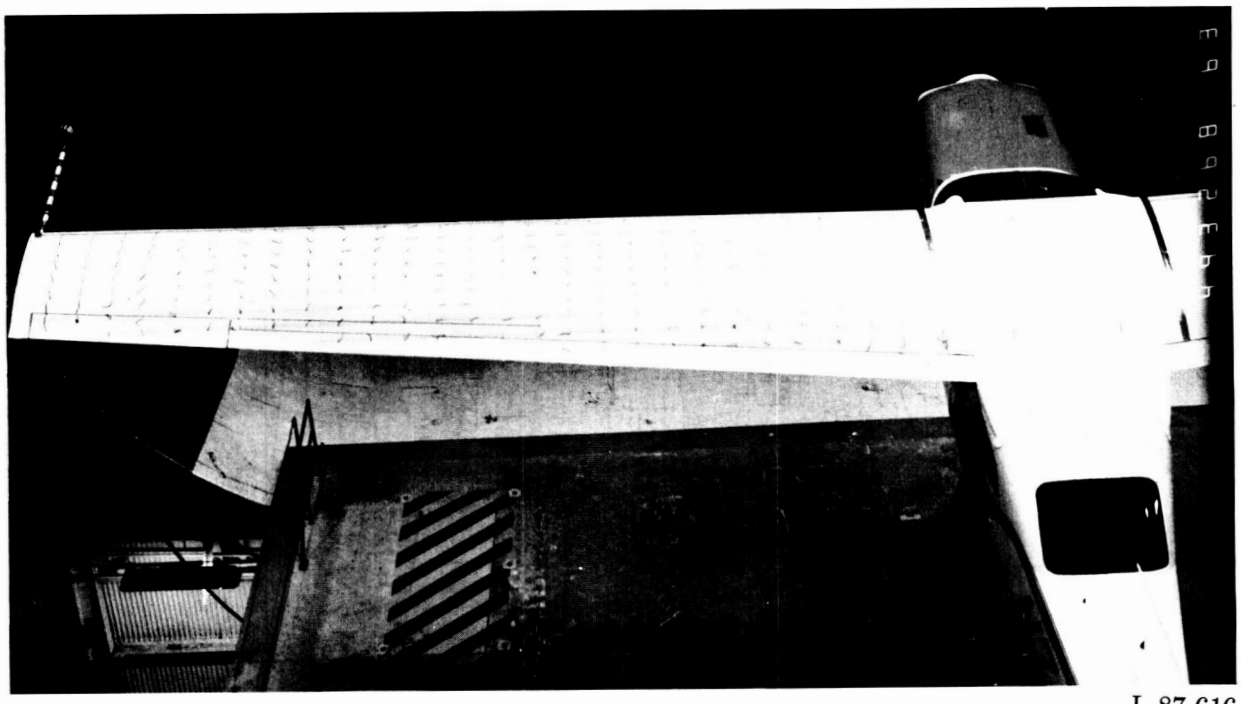

L-87-616

(f) $\alpha = 20°$.

Figure 24. Continued.

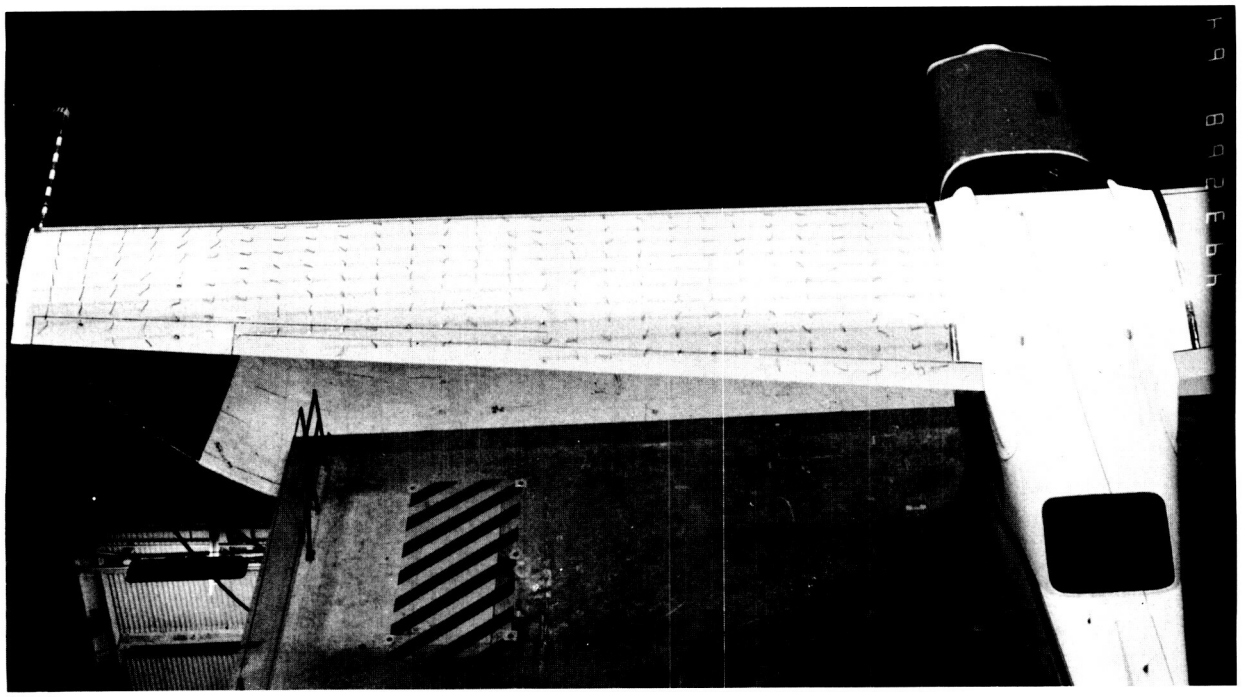

(g) $\alpha = 25°$.

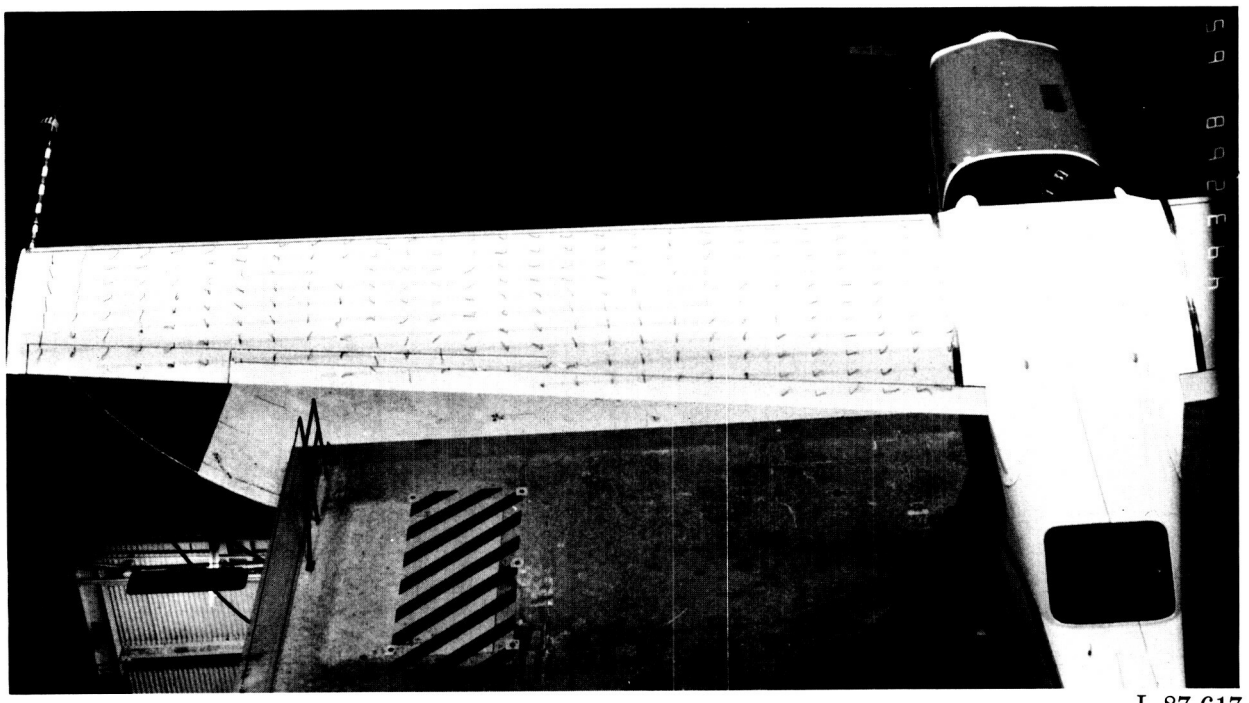

L-87-617

(h) $\alpha = 30°$.

Figure 24. Concluded.

(a) $\alpha = 15°$.

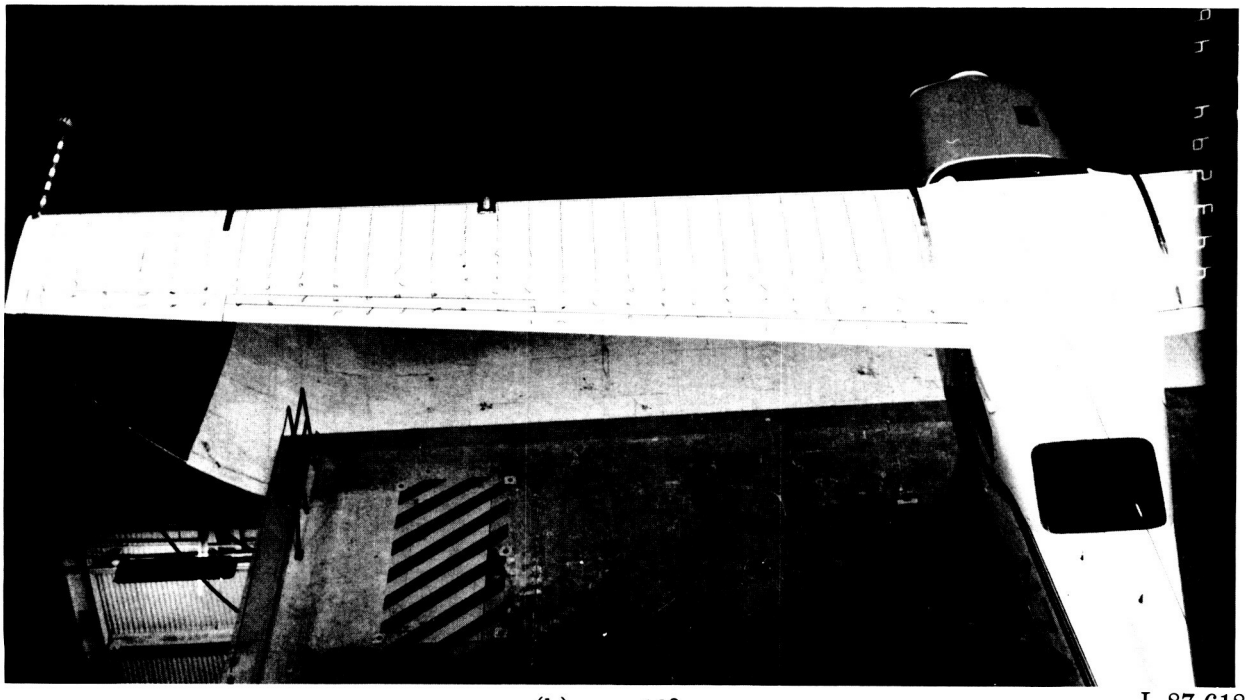

(b) $\alpha = 16°$.

L-87-618

Figure 25. Tuft flow-visualization photographs of basic configuration with droop/V.G. modification. Transition fixed at $x/c = 0.05$; all controls at zero; $C_T = 0$; $R = 2.0 \times 10^6$.

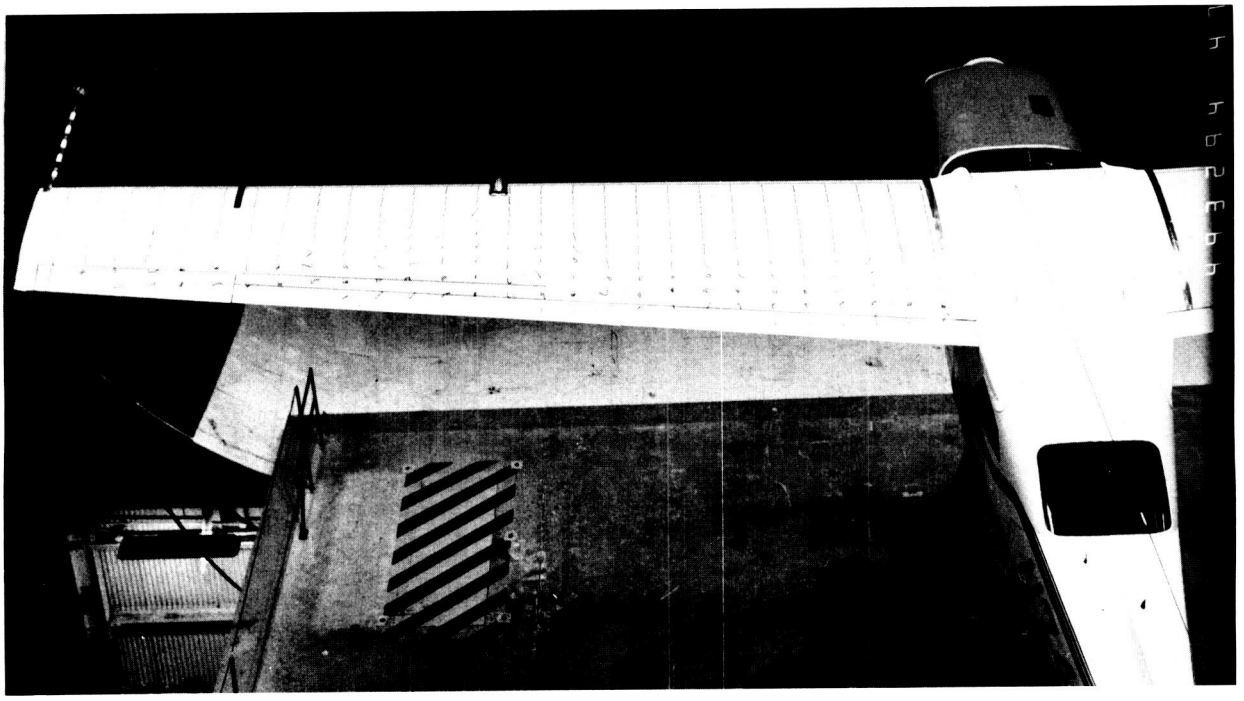

(c) $\alpha = 17°$.

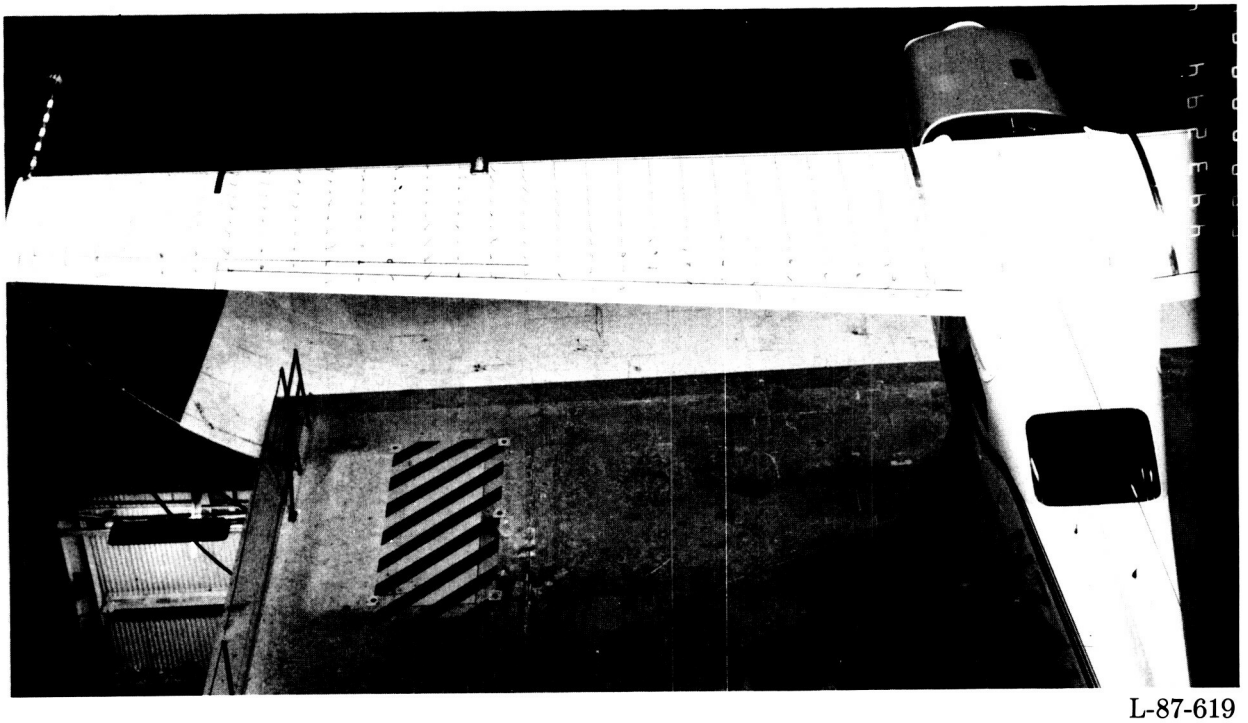

L-87-619

(d) $\alpha = 18°$.

Figure 25. Continued.

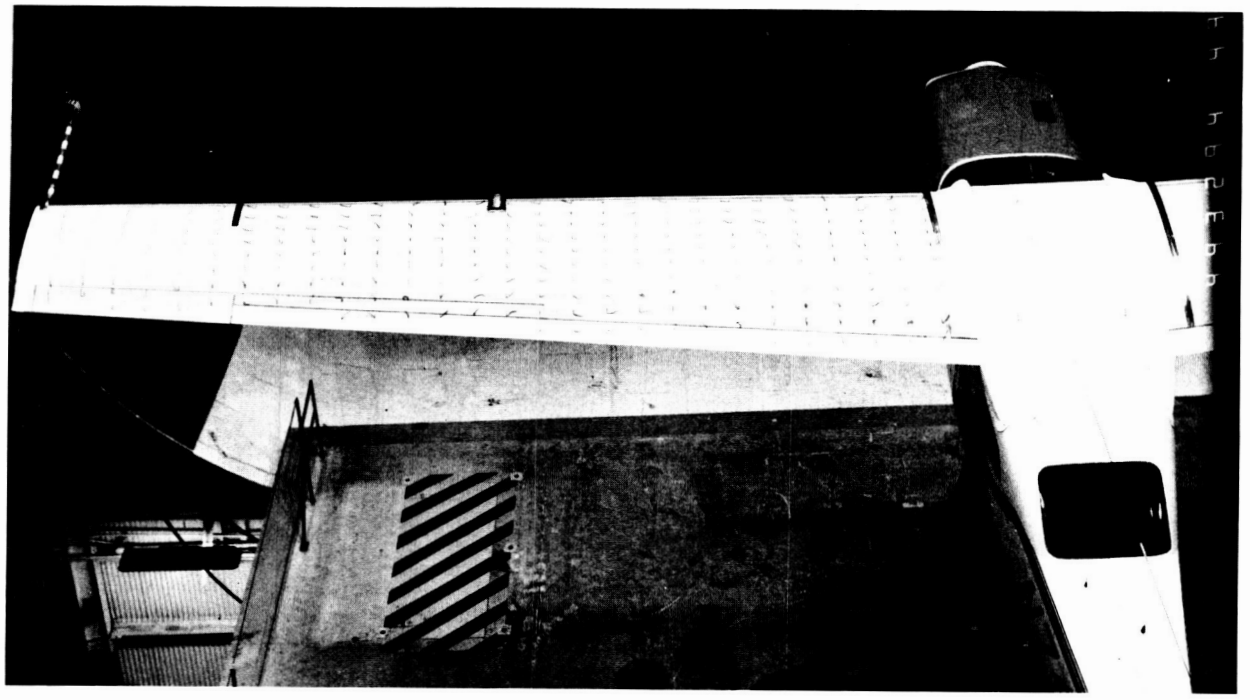

(e) $\alpha = 19°$.

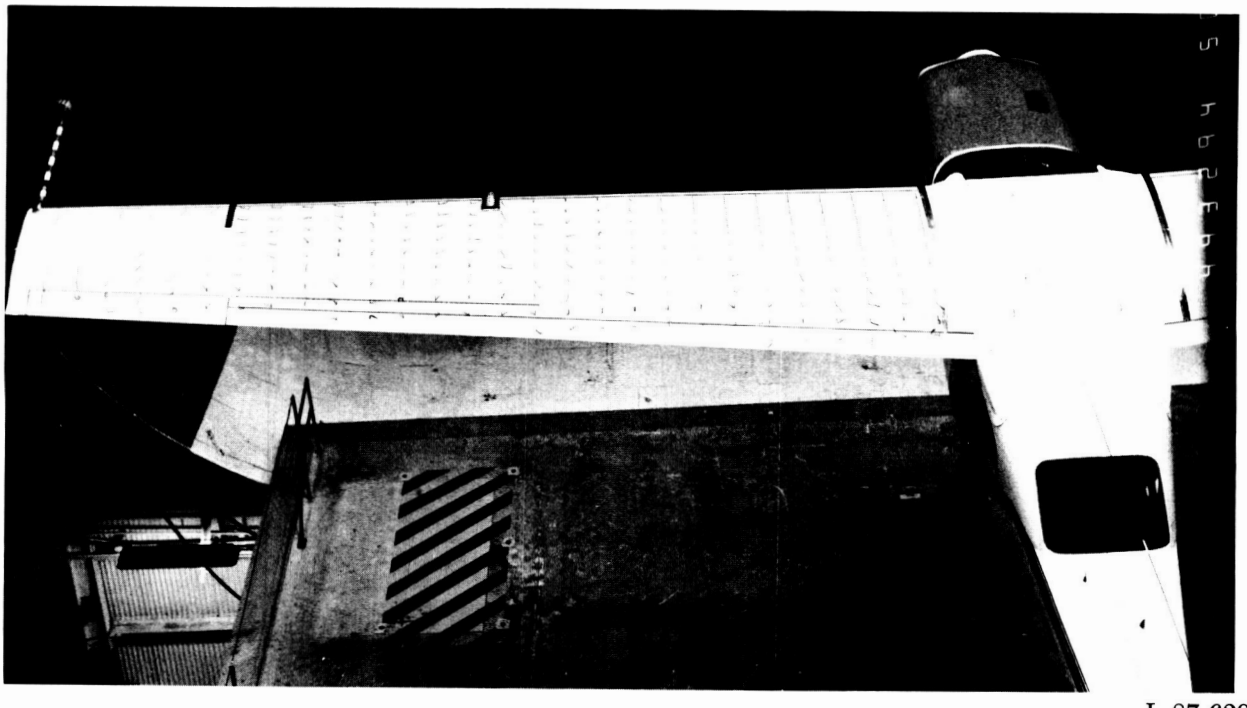

L-87-620

(f) $\alpha = 20°$.

Figure 25. Continued.

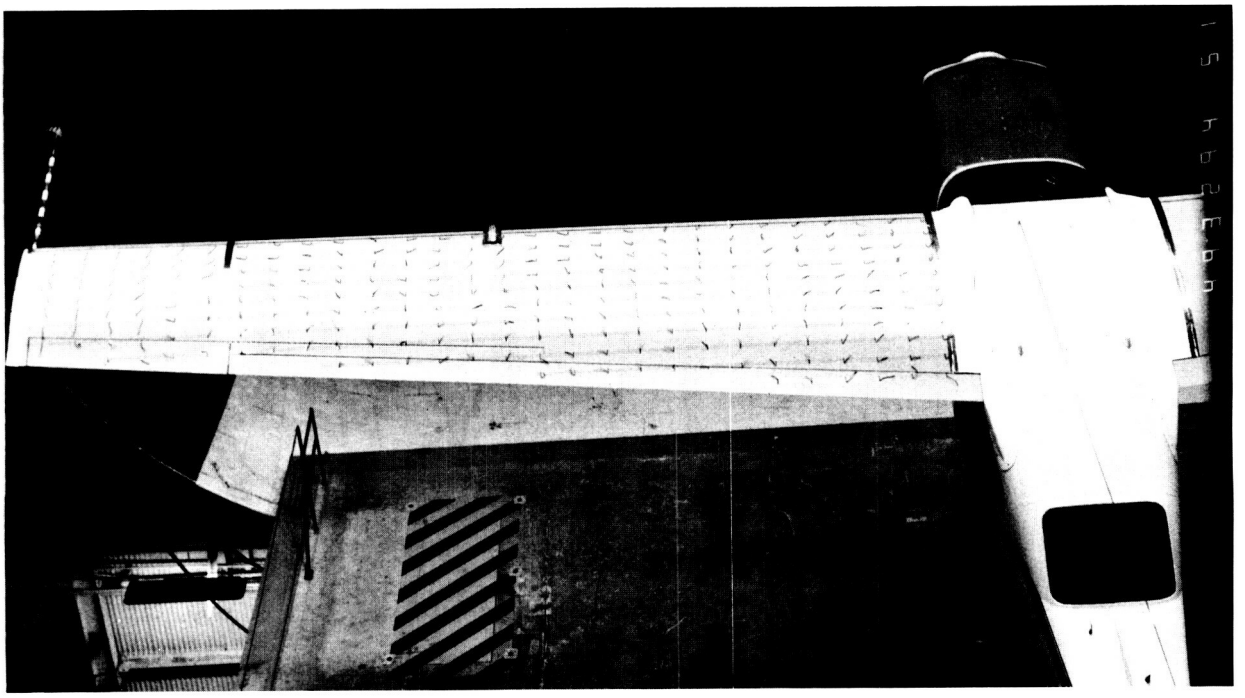

(g) $\alpha = 25°$.

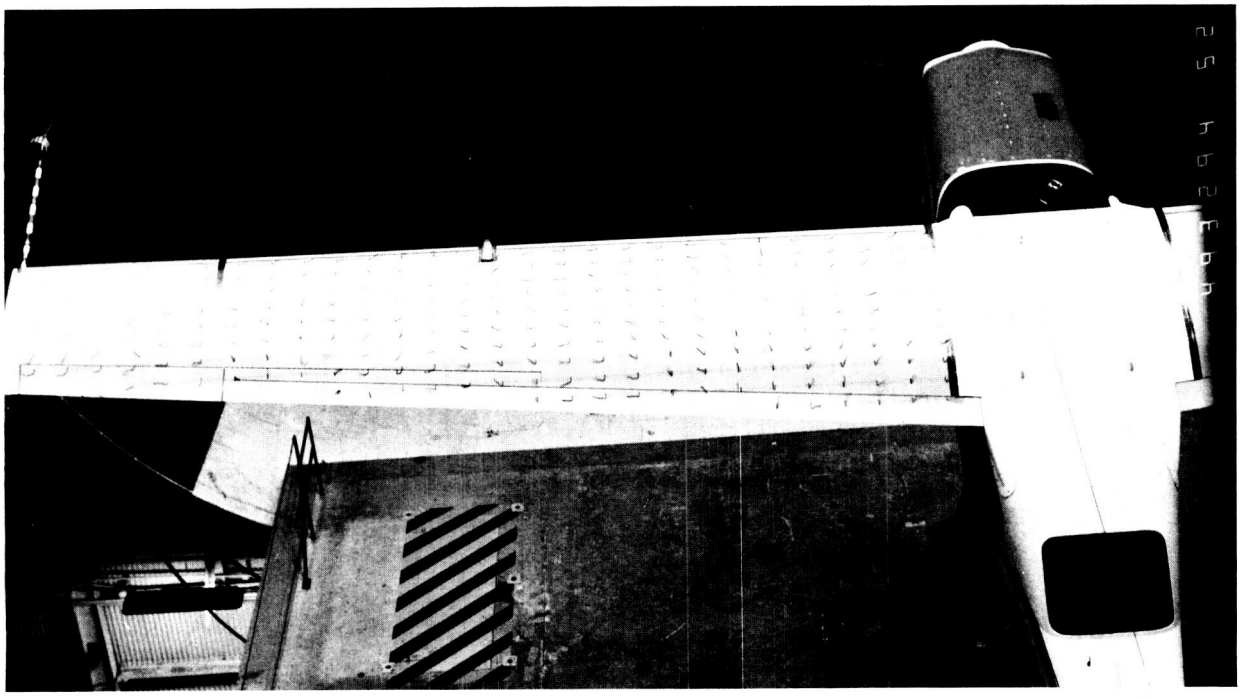

L-87-621

(h) $\alpha = 30°$.

Figure 25. Concluded.

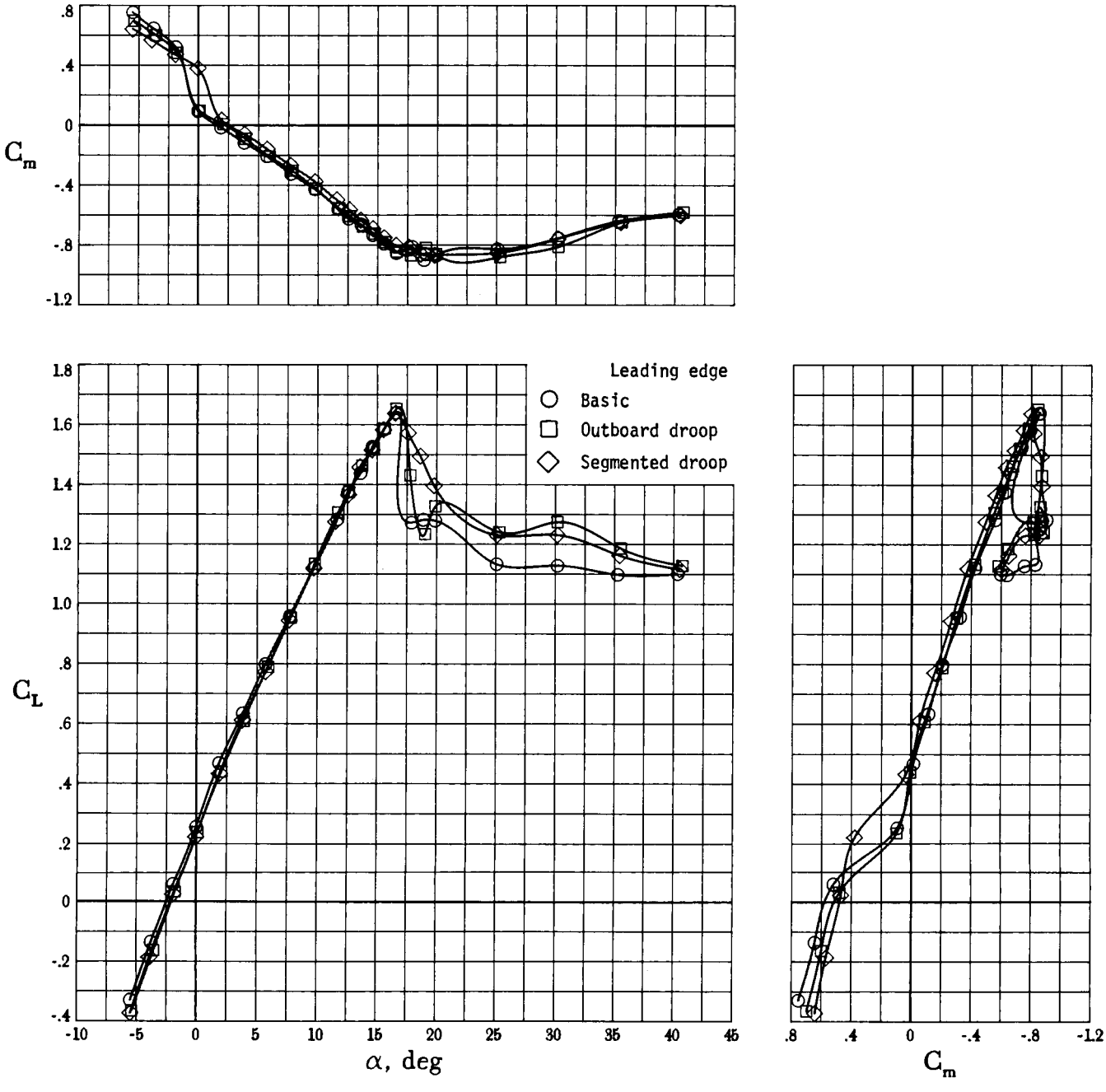


(a) Lift and pitching moment.

Figure 26. Effect of outboard-droop and segmented-droop leading-edge modifications on longitudinal characteristics of basic configuration. All controls at zero; $C_T = 0$; $R = 2.0 \times 10^6$.

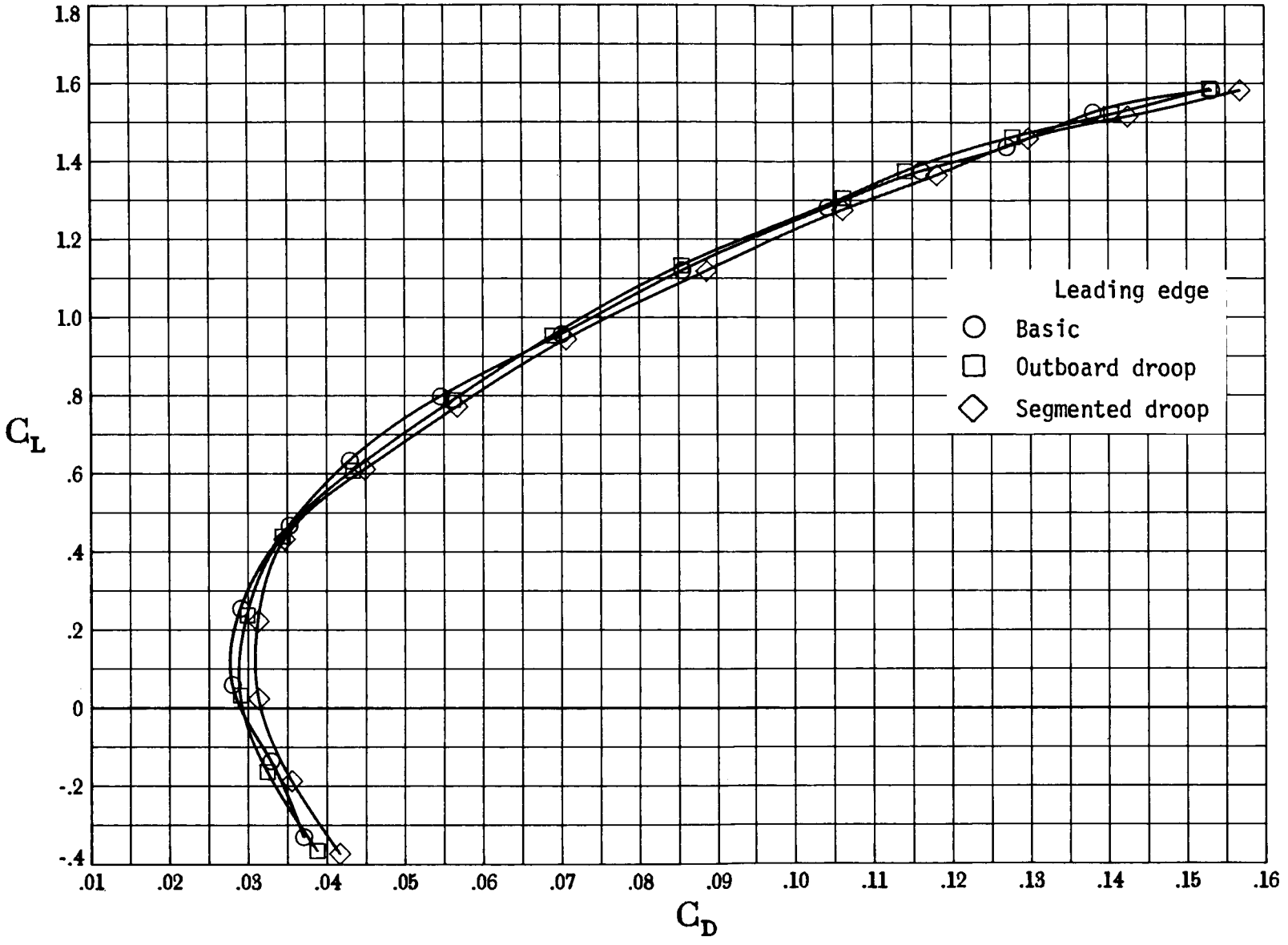


(b) Lift-drag polars.

Figure 26. Concluded.

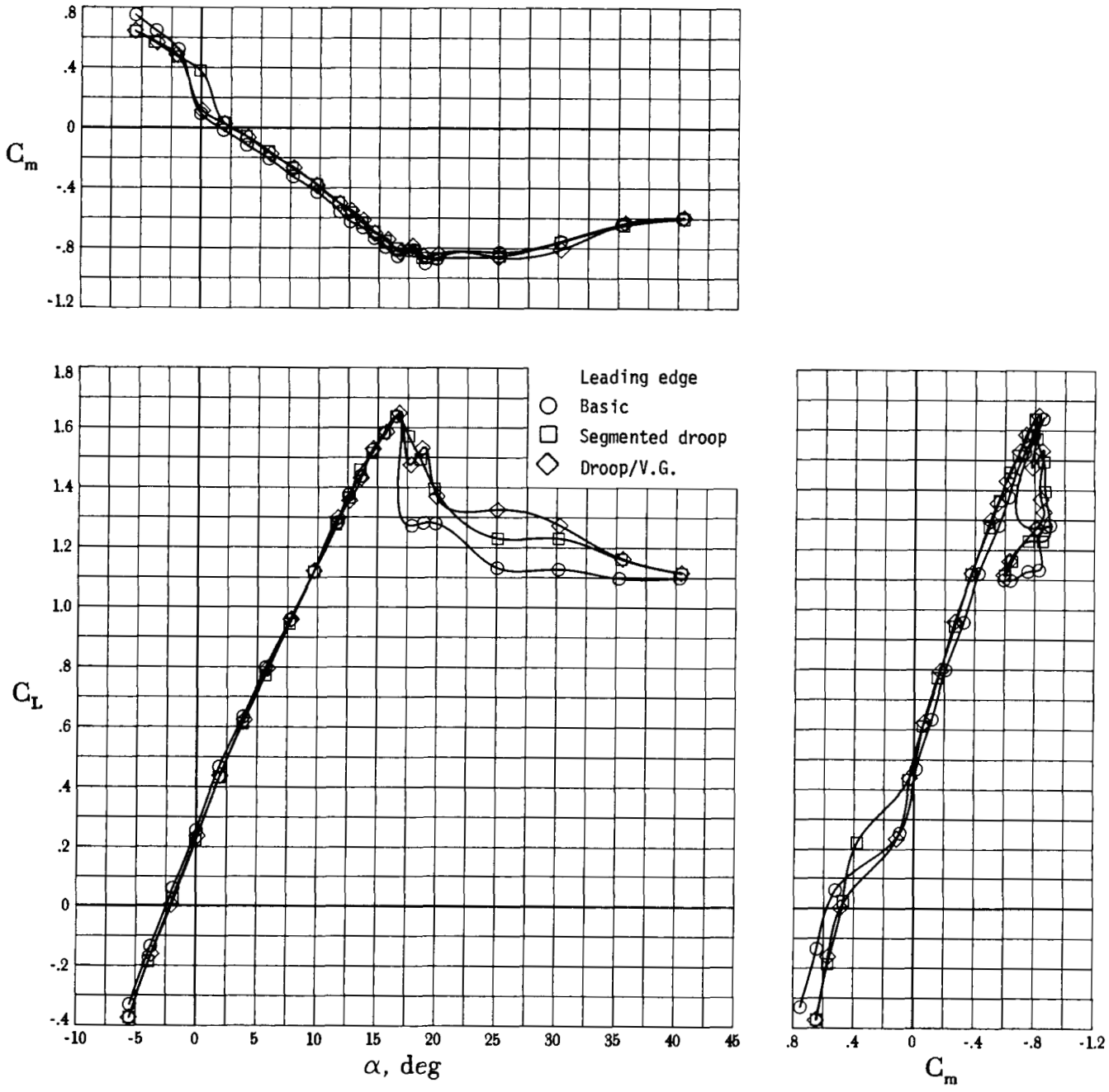


(a) Lift and pitching moment.

Figure 27. Effect of segmented-droop and droop/V.G. leading-edge modifications on longitudinal characteristics of basic configuration. All controls at zero; $C_T = 0$; $R = 2.0 \times 10^6$.

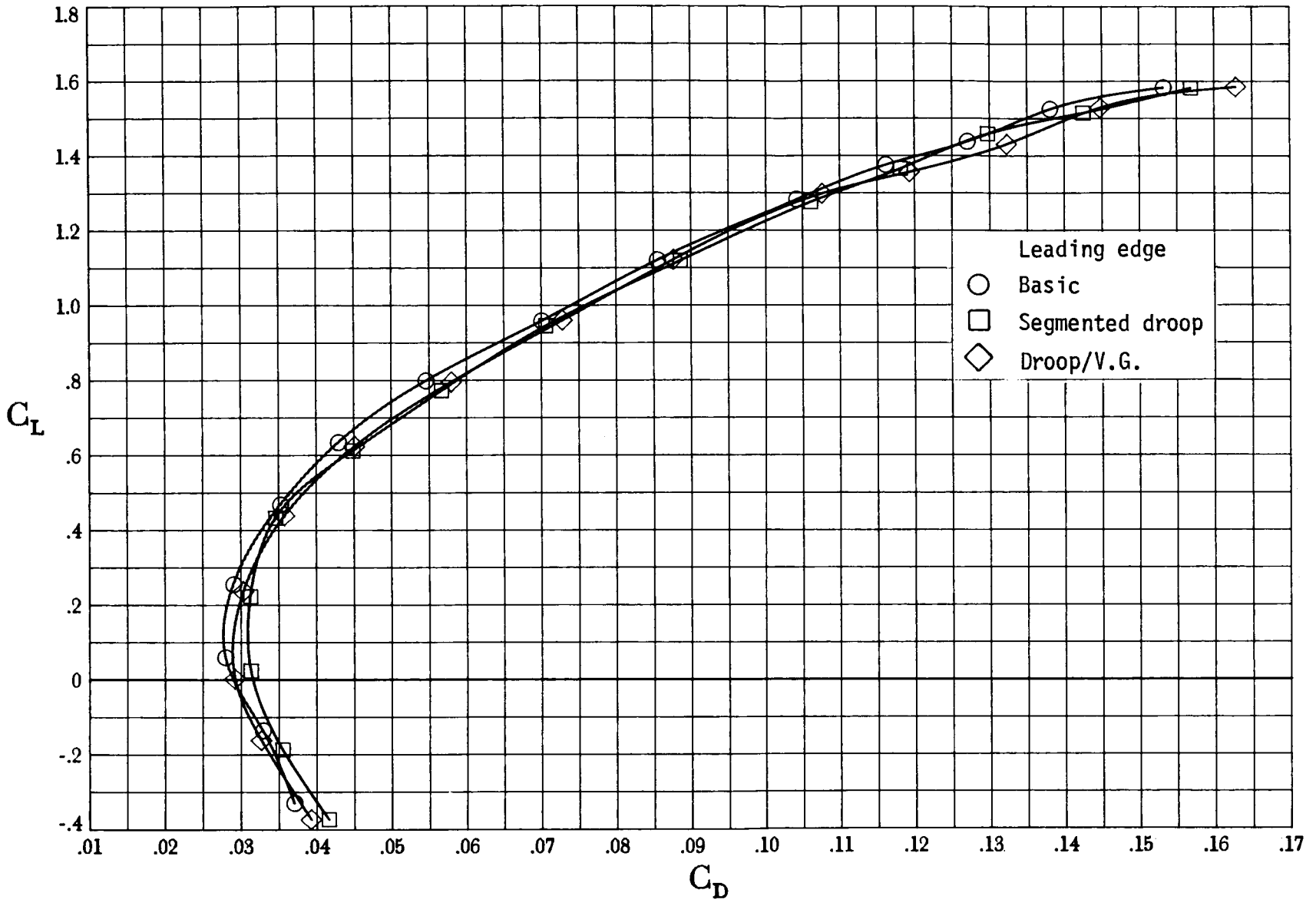


(b) Lift-drag polars.

Figure 27. Concluded.

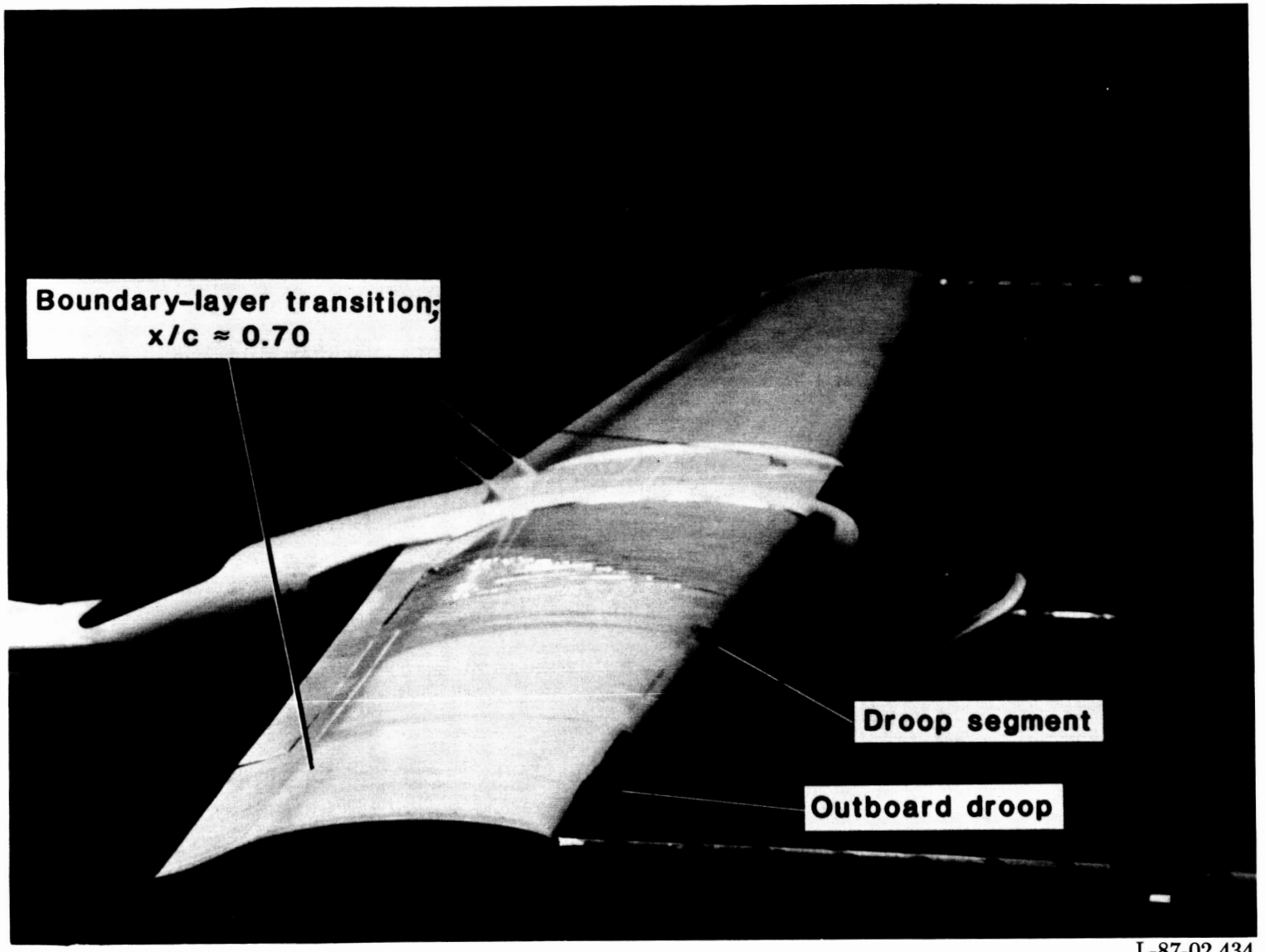


L-87-02,434

Figure 28. Boundary-layer transition characteristics of basic configuration with segmented-droop leading-edge modification at $\alpha = 1°$. All controls at zero; $C_T = 0$; $R = 2.4 \times 10^6$.

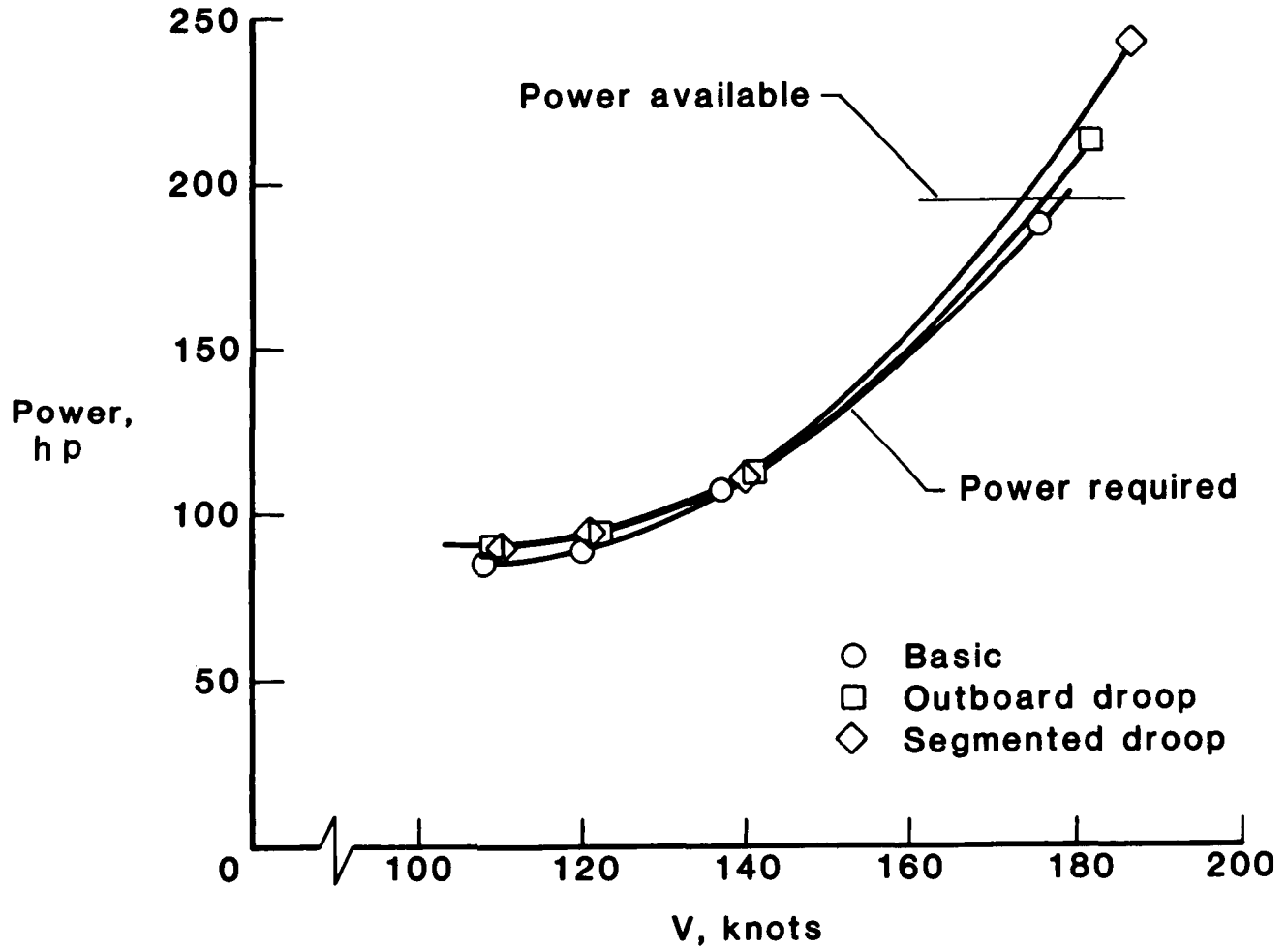


(a) Outboard-droop and segmented-droop leading-edge modifications.

Figure 29. Effect of leading-edge modifications on calculated cruise performance of basic configuration. $h = 10\,000$ ft; $W = 3500$ lb; Power = 75 percent; $\eta = 0.80$; Propeller $\Delta C_D = -0.0015$. Results based on trimmed lift and drag calculated from tests with $C_T = 0$ and $R = 2.0 \times 10^6$.

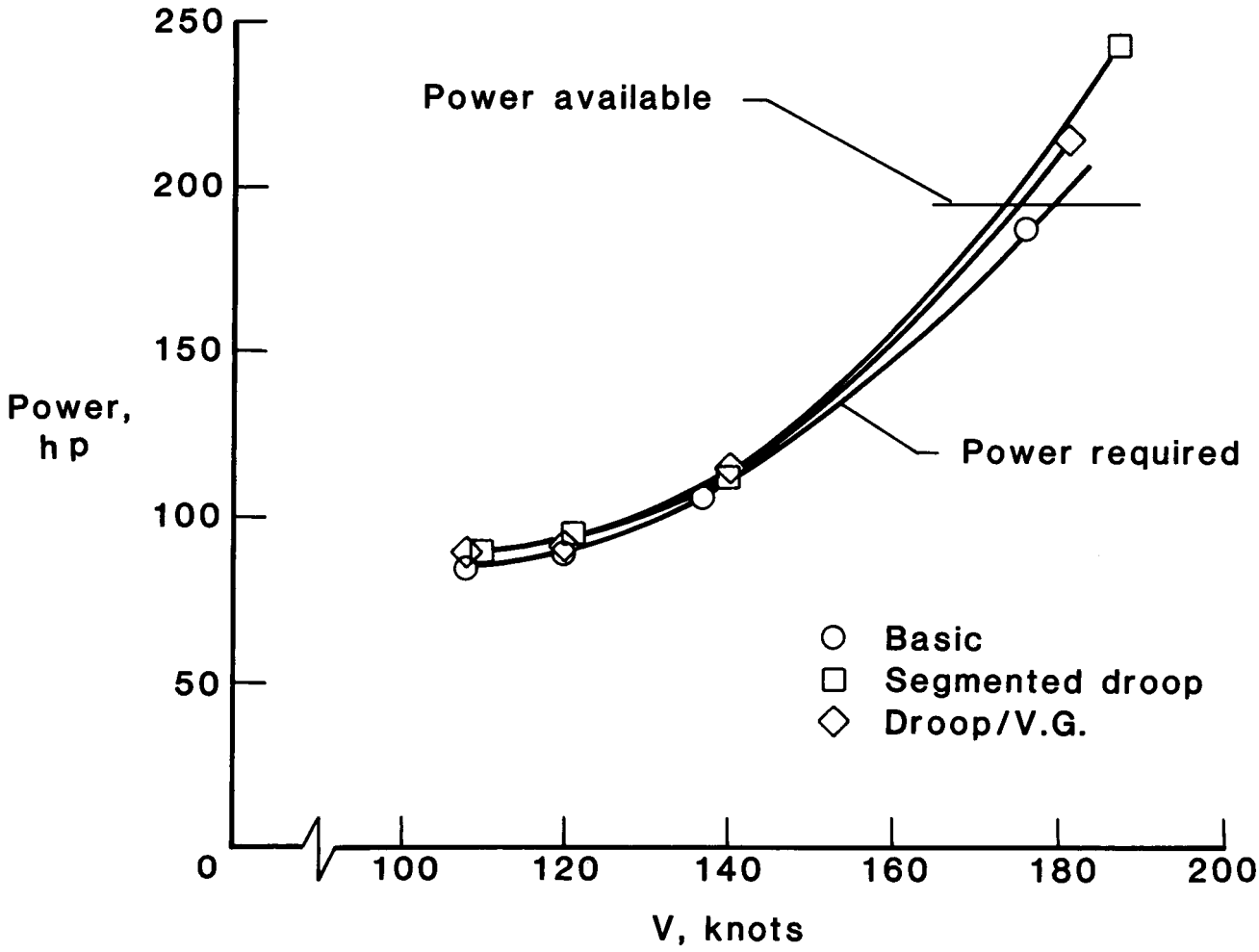


(b) Segmented-droop and droop/V.G. leading-edge modifications.

Figure 29. Concluded.

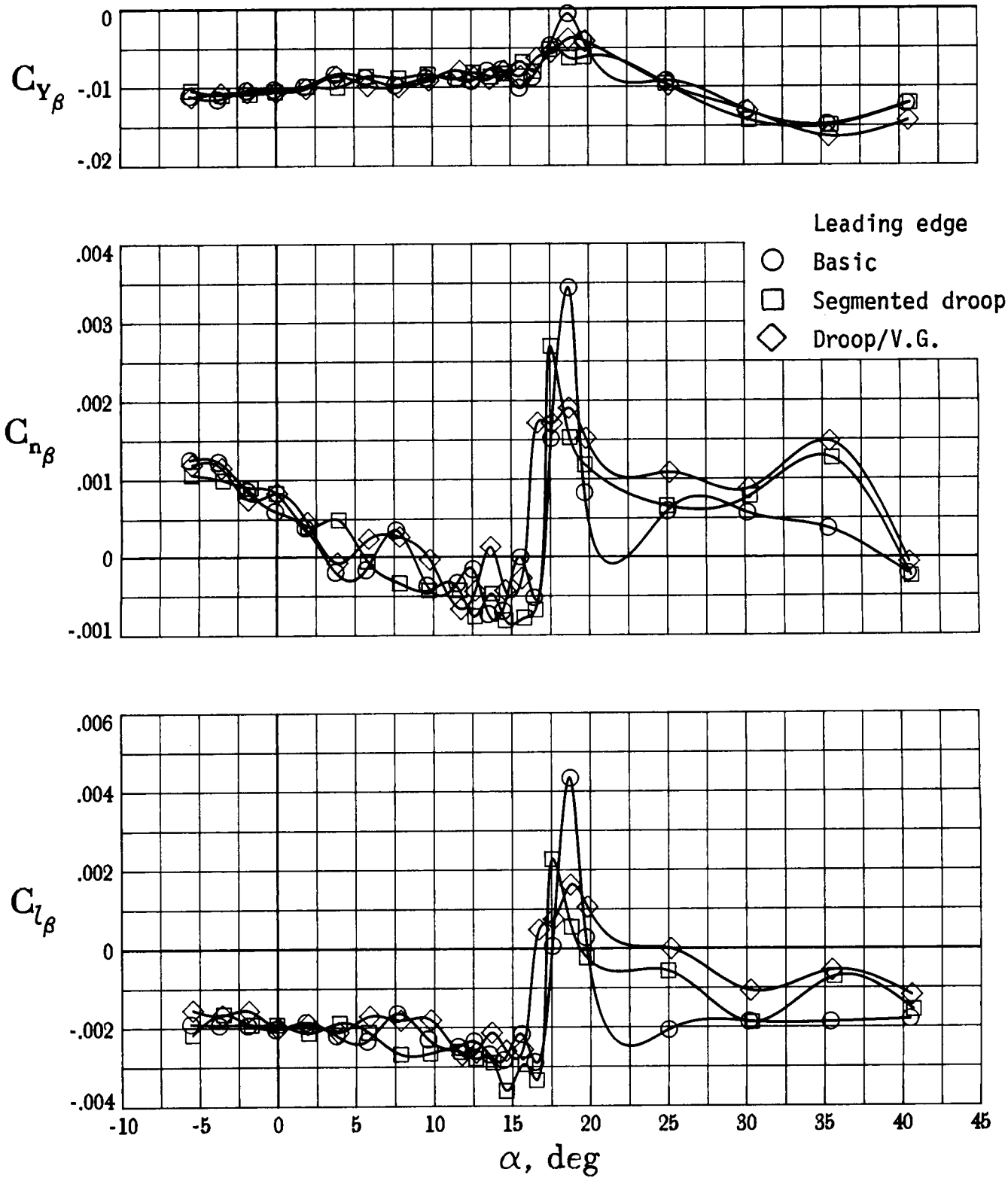


Figure 30. Effect of leading-edge modifications on lateral-directional stability characteristics of basic configuration. All controls at zero; $C_T = 0$; $R = 2.0 \times 10^6$.

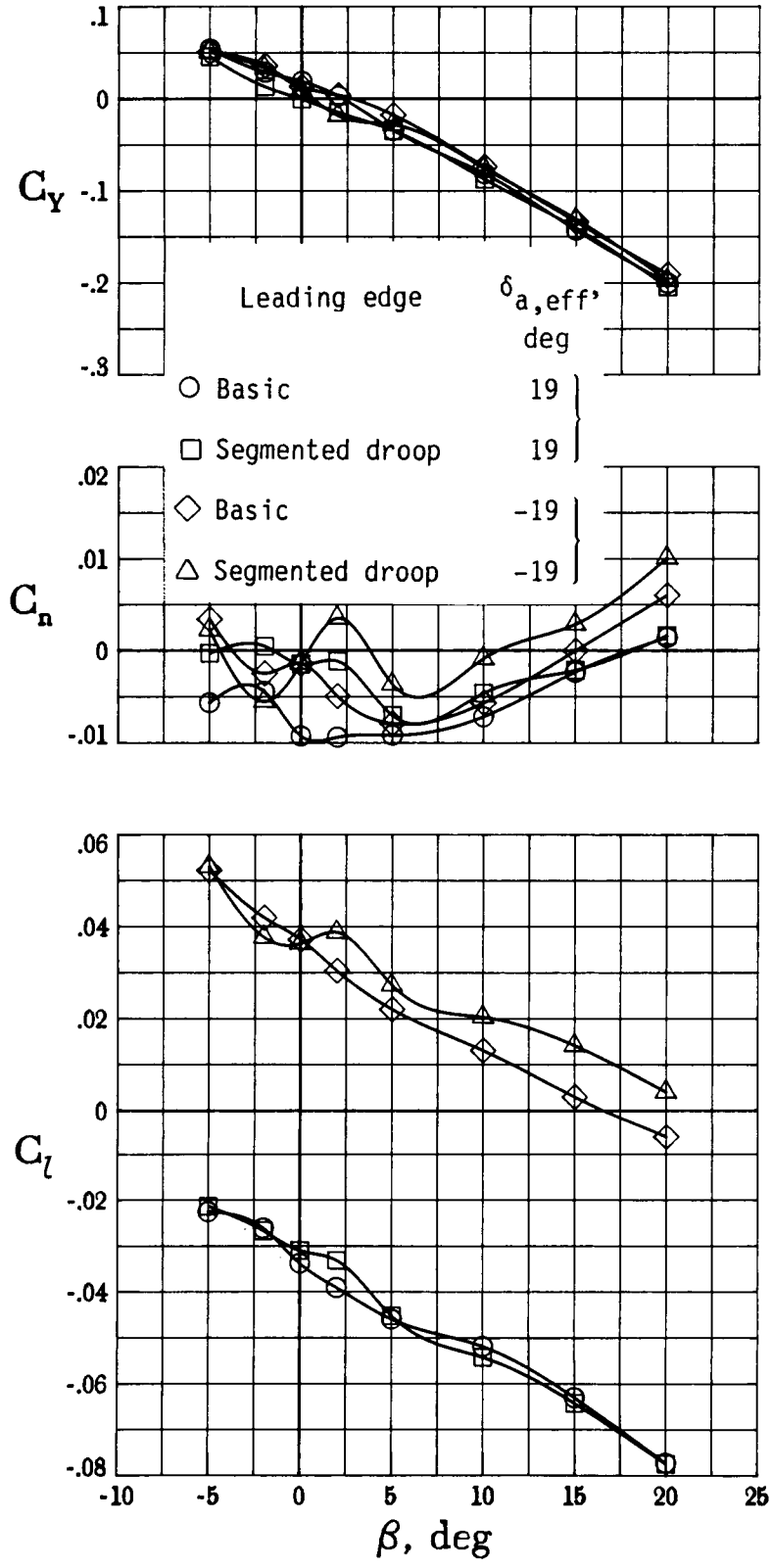


Figure 31. Effect of leading-edge modifications on combined aileron and spoiler characteristics of basic configuration at $\alpha = 15°$. All other controls at zero; $C_T = 0$; $R = 2.0 \times 10^6$.

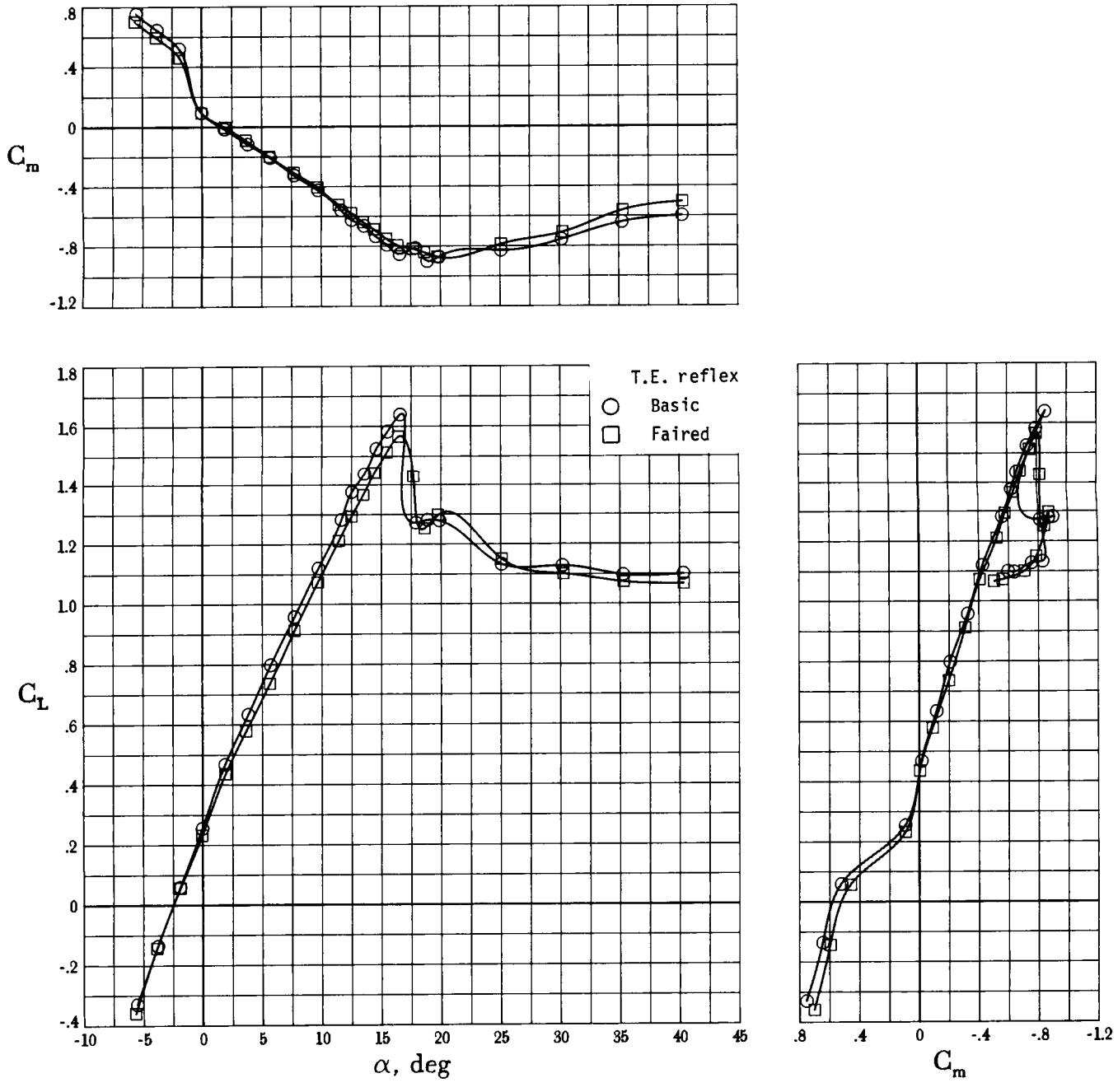


(a) Lift and pitching moment.

Figure 32. Effect of fairing trailing-edge reflex on longitudinal characteristics of basic configuration. All controls at zero; $C_T = 0$; $R = 2.0 \times 10^6$.

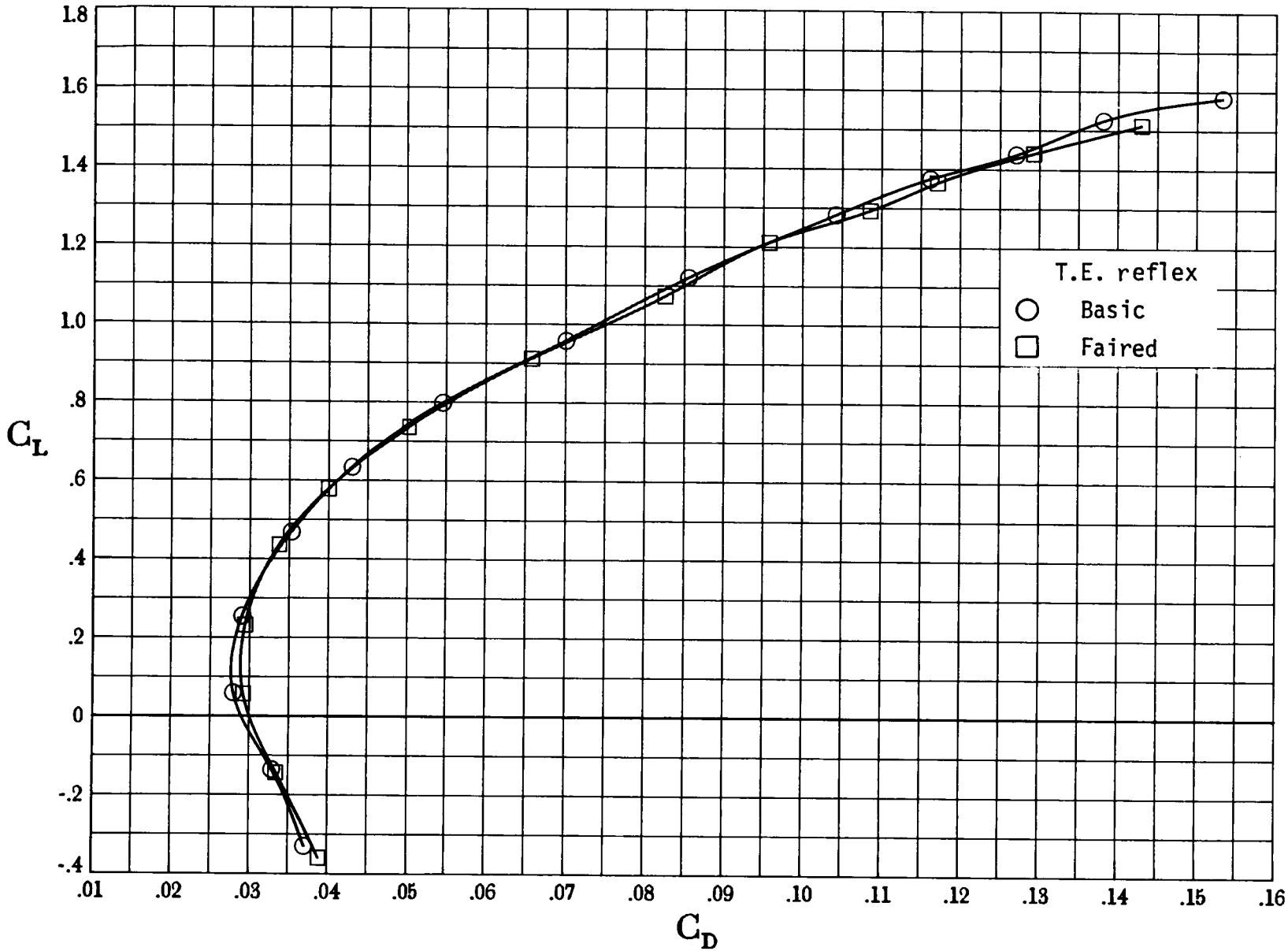


(b) Lift-drag polars.

Figure 32. Concluded.

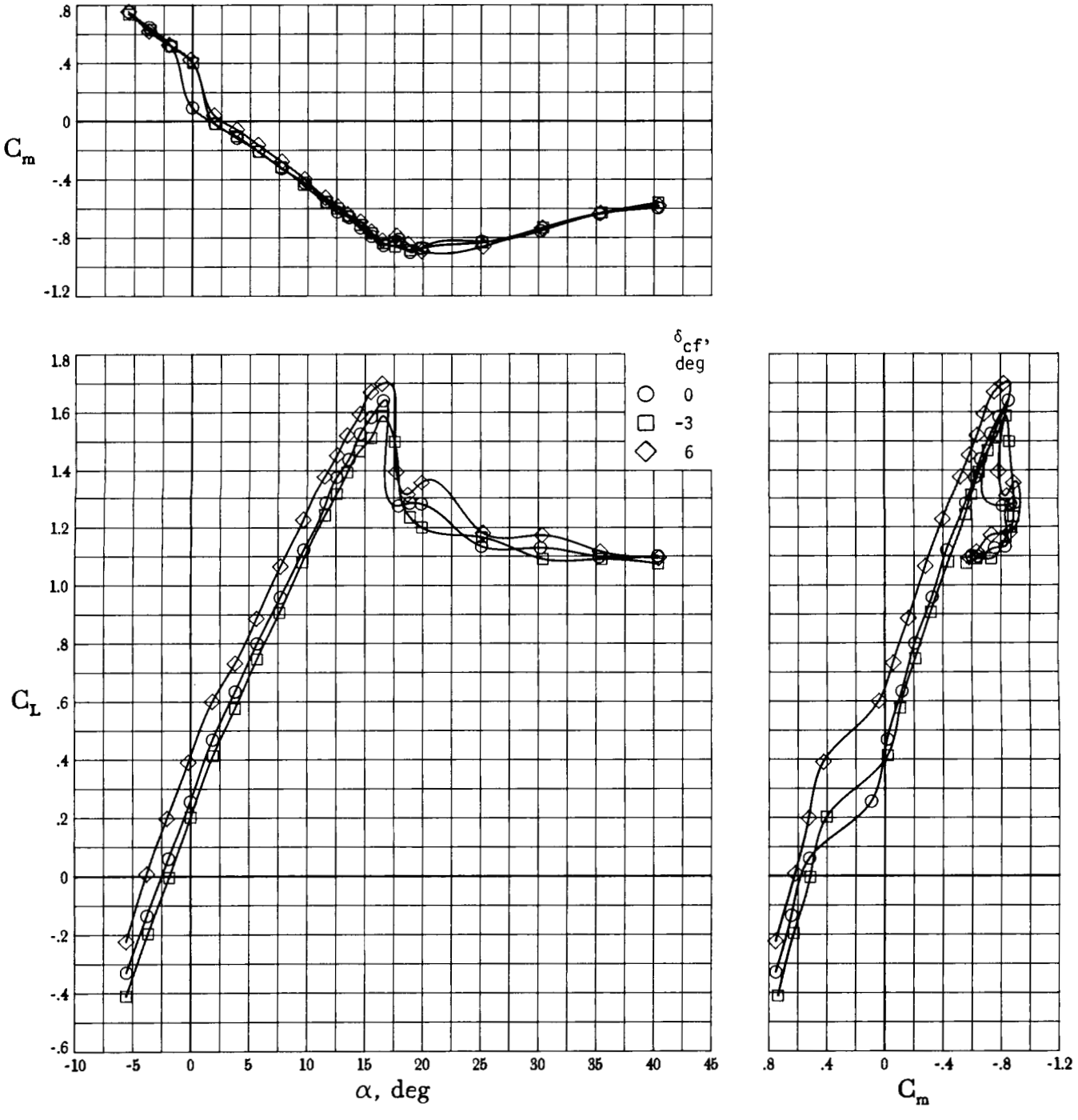


(a) Lift and pitching moment with small flap deflections.

Figure 33. Effect of cruise flap deflections on longitudinal characteristics of basic configuration. All other controls at zero; $C_T = 0$; $R = 2.0 \times 10^6$.

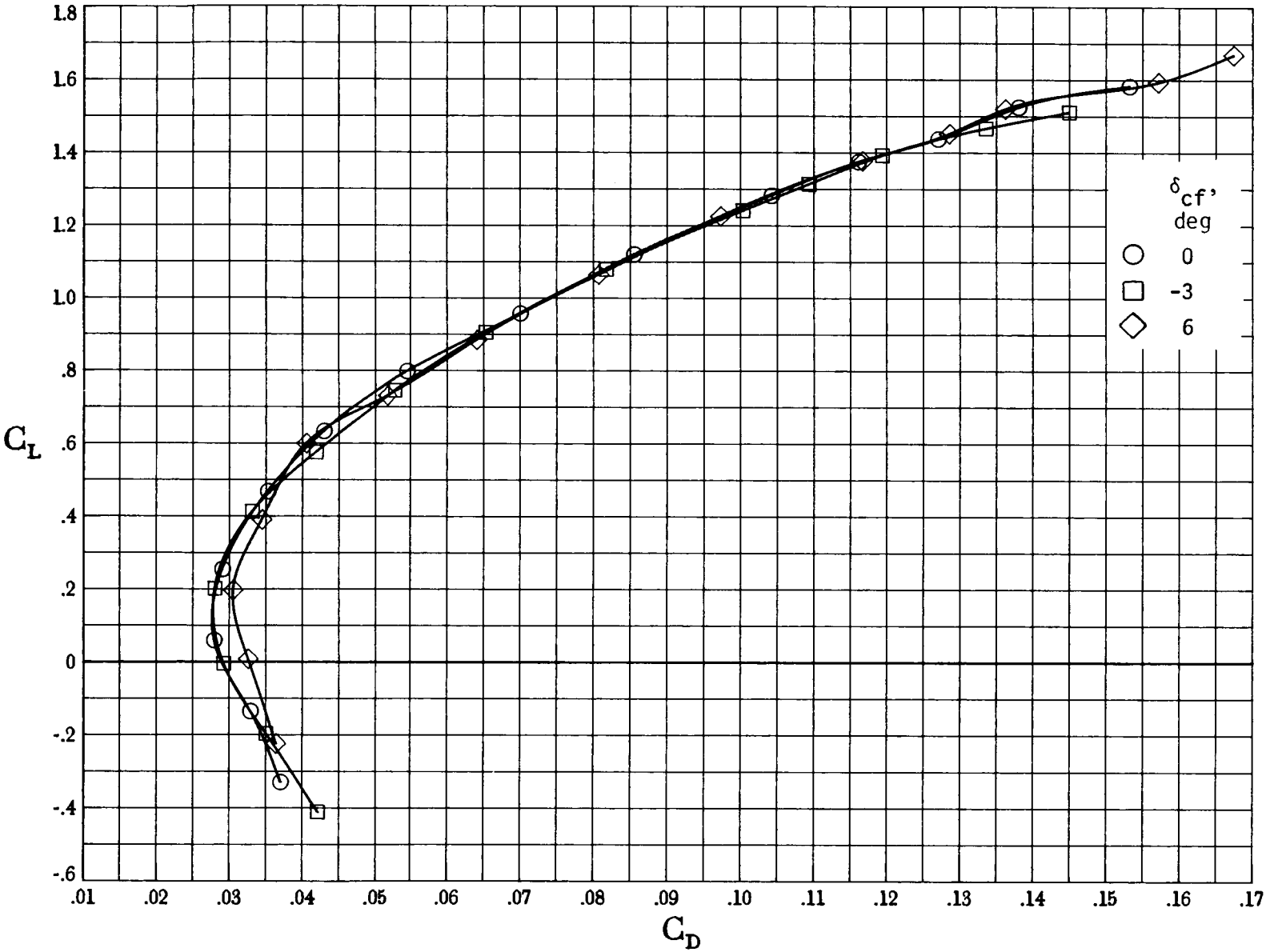


(b) Lift-drag polars with small flap deflections.

Figure 33. Continued.

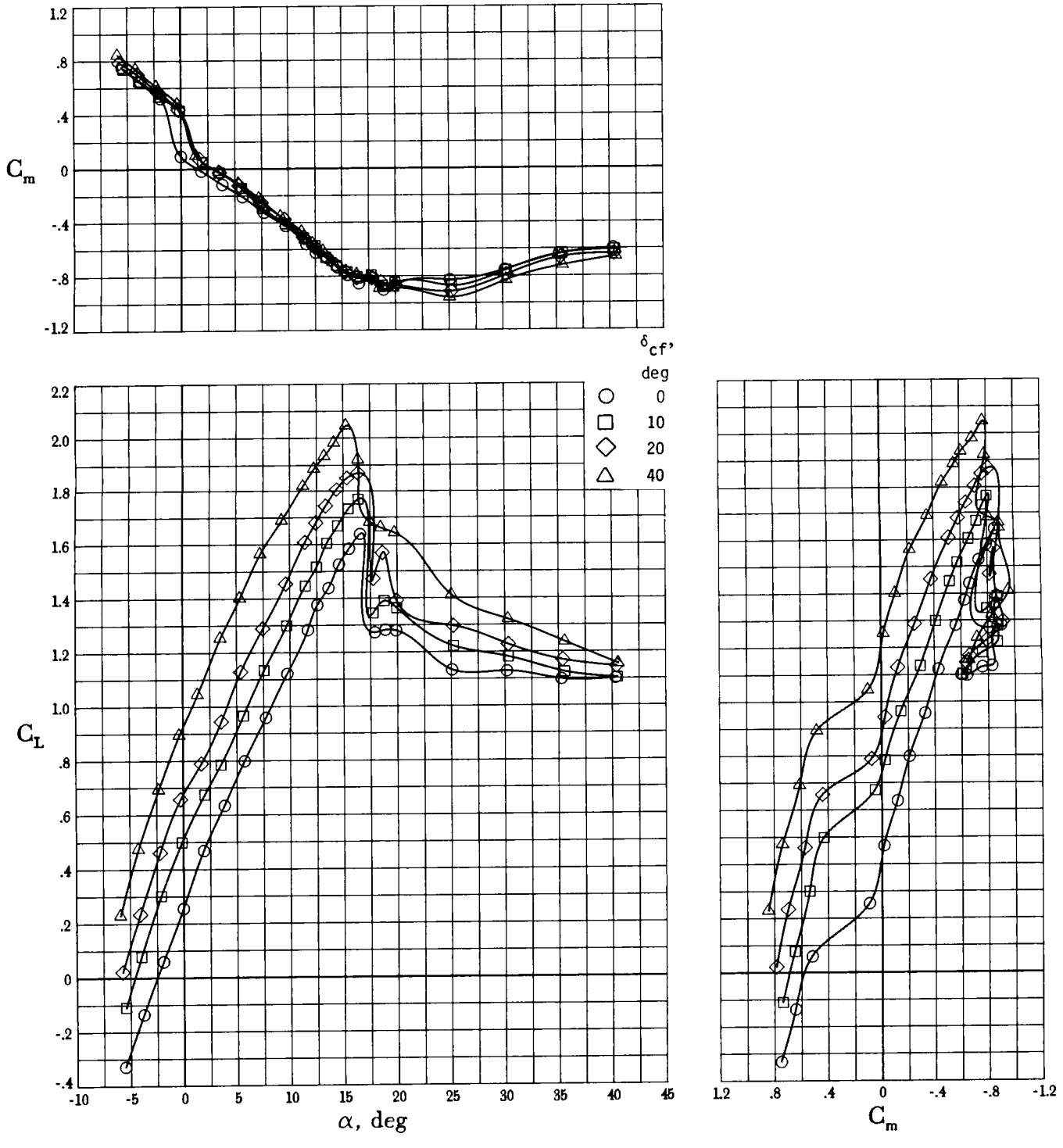


(c) Lift and pitching moment with large flap deflections.

Figure 33. Continued.

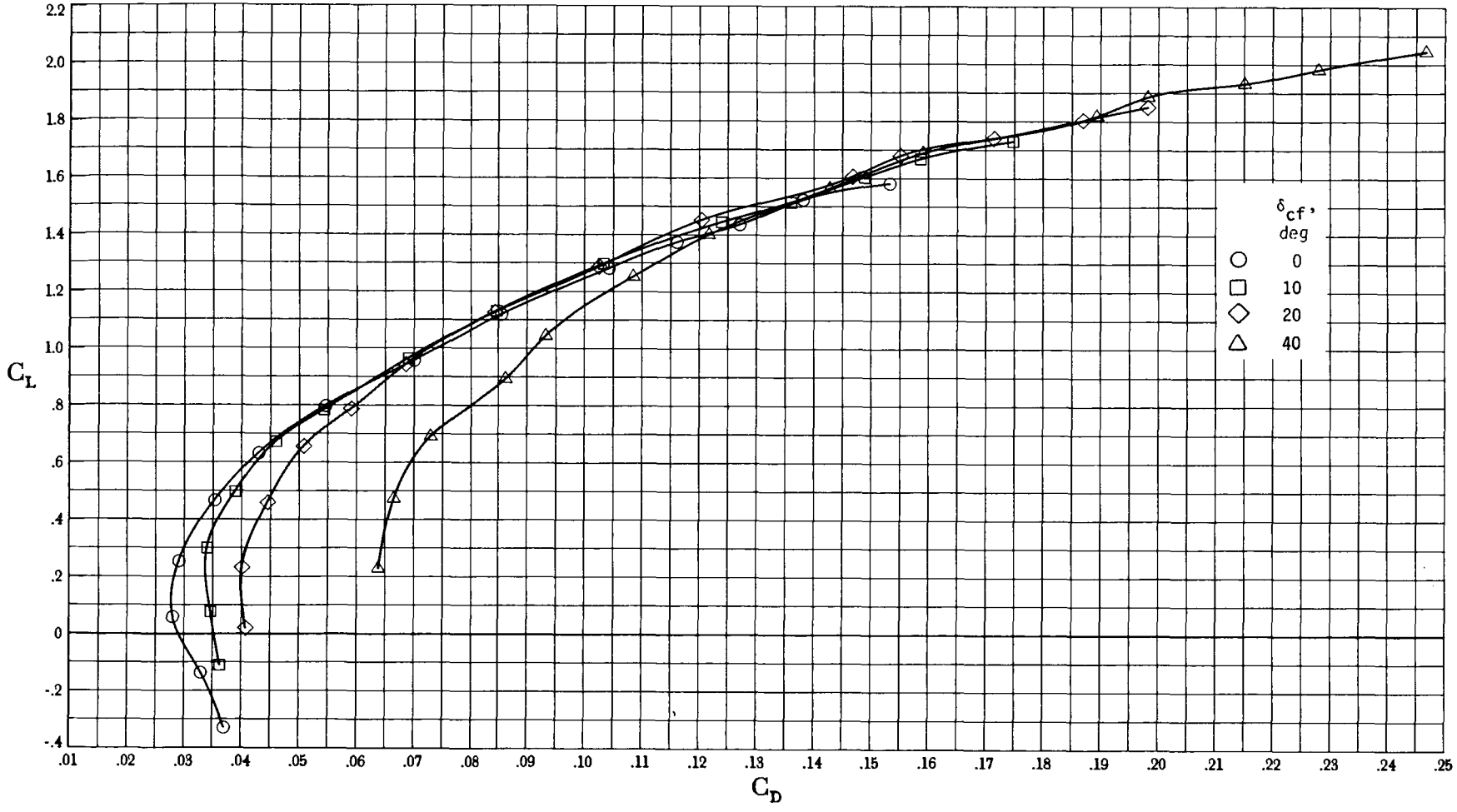


(d) Lift-drag polars with large flap deflections.

Figure 33. Concluded.

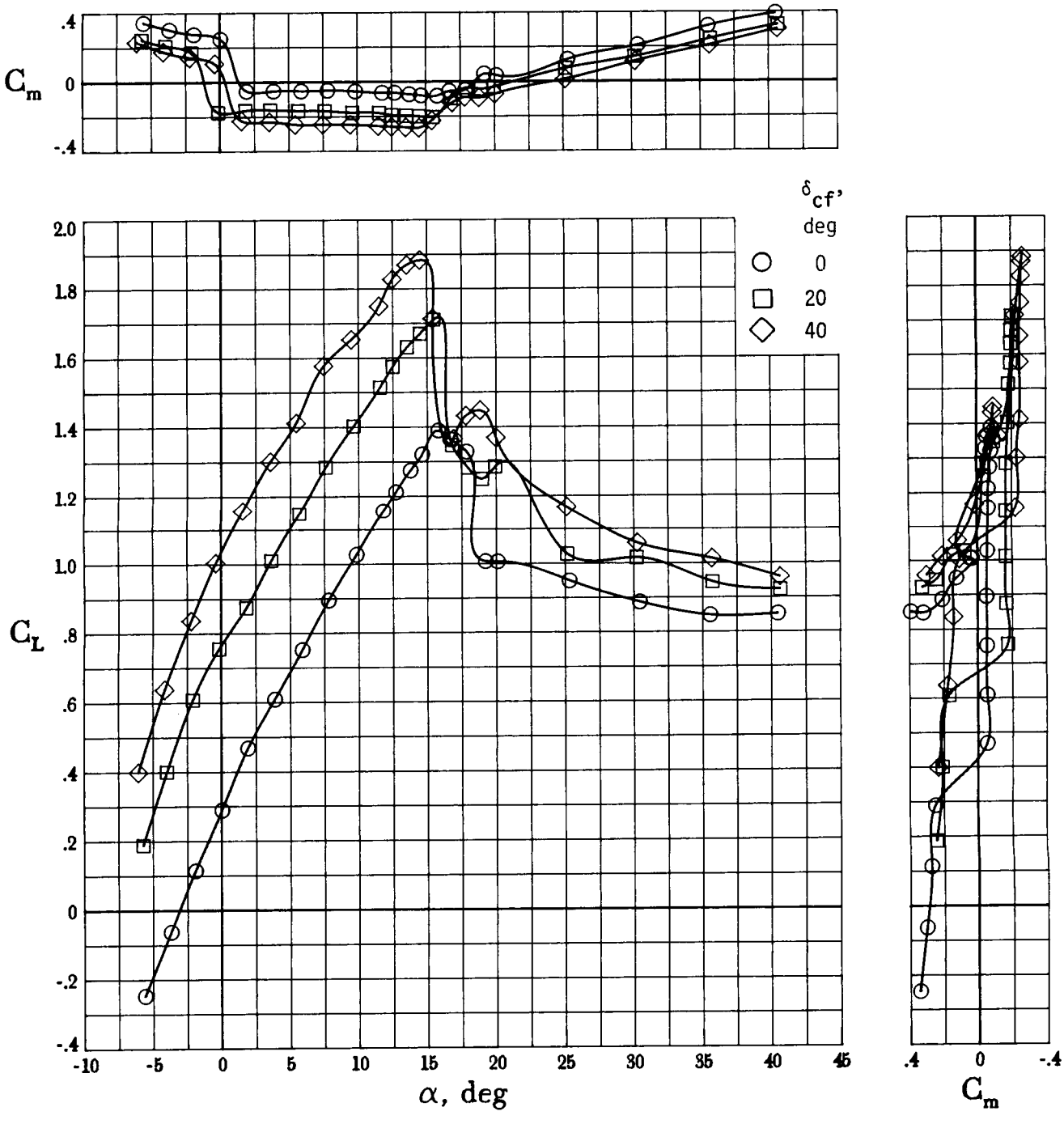


(a) Lift and pitching moment.

Figure 34. Effect of cruise flap deflections on longitudinal characteristics of basic configuration with engine cowl faired, propeller off, and horizontal and vertical tails removed. All other controls at zero; $C_T = 0$; $R = 2.0 \times 10^6$.



C-2

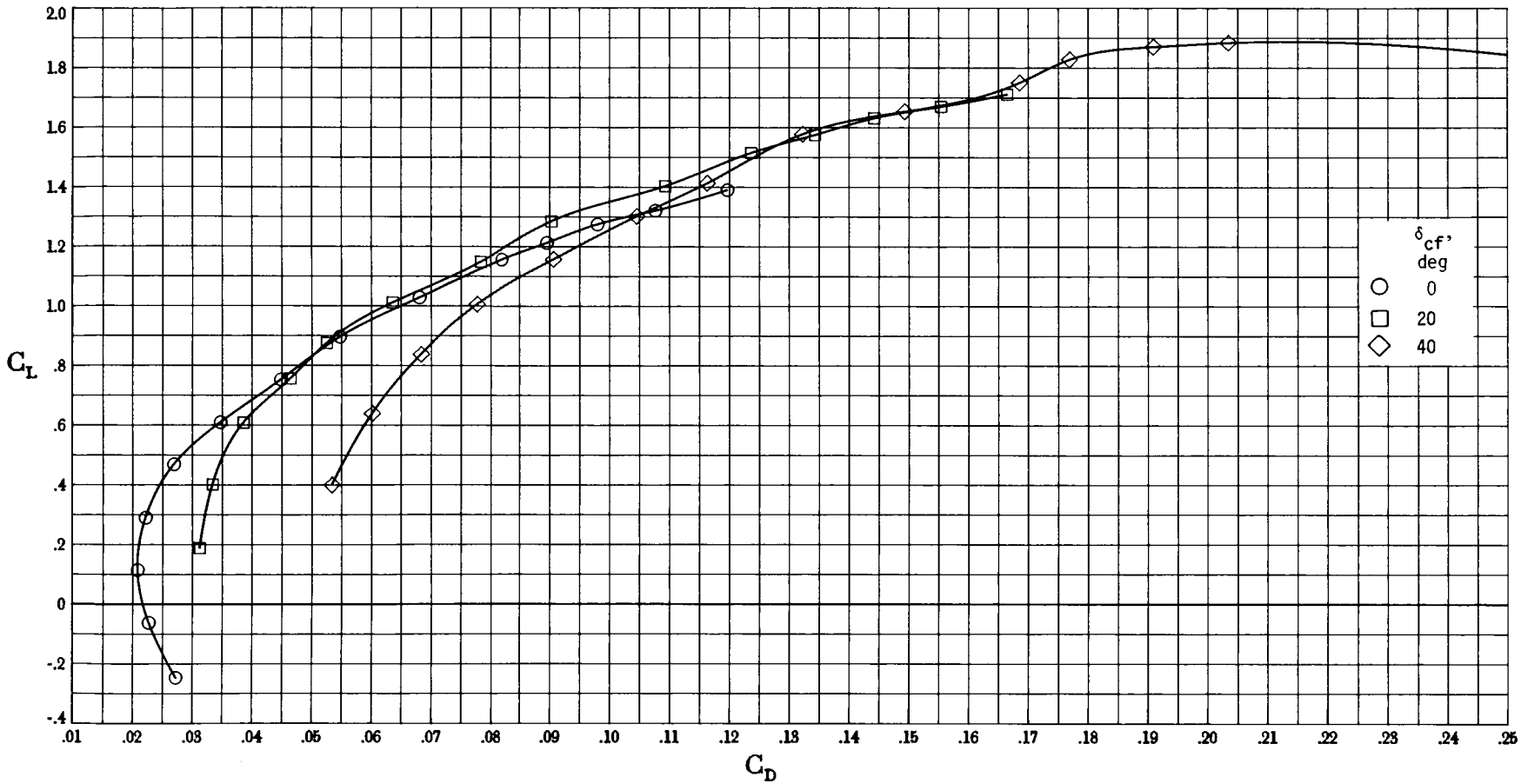


(b) Lift-drag polars.

Figure 34. Concluded.

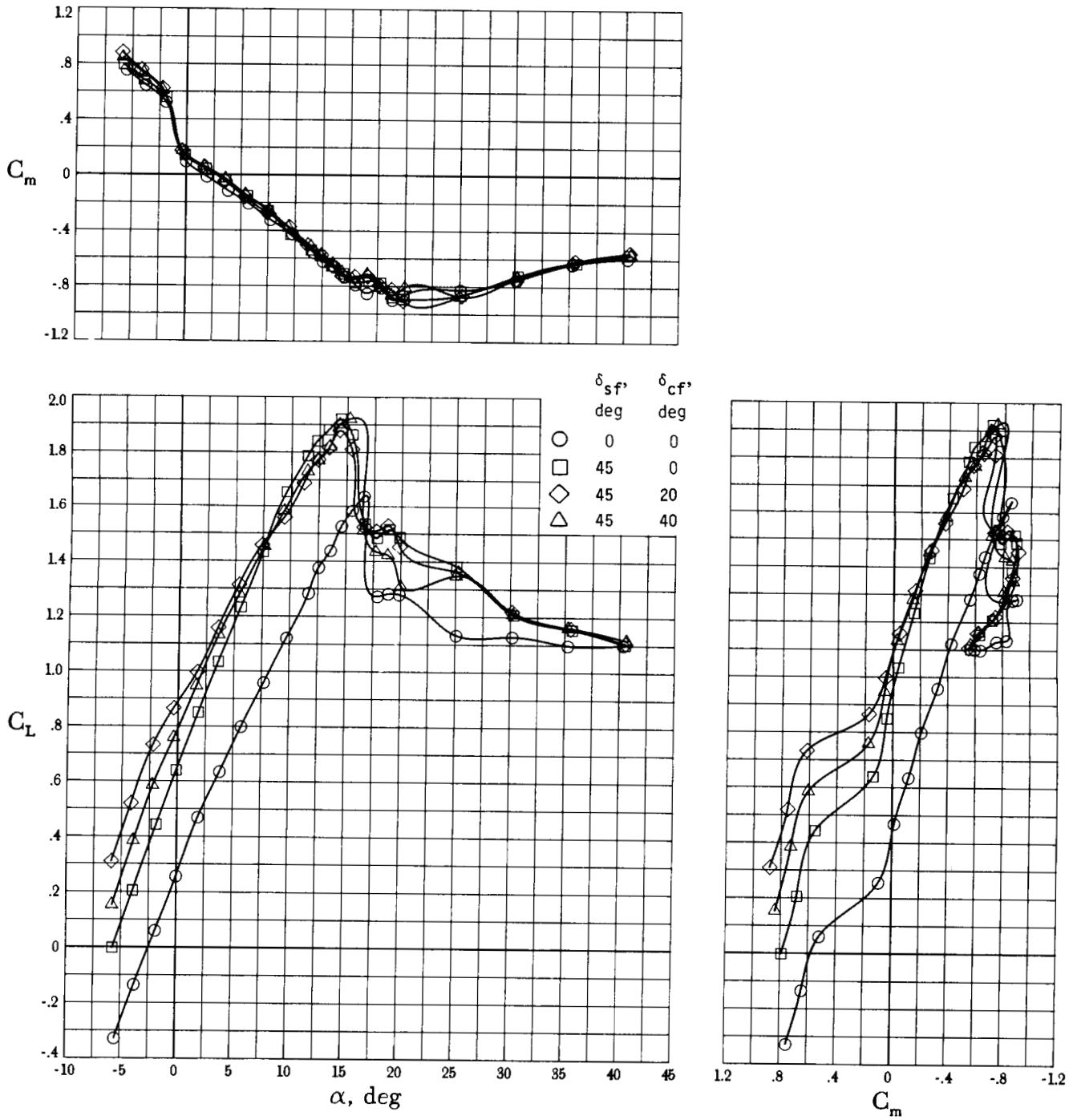


(a) Lift and pitching moment.

Figure 35. Effect of combined split flap and cruise flap deflections on longitudinal characteristics of basic configuration. All other controls at zero; $C_T = 0$; $R = 2.0 \times 10^6$.

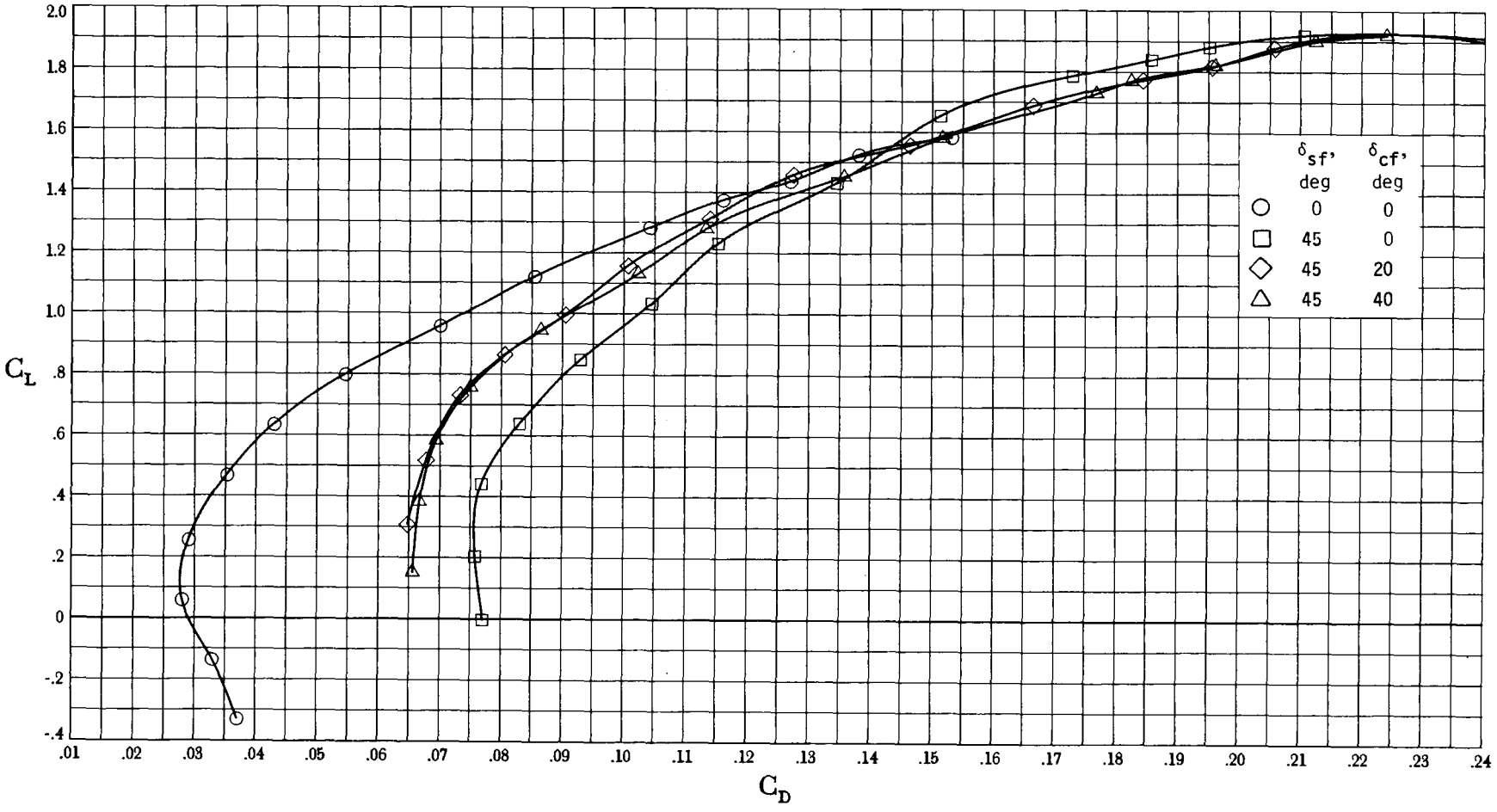


(b) Lift-drag polars.

Figure 35. Concluded.

(a) $\alpha = 15°$.

L-87-622

(b) $\alpha = 16°$.

Figure 36. Tuft flow-visualization photographs of basic configuration with $\delta_{cf} = 40°$. Transition fixed at $x/c = 0.05$; all other controls at zero; $C_T = 0$; $R = 2.0 \times 10^6$.

(c) $\alpha = 17°$.

L-87-623

(d) $\alpha = 18°$.

Figure 36. Concluded.

(a) $\alpha = 15°$.

L-87-624

(b) $\alpha = 16°$.

Figure 37. Tuft flow-visualization photographs of basic configuration with outboard-droop leading-edge modification and $\delta_{cf} = 40°$. Transition fixed at $x/c = 0.05$; all other controls at zero; $C_T = 0$; $R = 2.0 \times 10^6$.

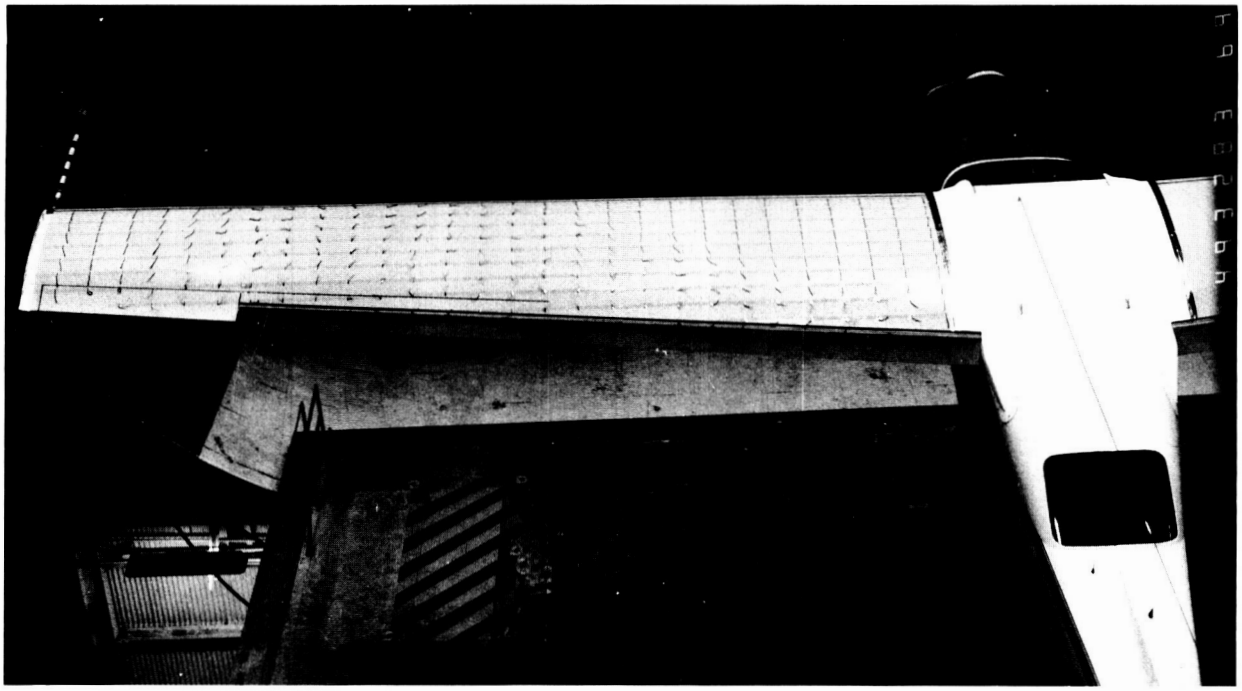

(c) $\alpha = 17°$.

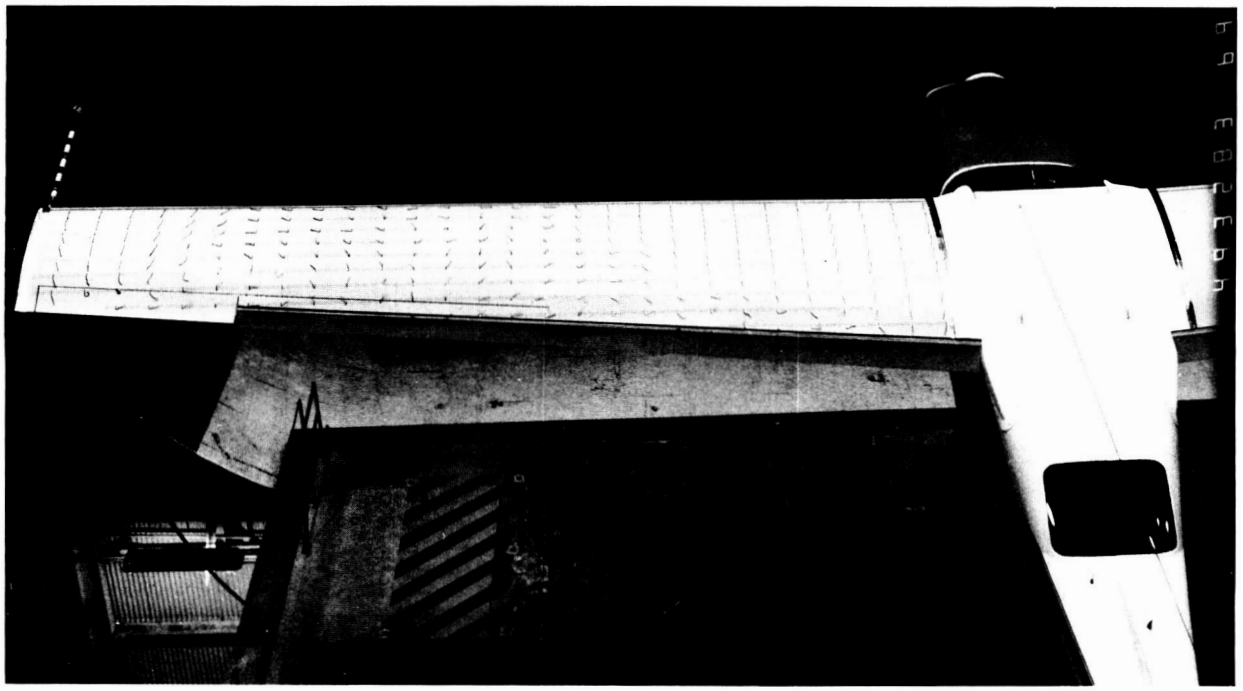

L-87-625

(d) $\alpha = 18°$.

Figure 37. Continued.

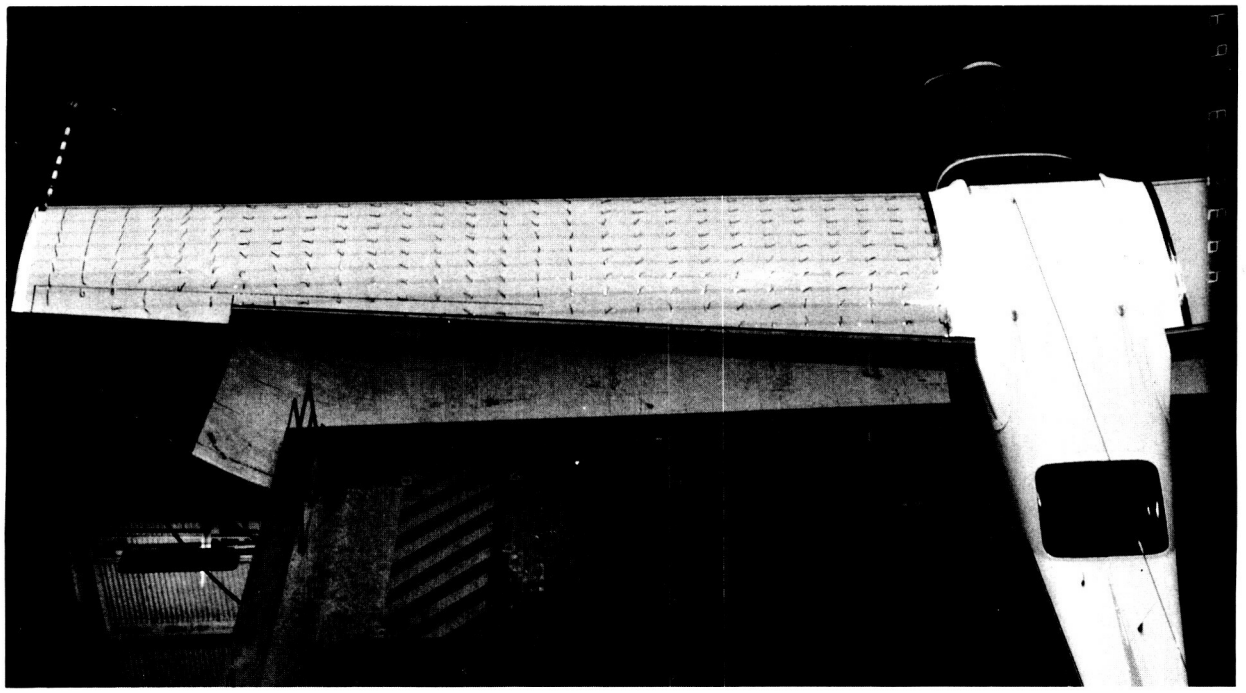

(e) $\alpha = 19°$.

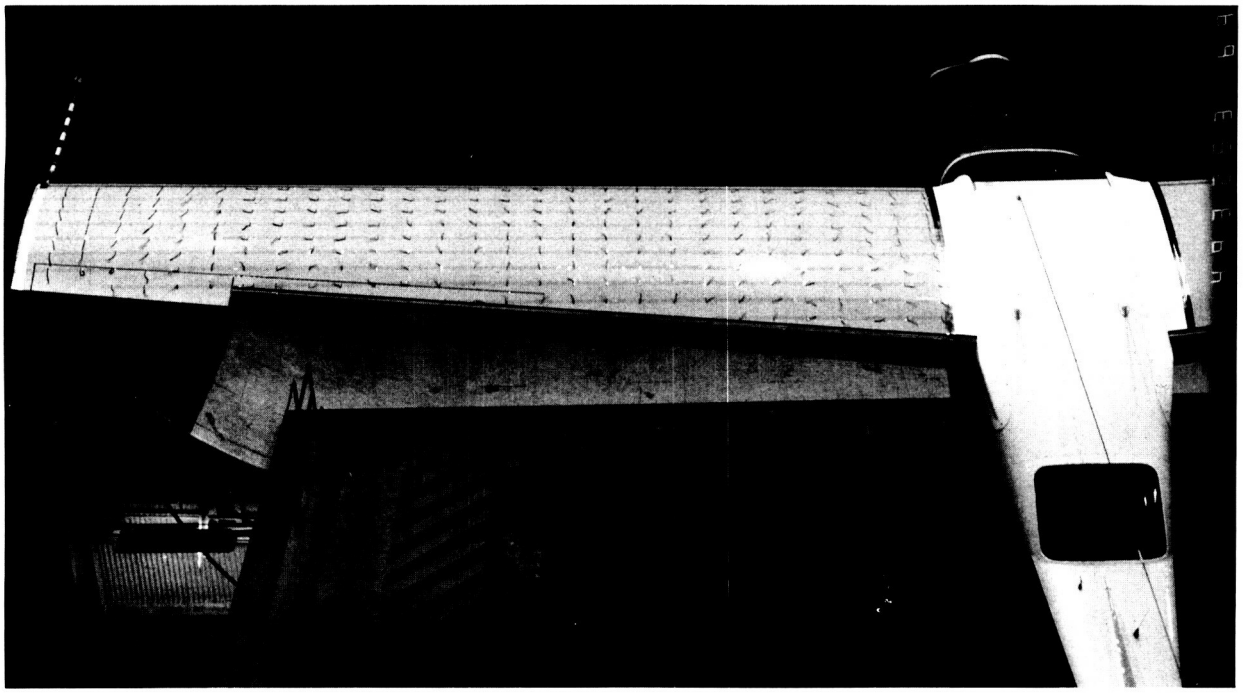

L-87-626

(f) $\alpha = 20°$.

Figure 37. Continued.

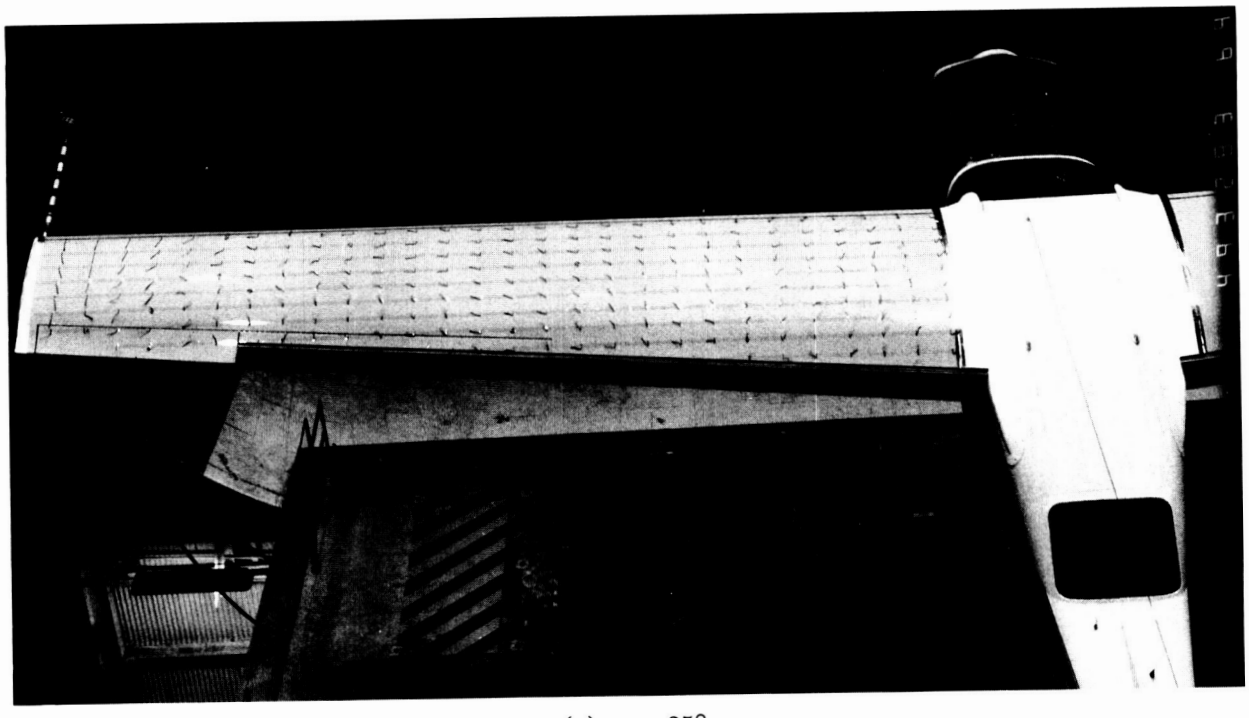

(g) $\alpha = 25°$.

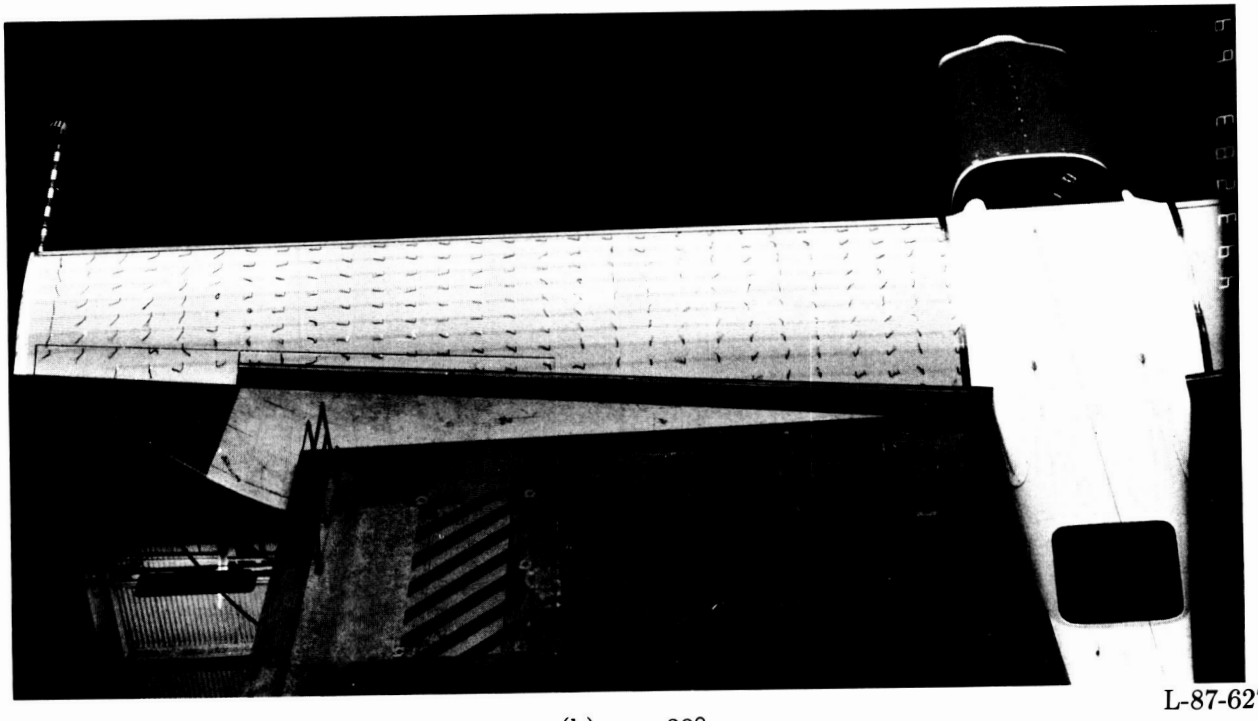

L-87-627

(h) $\alpha = 30°$.

Figure 37. Concluded.

(a) $\alpha = 15°$.

(b) $\alpha = 16°$.

L-87-628

Figure 38. Tuft flow-visualization photographs of basic configuration with segmented-droop leading-edge modification and $\delta_{cf} = 40°$. Transition fixed at $x/c = 0.05$; all other controls at zero; $C_T = 0$; $R = 2.0 \times 10^6$.

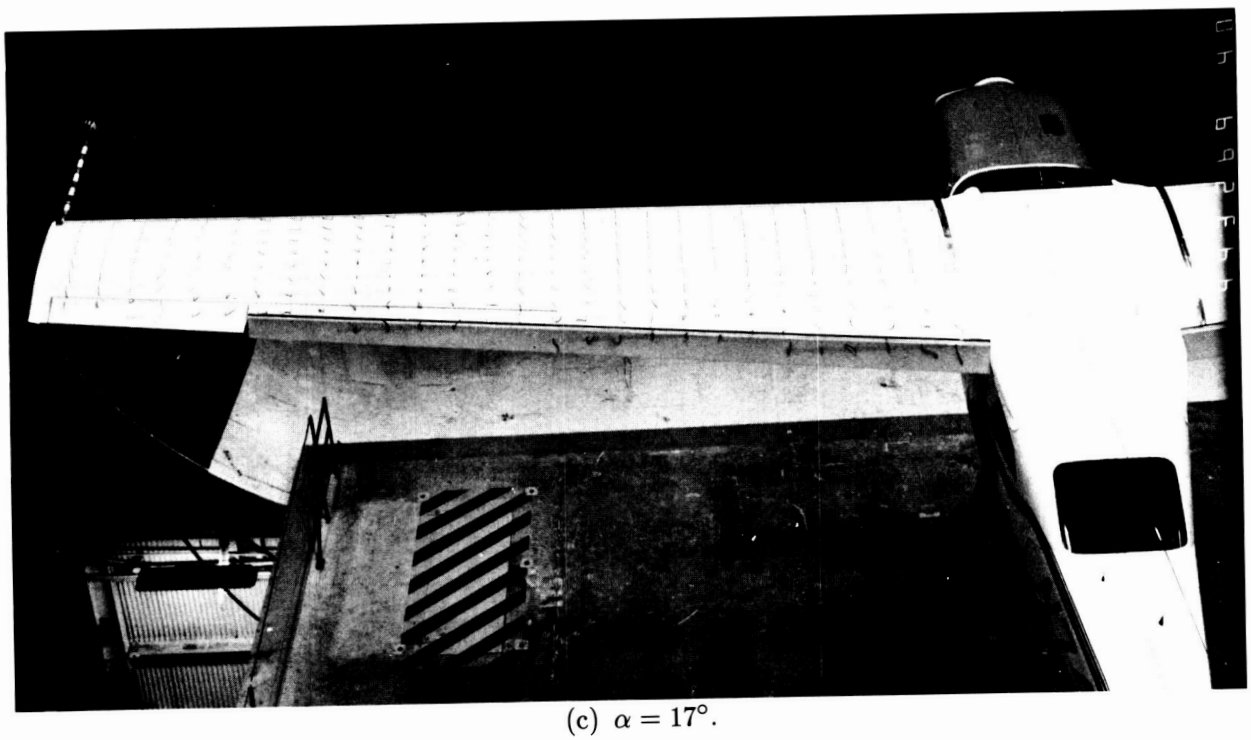

(c) $\alpha = 17°$.

(d) $\alpha = 18°$.

L-87-629

Figure 38. Continued.

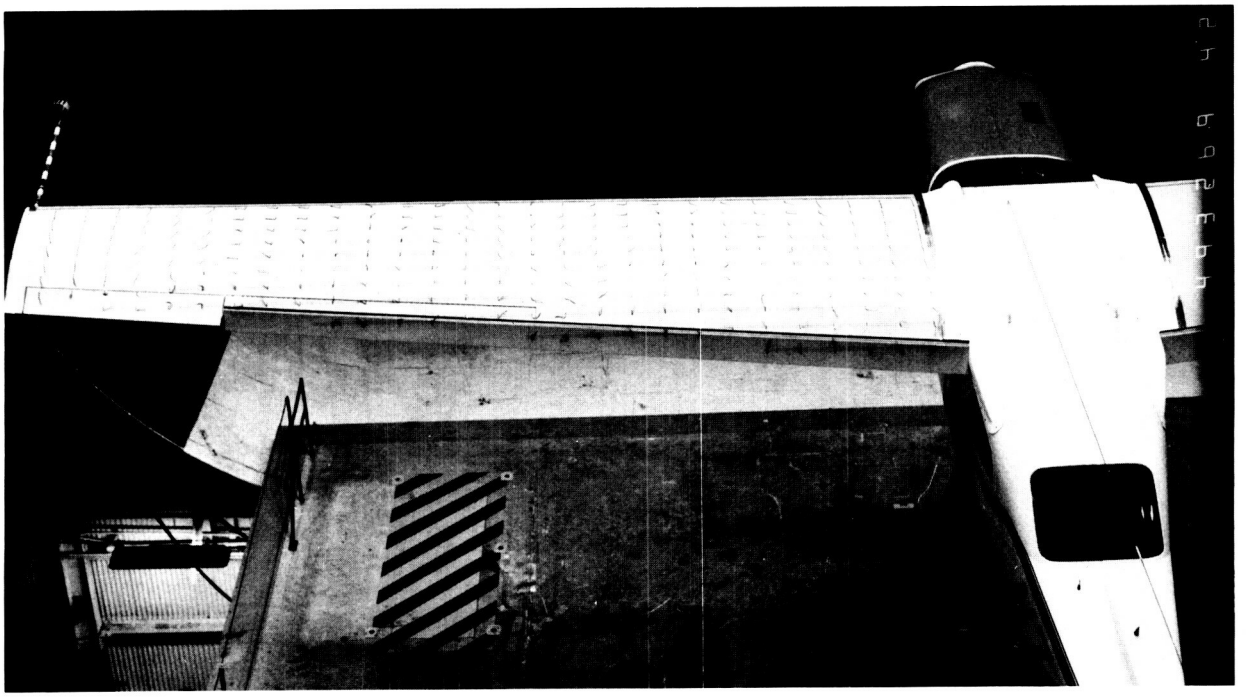

(e) $\alpha = 19°$.

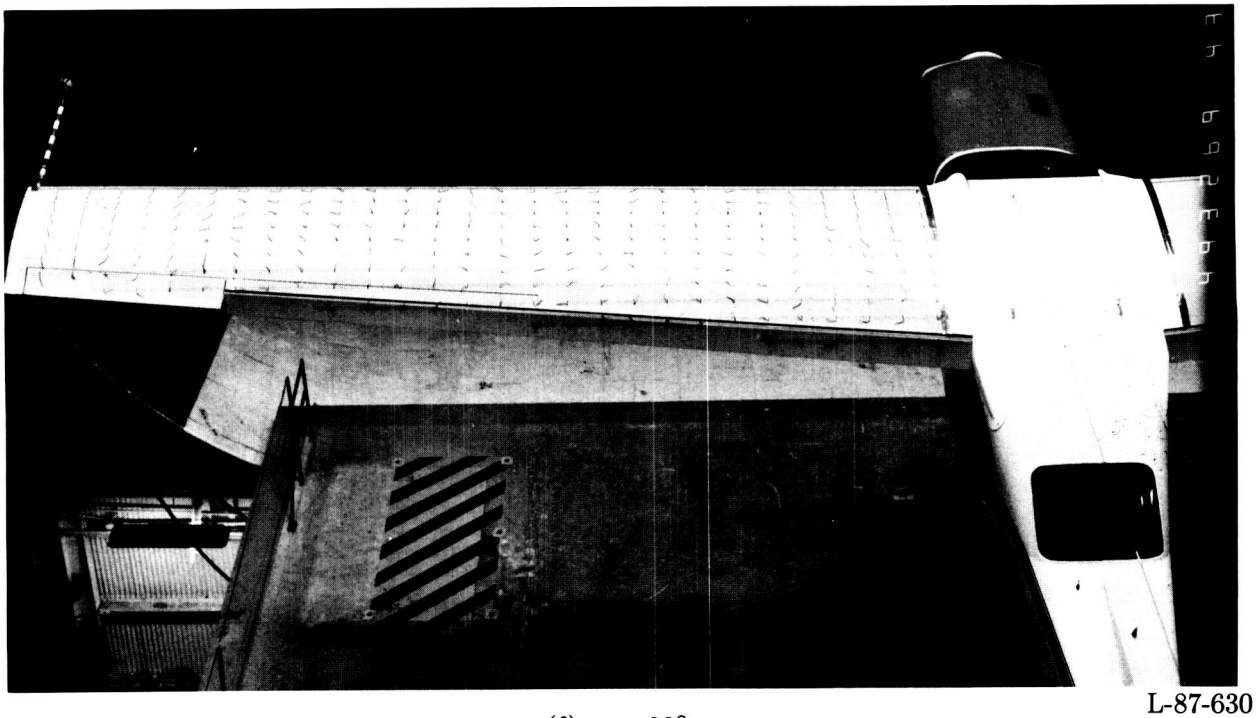

L-87-630

(f) $\alpha = 20°$.

Figure 38. Continued.

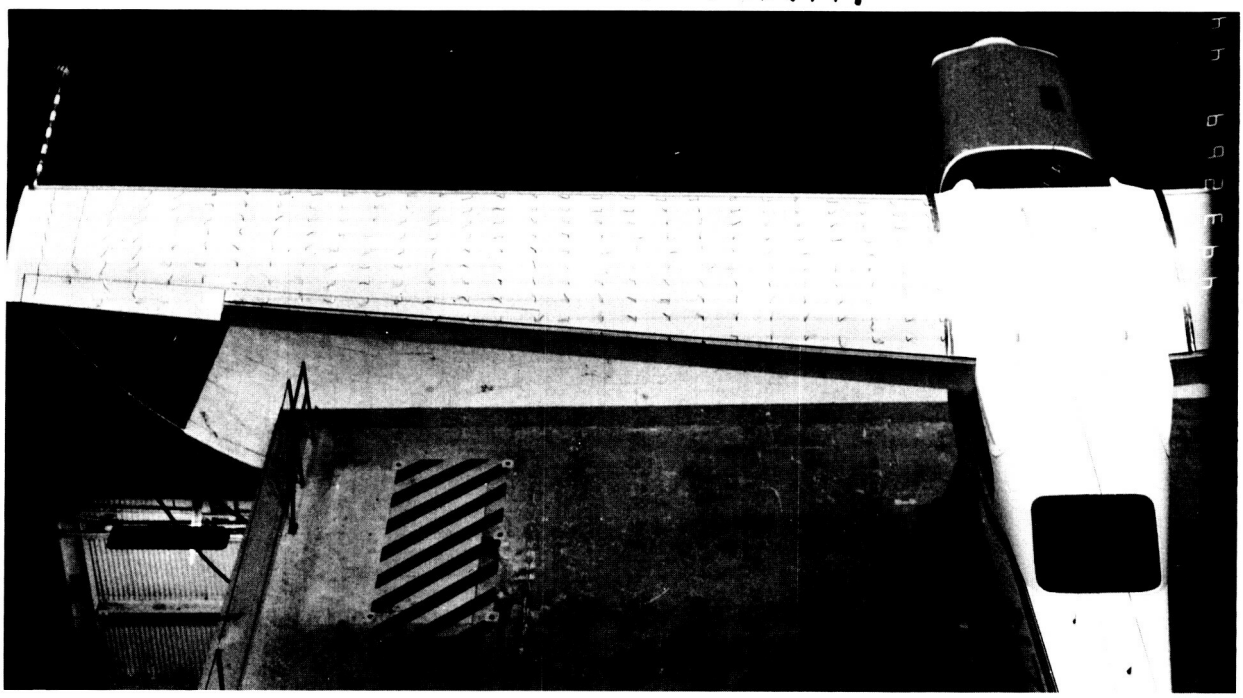

(g) $\alpha = 25°$.

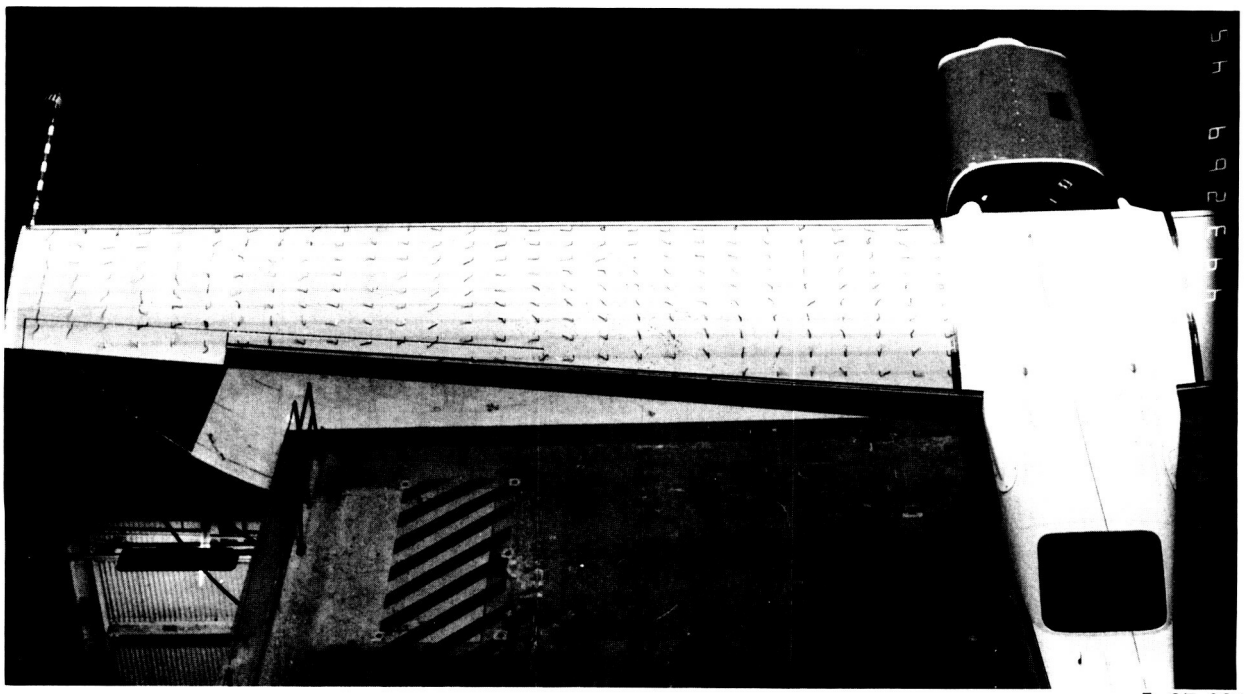

L-87-631

(h) $\alpha = 30°$.

Figure 38. Concluded.

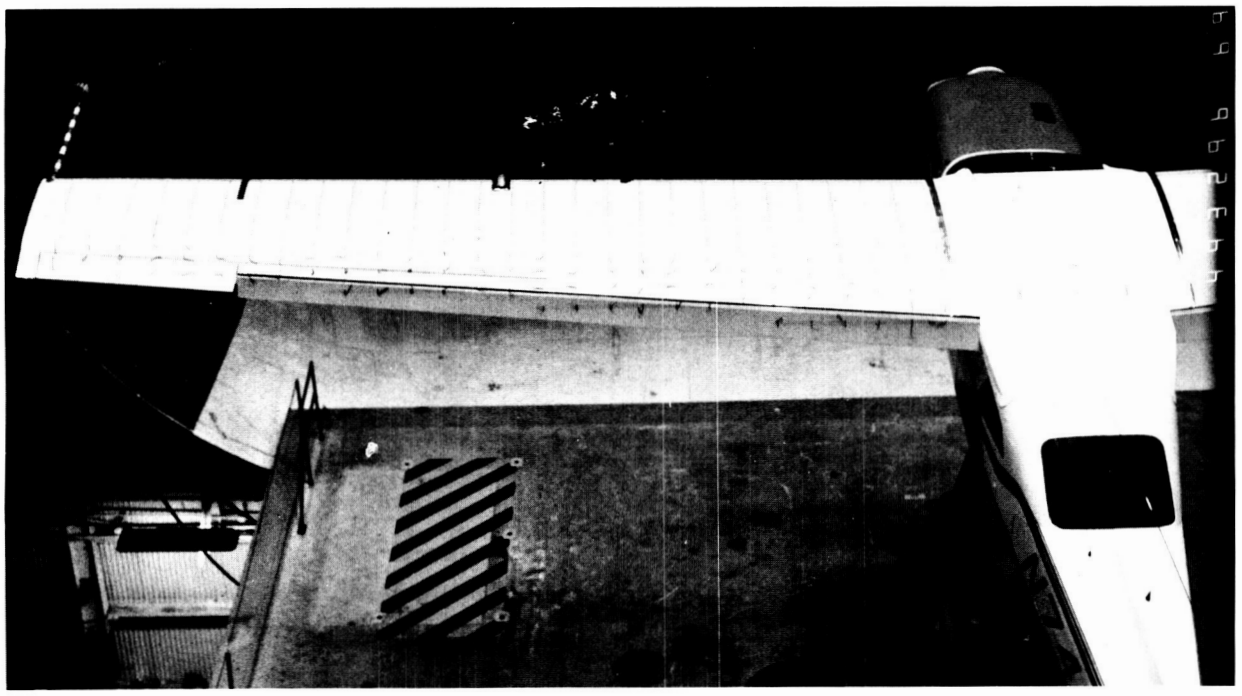

(a) $\alpha = 15°$.

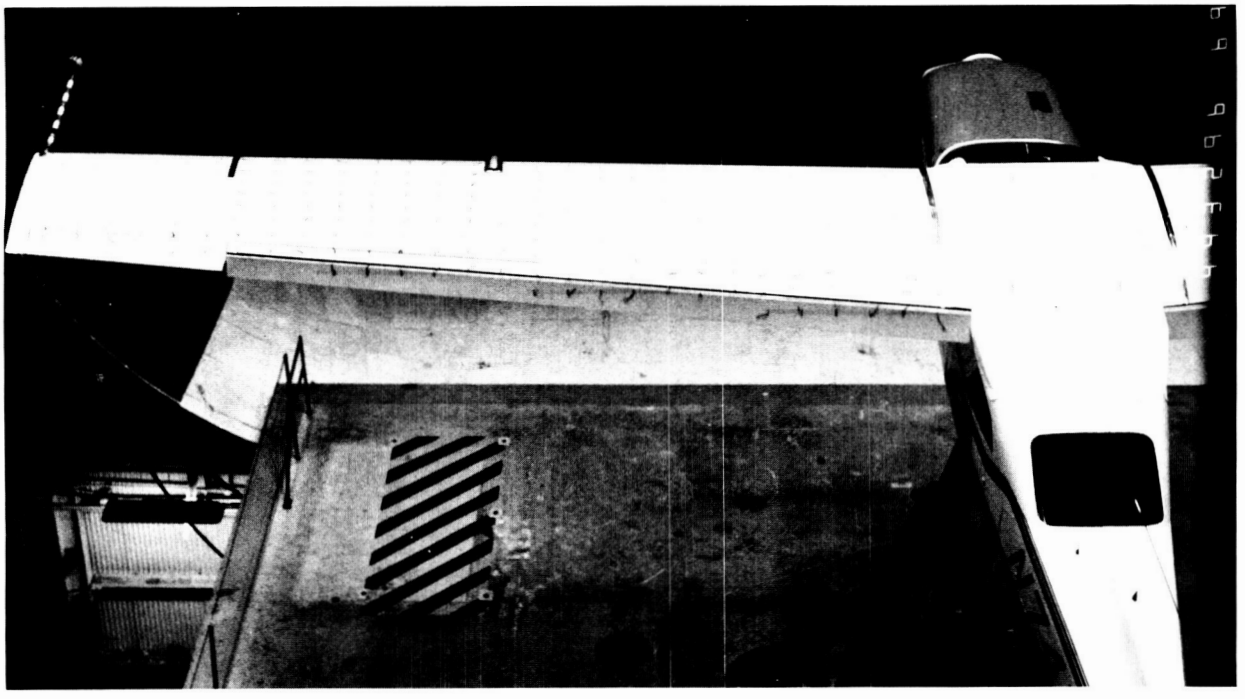

L-87-632

(b) $\alpha = 16°$.

Figure 39. Tuft flow-visualization photographs of basic configuration with droop/V.G. leading-edge modification and $\delta_{cf} = 40°$. Transition fixed at $x/c = 0.05$; all other controls at zero; $C_T = 0$; $R = 2.0 \times 10^6$.

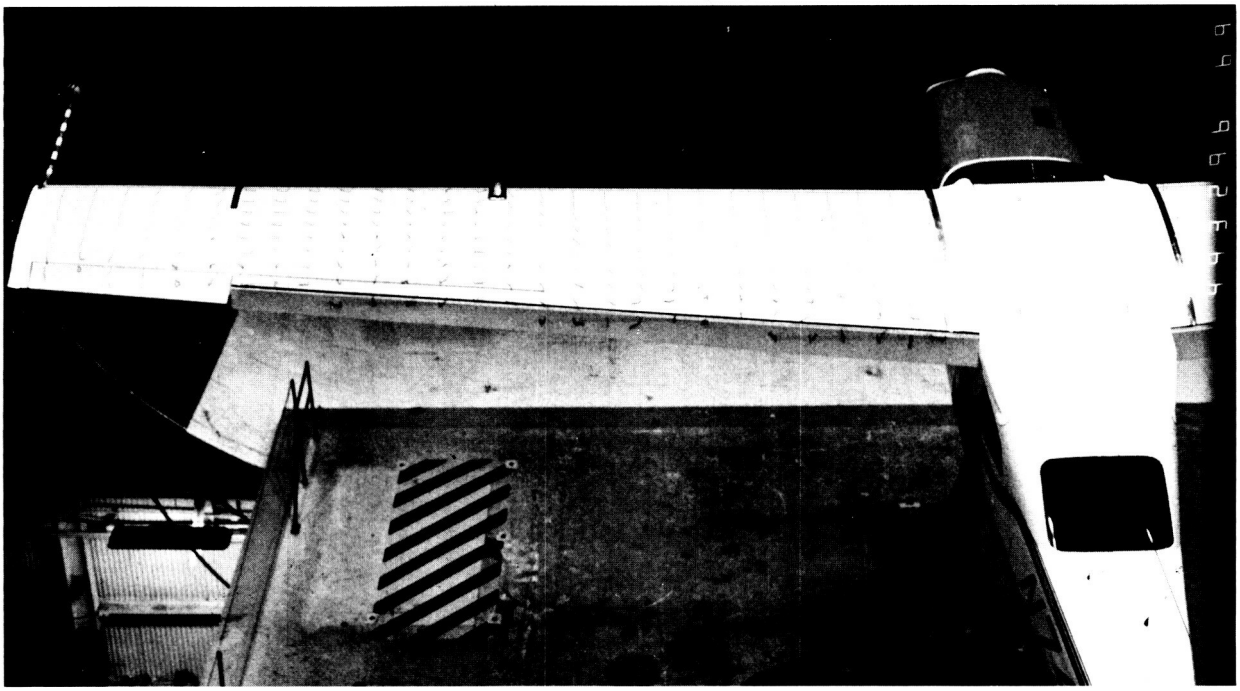

(c) $\alpha = 17°$.

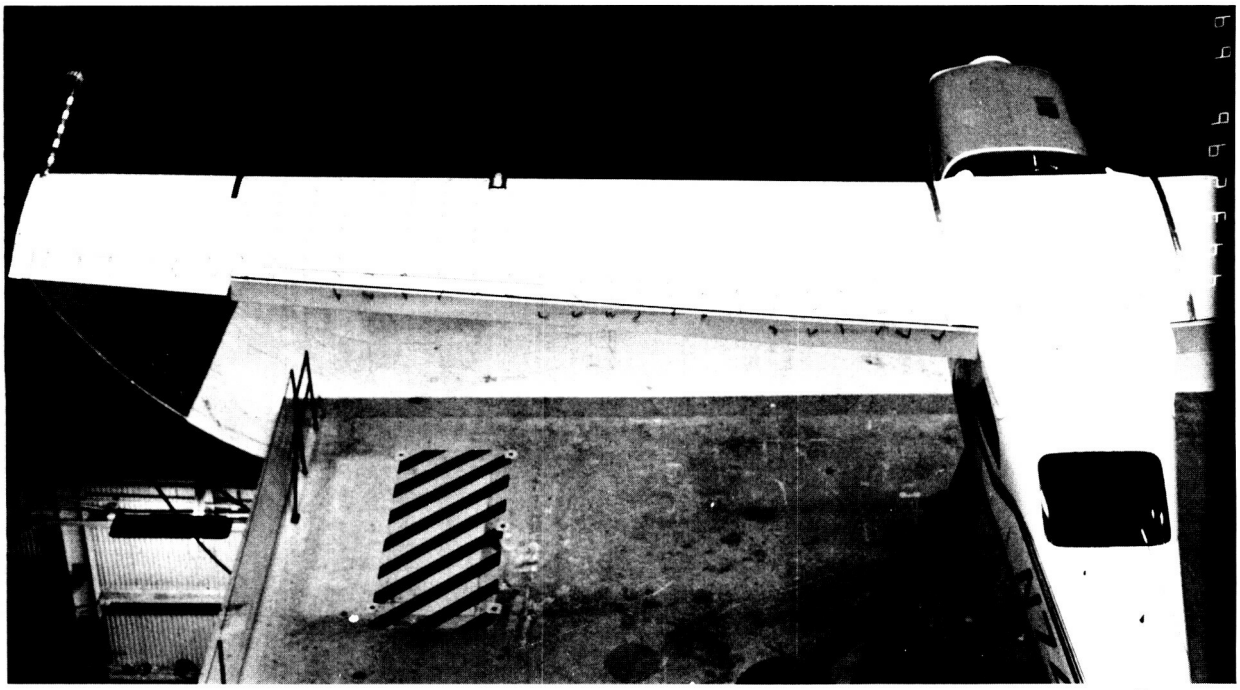

L-87-633

(d) $\alpha = 18°$.

Figure 39. Continued.

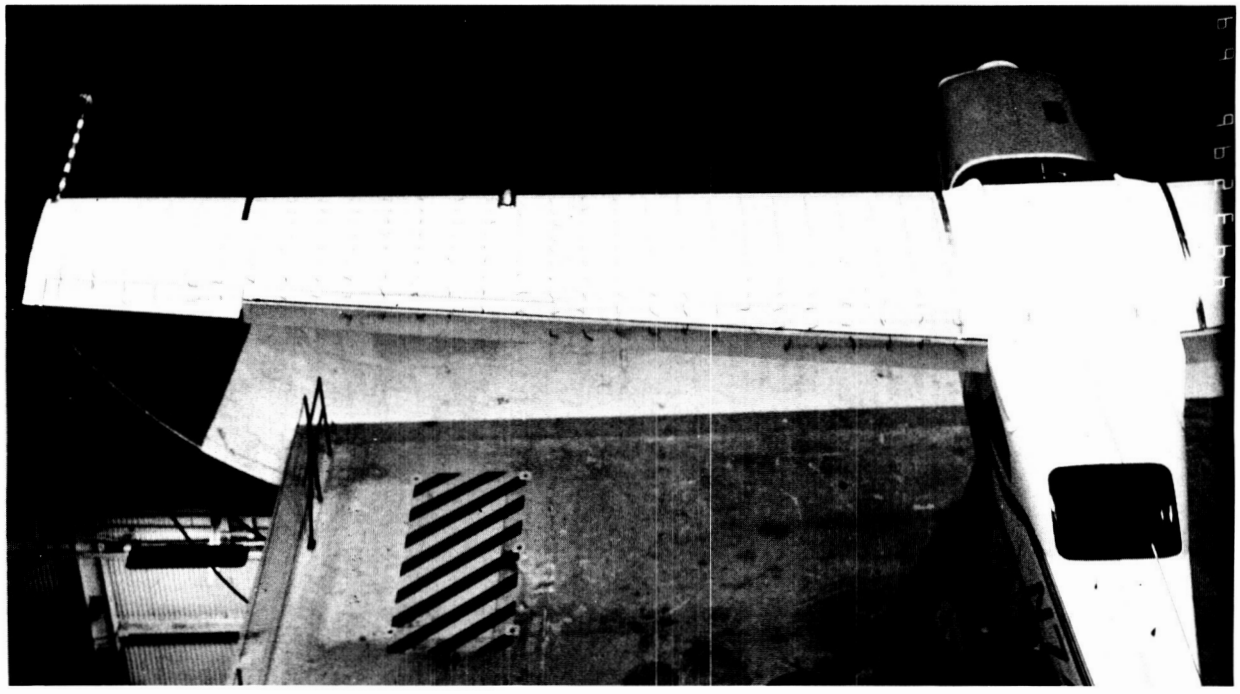

(e) $\alpha = 19°$.

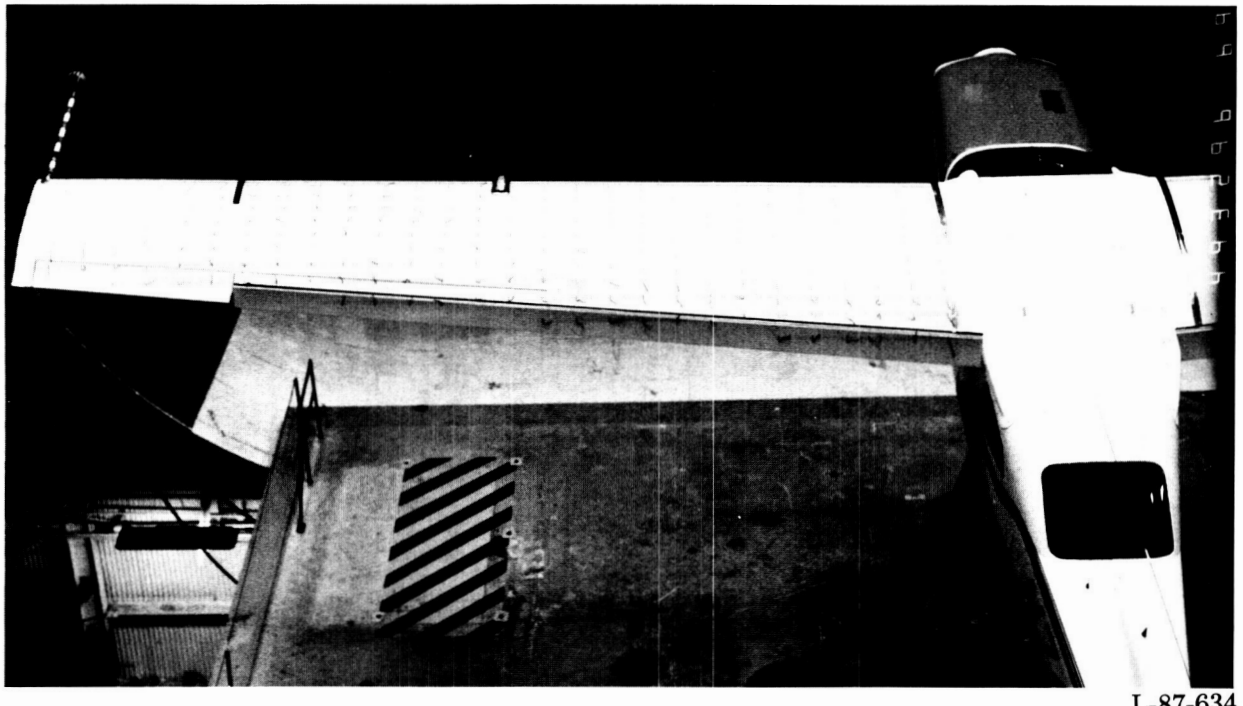

L-87-634

(f) $\alpha = 20°$.

Figure 39. Continued.

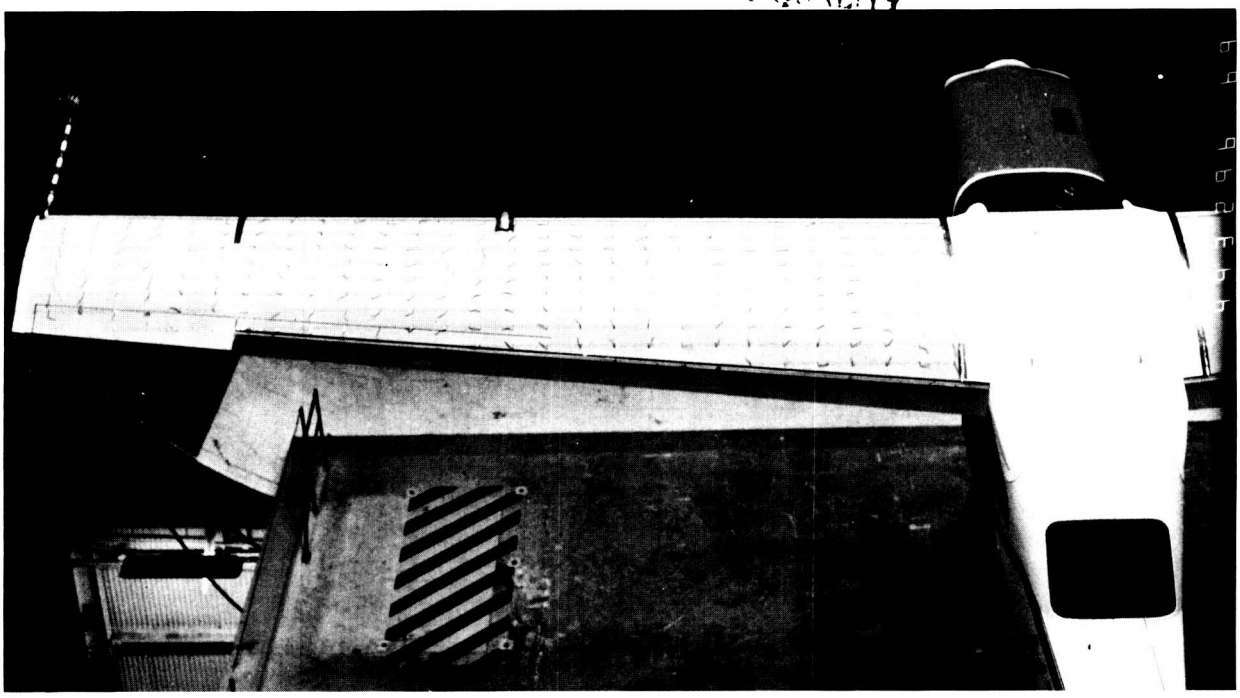

(g) $\alpha = 25°$.

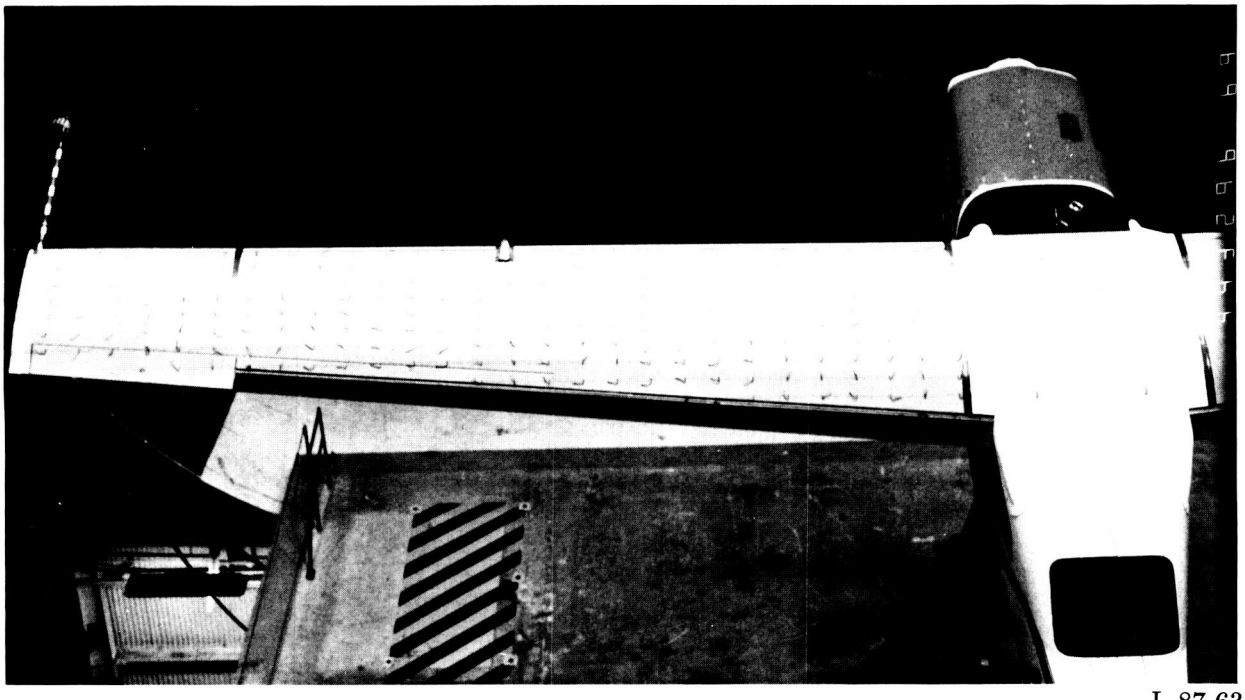

L-87-635

(h) $\alpha = 30°$.

Figure 39. Concluded.

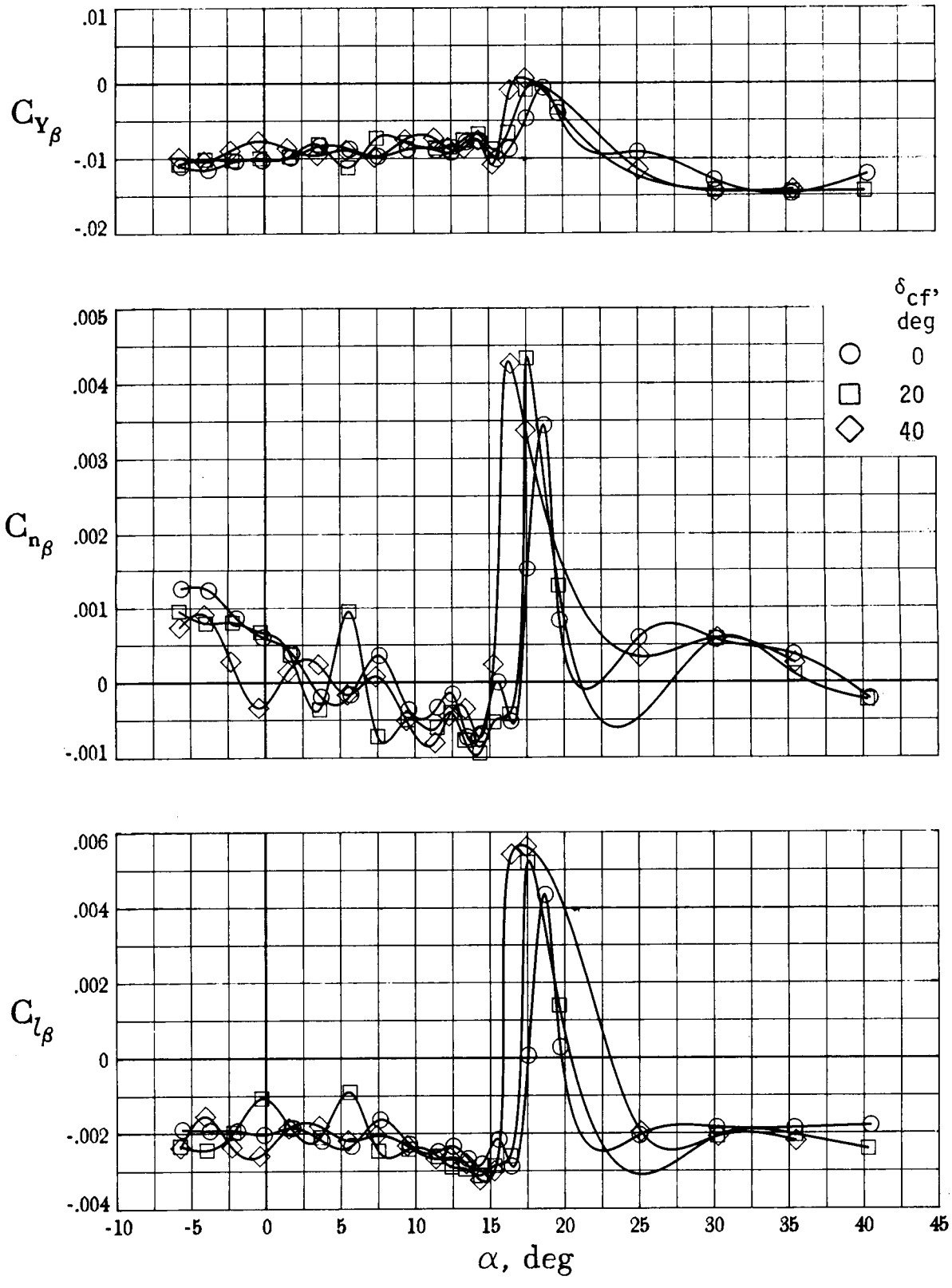


Figure 40. Effect of cruise flap deflections on lateral-directional stability characteristics of basic configuration. All other controls at zero; $C_T = 0$; $R = 2.0 \times 10^6$.

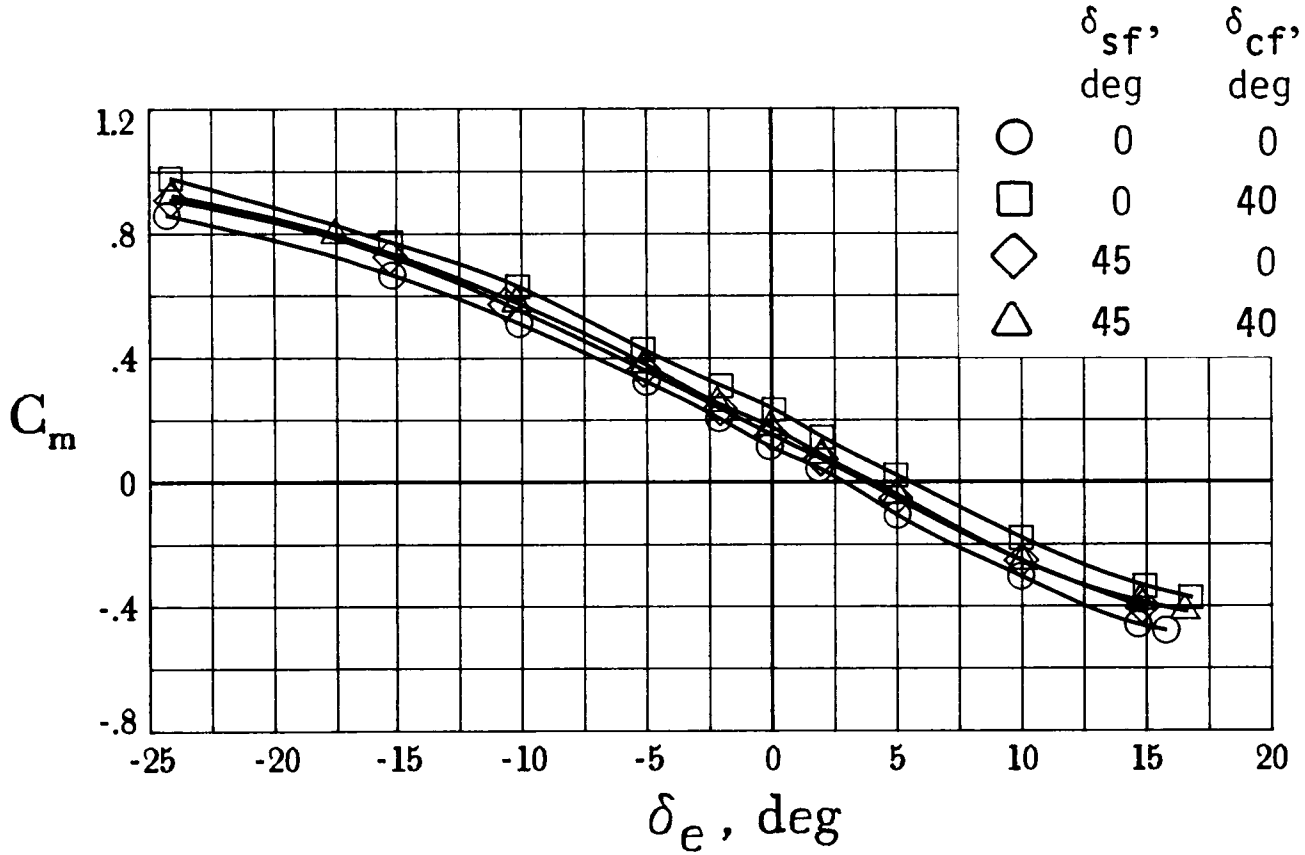


(a) $\alpha = 0°$.

Figure 41. Effect of split flap and cruise flap deflections on elevator characteristics of basic configuration. All other controls at zero; $C_T = 0$; $R = 2.0 \times 10^6$.

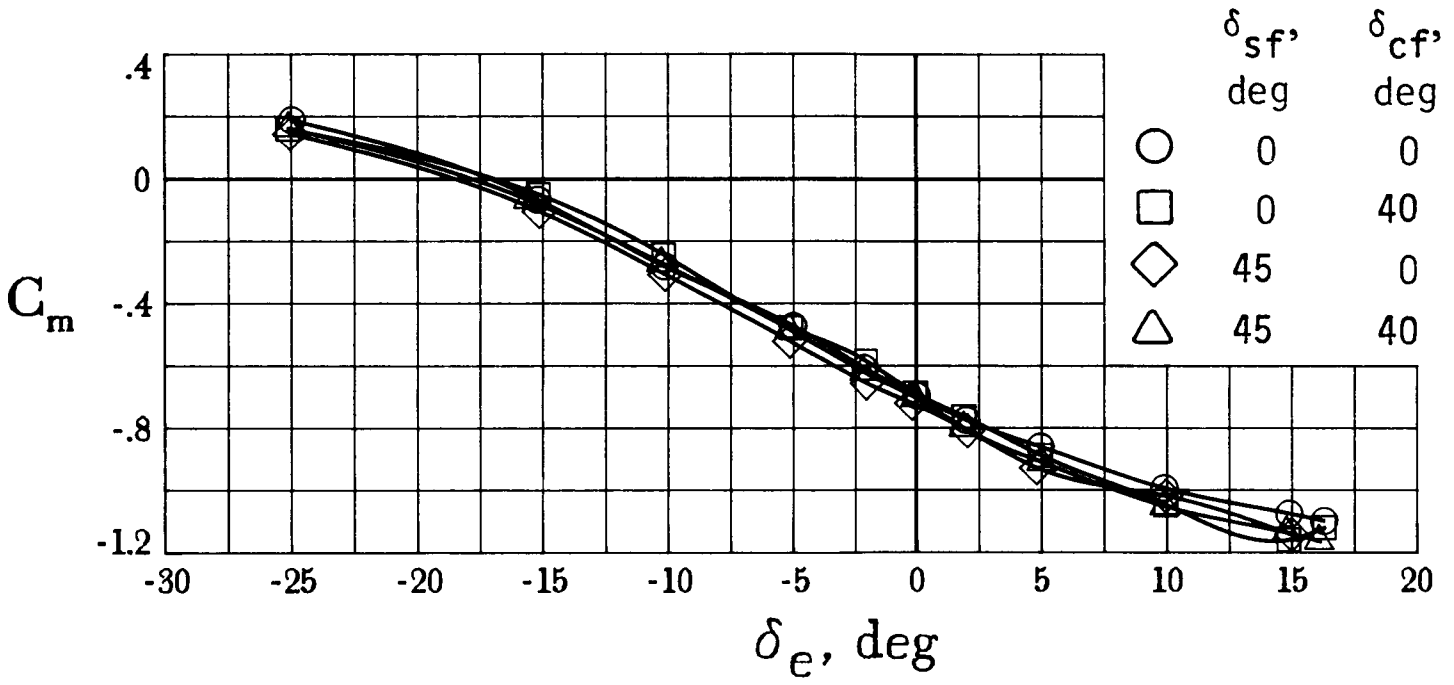


(b) $\alpha = 15°$.

Figure 41. Concluded.

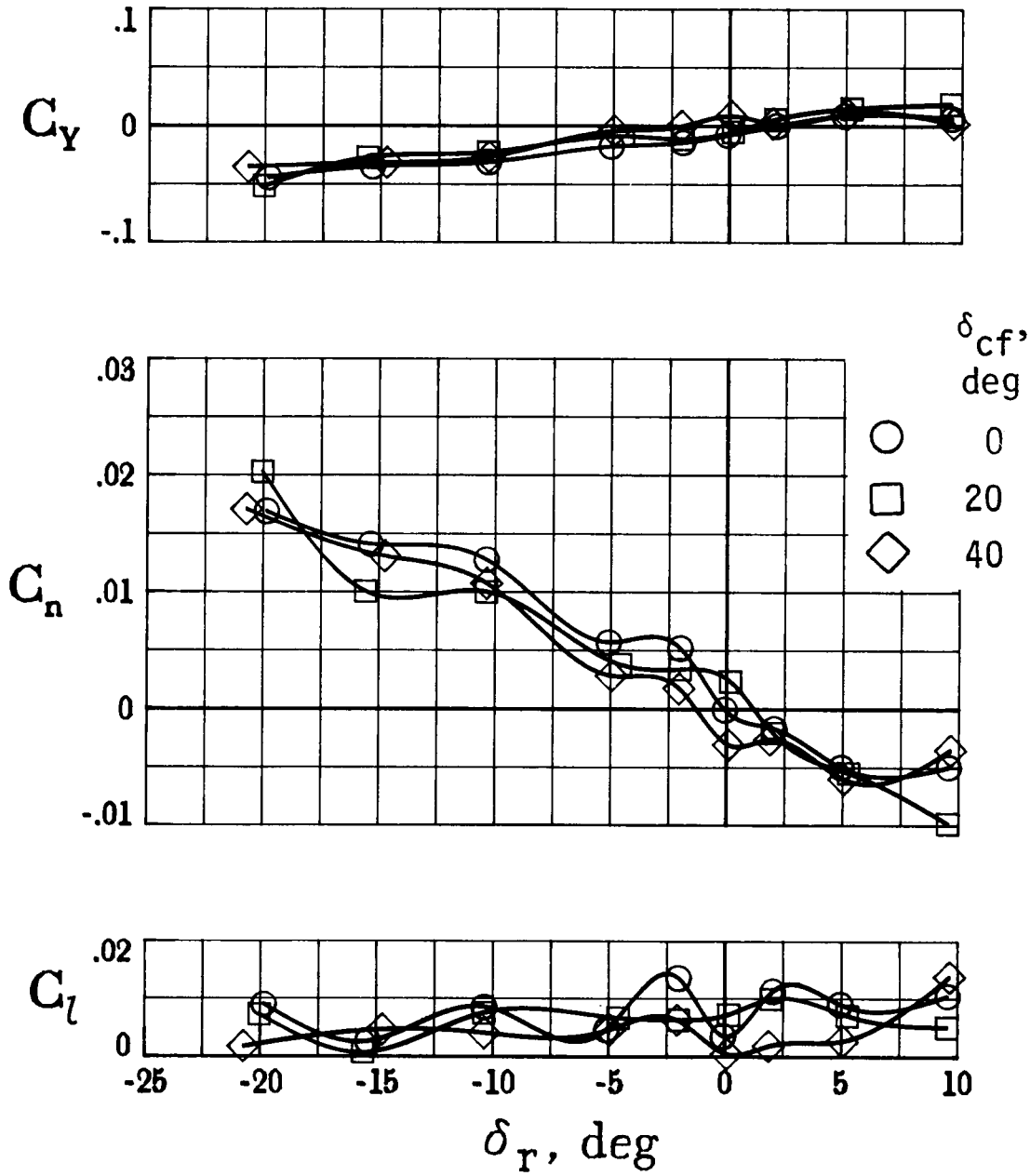


(a) $\alpha = 0°$.

Figure 42. Effect of cruise flap deflections on rudder characteristics of basic configuration. All other controls at zero; $C_T = 0$; $R = 2.0 \times 10^6$.

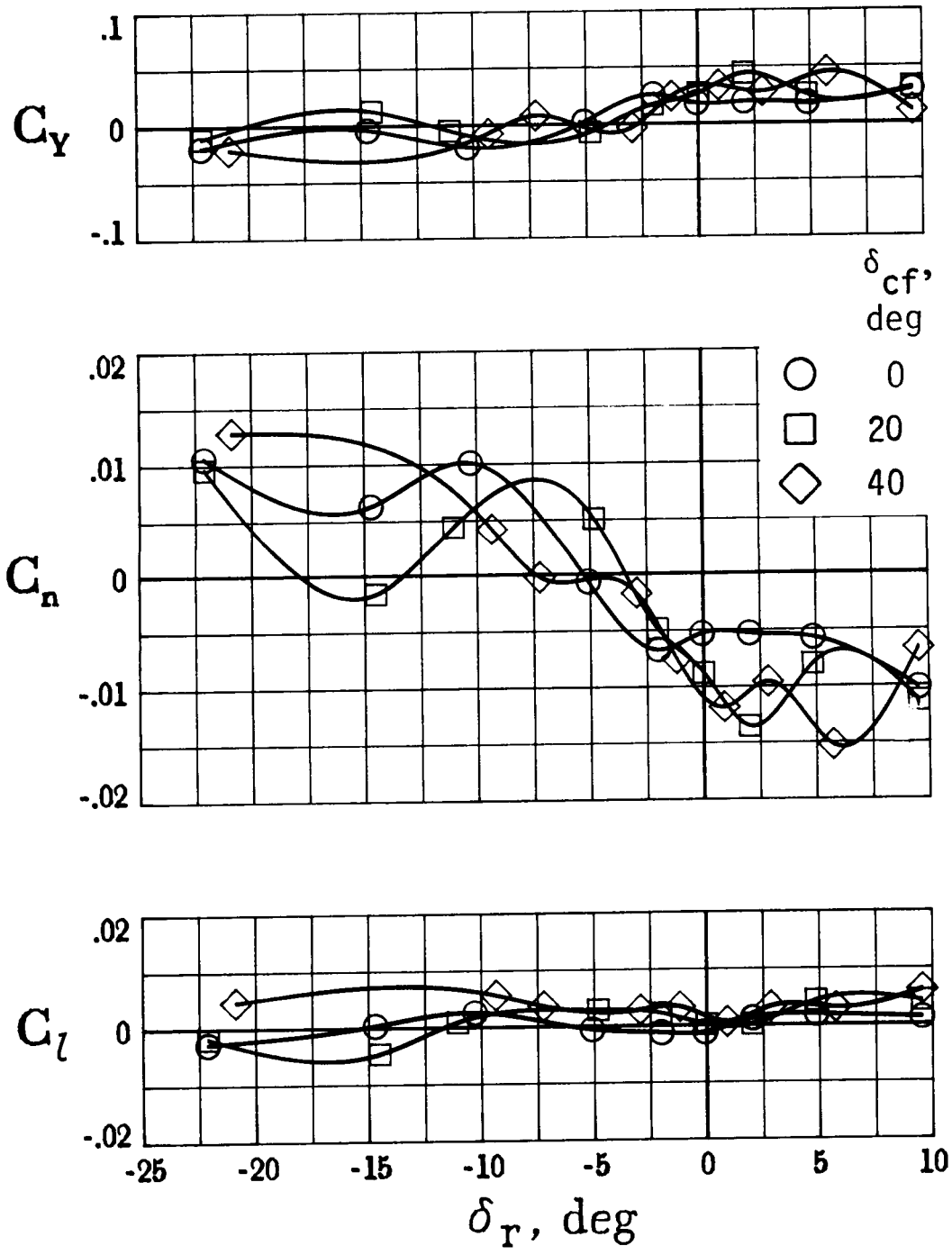


(b) $\alpha = 15°$.

Figure 42. Concluded.

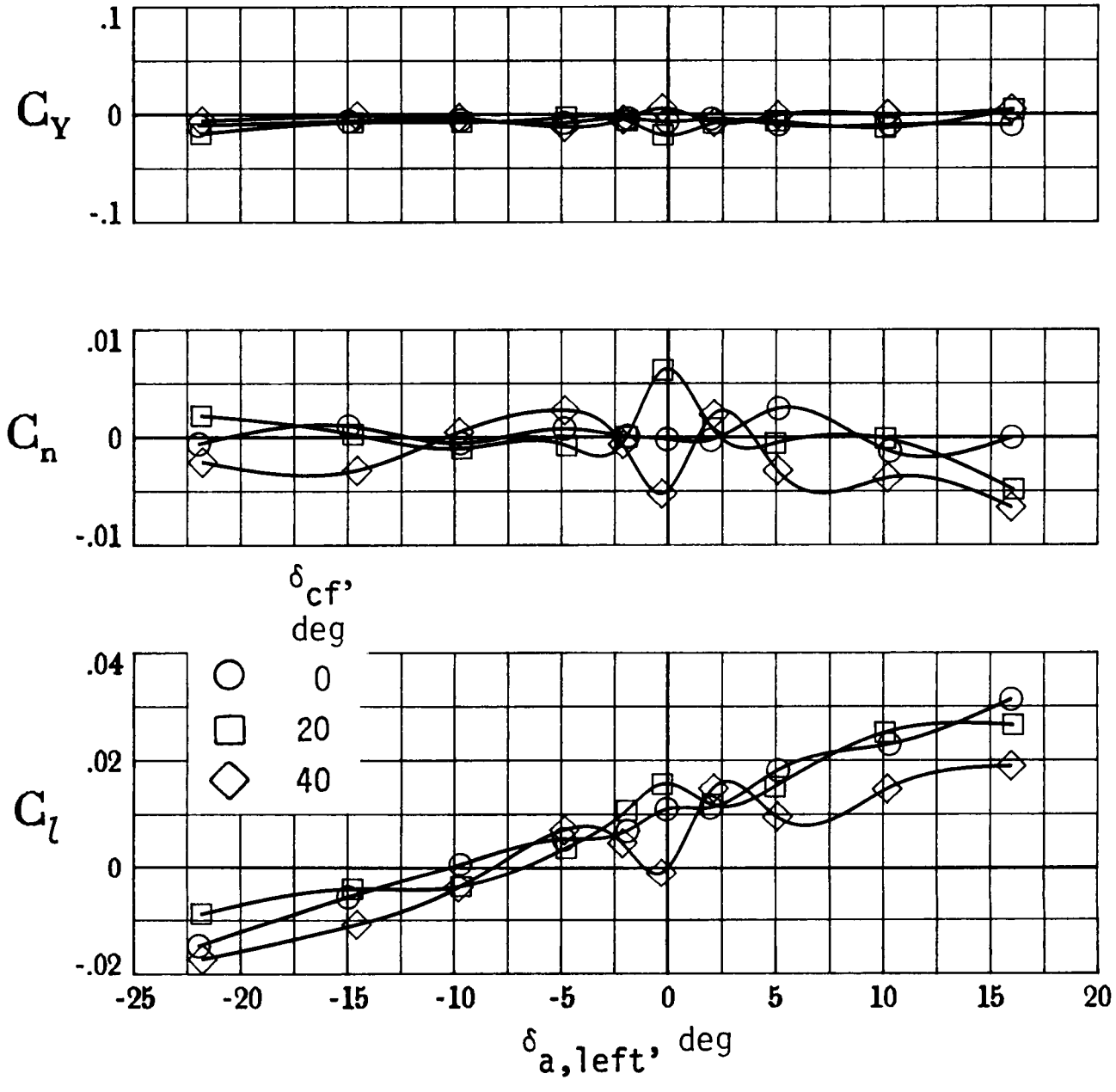


(a) $\alpha = 0°$.

Figure 43. Effect of cruise flap deflections on left-aileron characteristics of basic configuration. All other controls at zero; $C_T = 0$; $R = 2.0 \times 10^6$.

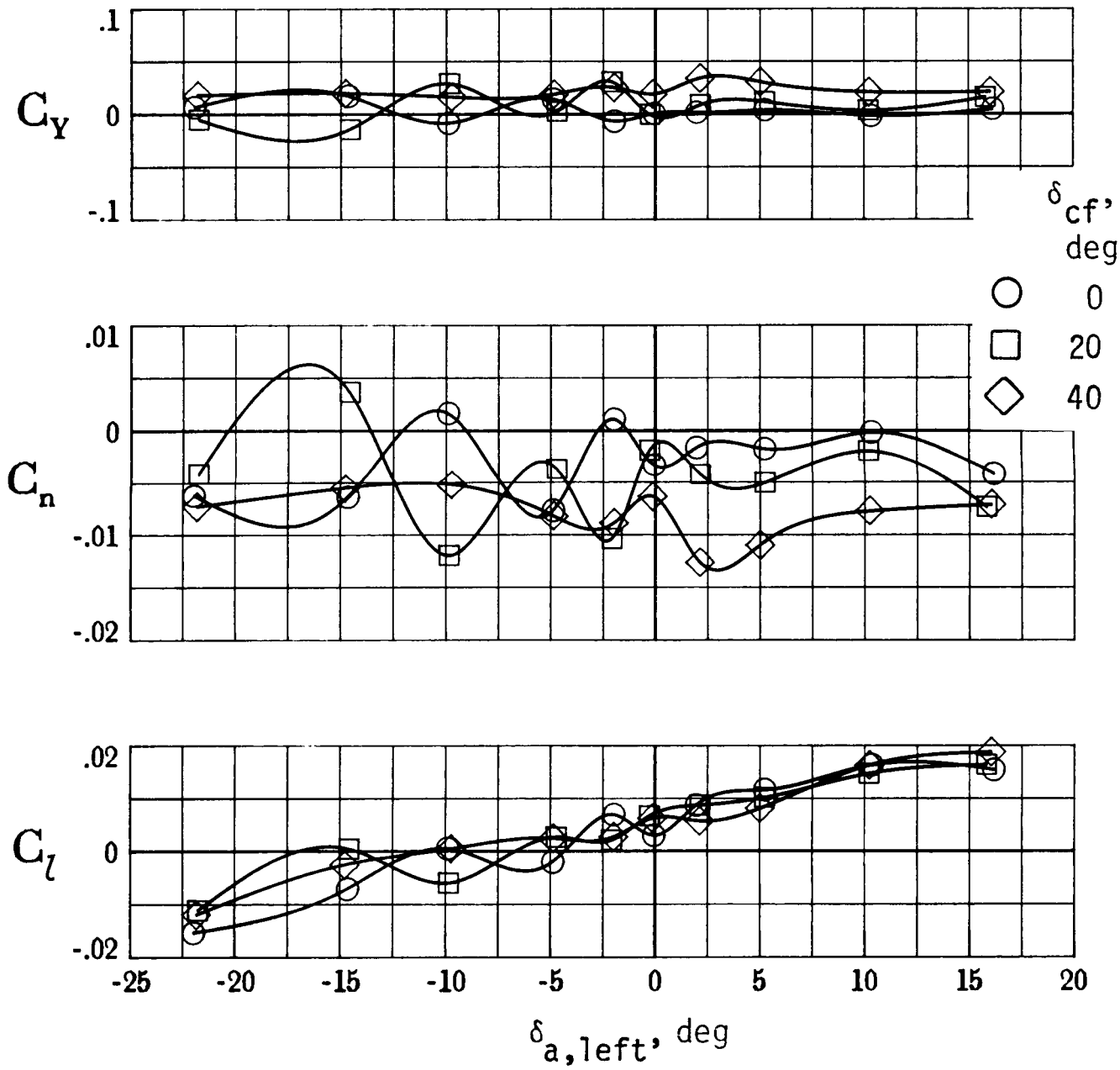


(b) $\alpha = 15°$.

Figure 43. Concluded.

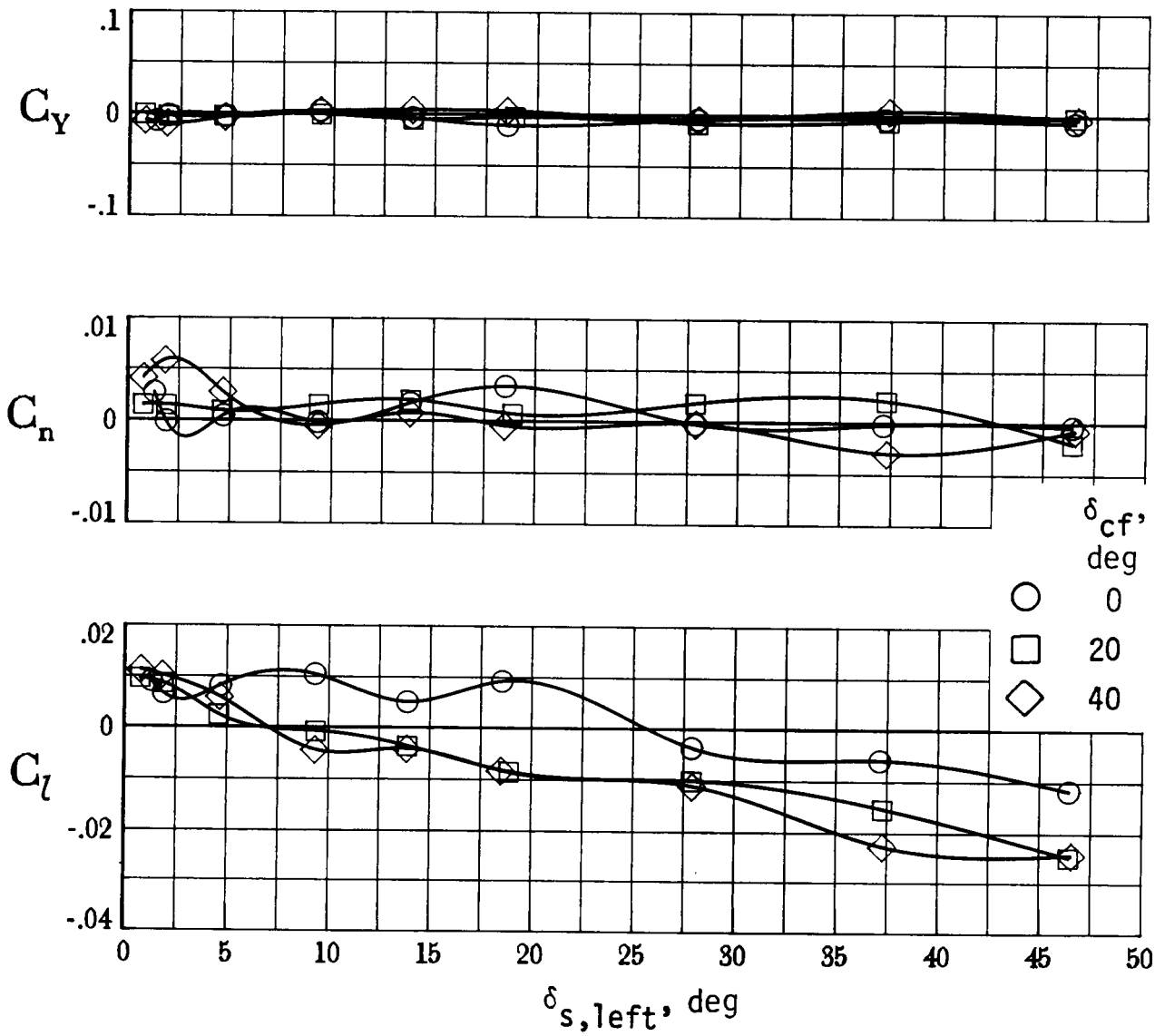


(a) $\alpha = 0°$.

Figure 44. Effect of cruise flap deflections on left-spoiler characteristics of basic configuration. All other controls at zero; $C_T = 0$; $R = 2.0 \times 10^6$.

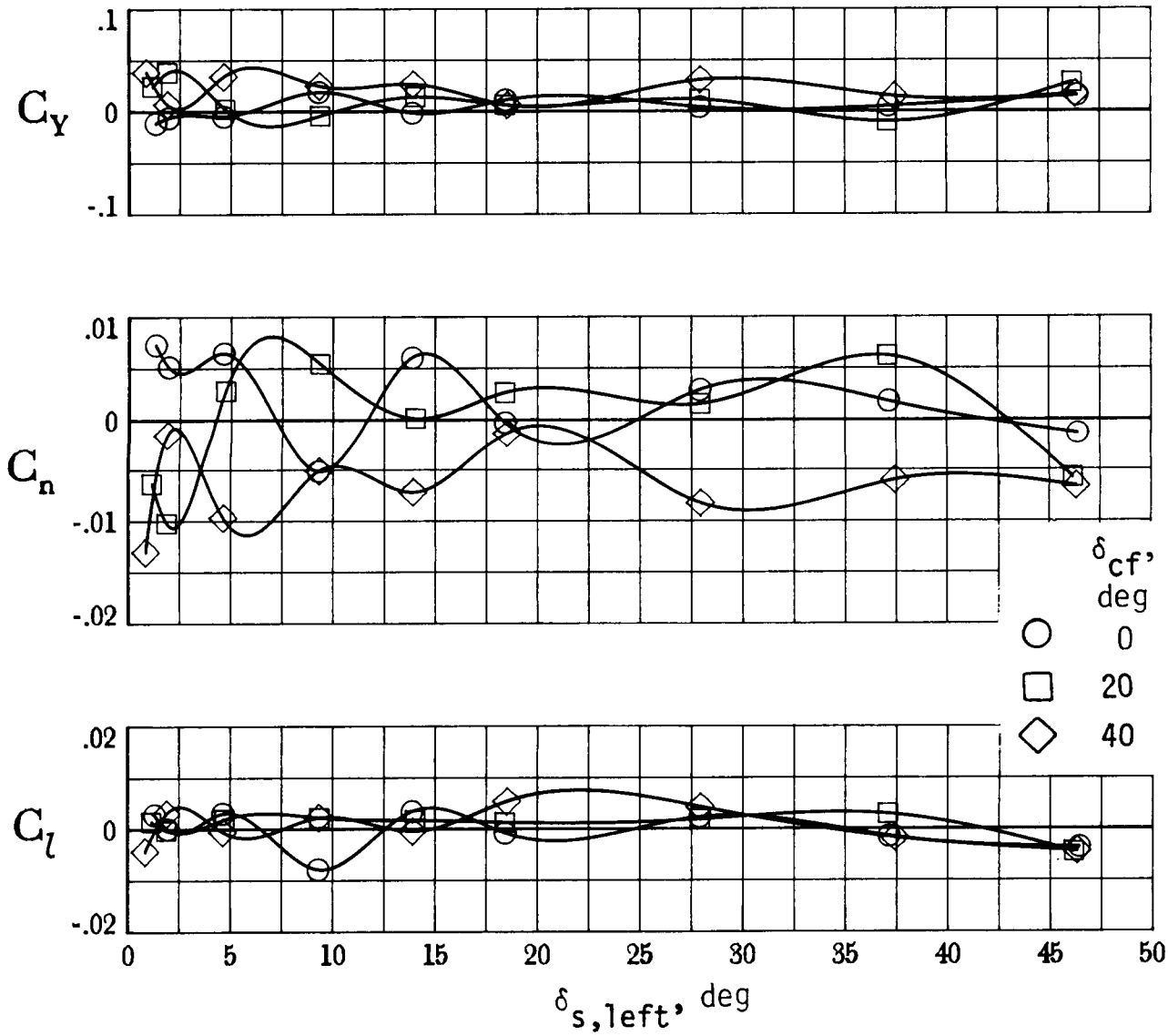


(b) $\alpha = 15°$.

Figure 44. Concluded.

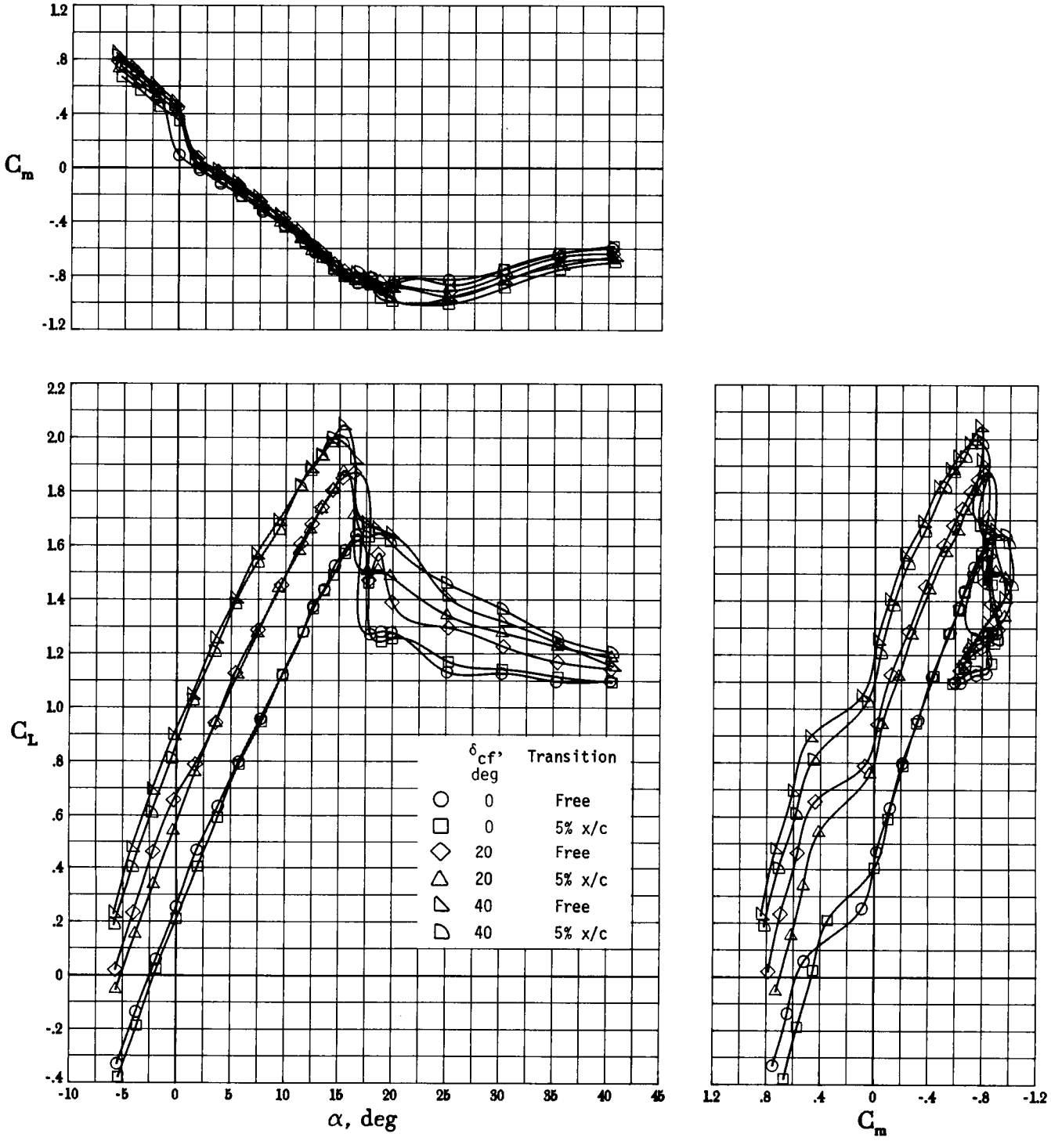


(a) Lift and pitching moment.

Figure 45. Effect of transition on cruise flap characteristics of basic configuration. All other controls at zero; $C_T = 0$; $R = 2.0 \times 10^6$.

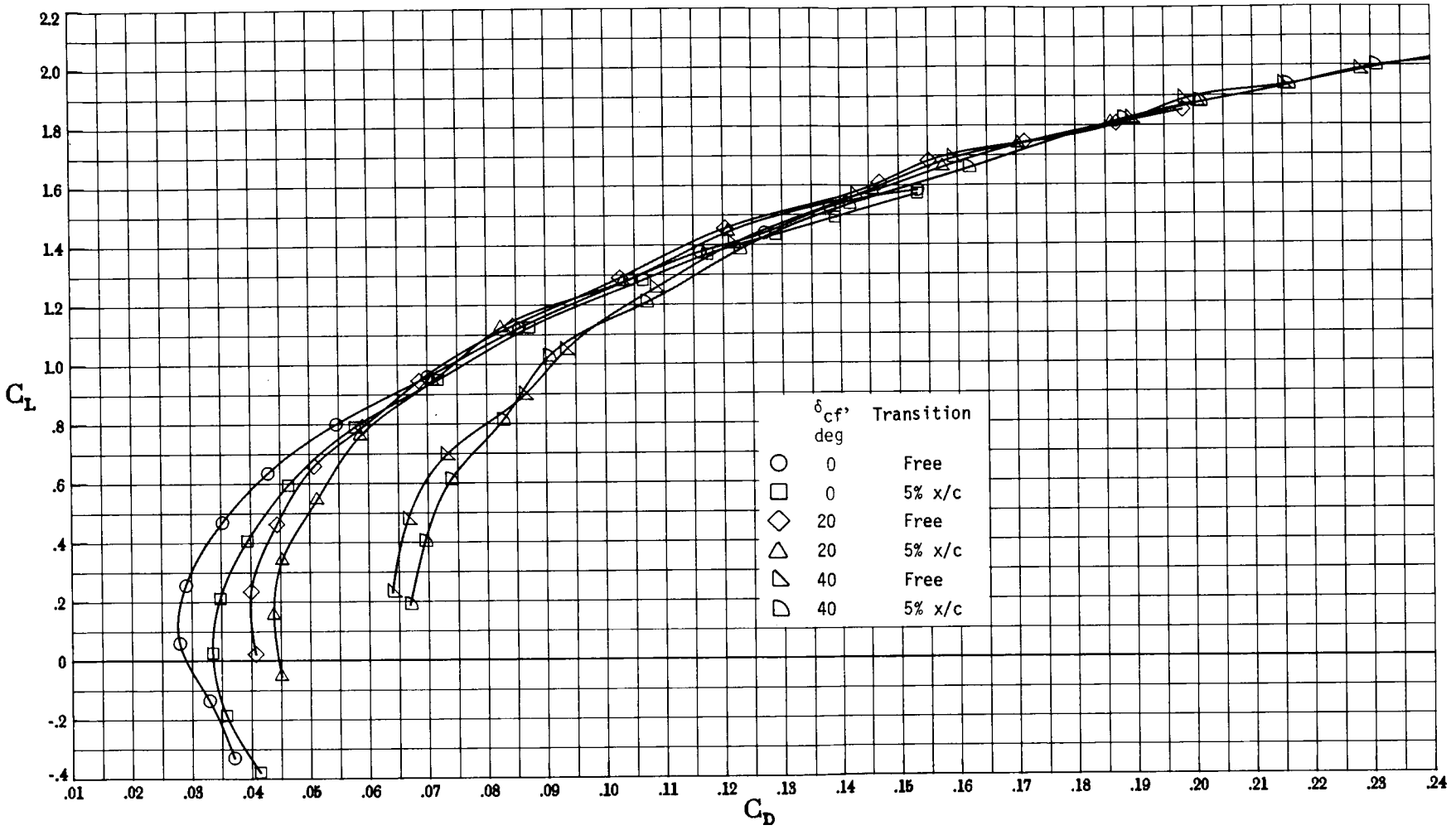


(b) Lift-drag polars.

Figure 45. Concluded.

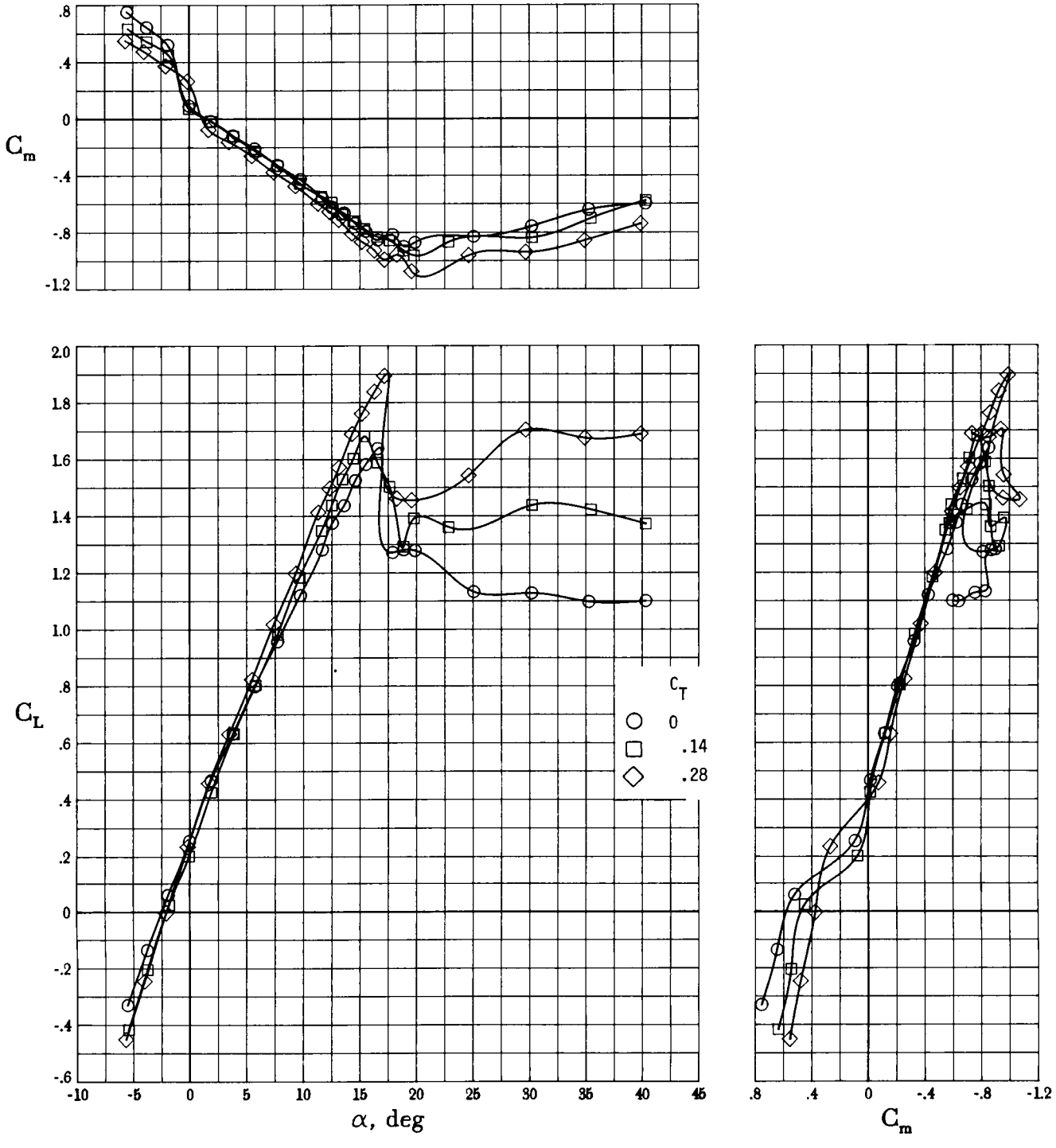


(a) Lift and pitching moment.

Figure 46. Effect of power on longitudinal characteristics of basic configuration. All controls at zero; $R = 2.0 \times 10^6$.

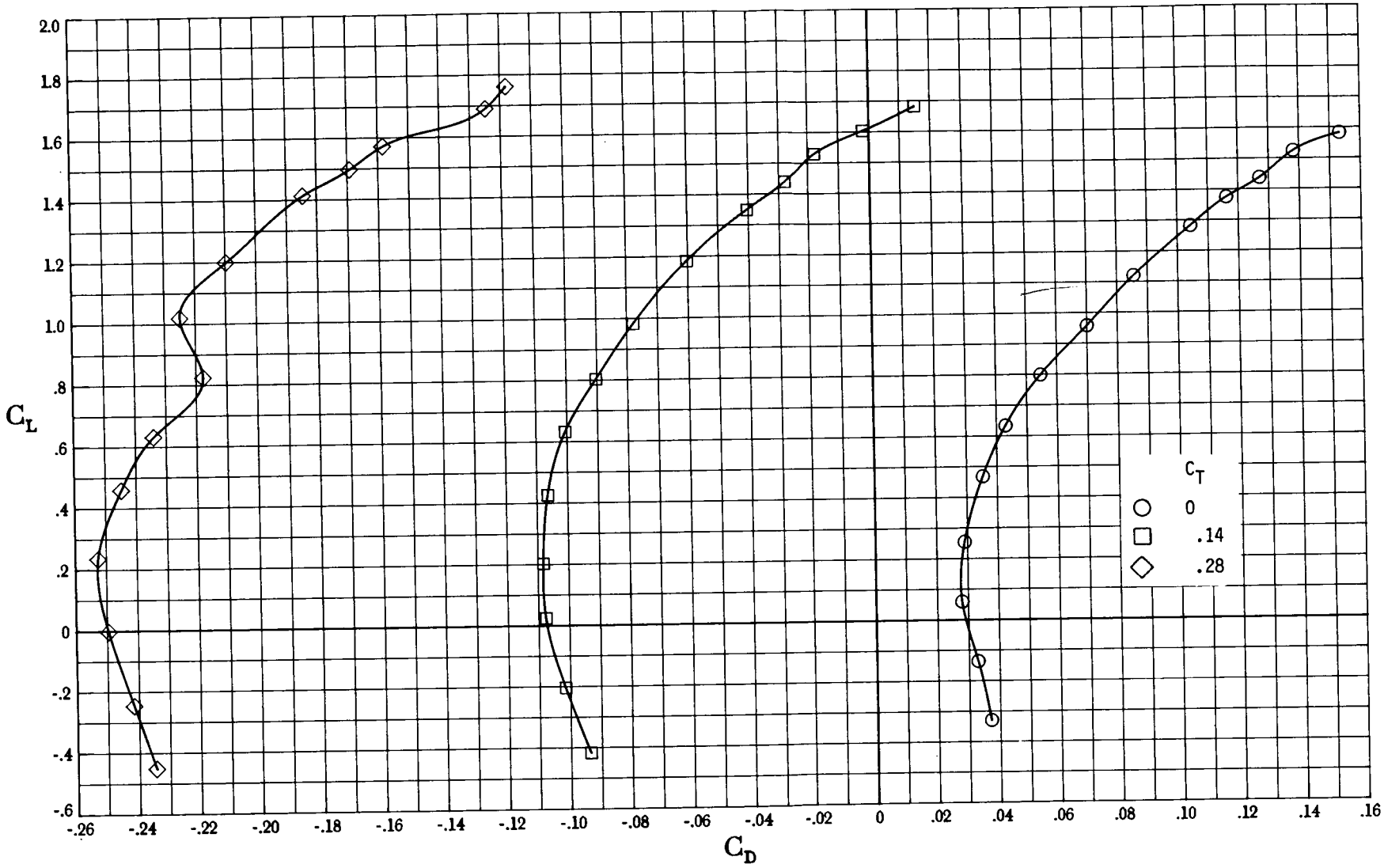


(b) Lift-drag polars.

Figure 46. Concluded.

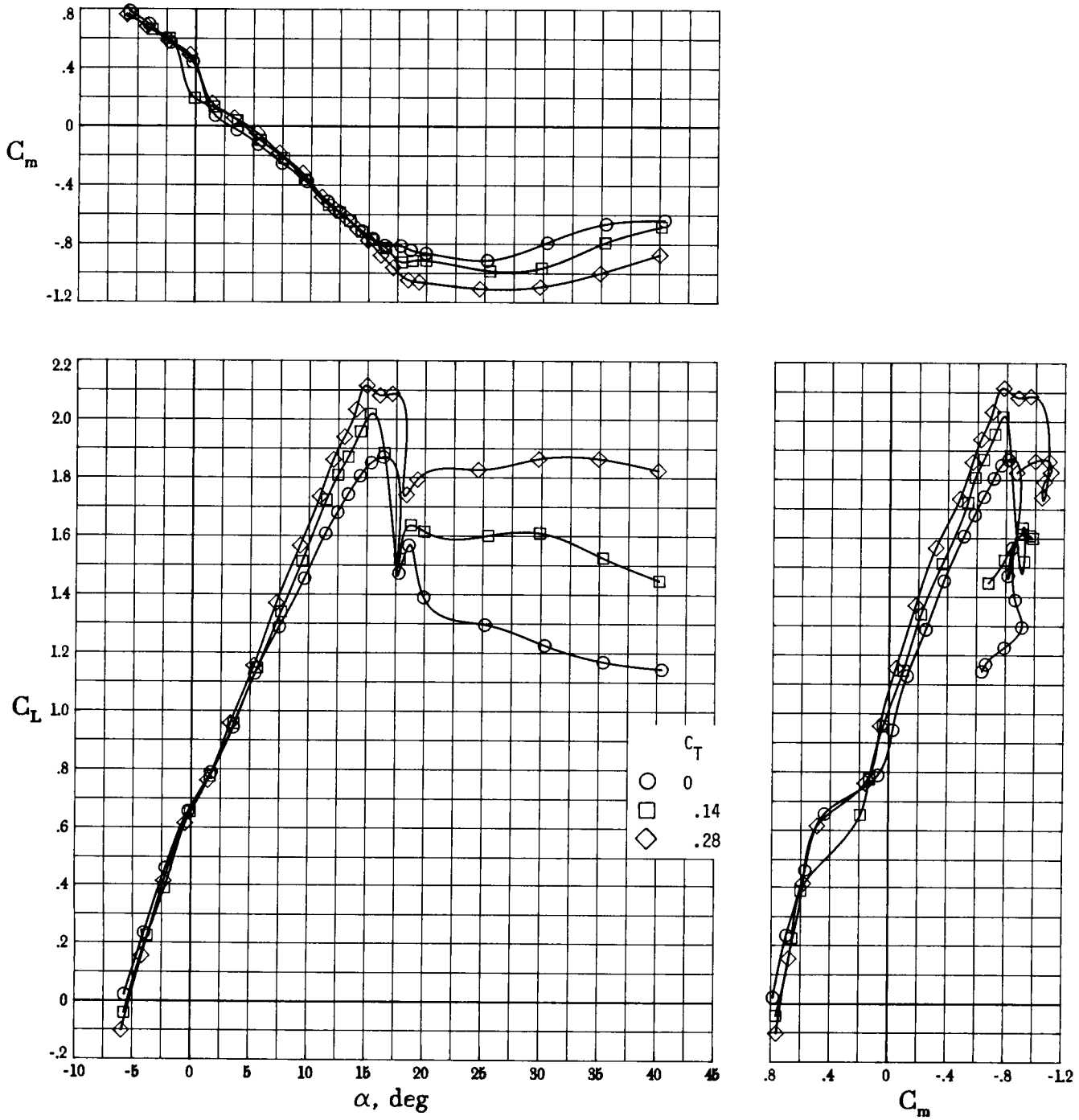


(a) Lift and pitching moment.

Figure 47. Effect of power on longitudinal characteristics of basic configuration with $\delta_{cf} = 20°$. All other controls at zero; $R = 2.0 \times 10^6$.

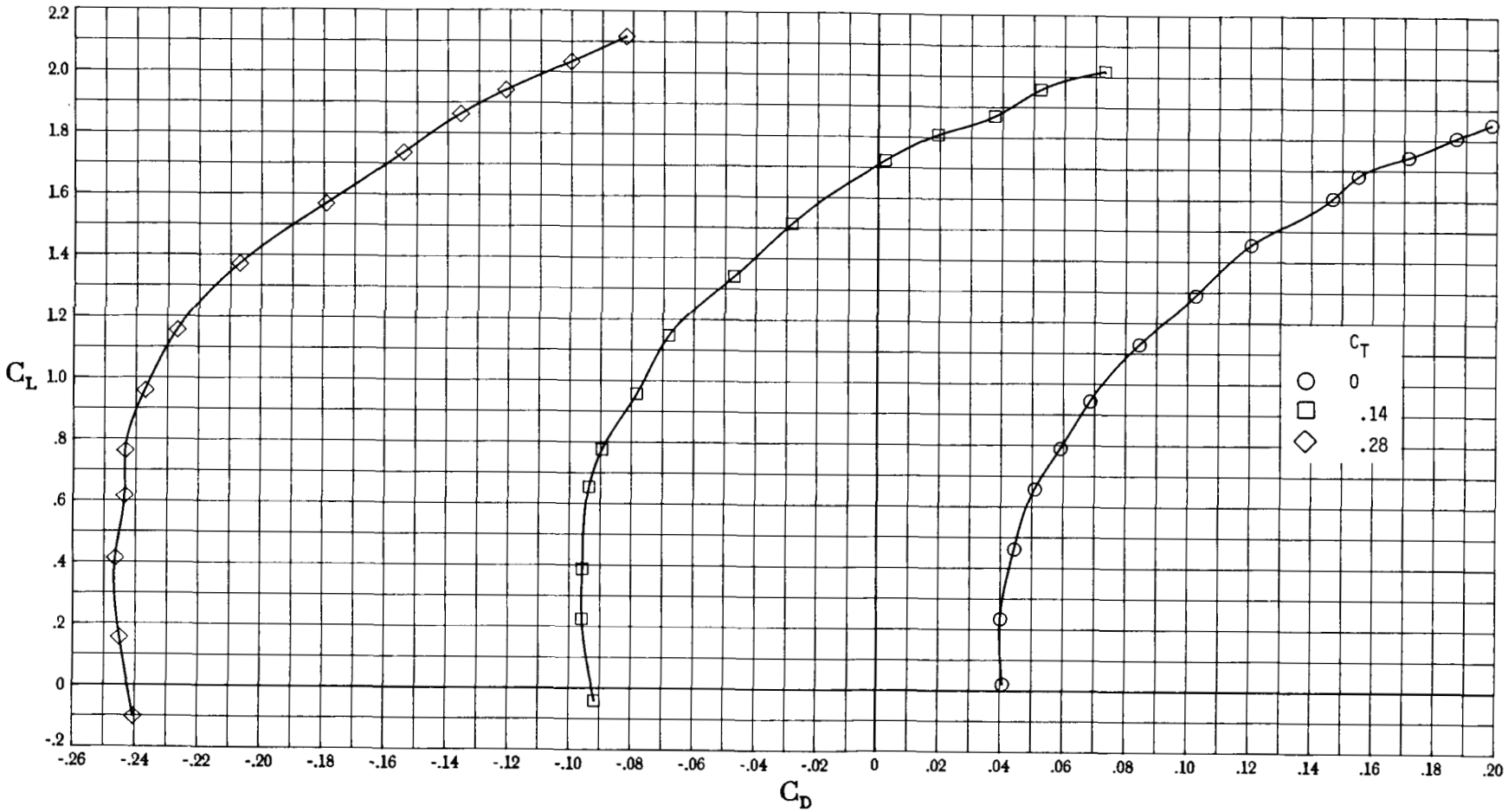


(b) Lift-drag polars.

Figure 47. Concluded.

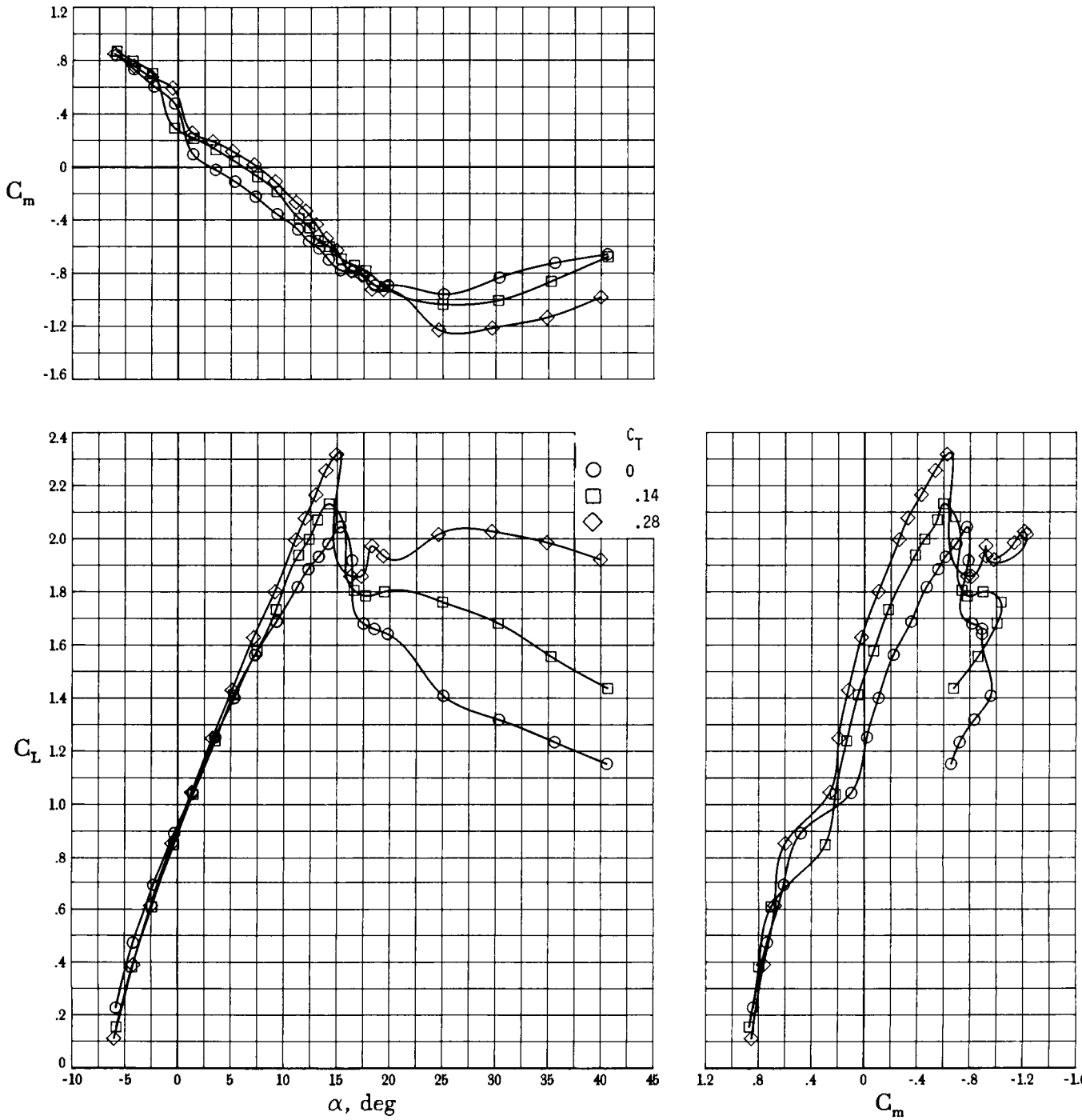


(a) Lift and pitching moment.

Figure 48. Effect of power on longitudinal characteristics of basic configuration with $\delta_{cf} = 40°$. All other controls at zero; $R = 2.0 \times 10^6$.

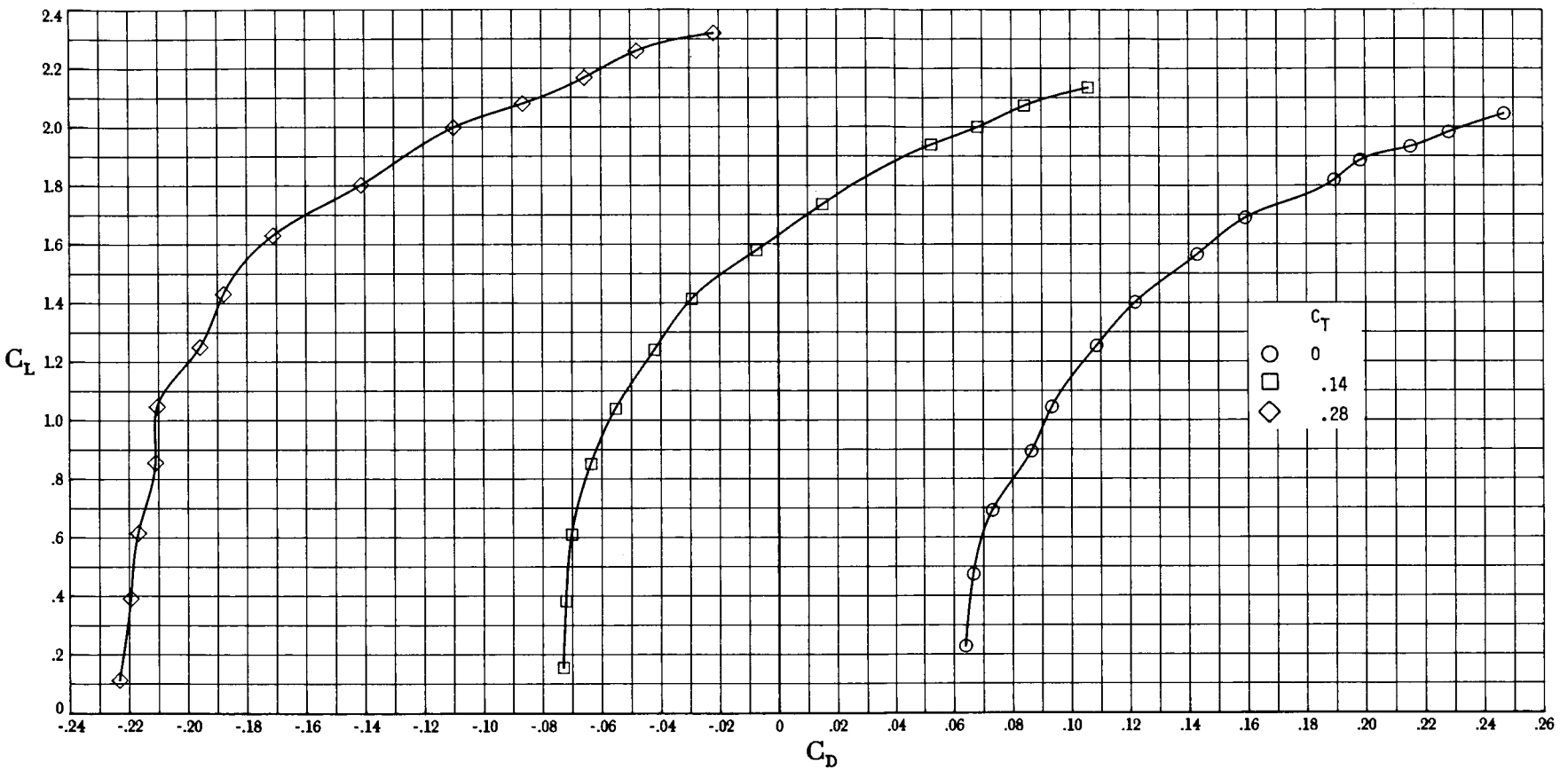


(b) Lift-drag polars.

Figure 48. Concluded.

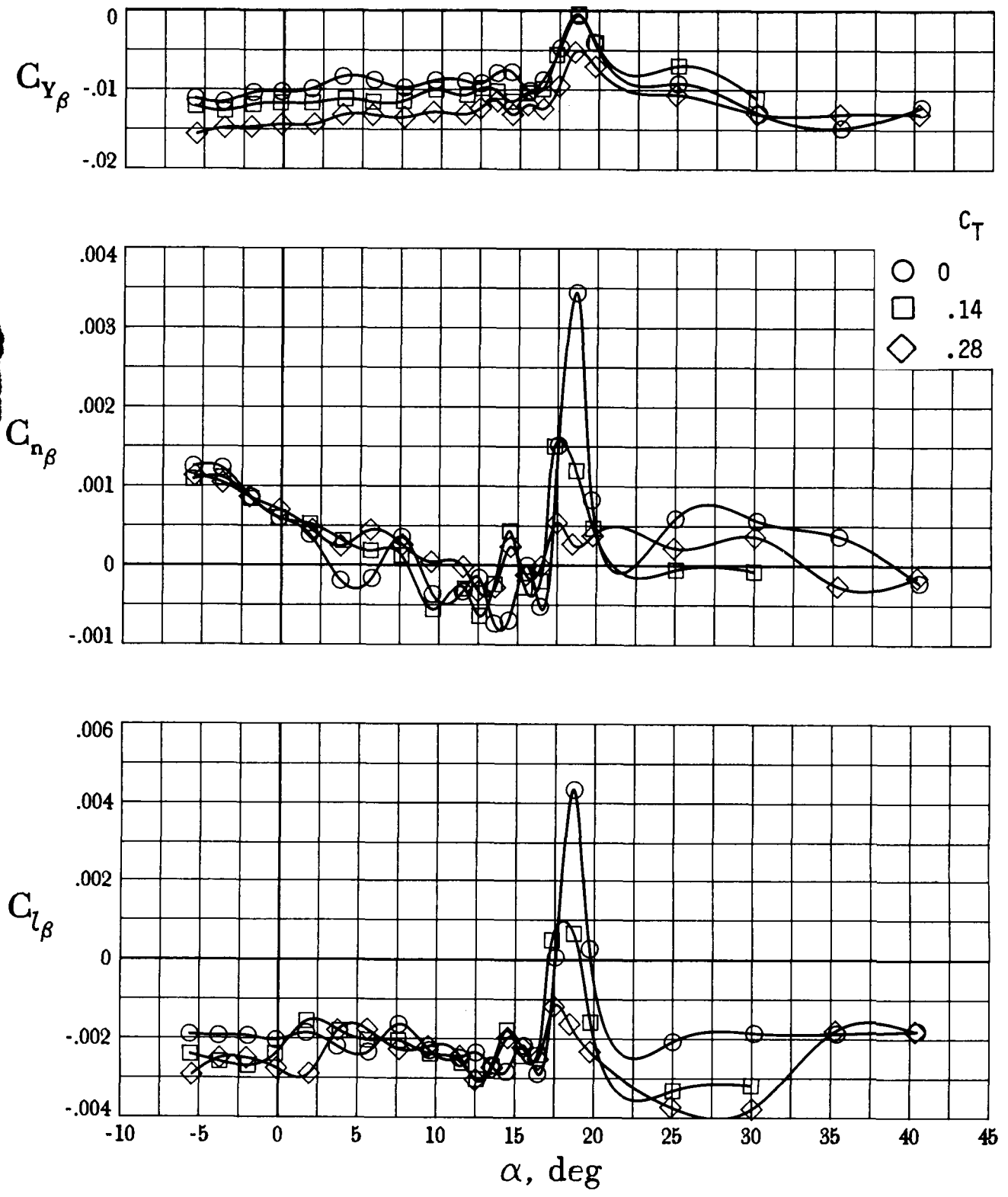


Figure 49. Effect of power on lateral-directional stability characteristics of basic configuration. All controls at zero; $R = 2.0 \times 10^6$.

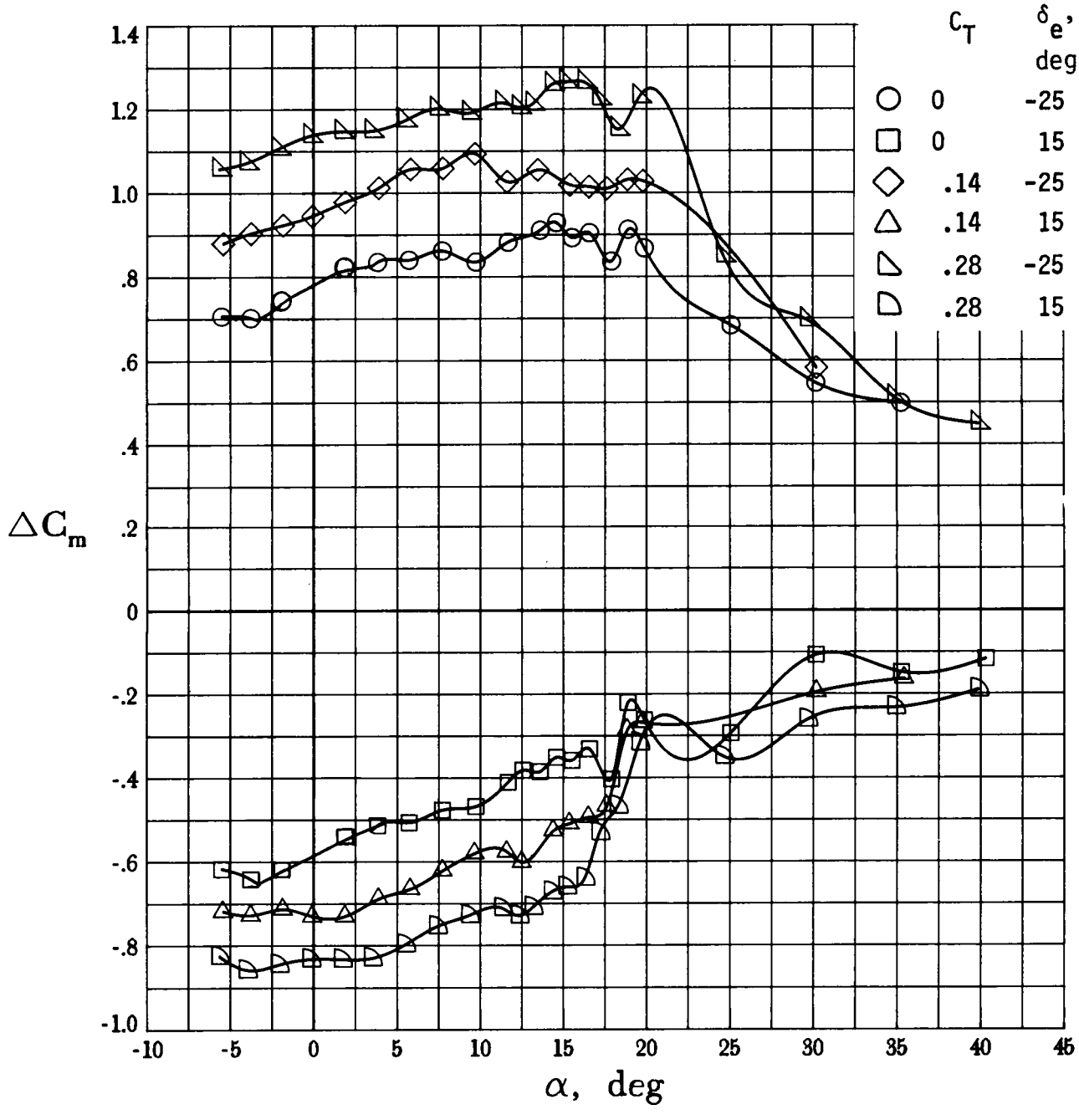


Figure 50. Effect of power on elevator characteristics of basic configuration. All other controls at zero; $R = 2.0 \times 10^6$.

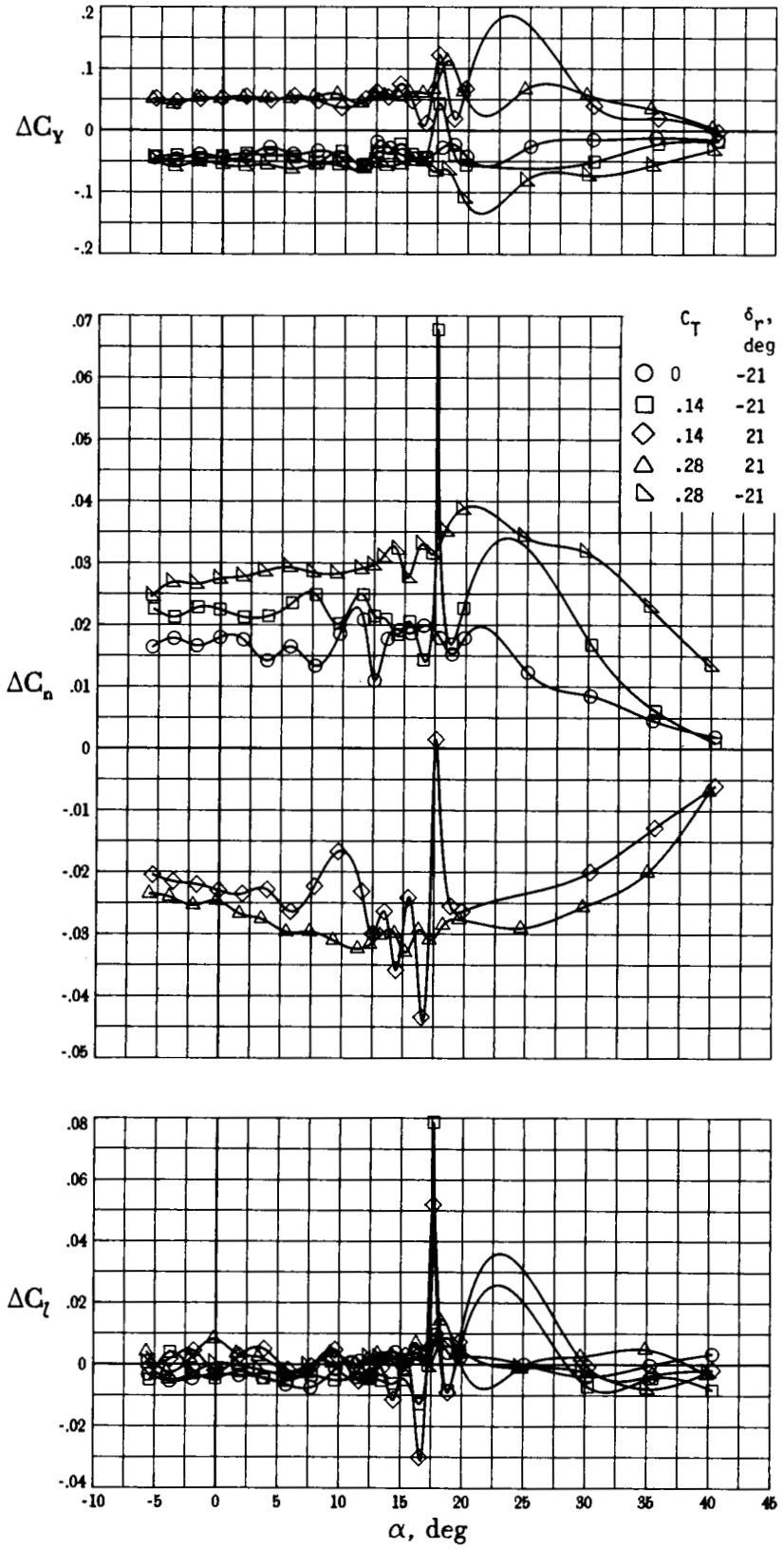


Figure 51. Effect of power on rudder characteristics of basic configuration. All other controls at zero; $R = 2.0 \times 10^6$.

NASA
National Aeronautics and Space Administration

# Report Documentation Page

| 1. Report No. | 2. Government Accession No. | 3. Recipient's Catalog No. |
|---|---|---|
| NASA TP-2772 | | |

| 4. Title and Subtitle | 5. Report Date |
|---|---|
| Wind-Tunnel Investigation of a Full-Scale General Aviation Airplane Equipped With an Advanced Natural Laminar Flow Wing | November 1987 |
| | 6. Performing Organization Code |
| 7. Author(s) | 8. Performing Organization Report No. |
| Daniel G. Murri and Frank L. Jordan, Jr. | L-16283 |
| 9. Performing Organization Name and Address | 10. Work Unit No. |
| NASA Langley Research Center<br>Hampton, VA 23665-5225 | 505-61-41-01 |
| | 11. Contract or Grant No. |
| 12. Sponsoring Agency Name and Address | 13. Type of Report and Period Covered |
| National Aeronautics and Space Administration<br>Washington, DC 20546-0001 | Technical Paper |
| | 14. Sponsoring Agency Code |

15. Supplementary Notes

16. Abstract

An investigation was conducted in the Langley 30- by 60-Foot Tunnel to evaluate the performance, stability, and control characteristics of a full-scale general aviation airplane equipped with an advanced natural laminar flow wing. The study focused on the effects of natural laminar flow and premature boundary-layer transition on performance, stability, and control, and also on the effects of several wing leading-edge modifications on the stall/departure resistance of the configuration. Data were measured over an angle-of-attack range from $-6°$ to $40°$ and an angle-of-sideslip range from $-6°$ to $20°$. The Reynolds number was varied from $1.4 \times 10^6$ to $2.4 \times 10^6$ based on the mean aerodynamic chord. Additional measurements were made using hot-film and sublimating chemical techniques to determine the condition of the wing boundary layer, and wool tufts were used to study the wing stall characteristics. The investigation showed that large regions of natural laminar flow existed on the wing which would significantly enhance the cruise performance of the configuration. Also, because of the characteristics of the airfoil section, artificially tripping the wing boundary layer to a turbulent condition did not significantly affect the lift, stability, and control characteristics. The addition of a leading-edge droop arrangement was found to increase the stall angle of attack at the wingtips and, therefore, was considered to be effective in improving the stall/departure resistance of the configuration. Also, the addition of the droop arrangement resulted in only minor increases in drag.

| 17. Key Words (Suggested by Authors(s)) | 18. Distribution Statement |
|---|---|
| Natural laminar flow<br>General aviation<br>Stall resistance<br>Wing leading-edge droop<br>Stability and control | Unclassified—Unlimited<br><br>Subject Category 02 |

| 19. Security Classif.(of this report) | 20. Security Classif.(of this page) | 21. No. of Pages | 22. Price |
|---|---|---|---|
| Unclassified | Unclassified | 134 | A07 |



For sale by the National Technical Information Service, Springfield, Virginia 22161-2171